2018

Novel Bandpass Filter Design based on Synchronous Filtering

Kanlun Li
Lehigh University

Novel Bandpass Filter Design Based on Synchronous Filtering

by

Kanlun Li

Presented to the Graduate and Research Committee
of Lehigh University
in Candidacy for the Degree of
Doctor of Philosophy

in

Electrical Engineering

Lehigh University

January 2018

Approved and recommended for acceptance as a dissertation in partial fulfillment of the requirements for the degree of Doctor of Philosophy.

_____

Date

_____

Prof. Douglas R. Frey (Advisor), Chair

_____

Accepted Date

Committee Members:

_____

Prof. D. Richard Decker

_____

Prof. Miltiadis K. Hatalis

_____

Prof. Ramamirtham Venkataraman

Acknowledgements

My gratitude goes out to many people who have assisted with my research work and/or contributed to my personal well-being.

Foremost, I would like to thank my advisor, Professor Douglas Frey, who has supported and advised me during my master's and doctoral study. Thank you for inspiring me with your genuine passion and steady effort toward circuit design, for taking me on the journey of creating, for keeping up my spirits with humor and patience. Your unique way of explaining circuits and systems made those complicated concepts and schematics easy for me to understand, your sharp insight into the project always led me to smart design ideas and got me through the research bottleneck. It has been a tough path to finally complete my doctorate, but I feel my effort towards becoming a good circuit designer would never end.

I would also like to thank the members of my committee, Professor D. Richard Decker, Professor Miltiadis K. Hatalis and Professor Ramamirtham Venkataraman, for reviewing this dissertation. Their comments and advice are greatly appreciated.

My thanks go out to Prof. Svetlana Tatic-Lucic, who supported and supervised me in my first two years at Lehigh University. I would like to thank Prof. Nelson Tansu for keeping encouraging me and emphasizing the value of hard work and integrity, and Prof. Bill Haller, who has successfully instilled in me the passion and proud of a Lehigh engineer. I would also like to thank Ted Bowen and David Morrisette, for providing prompt technical support that has made my research work more efficient.

My experience at Lehigh University would not have been the same without the teaching assistant work. I would like to thank the Electrical and Computer Engineering

Department for providing me the opportunity and I am grateful to Professor Douglas Frey for his kind guidance in how to give quality recitation and lab instruction. I would also like to thank my students over the years who have made me more outgoing and thoughtful.

I would like to thank the friends during my study at Lehigh University: Gaoshan Jing, Markus Gnerlich, Tianyi Zhou, Jing Zhang, Thomas Charisolis, Xi Luo, Zi Wang, Yongyang Huang, Eva Chen, Andre Sukernik, etc.

Finally, I deeply appreciate my parents for their unconditional love, generous support and endless patience that make me strong. Special thanks go out to my husband Bo, for being understanding and supportive.

Table of Contents

List of Tables

List of Figures

Abstract

The design of high-performance low-noise bandpass filtering systems has been studied from several aspects: (1) applying the synchronous filtering idea to the development of externally linear, time-invariant filters which can be internally nonlinear and/or time-varying, (2) seeking solutions to improve the noise performance of these filters, from parameter configuration to architecture design, and (3) implementing the systems of interest as transistor level circuits and verifying their function.

Particularly, the state space representations for a biquad AM mode synchronous bandpass filter and a biquad FM mode synchronous complex filter have been proposed and realized with ideal Gm-C networks and log-domain circuits. Both systems utilize the modulator-core filter-modulator architecture to synchronize the internal signal processing. The core filter in an AM mode synchronous filter has constant center frequency and time-variant bandwidth, and the terminal modulators perform amplitude modulation to maintain the system's external linearity and input/output characteristics. An FM mode synchronous filter typically has time-invariant bandwidth and performs frequency modulation before and after the signal filtering. Depending on whether the center frequency and terminal modulating frequency vary with time, there are static and dynamic types of FM mode synchronous filters. They both have the advantage of being able to filter the high frequency input signals in a low frequency range, which greatly alleviates the design and integration challenge due to the high frequency limitation of active components. Moreover, some dynamic filters effectively suppress the injected single-tone noise and generate an output with much higher SNR in comparison to the output from a static filter that implements the same transfer function.

As a variation of an AM mode synchronous bandpass filter, the system derived by removing its back end modulator has been verified to have impressive noise reduction capability when processing noisy AM signals. Furthermore, it inspired the development of a feedback filtering system, the effective bandwidth of which could be tuned by scaling the feedback signal that time varies the core filter's instantaneous bandwidth. It further provides an innovative approach to the design of a high-Q filter with superior immunity to internal noise, using a filter with very low Q factor. Finally, a design that combines the feedback architecture and the biquad FM mode synchronous complex filter is proposed and implemented as a log-domain filtering circuit. Appealing features of this system include wide dynamic range, flexible bandwidth and center frequency tunability. Since there is a low requirement for the high-frequency performance of active components, these filters make a good fit for monolithic integration, and greatly improved immunity to in-filter noise in comparison to that of an open loop complex filter with similar external filtering capability.

Chapter 1 Introduction to Synchronous Filtering

1.1 General Description

Motivated by the desire to create integrated circuits that have certain filtering functions, analog circuit designers have successfully developed basic filter blocks during the past several decades, such as operational amplifiers and transconductance amplifiers. They have also introduced and improved some new filtering paradigms, such as switched capacitor filters, delta sigma converters, etc. In recent years, the integration of high-frequency tunable filters has drawn more attention. For example, an electronically tunable anti-aliasing filter for use in digital video was reported in [1], [2-4] discussed the topologies of high-frequency filters in both bipolar and CMOS technology. However, they all suffer from the high-frequency limitations of the active elements. To alleviate this issue, researchers have focused their effort mainly on two aspects: incorporating current-mode elements into the design[5-10] and developing new filtering system architectures. We leave the design methodology and implementation detail of log-domain filters, a pure current-mode filtering paradigm, to Chapter 2 and introduce the synchronous filtering technique in this chapter, which is associated with the architecture design and has yielded many high performance filters for RF receivers, transmission and audio recording.

Take high-Q high-center frequency bandpass filters for instance, due to the high-frequency limitations of available active components, monolithic implementation of these filters is barely acceptable as it generally suffers from poor selectivity, narrow dynamic range and low noise immunity at high frequencies. To tackle this problem, a classic architecture, which introduces modulators to work in conjunction with a lower-

frequency core filter, has been devised and widely adopted in modern radio receivers. A desirable point of this solution is utilizing modulators to lower the frequency range of signals to be processed so that the high-Q high-frequency filter is no longer required by an RF receiver. In practice, such an architecture is widely employed in the so-called high intermediate frequency (IF), low-IF, and zero-IF systems. Inspired by this prevalent architecture, Frey proposed the concept and mathematics regarding synchronous filtering in 2006[11], which provided an elegant guideline for the development of a variety of synchronous filters. The paper articulated how a given time invariant filter can be implemented using the combination of modulators and a core filter, proved that the developed system has identical zero-input response as the original filter does, and introduced for the first time a companding complex filter as an instance of synchronous filters.

It is straightforward to demonstrate the synchronous filtering idea with the block diagram of a synchronous filter. In general, the system incorporates a core filter and a pair of modulators set up at the front end and back end respectively, which are abstracted as multipliers in Fig. 1.1. They work in a matching mode to implement a system that is functionally equivalent to a standalone filter (with no modulators). As an example that will be verified later, a high-center frequency high-Q filter could be realised with this architecture where the core filter is only required to have a much lower center frequency and a much smaller quality factor. The main purpose of the front end modulator is to down convert the received RF signal so that the core filter could process it in a lower frequency range. The back end modulator is utilized to apply another frequency-domain shifting on the output of the core filter, which is an indispensable piece for drawing the

function equivalence. The core filter in a synchronous filtering system could even have time-variant center frequency, which will not change the system's external linearity and overall function as long as the front end and back end modulators are synchronized accordingly. There is a potential that certain variation patterns for the core filter center frequency and terminal modulating frequencies could make the synchronous filter superior to its standalone-filter counterpart in noise suppression. Furthermore, a synchronous filter could have time-variant bandwidth too, as will be shown in Chapter 2, a system derived from such a filter is capable of heavily suppressing the input noise while maintaining the useful information signals.

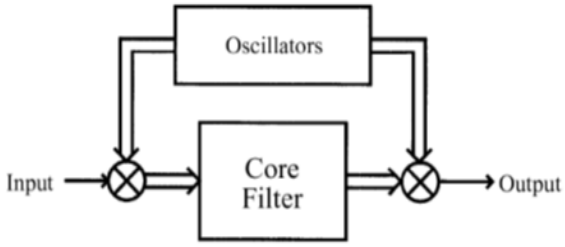

Figure 1.1 Generic block diagram of a synchronous filter.

1.2 State Space Representation of LTI Systems

The mathematical model of synchronous filtering to be introduced is developed in the context of a system state space representation, as the state-space-based filter design has been studied rigorously and employed to yield many modern filter topologies [12]. A brief review on the state space representation of linear time-invariant (LTI) systems is given below[13] before the derivation of the synchronous filtering models.

1.2.1 Formulation of the State Space Model

In general, state variables, state equations and output equations are three important elements in the state-space model. The state variables of a dynamical system refer to a minimum set of variables that could be used to fully describe the system and its response to any given set of inputs. It is asserted that the mathematical model of a state-determined system in terms of a minimum set of state variables $x_i(t), i = 1, \dots, n$, together with knowledge of those variables at an initial time t_0 and the system inputs for time $t > t_0$, are sufficient to predict the future system state and outputs for all time $t > t_0$. Many electrical networks may be represented by state-determined system models, where the number of state variables, n, is equal to the number of independent energy storage elements in the system, such as capacitors and inductors. A variety of different state variable sets may be selected to yield a complete system description, and it could be formulated in terms of physical and measureable variables, or in terms of variables that are not directly measurable. The crucial point is that any set of state variables must provide a complete description of the system with the possible minimum size. In electrical networks, capacitor voltage and inductor current are the natural choices for state variables. The state equations for an LTI system of order *n* and with *r* inputs are a set of *n* coupled first-order linear differential equations with constant coefficients. This set of *n* equations defines the derivatives of the state variables to be a weighted sum of the state variables and the system input. A compact expression for the state equations in a matrix form is:

$$\frac{d}{dt}\begin{bmatrix} x_1 \\ x_2 \\ \vdots \\ x_n \end{bmatrix} = \begin{bmatrix} a_{11} & a_{12} & \dots & a_{1n} \\ a_{21} & a_{22} & \dots & a_{2n} \\ \vdots & \vdots & \vdots & \vdots \\ a_{n1} & a_{n2} & \dots & a_{nn} \end{bmatrix}\begin{bmatrix} x_1 \\ x_2 \\ \vdots \\ x_n \end{bmatrix} + \begin{bmatrix} b_{11} & \dots & b_{1r} \\ b_{21} & \dots & b_{2r} \\ \vdots & \vdots & \vdots \\ b_{n1} & \dots & b_{nr} \end{bmatrix}\begin{bmatrix} u_1 \\ \vdots \\ u_r \end{bmatrix} \qquad (1.1)$$

which may be abstracted as

$$\dot{\bar{x}} = A\bar{x} + B\bar{u} \qquad (1.2)$$

where the state vector $\bar{x}$ is a column vector of length n, the input vector $\bar{u}$ is a column vector of length r, A is an n×n square matrix of the constant coefficients a_{ij} and it is known as the system state matrix, B is an n×r matrix of the coefficients b_{ij} that weight the inputs. The system state at any instant may be interpreted as a point in an n-dimensional state space, and the dynamic state response $\bar{x}(t)$ can be interpreted as a path or trajectory traced out in the state space.

The system output is defined as any system variable of interest. An important property of the linear state equation description is that all system variables may be represented by a linear combination of the state variables x_i and the system inputs u_i. An arbitrary output variable in a system of order *n* with *r* inputs may be formulated as:

$$y(t) = c_1x_1 + c_2x_2 + \cdots + c_nx_n + d_1u_1 + \cdots + d_ru_r \qquad (1.3)$$

where c_i and d_i are constants. If a total of *m* system variables are defined as outputs, the output equations could be expressed in the following matrix form:

$$\begin{bmatrix} y_1 \\ y_2 \\ \vdots \\ y_m \end{bmatrix} = \begin{bmatrix} c_{11} & c_{12} & \dots & c_{1n} \\ c_{21} & c_{22} & \dots & c_{2n} \\ \vdots & \vdots & \vdots & \vdots \\ c_{m1} & c_{m2} & \dots & c_{mn} \end{bmatrix}\begin{bmatrix} x_1 \\ x_2 \\ \vdots \\ x_n \end{bmatrix} + \begin{bmatrix} d_{11} & \dots & d_{1r} \\ d_{21} & \dots & d_{2r} \\ \vdots & \vdots & \vdots \\ d_{m1} & \dots & d_{mr} \end{bmatrix}\begin{bmatrix} u_1 \\ \vdots \\ u_r \end{bmatrix} \qquad (1.4)$$

which is also written as:

$$\bar{y} = C\bar{x} + D\bar{u} \qquad (1.5)$$

where $\bar{y}$ is a column vector of the output variables $y_i(t)$, C is an $m \times n$ matrix of the constant coefficients c_{ij} that weight the state variables, and D is an $m \times r$ matrix of the constant coefficients d_{ij} that weight the system inputs. For many physical systems the matrix D is the null matrix, and the output equation reduces to a linear combination of the weighted state variables:

$$\bar{y} = C\bar{x} \qquad (1.6)$$

The complete system model for a LTI system consists of a set of n state equations, defined in terms of the matrices A and B, plus a set of output equations that relate any output variables of interest to the state variables and input, and expressed in terms of C and D matrices. The matrices A and B are properties of the system and are determined by the system structure and elements. The output equation matrices C and D are determined by the particular choice of output variables. Fig.1.2 provides an explicit demonstration on the idea of state space representation. It shows the matrix operation from input to output in terms of the matrices A, B, C and D**,** without the specific path of individual state variables.

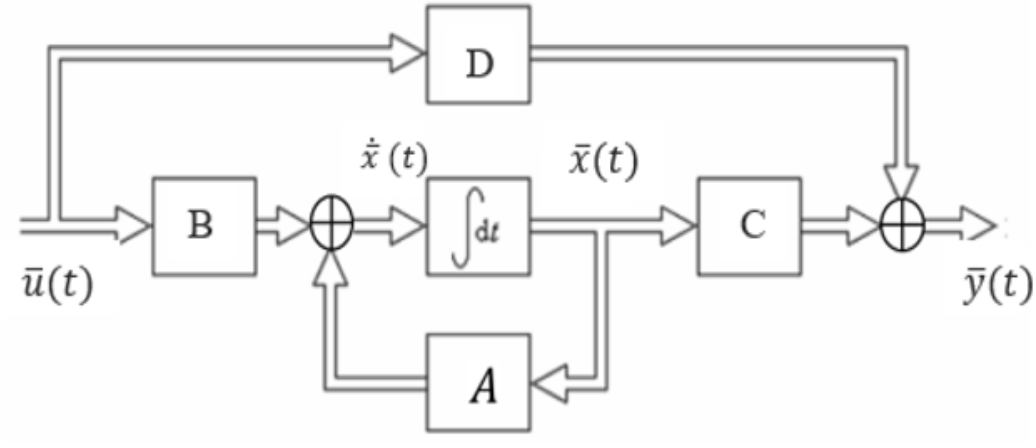

Figure 1.2 Vector block diagram for a LTI system described by state-space system dynamics.

1.2.2 Complete System Response

Eqn. (1.2) and eqn. (1.5) together provide a system state space representation. Given sufficient initial conditions, it is possible to predict the future system state and outputs for all time. A very straightforward approach to solving these equations is using Laplace and inverse Laplace transforms. Suppose the Laplace transform of the state vector $\bar{x}(t)$ is $\bar{X}(s)$, by utilizing the time-differentiation property of Laplace transform, the frequency-domain representation of $\bar{X}(s)$ is derived as:

$$\bar{X}(s) = \Phi(s)\bar{x}(0) + \Phi(s)B\bar{U}(s) \quad (1.7)$$

where $\Phi(s) = (sI - A)^{-1}$. Then the time domain representation of eqn. (1.7) is the solution to eqn. (1.2), which could be derived by applying inverse Laplace transform to each term in eqn. (1.7). Specifically,

$$\bar{x}(t) = \varphi(t)\bar{x}(0) + \int_0^t \varphi(t-\tau)B\bar{u}(\tau)d_\tau \quad (1.8)$$

where $\varphi(t)$ is the inverse Laplace transform of $\Phi(s)$. Substitute $\bar{x}(t)$ in eqn. (1.5), the system complete response is naturally developed to be:

$$\bar{y}(t) = C\varphi(t)\bar{x}(0) + \int_0^t C\varphi(t-\tau)B\bar{u}(\tau)d_\tau + D\bar{u}(t) \quad (1.9)$$

Derivation of the system transfer function from a state space representation is straightforward. As a transfer function is associated with the zero state system response, initial condition of the selected set of state variables is not of our concern here. In particular, setting $\bar{x}(0) = 0$ in eqn. (1.7):

$$\bar{X}(s) = \Phi(s)B\bar{U}(s) \quad (1.10)$$

Writing eqn. (1.5) in S domain and substituting $X(s)$ with the above expression, the system transfer function is derived as:

$$\bar{Y}(s) = C\bar{X}(s) + D\bar{U}(s) \quad (1.11)$$

Deriving State Space Description from the Transfer Function

$$H(s) = C\Phi(s)B + D \quad (1.12)$$

As the state space model of a LTI system is not unique, the mapping of any given transfer function to the time domain yields a variety of different dynamical equation sets. A convenient state-space model formulation technique that is widely used in control theory is presented here. Suppose without loss of generality the system is of order *n* and has a transfer function:

$$H(s) = \frac{b_n s^n + b_{n-1} s^{n-1} + \cdots + b_0}{a_n s^n + a_{n-1} s^{n-1} + \cdots + a_0} = \frac{b_n + b_{n-1} s^{-1} + \cdots + b_0 s^{-n}}{a_n + a_{n-1} s^{-1} + \cdots + a_0 s^{-n}} \quad (1.13)$$

Define a dummy variable $Z(s)$ and split the transfer function into two equations:

$$\bar{Z}(s) = \frac{1}{a_n + a_{n-1} s^{-1} + \cdots + a_0 s^{-n}} \bar{U}(s) \quad (1.14)$$

$$\bar{Y}(s) = (b_n + b_{n-1} s^{-1} + \cdots + b_0 s^{-n}) \bar{Z}(s) \quad (1.15)$$

Rearranging eqn. (1.14) to specify $Z(s)$ in terms of the system input and a weighted sum of successive integrations of itself, an equation associated with a system that includes a feedback structure is derived as eqn. (1.16). The resulting block diagram of the system is shown in Fig. 1.3, where a string of n cascaded integrators together with $Z(s)$ defined at the input of the first integrator is used to generate the feedback terms in the equation. Moreover, eqn. (1.15) is implemented easily by combining the output of each integrator.

$$\bar{Z}(s) = \frac{1}{a_n} \bar{U}(s) - \left(\frac{a_{n-1}}{a_n} \frac{1}{s} + \cdots + \frac{a_1}{a_n} \frac{1}{s^{n-1}} + \frac{a_0}{a_n} \frac{1}{s^n}\right) \bar{Z}(s) \quad (1.16)$$

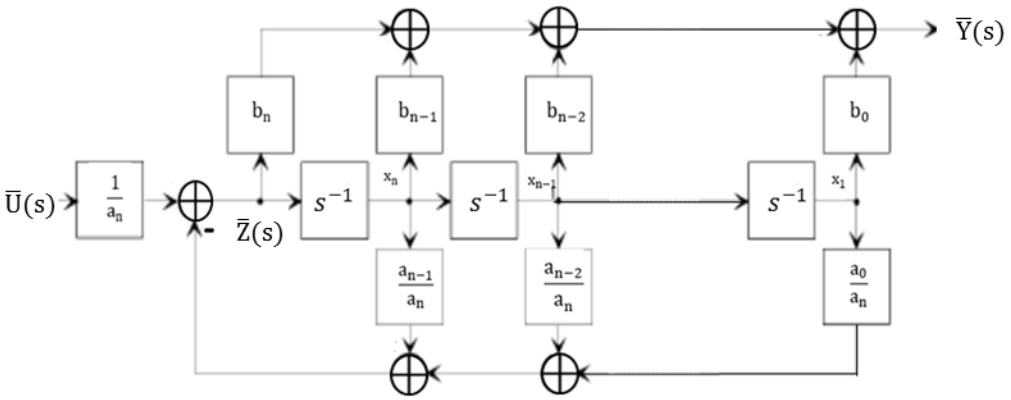

Figure 1.3 Block diagram of the system corresponding to eqn. (1.15) and eqn. (1.16).

Due to the direct cascade of each integrator, the state equations of the system take a very simple form if we assign the state variables $x_i(t)$ to the output of the n integrators. By inspection, a set of state equations may be formulated as follows:

$$\begin{bmatrix} \dot{x}_1 \\ \dot{x}_2 \\ \vdots \\ \dot{x}_{n-2} \\ \dot{x}_{n-1} \\ \dot{x}_n \end{bmatrix} = \begin{bmatrix} 0 & 1 & \cdots & 0 & 0 \\ 0 & 0 & \cdots & 0 & 0 \\ \vdots & \vdots & \ddots & \vdots & \vdots \\ 0 & 0 & \cdots & 1 & 0 \\ 0 & 0 & \cdots & 0 & 1 \\ -a_0/a_n & -a_1/a_n & \cdots & -a_{n-2}/a_n & -a_{n-1}/a_n \end{bmatrix} \begin{bmatrix} x_1 \\ x_2 \\ \vdots \\ x_{n-2} \\ x_{n-1} \\ x_n \end{bmatrix} + \begin{bmatrix} 0 \\ 0 \\ \vdots \\ 0 \\ 0 \\ 1/a_n \end{bmatrix} \bar{u}(t) \tag{1.17}$$

This version of the state equations are known as the phase variable or companion form, where the each row of the state matrix **A**, except the bottom one, is filled of zeroes except for one entry in the position just above the leading diagonal. The corresponding output equation could be derived by noting that $X_i(s) = \bar{Z}(s)/s^{(n+1-i)}$ and applying the inverse Laplace transform. In particular, eqn. (1.15) and eqn. (1.16) are converted into the time domain as:

$$\bar{y}(t) = b_0 x_1 + b_1 x_2 + b_2 x_3 + \cdots + b_{n-1} x_n + b_n \bar{z}(t) \tag{1.18}$$

$$\bar{z}(t) = -\left(\frac{a_0}{a_n} x_1 + \frac{a_1}{a_n} x_2 + \cdots + \frac{a_{n-1}}{a_n} x_n\right) + \frac{1}{a_n} \bar{u}(t) \tag{1.19}$$

Expressing $z(t)$ in eqn. (18) in terms of x_i and $\mathrm{u(t)}$, the output equation is derived as:

$$\bar{\mathrm{y}}(\mathrm{t}) = \left[\mathrm{b}_0 - \frac{\mathrm{b}_\mathrm{n}\mathrm{a}_0}{\mathrm{a}_\mathrm{n}} \quad \mathrm{b}_1 - \frac{\mathrm{b}_\mathrm{n}\mathrm{a}_1}{\mathrm{a}_\mathrm{n}} \quad \cdots \quad \mathrm{b}_{\mathrm{n}-1} - \frac{\mathrm{b}_\mathrm{n}\mathrm{a}_{\mathrm{n}-1}}{\mathrm{a}_\mathrm{n}}\right]\begin{bmatrix}\mathrm{x}_1\\ \mathrm{x}_2\\ \vdots\\ \mathrm{x}_\mathrm{n}\end{bmatrix} + \frac{\mathrm{b}_\mathrm{n}}{\mathrm{a}_\mathrm{n}}\bar{\mathrm{u}}(\mathrm{t}) \qquad (1.20)$$

1.2.3 State Space Transformation

Eqn. (1.17) and eqn. (1.20) give a state space description derived from the given transfer function. Since any linear transformation on the state space preserves the transfer function, a transfer function could in principle be realized by infinite electrical networks. However, some might have highly complicated schematics, some have poor dynamic range or high noise sensitivity, etc. Therefore, a smart state space transformation plays a critical role in deriving a state space model that leads to the design of a compact and high performance circuit. For example, diagonalization of the state matrix is one of the most provocative transformation approaches. It generates a state-space model that has a greatly simplified state transition matrix and could be implemented by an electrical network of low complexity. Recall the relationship between a matrix, its eigenvalues and its eigenvectors:

$$\mathrm{A}[\bar{\mathrm{v}}_1 \quad \bar{\mathrm{v}}_2 \quad \cdots \quad \bar{\mathrm{v}}_\mathrm{N}] = \mathrm{AV} = [\lambda_1\bar{\mathrm{v}}_1 \quad \lambda_2\bar{\mathrm{v}}_2 \quad \cdots \quad \lambda_\mathrm{N}\bar{\mathrm{v}}_\mathrm{N}] = \mathrm{V}\mathrm{diag}(\lambda_1, \lambda_2, \cdots, \lambda_\mathrm{N}) = \mathrm{V}\Lambda \qquad (1.21)$$

where $\bar{\mathrm{v}}_\mathrm{i}$ is the eigenvector corresponding to λ_i, 'diag()' denotes a diagonal matrix,

$$\mathrm{V} \equiv [\bar{v}_1 \quad \bar{v}_2 \quad \cdots \quad \bar{v}_N], \ \Lambda \equiv diag(\lambda_1, \lambda_2, \cdots, \lambda_N)$$

The diagonal matrix Λ could be taken as a transformed version of A, as shown in eqn. (1.22), which indicates that A could be easily diagonalized by determining its eigenvectors.

$$\Lambda = \mathrm{V}^{-1}\mathrm{AV} \qquad (1.22)$$

Based on the above example, a generic state space transformation is presented below. Suppose the originally derived system state space representation is given by eqn. (1.2) and eqn. (1.5). Because any new set of state variables is able to be expressed as a linear combination of the original state variables and the input, let $\bar{w} = M\bar{x} + \mathrm{Q}\bar{u}$, where both M and Q are nonsingular $N \times N$ matrices, and M is known as the transformation matrix. Substitute $\bar{x}$ in eqn. (1.2) and eqn. (1.5) with $M^{-1}(\bar{w} - \mathrm{Q}\bar{u})$ according to the definition:

$$\dot{\bar{\mathrm{w}}} = \hat{\mathrm{A}}\bar{\mathrm{w}} + \hat{\mathrm{B}}\bar{\mathrm{u}} + \mathrm{L}(\bar{\mathrm{u}}, \dot{\bar{\mathrm{u}}}) \quad (1.23)$$

$$\bar{y} = \hat{\mathrm{C}}\bar{\mathrm{w}} + (\mathrm{D} - \hat{\mathrm{C}}Q)\bar{\mathrm{u}} \quad (1.24)$$

where $\hat{\mathrm{A}} = \mathrm{MAM}^{-1}$, $\hat{\mathrm{B}} = \mathrm{MB}$, $\mathrm{L}(\bar{\mathrm{u}}, \dot{\bar{\mathrm{u}}}) = \mathrm{Q}\dot{\bar{\mathrm{u}}} - \mathrm{MAM}^{-1}\mathrm{Q}\bar{\mathrm{u}}$, $\hat{\mathrm{C}} = \mathrm{CM}^{-1}$.

Note that although the derivative of the input exists in the state equation, the transfer function derived from eqn. (1.23) and eqn. (1.24) is exactly the same as shown in eqn. (1.12). To get rid of the derivative term, Q is typically set to be a null matrix and the resulting state space description is simplified as:

$$\dot{\bar{\mathrm{w}}} = \hat{\mathrm{A}}\bar{\mathrm{w}} + \hat{\mathrm{B}}\bar{\mathrm{u}} = \mathrm{MAM}^{-1}\bar{\mathrm{w}} + \mathrm{MB}\bar{\mathrm{u}} \quad (1.25)$$

$$\bar{y} = \hat{\mathrm{C}}\bar{\mathrm{w}} + \mathrm{D}\bar{\mathrm{u}} = C\mathrm{M}^{-1}\bar{\mathrm{w}} + \mathrm{D}\bar{\mathrm{u}} \quad (1.26)$$

An example is now provided to show the beauty of state space transformation in filter design. Consider the transfer function for a standard second order bandpass filter:

$$\mathrm{H(s)} = \frac{\bar{\mathrm{Y}}(\mathrm{s})}{\bar{\mathrm{U}}(\mathrm{s})} = \frac{\frac{\mathrm{w_0}}{\mathrm{Q}}\mathrm{s}}{\mathrm{s}^2 + \frac{\mathrm{w_0}}{\mathrm{Q}}\mathrm{s} + {\mathrm{w_0}}^2} \quad (1.27)$$

One particular state-space representation of the above filter is in given by eqn. (1.28):

$$\begin{vmatrix} \dot{\mathrm{x}}_1 \\ \dot{\mathrm{x}}_2 \end{vmatrix} = \begin{vmatrix} -\frac{\mathrm{w_0}}{\mathrm{Q}} & -\mathrm{w_0} \\ \mathrm{w_0} & 0 \end{vmatrix} \begin{vmatrix} \mathrm{x}_1 \\ \mathrm{x}_2 \end{vmatrix} + \begin{vmatrix} \frac{\mathrm{w_0}}{\mathrm{Q}} \\ 0 \end{vmatrix} \mathrm{u}, \quad \mathrm{y} = |1 \quad 0| \begin{vmatrix} \mathrm{x}_1 \\ \mathrm{x}_2 \end{vmatrix} \quad (1.28)$$

Suppose that the state variables x_1 and x_2 are associated with the capacitor voltage and the inductor current, respectively. The state equations, after appropriate scaling, could be taken as a nodal equation and a loop equation of an RLC circuit. Accordingly, the output equation could be translated to mean that the circuit output is given by the capacitor voltage. Fig. 1.4 shows the RLC implementation of eqn. (1.28) with state variables labeled, and the constraints on the component are: $R = 1/Q, L = C = 1/w_0$.

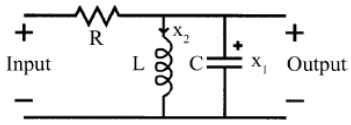

Figure 1.4 RLC circuit implementation of eqn. (1.28)

After state space transformation with the transformation matrix *M* in eqn. (1.30), the original state space model finds an equivalent new version of eqn. (30). Fig. 1.5 gives a common circuit realisation for the new state-space representation that contains a pair of lossy integrators built with op amps and necessary surrounding circuitry. The choosing of resistors and capacitors needs to follow the equations below the schematic so as to implement the expected center frequency and quality factor.

$$M = \begin{bmatrix} 1 & \gamma + \lambda \\ -1 & -\gamma + \lambda \end{bmatrix} \tag{1.29}$$

$$\begin{vmatrix} \dot{x_1} \\ \dot{x_2} \end{vmatrix} = \begin{vmatrix} -\frac{w_0}{2Q} & -w_A \\ w_A & -\frac{w_0}{2Q} \end{vmatrix} \begin{vmatrix} x_1 \\ x_2 \end{vmatrix} + \frac{w_0}{Q} \begin{vmatrix} 1 \\ -1 \end{vmatrix} u$$

$$y = \frac{1}{2\lambda} |(-\gamma + \lambda) \quad -(\gamma + \lambda)| \begin{vmatrix} x_1 \\ x_2 \end{vmatrix} \tag{1.30}$$

where $\gamma = 1/2Q;\ \lambda = \sqrt{1 - (1/2Q)^2};\ w_A = \sqrt{1 - (1/2Q)^2} w_0$.

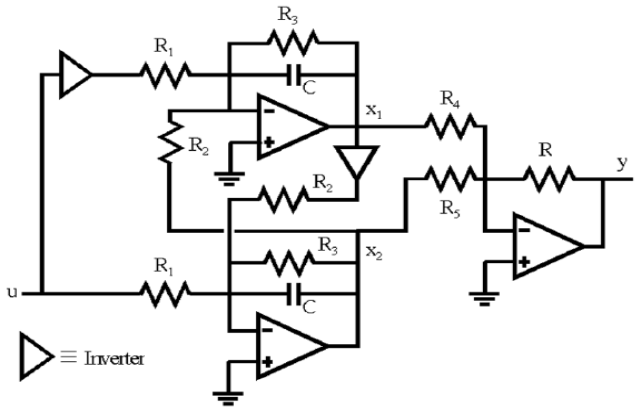

$R_1 = Q/(w_0C), R_2 = 1/(\lambda w_0C), R_3 = 2Q/(w_0C), R_4 = 2R\lambda/(\lambda - \gamma), R_5 = 2R\lambda/(\lambda + \gamma)$

Figure 1.5 Op-amp circuit implementation of eqn. (1.30).

1.3 State Space Representation of Synchronous Filters

1.3.1 FM Mode Synchronous Filtering

A state space transformation yields a new state space description, which almost certainly leads to an alternate electrical network that implements the target transfer function. However, if the transfer function is very difficult to implement due to component limitations, a random state space transformation barely alleviates the design challenge. This is because the resulting circuit, although it has a different schematic, still processes signals in the same frequency range. For instance, the transfer function of a second-order bandpass filter is implemented by two completely different circuits, as shown in Fig. 1.4 and Fig. 1.5, but neither of them is a good candidate for implementing a high-center frequency high-Q filter, due to the performance degradation of the electronic components in a very high frequency range. To tackle the challenge in developing a generally acceptable monolithic bandpass filter with very high center frequency and very high Q factor, the modulator-core filter-modulator architecture has been widely employed in RF systems, where the core filter has a much lower center

frequency and a much smaller Q factor. We now introduce how to utilize a state space transformation to develop the mathematical model of such an architecture from the state space representation of the target high-center frequency high-Q filter[11].

Suppose that a time-varying matrix, $M(t)$, were used in the state space transformation of the original dynamical equations specifying the target filter, which are abstracted as eqn. (1.2) and eqn. (1.5). The resulting equation set is derived as:

$$\dot{\mathrm{x}} = \mathrm{A}\bar{\mathrm{x}} + \mathrm{B}\bar{u} \quad \rightarrow \quad \dot{\bar{w}} = \hat{A}\bar{w} + G(t)\bar{u} \qquad (1.31)$$

$$\mathrm{y} = \mathrm{C}\bar{\mathrm{x}} + \mathrm{D}\bar{u} \quad \rightarrow \quad y = H(t)\bar{w} + D\bar{u}$$

where $\widehat{\mathrm{A}} = \mathrm{M(t)AM^{-1}(t)} + \dot{\mathrm{M}}\mathrm{(t)M^{-1}(t)}$, $\mathrm{G(t)} = \mathrm{M(t)B}$, $\mathrm{H(t)} = \mathrm{CM^{-1}(t)}$. In general, $\hat{A}$ is a time-varying matrix. However, since eqn. (1.31) represents a system where the core filter has time-invariant center frequency and Q factor, it is appropriate to assume $\hat{A}$ as a constant matrix in this particular case. This assumption actually sets some implicit constraints on the choice of $M(t)$ and the original state matrix A. Namely, the expected constant state matrix $\hat{A}$ exists only if eqn. (1.32) has a solution for $M(t)$.

$$\dot{M}(t) = \hat{A}M(t) - M(t)A \qquad (1.32)$$

It is not within the scope of our research to seek for the analytical solution of eqn. (1.32), but if A,$\hat{A}$ and $M(t)$ commute, the solution could easily be formulated as:

$$M(t) = Ke^{(\hat{A}-A)t} = Ke^{\hat{A}t}e^{-At} \qquad (1.33)$$

where K is a constant matrix that commutes with $\widehat{\mathrm{A}}$. Note that the core filter in the resulting system differs from the target filter only in the center frequency and quality factor, A and $\hat{A}$ should share the same matrix format and be different in some entries. Based on the above constraints, one possible formation of A and $\hat{A}$ is:

$$A = \begin{bmatrix} a_{11} & a_{12} \\ -a_{12} & a_{11} \end{bmatrix}, \quad \hat{A} = \begin{bmatrix} \widehat{a_{11}} & \widehat{a_{12}} \\ -\widehat{a_{12}} & \widehat{a_{11}} \end{bmatrix} \tag{1.34}$$

where all the entries are real, the diagonal entries are identical and the off-diagonal entries are opposite in sign. It could then be derived with the Cayley-Hamilton theorem:

$$e^{At} = e^{a_{11}t} \begin{bmatrix} \cos(a_{12}t) & \sin(a_{12}t) \\ -\sin(a_{12}t) & \cos(a_{12}t) \end{bmatrix} = e^{a_{11}t}\Phi(a_{12}t) \tag{1.35}$$

where $\Phi(\Omega) = \begin{bmatrix} \cos(\Omega) & \sin(\Omega) \\ -\sin(\Omega) & \cos(\Omega) \end{bmatrix}$. Note that function $\Phi(\,)$ has some interesting properties:

$$\Phi(\theta_1)\,\Phi(\theta_2) = \Phi(\theta_2)\Phi(\theta_1) = \Phi(\theta_1 + \theta_2) \tag{1.36}$$

$$\Phi^{-1}(\theta) = \Phi^{T}(\theta) = \Phi(-\theta)$$

Accordingly, the transformation matrix defined in eqn. (1.33) is derived as:

$$M(t) = Ke^{(\widehat{a_{11}} - a_{11})t} \begin{vmatrix} \cos((a_{12} - \widehat{a_{12}})t) & \sin((a_{12} - \widehat{a_{12}})t) \\ -\sin((a_{12} - \widehat{a_{12}})t) & \cos((a_{12} - \widehat{a_{12}})t) \end{vmatrix}$$

$$= Ke^{(\widehat{a_{11}} - a_{11})t}\Phi((a_{12} - \widehat{a_{12}})) \tag{1.37}$$

And a possible choice for K is a unitary matrix in the same format as A:

$$K = \begin{vmatrix} \cos(\theta_K) & \sin(\theta_K) \\ -\sin(\theta_K) & \cos(\theta_K) \end{vmatrix} = \Phi(\theta_K) \tag{1.38}$$

Therefore,

$$M(t) = e^{(\widehat{a_{11}} - a_{11})t} \begin{vmatrix} \cos((a_{12} - \widehat{a_{12}})t + \theta_K) & \sin((a_{12} - \widehat{a_{12}})t + \theta_K) \\ \sin((a_{12} - \widehat{a_{12}})t + \theta_K) & \cos((a_{12} - \widehat{a_{12}})t + \theta_K) \end{vmatrix} \tag{1.39}$$

To minimize clutter in the mathematics, assume $\widehat{a_{11}} = a_{11}$, $\theta_K = 0$ and define $a_{12} - \widehat{a_{12}} = w_M$. Eqn. (1.39) is simplified to yield

$$M(t) = \begin{vmatrix} \cos(w_M t) & \sin(w_M t) \\ -\sin(w_M t) & \cos(w_M t) \end{vmatrix} = \Phi(w_M t) \tag{1.40}$$

Applying $M(t)$ to the transformation defined in eqn. (1.31), the synchronous filtering system is now specified by a new set of matrices:

$$\hat{A} = M(t)AM^{-1}(t) + \dot{M}(t)M^{-1}(t) = \Phi(w_M t)A\Phi^{-1}(w_M t) + \dot{\Phi}(w_M t)\Phi^{-1}(w_M t)$$

$$= A + w_M \begin{bmatrix} -\sin(w_M t) & \cos(w_M t) \\ -\cos(w_M t) & -\sin(w_M t) \end{bmatrix} \begin{bmatrix} \cos(w_M t) & -\sin(w_M t) \\ \sin(w_M t) & \cos(w_M t) \end{bmatrix}$$

$$= \begin{bmatrix} a_{11} & a_{12} \\ -a_{12} & a_{11} \end{bmatrix} + \begin{bmatrix} 0 & w_M \\ -w_M & 0 \end{bmatrix} = \begin{bmatrix} a_{11} & a_{12} + w_M \\ -(a_{12} + w_M) & a_{11} \end{bmatrix} \quad (1.41a)$$

$$\bar{g}(t) = M(t)\bar{b} = \begin{vmatrix} \cos(w_M t) & \sin(w_M t) \\ -\sin(w_M t) & \cos(w_M t) \end{vmatrix} \begin{vmatrix} b_1 \\ b_2 \end{vmatrix} = b_0 \begin{vmatrix} \sin(w_M t + \beta) \\ \cos(w_M t + \beta) \end{vmatrix}$$

where $b_0 = \sqrt{{b_1}^2 + {b_2}^2}$, $\beta = tan^{-1}(b_1/b_2)$; (1.41b)

$$\bar{h}^T = \bar{c}^T M^{-1}(t) = |c_1 \quad c_2| \begin{vmatrix} \cos(w_M t) & -\sin(w_M t) \\ \sin(w_M t) & \cos(w_M t) \end{vmatrix}$$

$$= c_0 |\sin(w_M t + \alpha) \quad \cos(w_M t + \alpha)|.$$

where $c_0 = \sqrt{{c_1}^2 + {c_2}^2}$, $\alpha = tan^{-1}(c_1/c_2)$ (1.41c)

To prove that the derived system and the target filter have same zero input response, we reproduce the expression for zero input response of the target filter:

$$y_{ZI}(\mathrm{t}) = \bar{\mathrm{c}}^{\mathrm{T}} \phi(t)\bar{x}(0), \quad \text{where } \phi(t) = e^{At} \quad (1.42)$$

Using the property $M^{-1}(\mathrm{t})\mathrm{M}(\mathrm{t}) = \mathrm{I}$, rewrite eqn. (1.42) as:

$$y_{ZI}(\mathrm{t}) = \bar{\mathrm{c}}^{\mathrm{T}} M^{-1}(\mathrm{t})\mathrm{M}(\mathrm{t})\phi(t)M^{-1}(0)\mathrm{M}(0)\bar{x}(0) = \bar{h}^T(t)(\,\mathrm{M}(\mathrm{t})\phi(t)M^{-1}(0))\bar{w}(0) \quad (1.43)$$

Note that $\mathrm{M}(\mathrm{t}) = Ke^{\hat{A}t}e^{-At}$, the three matrices commute and $\mathrm{M}(0) = K$, so

$$e^{\hat{A}t} = \mathrm{M}(\mathrm{t})e^{At}K^{-1} = \mathrm{M}(\mathrm{t})e^{At}M^{-1}(0) \quad (1.44)$$

Therefore, the zero input response of the synchronous filtering system is:

$$\hat{y}_{ZI}(\mathrm{t}) = \bar{h}^T(t)e^{\hat{A}t}\bar{w}(0) = \bar{h}^T(t)\mathrm{M}(\mathrm{t})e^{At}M^{-1}(0)\bar{w}(0) = y_{ZI}(\mathrm{t}) \quad (1.45)$$

Eqn. (1.45) suggests that the zero input response of the synchronous filtering system is completely determined by the initial conditions of the core filter, and it is exactly the same as that of the target filter. Furthermore, the phase offset α and β of the modulating signals could be removed without affecting the system zero input response.

FM Mode Synchronous Complex Filters

Complex filters, also called polyphase filters, are generally multiple input-multiple output blocks widely used in RF circuits. Besides the bandpass filtering function, a complex filter is able to reject the image of an RF signal[14-17]. Due to the employment of complex-domain signal processing[18], it has the ability to distinguish a positive frequency component from its negative counterpart by attenuating one of them to a negligible level when both are present. Potential realizations for a monolithic complex filter are passive RC networks or active networks. Passive RC complex filters have a high-image rejection ratio but limited selectivity, which means they suffer from strong adjacent channel interference, hence requiring extra filtering[14]. Although active complex filters can achieve both good adjacent channel interference rejection and image rejection, it's extremely hard to find an acceptable monolithic realization for the transfer function of a very high-frequency very high-Q complex filter. Utilizing the derived model above, we develop in this section the state space model of a biquad high-frequency high-Q complex filter in the FM mode synchronous filtering architecture[11].

One possible state space description of a second-order complex filter, given in eqn. (1.46), is almost identical to that of a second-order bandpass filter as defined by eqn. (1.30). Inspection of the state space models reveals that the intrinsic difference between

a standard biquad bandpass filter and a biquad complex filter is that their output is created via slightly different combinations of the state variables.

$$\begin{vmatrix} \dot{x}_1 \\ \dot{x}_2 \end{vmatrix} = \begin{vmatrix} -\frac{w_0}{2Q} & -w_A \\ w_A & -\frac{w_0}{2Q} \end{vmatrix} \begin{vmatrix} x_1 \\ x_2 \end{vmatrix} + \frac{w_0}{Q} \begin{vmatrix} 1 \\ -1 \end{vmatrix} u \quad , \qquad y = \frac{1}{2} |1 \quad -1| \begin{vmatrix} x_1 \\ x_2 \end{vmatrix} \tag{1.46}$$

where w_0 is the center frequency, Q is the quality factor, $w_A = \sqrt{1-(1/2Q)^2}\,w_0$. Suppose the equation set above represents a high-frequency high-Q factor complex filter. Note that the state matrix has the same format as matrix A specified in eqn. (1.34): identical diagonal entries and opposite off-diagonal entries. It suggests that the state space transformation developed above could be applied to eqn. (1.46) to derive a system in the modulator-core filter-modulator architecture that is functionally equivalent to the target complex filter.

To find out a proper transformation matrix $M(t)$, we need to define a proper state matrix, $\hat{A}$, for the core filter in the derived system first. As the core filter is expected to have low center frequency and low Q factor so that the signal filtering does not have to take place in a high frequency band, it is natural to write $\hat{A}$ in the same format as A but with different entry values, as eqn. (1.47). Constructing $\hat{A}$ in this form also makes the implementation of the core filter straightforward, as will be shown in Chapter 3.

$$\hat{A} = \begin{vmatrix} -\frac{\widehat{w_0}}{2\hat{Q}} & -\widehat{w_A} \\ \widehat{w_A} & -\frac{\widehat{w_0}}{2\hat{Q}} \end{vmatrix}$$

where $\widehat{w_0}$ is the core filter center frequency, $\widehat{Q}$ is the core filter quality factor

$$\widehat{w_A} = \sqrt{1-(1/2\hat{Q})^2}\,\widehat{w_0} \tag{1.47}$$

As $\hat{A}$ corresponds to a lower-frequency lower-Q core filter, $\widehat{w_A} < w_A$ and $\hat{Q} < Q$. Assume the two filters have same bandwidth, then $\frac{\widehat{w_0}}{\hat{Q}} = \frac{w_0}{Q}$. Define $w_A - \widehat{w_A} = w_M$, the transformation matrix $M(t)$ is derived as:

$$M(t) = \begin{bmatrix} \cos(w_M t) & \sin(w_M t) \\ -\sin(w_M t) & \cos(w_M t) \end{bmatrix} = \Phi(w_M t) \quad (1.48)$$

According to eqn. (1.41a),

$$\hat{A} = M(t)AM^{-1}(t) + \dot{M}(t)M^{-1}(t) = \begin{vmatrix} -w_0/2Q & -w_A \\ w_A & -w_0/2Q \end{vmatrix} + \begin{vmatrix} 0 & w_M \\ -w_M & 0 \end{vmatrix}$$

$$= \begin{vmatrix} -w_0/2Q & -(w_A - w_M) \\ w_A - w_M & -w_0/2Q \end{vmatrix} \quad (1.49a)$$

$$\bar{g}(t) = M(t)\bar{b} = (w_0/Q) \begin{bmatrix} \cos(w_M t) & \sin(w_M t) \\ -\sin(w_M t) & \cos(w_M t) \end{bmatrix} \begin{vmatrix} 1 \\ -1 \end{vmatrix}$$

$$= (w_0/Q) \begin{vmatrix} \cos(w_M t) - \sin(w_M t) \\ -\sin(w_M t) - \cos(w_M t) \end{vmatrix} \quad (1.49b)$$

$$\bar{h}^T = \bar{c}^T M^{-1}(t) = \left(\frac{1}{2}\right) |1 \quad -1| \begin{bmatrix} \cos(w_M t) & -\sin(w_M t) \\ \sin(w_M t) & \cos(w_M t) \end{bmatrix}$$

$$= (1/2)|\cos(w_M t) - \sin(w_M t) \quad -\sin(w_M t) - \cos(w_M t)| \quad (1.49c)$$

Now, simplify $\bar{g}(t)$ and $\bar{h}^T$ and formulate the derived state-space equations in eqn. (1.50), where the phase offset of $\frac{3\pi}{4}$ could be removed without affecting the system performance.

$$\begin{vmatrix} \dot{w}_1 \\ \dot{w}_2 \end{vmatrix} = \begin{vmatrix} -\frac{\widehat{w_0}}{2\hat{Q}} & -(w_A - w_M) \\ w_A - w_M & -\frac{\widehat{w_0}}{2\hat{Q}} \end{vmatrix} \begin{vmatrix} w_1 \\ w_2 \end{vmatrix} + \sqrt{2}(w_0/Q) \begin{vmatrix} sin\left(w_M t + \frac{3\pi}{4}\right) \\ cos\left(w_M t + \frac{3\pi}{4}\right) \end{vmatrix} u$$

$$y = \sqrt{2} \left| sin\left(w_M t + \tfrac{3\pi}{4}\right) \quad cos\left(w_M t + \tfrac{3\pi}{4}\right) \right| \begin{vmatrix} w_1 \\ w_2 \end{vmatrix} \quad (1.50)$$

The physical meaning of the above equation set is obvious: the state matrix $\hat{A}$ specifies the core filter; vectors $\bar{g}(t)$ and $\bar{h}^T$, respectively, represent the front end and back end modulators with modulating frequency approximately equals to the difference of w_0 and

$\widehat{w_0}$. Because $M(t)$ is consistently non-singular, the state space transformation from eqn. (1.46) to eqn. (1.50) is linear, and the derived synchronous filtering system is functionally equivalent to the target high-frequency high-Q complex filter. Due to the introduction of both end modulators, the core filter works in a comparatively lower frequency range so the required quality factor and center frequency are accordingly scaled down, and the high frequency limitations of the active components have less influence on the core filter's performance.

In the system specified by eqn. (1.50), the modulating frequency w_M is lower than $\mathrm{w_A}$, so the front end modulation is subheterodyne. It has been proven in [11] that the front end modulation could also be superheterodyne. To develop the corresponding system model, matrix T was introduced to generate the transpose of $\hat{A}$.

$$T = \begin{bmatrix} 0 & 1 \\ 1 & 0 \end{bmatrix} \quad (1.51)$$

Note that this matrix has some interesting properties:

$$T^{-1} = T \ \ and \ \ T^{-1}T = TT^{-1} = I \quad (1.52)$$

Moreover,

$$T\hat{A}T = T\hat{A}T^{-1} + \dot{T}T^{-1} = \hat{A}^T \quad (1.53)$$

Suppose that $\hat{A}^T$ specifies the lower-Q lower-frequency core filter in the synchronous system, then

$$\hat{A}^T = \begin{vmatrix} -\widehat{\mathrm{w}_0}/2\hat{Q} & -\widehat{\mathrm{w}_\mathrm{A}} \\ \widehat{\mathrm{w}_\mathrm{A}} & -\widehat{\mathrm{w}_0}/2\hat{Q} \end{vmatrix} = \begin{vmatrix} -w_0/2\mathrm{Q} & (\mathrm{w_A} - w_M) \\ -(w_A - \mathrm{w_M}) & -w_0/2\mathrm{Q} \end{vmatrix} \rightarrow w_M = w_A + \widehat{w_A} \quad (1.54)$$

Therefore, modulating frequency w_M in the new system approximately equals the sum of the center frequencies of the target filter and the system's core filter, which suggests superheterodyne front end modulation in the resulting synchronous filter.

Define matrices and state variable vector that specify the superheterodyne-mode system as $\hat{A}_T$, $\overline{g_T}(t)$, $\overline{h_T}^T$ and $\bar{v}$ to distinguish from $\hat{A}$, $\bar{g}(t)$, $\bar{h}^T(t)$ and $\bar{w}$ in the subheterodyne-mode system. According to eqn. (1.53), the generic formulation for the former set could be easily derived from the latter, using the T in eqn. (1.51) as the transformation matrix. Specifically,

$$\hat{A}_T = \widehat{A}^T = T\widehat{A}T^{-1} + \dot{T}T^{-1},\ \overline{g_T}(t) = T\bar{g}(t),\ \overline{h_T}^T = \bar{h}^T(t)T^{-1} = \bar{h}^T(t)T,\ \bar{v} = \mathrm{T}\bar{w} \tag{1.55}$$

Substitute the expression for $\hat{A}$, $\bar{g}(t)$, $\bar{h}^T(t)$ given in eqn. (1.41a) to eqn. (1.41c):

$$\hat{A}_T = \begin{bmatrix} a_{11} & -(a_{12}+w_M) \\ (a_{12}+w_M) & a_{11} \end{bmatrix} \tag{1.56a}$$

$$\overline{g_T}(t) = \begin{bmatrix} 0 & 1 \\ 1 & 0 \end{bmatrix} \begin{vmatrix} cos(w_M t) & sin(w_M t) \\ -sin(w_M t) & cos(w_M t) \end{vmatrix} \begin{vmatrix} b_1 \\ b_2 \end{vmatrix} = b_0 \begin{vmatrix} cos(w_M t+\beta) \\ sin(w_M t+\beta) \end{vmatrix},$$

where $b_0 = \sqrt{{b_1}^2 + {b_2}^2}, \beta = tan^{-1}(\frac{b_1}{b_2})$. (1.56b)

$$\bar{h}^T = |c_1 \quad c_2| \begin{vmatrix} \cos(w_M t) & -\sin(w_M t) \\ \sin(w_M t) & \cos(w_M t) \end{vmatrix} \begin{bmatrix} 0 & 1 \\ 1 & 0 \end{bmatrix}$$

$$= c_0 |\cos(w_M t+\alpha) \quad \sin(w_M t+\alpha)|$$

where $c_0 = \sqrt{{c_1}^2 + {c_2}^2}, \alpha = tan^{-1}(c_1/c_2)$. (1.56c)

Referring to the state space representation of the target complex filter in eqn. (1.46), the state space model of the superheterodyne FM-mode synchronous complex filter is derived as eqn. (1.57), by replacing a_{11}, a_{12}, b_1, b_2, c_1, c_2 in eqn. (1.56a) to eqn. (1.56c) with $-w_0/2\mathrm{Q}$, $-\mathrm{w_A}$, 1, -1, 1, -1, respectively.

$$\begin{vmatrix}\dot{v}_1\\ \dot{v}_2\end{vmatrix} = \begin{vmatrix}-w_0/2\mathrm{Q} & -(w_M - \mathrm{w_A})\\ (w_M - \mathrm{w_A}) & -w_0/2\mathrm{Q}\end{vmatrix}\begin{vmatrix}v_1\\ v_2\end{vmatrix} + \sqrt{2}(\mathrm{w_0/Q})\begin{vmatrix}\cos\left(w_M t + \frac{3\pi}{4}\right)\\ \sin\left(w_M t + \frac{3\pi}{4}\right)\end{vmatrix} u \quad (1.57)$$

$$\mathrm{y} = \sqrt{2}\left|\cos\left(w_M t + \frac{3\pi}{4}\right) \quad \sin\left(w_M t + \frac{3\pi}{4}\right)\right|\begin{vmatrix}v_1\\ v_2\end{vmatrix}, \text{ where } w_M = w_A + \widehat{w_A}.$$

Similar to the subheterodyne system, the phase offset of $\frac{3\pi}{4}$ in the modulating signals could be removed without affecting the system performance.

1.3.2 AM Mode Synchronous Filtering

Consider a second-order system and its transformed version given in eqn. (1.58):

$$\dot{\mathrm{x}} = \mathrm{A}\bar{\mathrm{x}} + \mathrm{bu} \quad \rightarrow \quad \dot{\bar{w}} = \hat{A}\bar{w} + \bar{g}(t)u$$

$$\mathrm{y} = \bar{\mathrm{c}}^{\mathrm{T}}\bar{\mathrm{x}} + \mathrm{du} \quad \rightarrow \quad y = \bar{h}^{T}\bar{w} + du$$

where $\mathrm{A} = \begin{vmatrix}a_{11} & a_{12}\\ a_{21} & a_{22}\end{vmatrix}, \mathrm{b} = \begin{vmatrix}\mathrm{b}_1\\ \mathrm{b}_2\end{vmatrix}, \bar{\mathrm{c}}^{\mathrm{T}} = |c_1 \quad c_2|, \mathrm{d} = 0$ are all constant matrices and

$$\widehat{\mathrm{A}} = \mathrm{M(t)AM^{-1}(t)} + \dot{\mathrm{M}}(\mathrm{t})\mathrm{M^{-1}(t)},\ \bar{\mathrm{g}}(\mathrm{t}) = \mathrm{M(t)\bar{b}},\ \bar{\mathrm{h}}^{\mathrm{T}} = \bar{\mathrm{c}}^{\mathrm{T}}\mathrm{M^{-1}(t)} \quad (1.58)$$

With the transformation matrix in eqn. (1.59) [19], we derive $\widehat{\mathrm{A}}, \bar{\mathrm{g}}(\mathrm{t})$ and $\bar{\mathrm{h}}^{\mathrm{T}}$ as eqn. (1.60):

$$\mathrm{M(t)} = \begin{vmatrix}\mathrm{p}_1(\mathrm{t}) & 0\\ 0 & \mathrm{p}_2(\mathrm{t})\end{vmatrix},\ \mathrm{p_i(t)} \text{ is either always positive or always negative} \quad (1.59)$$

$$\widehat{\mathrm{A}} = \begin{vmatrix}a_{11} + \frac{\dot{p}_1(t)}{p_1(t)} & \frac{\mathrm{p}_1(\mathrm{t})}{\mathrm{p}_2(\mathrm{t})}a_{12}\\ \frac{\mathrm{p}_2(\mathrm{t})}{\mathrm{p}_1(\mathrm{t})}a_{21} & a_{22} + \frac{\dot{p}_2(t)}{p_2(t)}\end{vmatrix},\ \bar{\mathrm{g}}(\mathrm{t}) = \begin{vmatrix}p_1(\mathrm{t})\mathrm{b}_1\\ p_2(\mathrm{t})\mathrm{b}_2\end{vmatrix},\ \bar{\mathrm{h}}^{\mathrm{T}} = |c_1/p_1(\mathrm{t}) \quad c_2/p_2(\mathrm{t})| \quad (1.60)$$

When $p_1(\mathrm{t}) = p_2(\mathrm{t}) = \mathrm{p(t)}$, the above matrices are simplified as:

$$\widehat{\mathrm{A}} = \begin{vmatrix}a_{11} + \frac{\dot{p}(t)}{p(t)} & a_{12}\\ a_{21} & a_{22} + \frac{\dot{p}(t)}{p(t)}\end{vmatrix},\ \bar{\mathrm{g}}(\mathrm{t}) = p(t)\begin{vmatrix}\mathrm{b}_1\\ \mathrm{b}_2\end{vmatrix},\ \bar{\mathrm{h}}^{\mathrm{T}} = \frac{1}{p(t)}|c_1 \quad c_2| \quad (1.61)$$

In the resulting system, the front end stage modulates the input signal by $c_1 p_1(t), c_2 p_2(t)$; the modulation results are then fed through a time-varying core filter specified by $\widehat{\mathrm{A}}$; to draw the external equivalence between this system and the original time-invariant system, another block that scales the core filter output with $\frac{c_1}{p_1(\mathrm{t})}, \frac{c_2}{p_2(\mathrm{t})}$ has to be included. As the derived system performs amplitude modulation at both ends to match the time-varying properties of the core filter, it could be taken as an AM mode synchronous filter. Such a technique finds prevalent application in companding (compressing and expanding) systems to improve signal integrity[20, 21], which have been used for many years in transmission and audio magnetic recording[22, 23]. A companding system typically consists of compressing the dynamic range of a signal to be transmitted or recorded, before noise and/or distortion in the transmission or recording medium gets a chance to corrupt it. At the receiving or playback end, the dynamic range is expanded again, so the output SNR could get improved. The need for companding in signal processing and its merit is now briefly introduced as follows[19]. Suppose the output of an analog signal processor consists of three types of components: useful signal, noise (internally generated noise and external interference) and distortion (harmonics, intermodulation, etc.). Denote the rms value of the signal, the noise and the distortion with S, N and D respectively. For a linear system, S is proportional to the input rms value, N is independent of the input. For large enough input signals, nonlinearities of the system components would result in output distortion, and the output signal might not be proportional to the input anymore, as shown in Fig. 1.6(a). For demonstration simplicity, we utilize the ratio of signal to noise-plus-distortion in decibel, given by

Fig.1.6(b), to represent the system input dynamic range: denote the minimum acceptable $(\frac{S}{N+D})_{dB}$ with which the input signal could be successfully processed as $(\frac{S}{N+D})_{accept,dB}$, then the usable dynamic range of the input signals is the quantity shown as DR in the same figure.

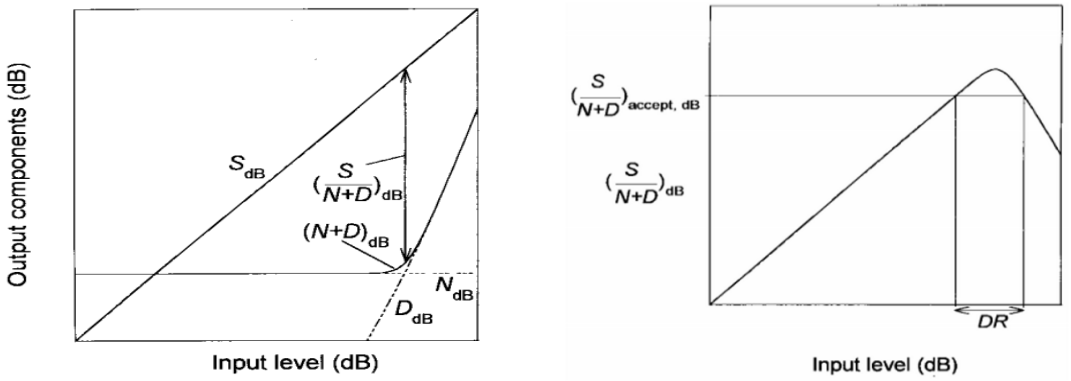

(a) (b)

Figure 1.6 (a) Three typical types of output components from a conventional signal processor: signal (S), noise (N), distortion (D), and noise-plus-distortion (N+D), represented as power in dB. (b) S/(N+D) in dB and the usable dynamic range (DR) for a specified minimum acceptable S/(N+D).

To widen the system's dynamic range, assuming the maximum signal level cannot be raised due to the limited supply voltage, then the noise floor should be reduced below the level shown in Fig. 1.6(a). This gives rise to the S/(N+D) curve in the solid line in Fig. 1.7, where the broken line is a replica of the curve in Fig. 1.6(b). Apparently, the new usable dynamic range is wider than the original one due to the lowered noise floor. However, lowering the noise floor usually causes some undesired issues for an integrated signal processor in practice. Take for instance a system where the main noise source of interest is thermal noise which is contributed by resistors or transconductors that along with some capacitors determine the critical frequencies of the filter. As the mean square value of the noise is inversely proportional to the total capacitance, large capacitances

should be used to keep the system noise low, which results in a much larger chip area. Moreover, as the associated transconductantors need to be scaled up by the same factor in order to maintain the system's original frequency response, the system dynamic power dissipation would increase by the same factor[24-26]. Note that the solid curve in Fig. 1.7 displays some amount of wasted value around its peak compared to the broken-line curve, which is resulted from the lowered system noise floor.

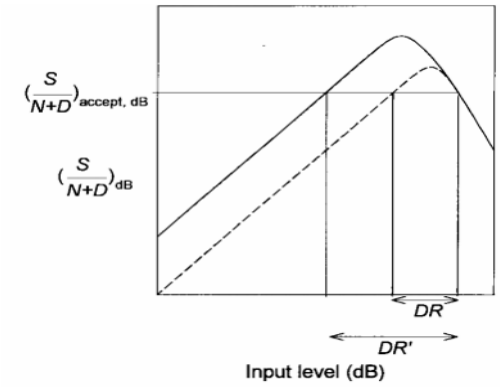

Figure 1.7 Solid line: the raised $\frac{S}{N+D}$ by lowering the system noise floor; broken line: the original system $\frac{S}{N+D}$. The dynamic range gets widened from DR to DR'.

The companding technique greatly relaxes the above limitations by operating on the dynamic range in a way shown in Fig. 1.8(a), where the center portion represents the level of the signal at a point inside the signal processor. It is also assumed that the noise generated in the processor itself is much higher than the input noise and is the dominant noise source, which is a very practical assumption for a high-Q design[27-29]. As the overload level inside a signal processor can be lower than the external overload level in some designs, the companded input signal leads to a flattened S/(N+D) curve, shown by the solid line in Fig. 1.8(b). The corresponding dynamic range, DR" is much larger than the original dynamic range DR; compared to the solid curve in Fig. 1.7 which is achieved

by lowering the system noise level, the S/(N+D) curve resulted by companding has lower peak value while yields a greatly enlarged usable dynamic range.

The input/output signal and its companded version could either be of the same type (e.g., both are voltage signals) or of different types. An interesting and popular application of the latter case is some current-mode companding filtering systems, where the input and output signals are current, while the core filter processes voltages signals across its capacitors. In these systems, the overload levels of input/output signals are not directly related to the supply-imposed voltage limitations, and the input/output dynamic ranges can be very different from what's attainable within the filter. Fig. 1.8 depicts the distinction between the original signal and its companded versions, as well as the associated dynamic range. When the companding technique is applied to a filtering system, the core filter's signal levels may be no longer proportional to the input, so the system is internally nonlinear, however, its overall input-output behavior remains linear if the system is implemented with appropriately synchronized circuits. Companding is accomplished by monitoring signal(s), either inside or outside the signal processor, and then accordingly modifying some gain-related quantities. Based on the gain controlling signals utilized, there are two main types of companding systems: instantaneous and syllabic. If the value of the gain-related quantities depends only on the value of signals in the signal path at the same instant, the companding action is called instantaneous. If a measure of the average strength of a signal, such as its rms value or envelope, is used as a gain control, then the resulting companding is syllabic. Syllabic companding was first used in speech transmission[20, 21], and it also finds application in audio recording and reproduction[22, 23]. It typically relies on an appropriately designed dynamical system

to evaluate the control signal's average strength and adjust the specific gain to compand related signals in the system.

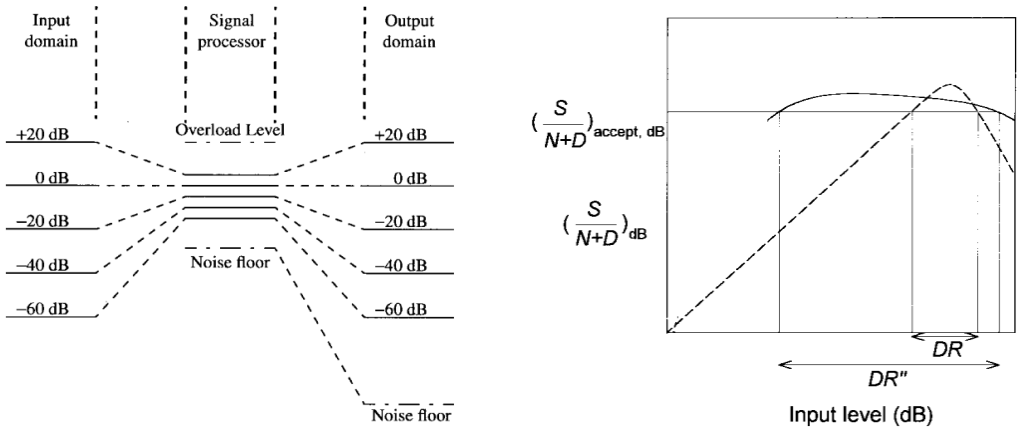

(a) (b)

Figure 1.8 (a) Schematic representation of companding. (b) Solid line: S/(N+D) curve of a companding system, broken line: S/(N+D) curve without companding.

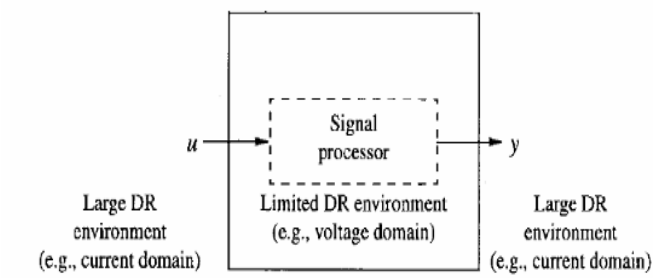

Figure 1.9 A companding system with the core signal processor being internally voltage-limited while having current signals as input and output. Typically, the system has an external dynamic range much larger than the dynamic range of the signal processor.

1.3.3 Combinational Synchronous Filtering

The framework of synchronous filtering systems allows us to go beyond what has already been developed[11]. Another transformation matrix, $M_{new}(t)$, is now defined as the product of $M(t)$ and a time-varying scalar, $p(t)$.

$$M_{new}(t) = p(t)M(t) = p(t)\Phi(w_M t + \theta_K) \quad (1.62)$$

where $p(t)$ has to be a strictly positive time function to guarantee $M_{new}(t)$ is nonsingular. Transforming the state matrix with the $M_{new}(t)$, we have

$$\begin{aligned}\hat{A}_{new}(t) &= p(t)M(t)AM^{-1}(t)\frac{1}{p(t)} + \frac{d}{dt}[p(t)M(t)]M^{-1}(t)\frac{1}{p(t)} \\ &= M(t)AM^{-1} + [\dot{p}(t)M(t) + p(t)\dot{M}(t)]M^{-1}(t)\frac{1}{p(t)} \\ &= M(t)AM^{-1} + \dot{M}(t)M^{-1}(t) + \frac{\dot{p}(t)}{p(t)}I \\ &= \hat{A} + \frac{\dot{p}(t)}{p(t)}I \end{aligned} \quad (1.63)$$

The complete system is now represented as:

$$\frac{d}{dt}\bar{w}_{new} = \hat{A}_{new}(t)\bar{w}_{new} + G_{new}(t)\bar{u} \quad (1.64)$$

$$y = H_{new}(t)\bar{w}_{new} + D\bar{u}$$

where $G_{new}(t) = p(t)G(t),\ H_{new}(t) = \frac{1}{p(t)}H(t),\ \bar{w}_{new} = p(t)\bar{w}.$

The system specified by eqn. (1.64) actually adds to the FM-mode synchronous filter a network that performs signal companding, represented by $p(t)$ in $G_{new}(t)$ and $\frac{1}{p(t)}$ in $H_{new}(t)$. So the front end and back end stages of the system perform both amplitude modulation and frequency modulation. In practice, $p(t)$ could be adjusted continuously to implement some automatic gain control that helps maximize the system's dynamic range. It has been reported in literature[30, 31] that one issue about the time-varying gain is that it might change the system signals and produce distortion when the core filtering block is involved in the companding process. Inspection reveals that the introduced time-varying diagonal terms in the state matrix, $\frac{\dot{p}(t)}{p(t)}$, amount to a time-varying Q factor of the system core filter. Electronically tuning the Q factor in most integrated filters is relatively easy, so this change does not pose a challenging implementation problem. The benefits resulting from the companding nature of the system will almost certainly

outweigh the cost of the increased circuit complexity. A conceptual representation of a companding synchronous filtering system is given in Fig. 1.10.

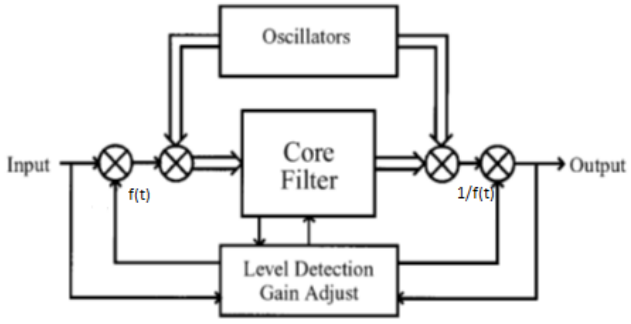

Figure 1.10 Block diagram for a companding synchronous filter system.

Taking the above second-order subheterodyne synchronous filter for instance, the specific expression of the matrices for the new model is derived as below:

$$\hat{A}_{new}(t) = \begin{vmatrix} -\frac{w_0}{2Q} + \frac{\dot{p}(t)}{p(t)} & -(w_A - w_M) \\ (w_A - w_M) & -\frac{w_0}{2Q} + \frac{\dot{p}(t)}{p(t)} \end{vmatrix} \quad (1.65a)$$

$$\bar{g}_{new}(t) = b_0 p(t) \begin{vmatrix} \sin(w_M t + \theta_K + \beta) \\ \cos(w_M t + \theta_K + \beta) \end{vmatrix}$$

where $b_0 = \sqrt{{b_1}^2 + {b_2}^2}$, $\beta = tan^{-1}(b_1/b_2)$; (1.65b)

$$\bar{h}^T_{new}(t) = c_0 \frac{1}{p(t)} |\sin(w_M t + \theta_K + \alpha) \quad \cos(w_M t + \theta_K + \alpha)|$$

where $c_0 = \sqrt{{c_1}^2 + {c_2}^2}$, $\alpha = tan^{-1}(c_1/c_2)$. (1.65c)

1.4 Overview of this Dissertation

In Chapter 1 we have given a brief introduction to the architecture and mathematical model of a few synchronous filtering systems. The objective of our research is to search for effective approaches or architectures related to synchronous filtering to improve the noise performance of analog filters. The subjects of our research

are a biquad bandpass filter and a biquad complex filter, the state space descriptions of which are given by eqn. (1.30) and eqn. (1.46) respectively.

In Chapter 2, log-domain filters and a particular technique to design log filters are introduced. A log-domain biquad bandpass filter is then designed and tested, based on which an AM mode synchronous bandpass filter is proposed and modified. The ideally modified filter, according to mathematical analysis, has superior capability in suppressing the input noise while maintaining the useful input components. It leads to the creation of a feedback filtering system capable of producing signals very similar to what is produced by the ideally modified filter under certain circumstances. What is more important, the feedback system provides a foundation for the development of a novel high noise performance feedback filter with tunable Q factor as will be articulated in Chapter 5.

Chapter 3 discusses a log-domain biquad complex filter and related synchronous filtering systems. Following a detailed implementation process, we verify the input-output function of the resulting FM mode static synchronous complex filter. We then transform it into a dynamic synchronous system with time-varying core filter center frequency and modulating frequencies. Two specific patterns for the center frequency variation are introduced and tested, to show that the overall dynamic system externally maintains the function of a standard complex filter.

In Chapter 4, after a brief review on the developed systems in previous chapters, we test their performance in dealing with the input noise and the injected in-filter noise, to explore approaches or architectures that might lead to the design of a filter with improved noise performance.

Inspired by some discoveries made in Chapter 4, we devised a novel method of utilizing feedback signals to tune the Q factor of a bandpass filter, which could be used to alter a low-Q bandpass filter into a much sharper one that has superior immunity to the in-filter noise. Mathematical analysis is provided to explain the Q-factor tuning mechanism. In Chapter 5, we detail the development of such a feedback filter, test its function and noise performance, and give a transistor-level design solution for a log-domain feedback complex filtering system. Important research discoveries are summarized in Chapter 6, followed by suggestions regarding future work that could be done.

Chapter 2 AM mode-synchronous-filtering Related Bandpass Filters

This chapter focuses on the transistor-level realization of an AM mode synchronous bandpass filter. A particular class of circuits known as log-domain filters are introduced first, as their unique features make them a good implementation solution for synchronous filters. A classic realization technique is then articulated, followed by a specific design case of applying the synchronous filtering approach to a biquad log-domain bandpass filter. Moreover, a feedback filtering system will be derived from the resulting synchronous filter.

2.1 Introduction to Log-domain Filters

The idea of 'log-domain filtering' was initially proposed by Adams in 1979[32]. It was motivated by the need from electronic music applications for filters that have tunable gain and cut-off or center frequency, wider tuning range and lower signal distortion. Adams claimed that a linear transfer function could be implemented by an internally nonlinear system with properly designed log-domain circuits. In general, a log filter takes a current signal as input and converts it into a voltage signal, which is its natural logarithm version, for the following processing. The processed voltage signal will be converted back into current signal so that the final output is a linearly filtered version of input. Adams' log-filter is illustrated in Fig. 2.1 and could be divided into three parts: front end, back end converting circuit and the filtering stage. Assuming ideal components are used in the filter implementation, we formulate the following equations:

$$V_i = \frac{1}{k}\ln\left(\frac{I_{in}}{I_s}\right), \quad C\frac{dV_C}{dt} = I_c = I_s e^{k(V_i - V_c)} - I_0, \quad I_{out} = I_s e^{k(V_C + V_{D_3})} = I_0 e^{kV_C} \quad (2.1)$$

where I_s is the reverse bias saturation current of an ideal diode,and k is the inverse of thermal voltage V_t of a PN junction. Based on the equations above, I_{out} and I_{in} are correlated:

$$\frac{dI_{out}}{dt} + \frac{kI_0}{C} I_{out} = \frac{kI_0}{C} I_{in} \qquad (2.2)$$

Eqn. (2.2) indicates that the system in Fig. 2.1 is a one-pole low-pass filter with unity low-frequency gain and a cutoff frequency of $w_0 = kI_0/C$. The transfer function is derived as:

$$Y(s) = \frac{I_{out}(s)}{I_{in}(s)} = \frac{w_0}{S+w_0} \qquad (2.3)$$

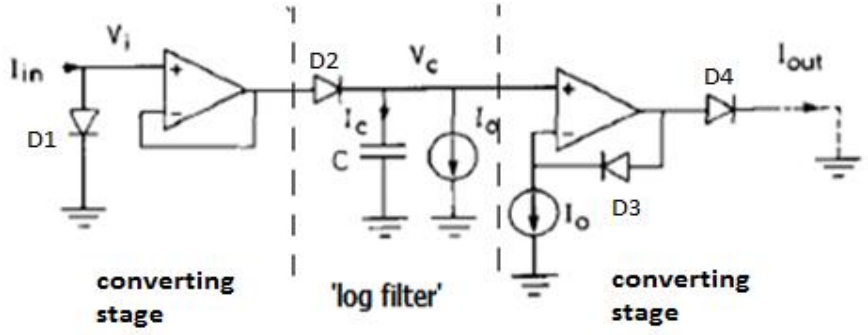

Figure 2.1 Adam's basic log-domain filter.

Another perspective on the 'log-filter' is to picture the input as an ac signal riding on a constant DC current I_0. In this sense, diode D_2 contributes a resistance equal to the dynamic impedance of a diode with I_0 flowing in it. Then the log-filter is equivalent to a first-order RC filter with $R = V_t/I_0$ and the cutoff frequency $w_0 = I_0/V_tC$. Adams therefore suggested that any active RC filter should have a log-domain counterpart where all the original resistors are replaced with an appropriate network of diodes and current sources.

Features of a log-domain filter include convenient tunability, accurate wide tuning range and current operational mode. In Adams' low pass filter, the cutoff frequency is proportional to dc current I_0, so it could be tuned with great ease by simply adjusting the magnitude of the current source. The relation between I_0 and w_0 is claimed to hold accurate over a range wider than three decades for I_0 in the literature [32]. On the other hand, since the log filter incorporates an electrical network designed upon the constitutive law for a forward-biased diode and Kirchhoff's current law (KCL), it's categorized as a current-mode filter. Therefore, it provides a potential solution to the high frequency limitation of many voltage-mode filters. A major shortcoming of Adams' design is the use of op-amps in signal processing such as logging, level shifting and exponentiation. Due to non-idealities of the op-amps, such as input offset voltage, bias current, input noise, etc., the filter would face serious performance degradation in practice. Another drawback of the design approach proposed by Adams is that it yields distortion when applied to the realization of filters of second or higher order. The defect manifests itself as some unwanted term(s) in the differential equation that specifies the implemented filter.

2.2 Implementation Technique

Inspired by Adam's log-domain filtering idea, Frey proposed in 1993[33] a distortionless synthesis procedure which provides an elegant guideline for the generation of many modern filter topologies. The technique uses a particular state-space representation derived from the system transfer function. After applying an exponential mapping and giving physical meaning for the state variables, the dynamical equations become explicitly implementable as each term is associated with some parameter in an

electrical network. To make this point clearer, the specific mathematical operation and a design example related to the synthesis technique will be introduced. Start with the generic dynamical equations:

$$\dot{\bar{x}} = A\,\bar{x} + bu, \qquad y = \bar{c}^{T}\bar{x} + du \tag{2.4}$$

where $\bar{x} = (x_1, x_2, \ldots, x_n)^T$ is the state vector, u is the input scalar and y the output scalar; A is an $n \times n$ matrix, b is an $n \times 1$ vector, $\bar{c}^T$ is a $1 \times n$ vector, and d is a scalar. Next, define the change of variables using exponential mapping:

$$x_i = e^{kV_i} \;\; , \; u = I_{dc}e^{kV_0} \tag{2.5}$$

where k is a positive real number, V_i is a nodal voltage associated with the state variable x_i, and I_{dc} is the value for a nominal dc current. Substitute the specific expression of $\bar{x}$ and u back into the state equation, then multiply both sides with $(C_i/k)e^{-kV_i}$:

$$C_i \frac{dV_i}{dt} = \left[\sum_{j=1}^{n} \frac{C_i}{k} A_{ij} e^{k(V_j - V_i)}\right] + \frac{C_i}{k} b_i I_{dc} e^{k(V_0 - V_i)}$$

$$= \left[\sum_{j=1}^{n} I_{aij}\, e^{k(V_j - V_i)}\right] + \; I_{bi} e^{k(V_0 - V_i)} \tag{2.6}$$

where $1 \leq i \leq n$, constants C_i are arbitrary, A_{ij} denotes the entry in the i^{th} row and the j^{th} column of matrix A,b_i is the i^{th} element of vector b, $I_{aij} = \frac{C_i}{k} A_{ij}$, $I_{bi} = \frac{C_i}{k} b_i I_{dc}$. The physical meaning of the above equation set is explicit if we take it as a series of nodal equations associated with the electrical parameters in a circuit. Defining V_i as the i^{th} node voltage, the left-hand side could be interpreted as the current flowing into a capacitor C_i, which has one end grounded and the other tied to the i^{th} node. This current is contributed by the variation of the capacitor variation. The right-hand side could be taken as the sum of currents entering or leaving the same capacitor, contributed by

surrounding circuitry. Using the same mapping method, the system input-output equation is rewritten as:

$$Y = (\sum_{i=1}^{n} \bar{c}_i e^{kV_i}) + dI_{dc} e^{kV_0} \quad (2.7)$$

where $\bar{c}_i$ denotes the i^{th} element in $\bar{c}^T$. Due to the introduced exponential mapping, it is now possible to implement a log filter with much less effort, using only current sources, capacitors and BJTs in active region or MOSFETs in subthreshold region.

Take the implementation of a first-order, unity gain lowpass filter which is specified by the transfer function below for instance:

$$H(s) = \frac{w_0}{s+w_0} \quad (2.8)$$

A possible set of dynamical equations that corresponds the transfer function is:

$$\dot{X} = -w_0 X + w_0 U, \qquad Y = X \quad (2.9)$$

where X is the state-variable, U is the input signal, Y is the system output and w_0 is the cutoff frequency of the filter. Apply the exponential mapping and define

$$X = I_s \, exp\left(\frac{V_1}{V_T}\right) = Y \, , \quad U = I_s \, exp\left(\frac{V_0}{V_T}\right) \quad (2.10)$$

Note in eqn. (2.9) the input vector U is strictly positive, which indicates that the input current has to be appropriately offset for the system to work as expected. Substitute the definition in eqn. (2.10) into the dynamical equations and multiply both sides with $\frac{V_T C}{X}$:

$$C\dot{V_T} = -w_0 C V_T + w_0 C V_T \, exp\left(\frac{V_0 - V_1}{V_T}\right) = -I_0 + I_s \, exp\left(\frac{V_{dc} + V_0 - V_1}{V_T}\right) \quad (2.11)$$

where $I_0 = w_0 C V_T$, $V_{dc} = V_T \ln(\frac{I_0}{I_s})$. At this point, the system dynamical equations have been transformed into a form which is very straightforward to implement. Fig. 2.2 shows the resulting log filter. An unobvious issue in the design is the necessity of forcing a

proper operating point for the system so that small signals get processed as expected and the dc component in the output is predictable. In this case, the solution is to set the bias current of Q2 to be I_0. By doing this, the dc level of the output should be the same as that of the input signal.

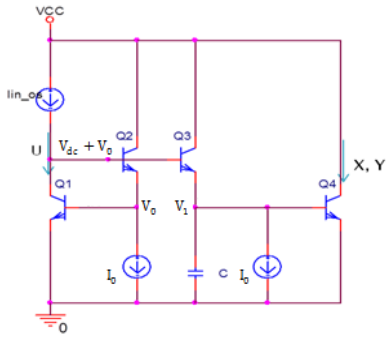

Figure 2.2 A first-order low pass log filter with cutoff frequency $w_0 = I_0/CV_T$.

Simulation was run in PSpice for design verification. As a prototype design, ideal components are used and the transistors are with β=10k so their base current is negligible. The particular filter designed is expected to have a cutoff frequency at 1kHz. Other related parameters are set up accordingly as: $I_0 = 500uA, C = 3.084uF$. Test results are shown below. The Bode plot verifies the filter's low-frequency unity gain, cutoff frequency and roll-off slope rate. In the transient test, the input signal is a sine wave current: $I_{in\_os} = 500uA + 400uA \cdot \sin(2\pi \cdot 1000t)$. No distortion is observed in the output waveform at steady state, and the amplitude and phase change matches what is specified by the transfer function of a first-order low pass filter.

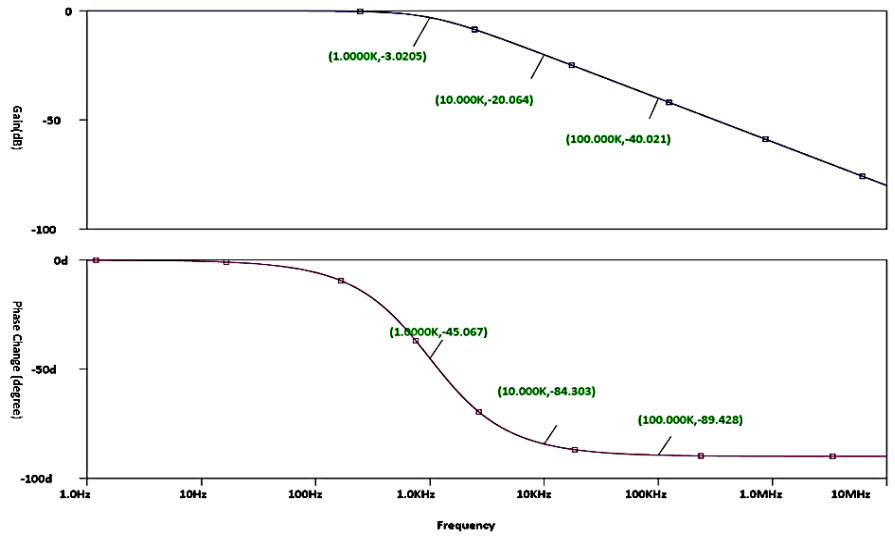

Figure 2.3 Bode plot of the log filter in Fig. 2.2.

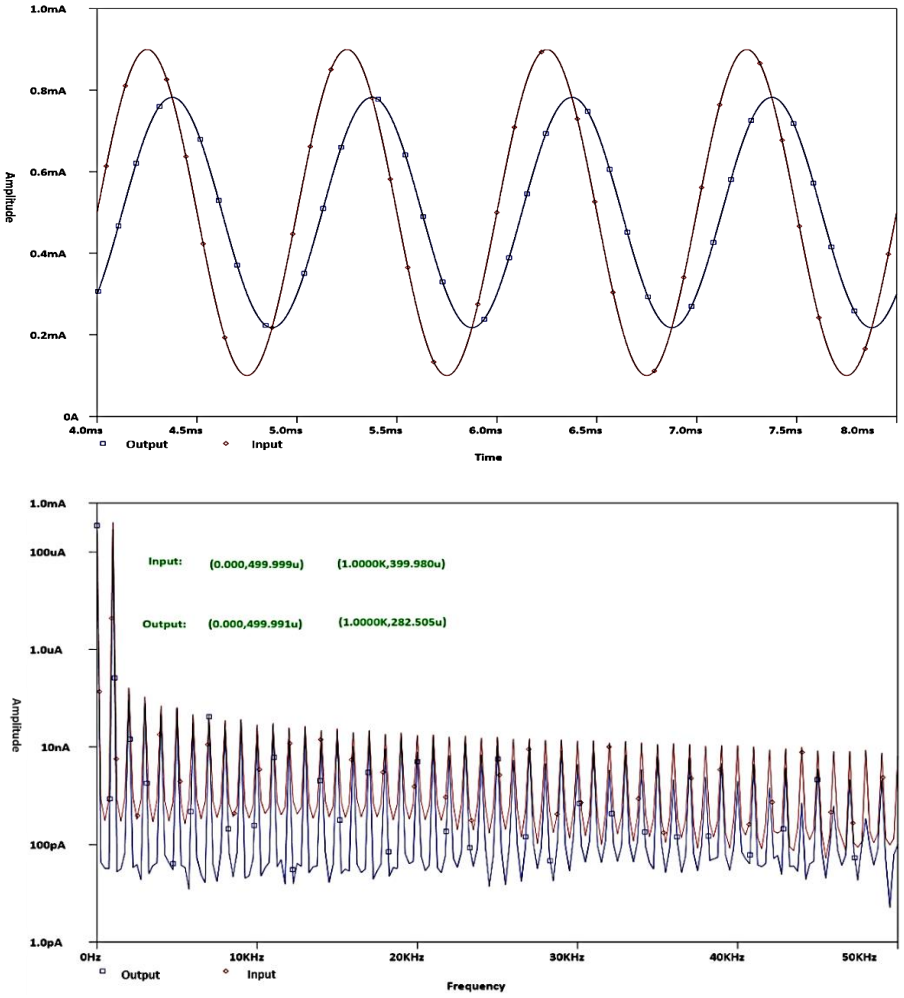

Figure 2.4 Input and output signals from the transient test. Upper graph: time-domain plots. Lower graph: Corresponding FFT spectra.

2.3 A Biquad Log-domain Bandpass Filter

2.3.1 Circuit Realization

As has been mentioned in Chapter 1, the state-space equation set below implements the transfer function of a standard second-order bandpass filter given by eqn. (2.13).

$$\begin{vmatrix} \dot{x_1} \\ \dot{x_2} \end{vmatrix} = \begin{vmatrix} -\frac{w_0}{Q} & -w_0 \\ w_0 & 0 \end{vmatrix} \begin{vmatrix} x_1 \\ x_2 \end{vmatrix} + \begin{vmatrix} \frac{w_0}{Q} \\ 0 \end{vmatrix} u \,,\; y = |1 \quad 0| \begin{vmatrix} x_1 \\ x_2 \end{vmatrix} \tag{2.12}$$

$$H(s) = \frac{Y(s)}{U(s)} = \frac{\frac{w_0}{Q}s}{s^2 + \frac{w_0}{Q}s + {w_0}^2} \tag{2.13}$$

where w_0 is the center frequency, $\sigma = \frac{w_0}{Q}$, and Q is the quality factor. According to the synthesis technique, an exponential mapping is first applied to the state equation set to transform it into a new form which is explicitly associated with a BJT transistor-level electrical network. Define the state variables as:

$$x_1 = I_s\, exp\left(\frac{v_1 - v_{I_{fc}}}{v_t}\right) = y_1\,, \quad x_2 = I_s\, exp\left(\frac{v_2}{v_t}\right) \tag{2.14}$$

where v_1 is a voltage of two-diode drop while v_2 is a one-diode drop voltage, $v_{I_{dc}}$ represents the base-emitter voltage of a BJT carrying dc current I_{dc}. The state equations are correspondingly transformed into:

$$C\dot{v}_1 = -\frac{I_{fc}}{Q} - I_s \exp\left(\frac{v_2 + v_{I_{fc}} + v_{I_{dc}} - v_1}{v_t}\right) + I_s \exp\left(\frac{v_{M_1} + v_{I_Q} - v_1}{v_t}\right) \tag{2.15}$$

$$C\dot{v}_2 = I_s \exp\left(\frac{v_1 - v_{I_{fc}} + v_{I_{fc}} - v_2}{v_t}\right) \tag{2.16}$$

Related current and voltage notations are explained below:

$$I_{fc} = w_0 C v_t,\; I_Q = \frac{I_{fc}}{Q},$$

$$v_{I_{fc}} = v_t l\, n\left(\frac{I_{fc}}{I_s}\right) = v_{I_{dc}} = v_t l\, n\left(\frac{I_{dc}}{I_s}\right), v_{M_1} = v_t\, ln\left(\frac{u_{M1}}{I_s}\right) + v_t\, ln\left(\frac{I_{fc}}{I_s}\right), v_{I_Q} = v_t\, ln\left(\frac{I_Q}{I_s}\right).$$

Physical meaning of the yielded equations is obvious. For both equations, the left hand side represents a current flowing into a capacitor which is contributed by the variation of the voltage across the capacitor, and the right hand side terms are current flows generated by surrounding circuitry to balance out the current on the left hand side. Fig. 2.5 shows a possible circuit realization of the filter which incorporates two interacting capacitors. The input to the circuit, I_{in_os}, is a current with offset I_{dc}. The circuitry in the broken-line box implements a negative transconductance with a translinear loop. The operating point of each capacitor voltage is forced by circuitry enclosed by the solid line. Specifically, $V_{c\_left} = v_{I_{fc}} + v_{I_{dc}}$, $V_{c\_right} = v_{I_{dc}}$. The collector currents labeled as Y_BPF and Y_LPF are possible circuit outputs: the former provides a band-pass filtered version and the latter is a low-pass filtered version of the input current. This result could be derived from the state-space representation of eqn. (2.12):

$$\frac{X_2(s)}{U(s)} = \frac{w_0}{S} H(s) = \frac{\frac{{w_0}^2}{Q}}{s^2 + \frac{w_0}{Q}s + {w_0}^2} \qquad (2.17)$$

The design in Fig. 2.5 could be modified into another bandpass filter whose peak gain is proportional to the quality factor. As shown in Fig. 2.6, the new circuit has a much simpler schematic. Since no circuitry is designed to balance I_Q for the left capacitor, it is required I_Q to be much smaller than I_{fc}, which indicates that the bandpass filter needs to be set with a high Q to avoid performance degradation. On the other hand, because the filter's mid-band gain is proportional to Q, the amplitude of input current needs to be adjusted properly to ensure a distortionless output. The transfer functions realized by

the circuit are given by eqn.(2.18). Different from the bandpass filtered output, the low-pass filtering output has a unity passband gain that is independent of Q. Both filters in Fig. 2.5 and Fig. 2.6 are electronically tunable: varying the amplitude of current sources labeled with Ifc or IQ, we can easily adjust the filter's center frequency or quality factor.

$$H_1(s) = \frac{Ybp(s)}{U(s)} = \frac{w_0 s}{s^2 + \frac{w_0}{Q}s + {w_0}^2} \qquad H_2(s) = \frac{Ylp(s)}{U(s)} = \frac{{w_0}^2}{s^2 + \frac{w_0}{Q}s + {w_0}^2} \qquad (2.18)$$

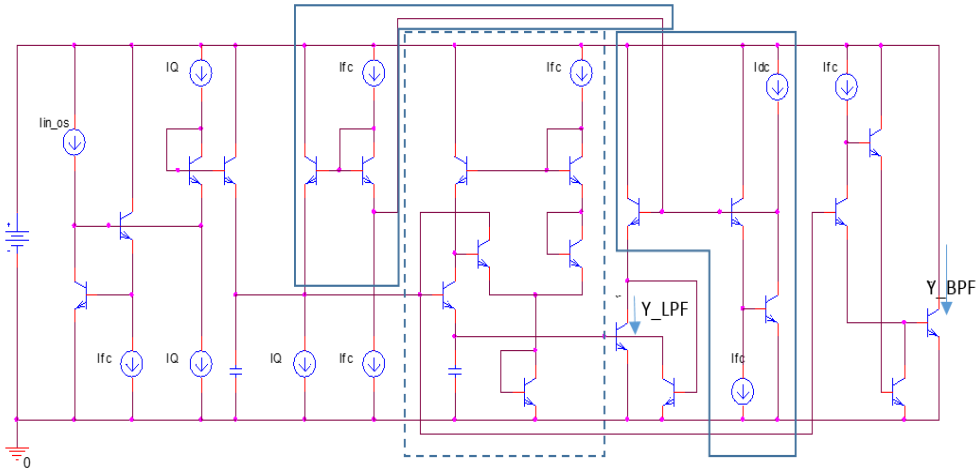

Figure 2.5 A unity gain, electronically tunable second-order log-domain bandpass filter.

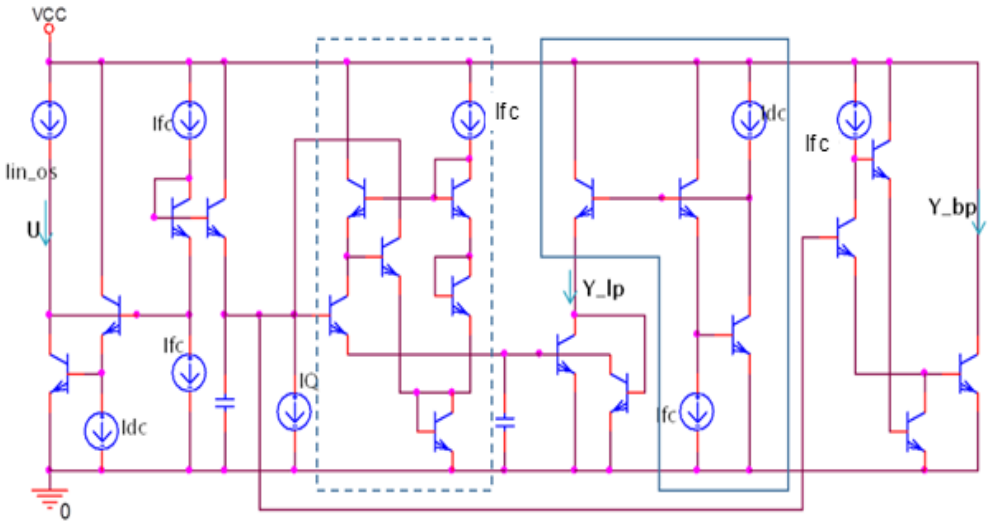

Figure 2.6 A non-unity gain, electronically tunable second-order log-domain bandpass filter.

2.3.2 Simulation Results

Both ac test and transient test are run under PSpice to verify the function and performance of our design. The purpose of the ac test was to generate the system's Bode plot and verify the filter's tunability, and the transient test was mainly for checking out the integrity of output current signals. Ideal sources and capacitors were used in the design. Unless otherwise mentioned, all the NPN transistors take the QbreakN model (in Cadence) with β_f set to 10k. Other parameters are: $I_{dc} = 0.5mA, C = 3.076nF$.

ac test

According to the design technique, I_{fc} is proportional to the bandpass filter center frequency. Therefore, adjusting current sources "I_{fc}" easily tunes the center frequency. Also, the Q factor is determined by the ratio of I_{fc} to I_Q, so if I_Q stays the same while I_{fc} is tuned, both the center frequency and the Q factor will be scaled by the same factor and the filter bandwidth would remain unchanged. On the other hand, if I_{fc} is fixed and I_Q is tuned, then the center frequency will remain the same while the Q factor and the bandwidth will be scaled together. The above expected properties need to be verified by Bode plots and related measurement data from the ac test. The lowpass filtering function of the filter can be verified with Bode plot too.

1. Tests on the unity-gain filter in Fig. 2.5

1) Center frequency tunability

Setup

Input: ac=1, dc offset $= 500$u. Output: $\mathrm{I_{out}} =$ Y_BPF

Current sources setup: IQ=10u, Ifc sweeping: 320u, 410u, 500u, 660u, 720u

Simulation Results

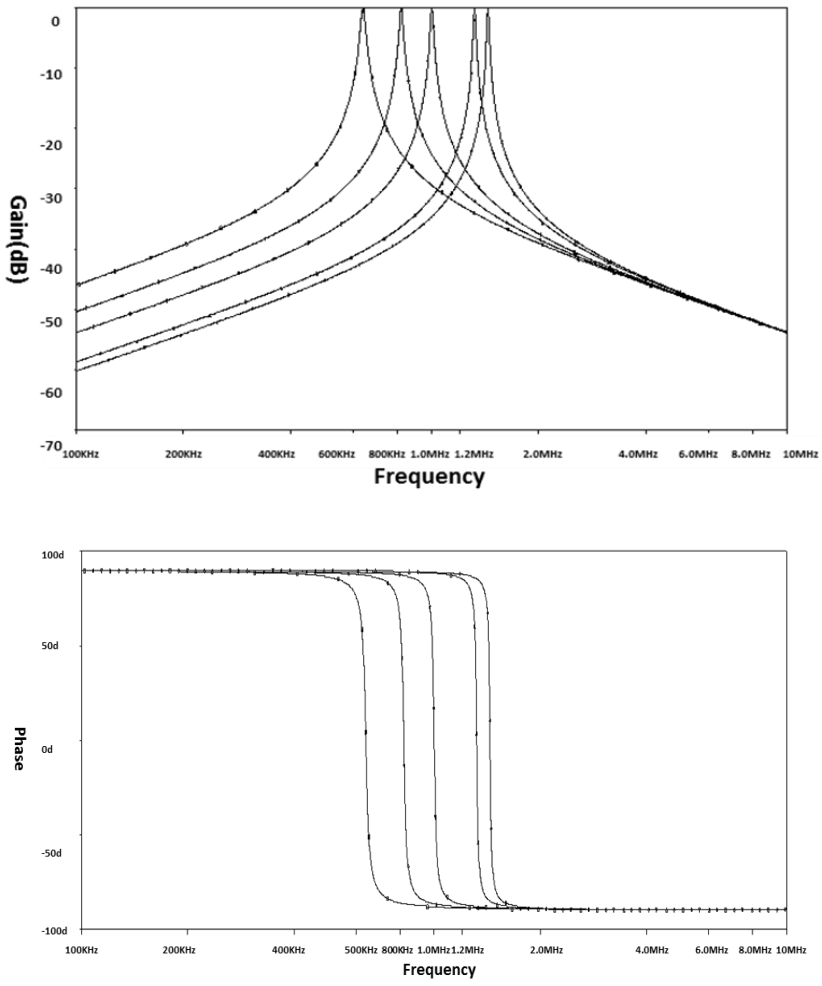

Figure 2.7 Bode plots of the bandpass filter in Fig. 2.5 under the center frequency tunability test.

Test Setup	Ifc (A)	320u	410u	500u	660u	720u
	IQ (A)	10u	10u	10u	10u	10u
Test Results	Center Frequency (Hz)	**640.143k**	**820.183k**	**1.000M**	**1.320M**	**1.440M**
	Quality Factor	**32.026**	**41.025**	**50.029**	**65.988**	**71.972**
	Bandwidth (Hz)	**19.987k**	**19.992k**	**19.997k**	**20.007k**	**20.012k**
	Peak Gain (dB)	-0.013	-0.015	-0.017	-0.022	-0.024
	Phase Angle Zero Cross (Hz)	640.143k	820.183k	1000.440k	1320.290k	1440.330k

Table 2-1 Measurement data from the center frequency tunability test on the filter in Fig. 2.5.

Observation

Varying I_{fc} and keeping the I_Q scales the center frequency and Q factor of the bandpass filter simultaneously with the same factor, while the bandwidth is almost unaffected. The peak gain of this filter is unity and is barely influenced by the tuning of I_{fc}. In each test case, the phase change starts to drop from 90 degrees as the input frequency increases, approximately hitting 0 when the input frequency equals the filter's center frequency and asymptotically approaches -90 degrees as the input frequency becomes extremely high.

2) Quality factor tunability

Setup

Input: ac=1, dc offset $= 500$u.

Current sources setup: Ifc =500u, IQ sweeping: 2u, 5u, 10u, 20u, 50u.

Simulation Results

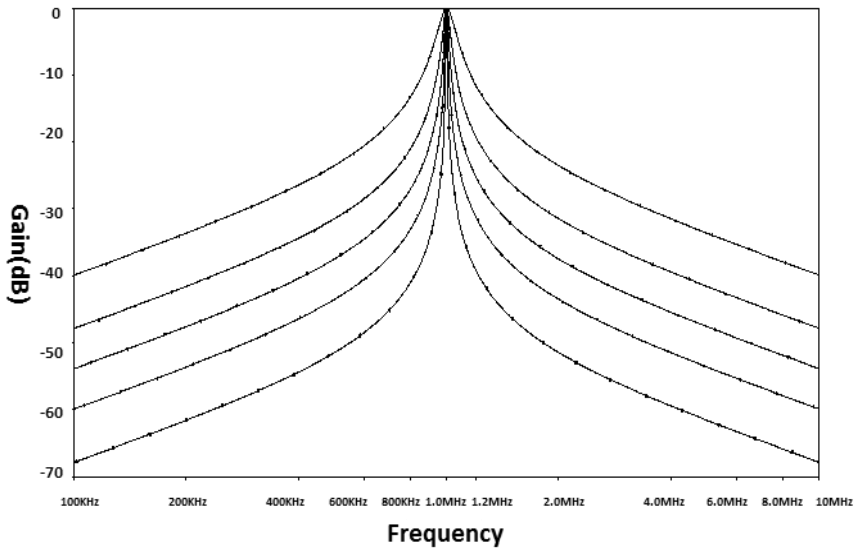

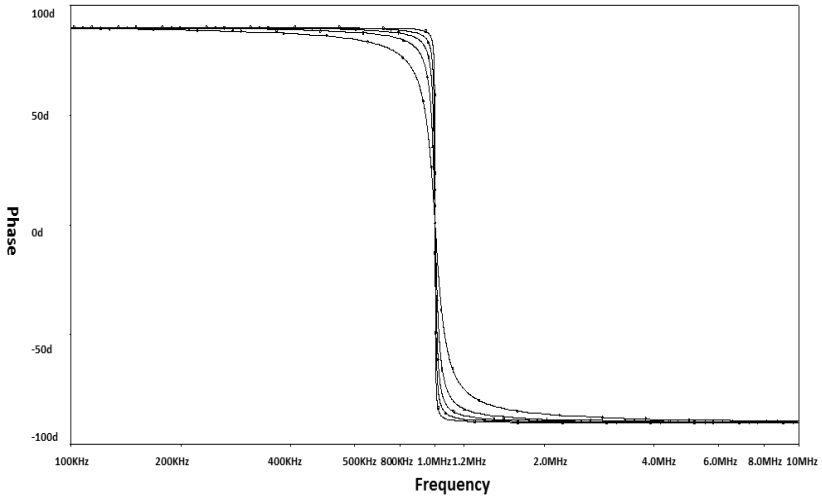

Figure 2.8 Bode plots of the bandpass filter in Fig. 2.5 under the Q factor tunability test.

Test Setup	Ifc (A)	500u	500u	500u	500u	500u
	IQ (A)	2u	5u	10u	20u	50u
Test Results	Center Frequency (Hz)	**1.000M**	**1.000M**	**1.000M**	**1.000M**	**1.000M**
	Quality Factor	**248.085**	**99.832**	**49.973**	**25.012**	**10.019**
	Bandwidth (Hz)	**4.031k**	**10.019k**	**20.015k**	**39.989k**	**99.830k**
	Peak Gain (dB)	-0.087	-0.035	-0.017	-0.009	-0.003
	Phase Angle Zero Cross (Hz)	1000.220k	1000.220k	1000.220k	1000.220k	1000.220k

Table 2-2 Measurement data from the Q factor tunability test on the filter in Fig. 2.5.

Observation

Varying I_Q while keeping the value of I_{fc} changes the quality factor and bandwidth of the filter, but the center frequency is almost unaffected. Also, the peak gain of this filter is barely affected during the tuning of quality factor. Comparing the measured Q factors to the target values, it's discovered that the tuning for a higher Q is less accurate, which might because it requires a very low I_Q current. But even in the tuning for Q=250, the error is measured to be smaller than 1%. The phase spectrum again verifies that the filter center frequency does not change during the tuning of I_Q, as long

as I_{fc} is fixed. The test results from 1) and 2) suggest that I_{fc} and I_Q can be adjusted together to set up the bandpass filter with any random combination of fc and Q within certain range.

3) Low-pass filtering function

Setup

Input: ac=1, dc offset $= 500\text{u}$. Output: $\text{I}_{\text{out}} = \text{Y\_LPF}$

Current sources: I_{fc} =500u, I_Q sweeping: 2u, 5u, 10u, 20u, 50u

Simulation Results

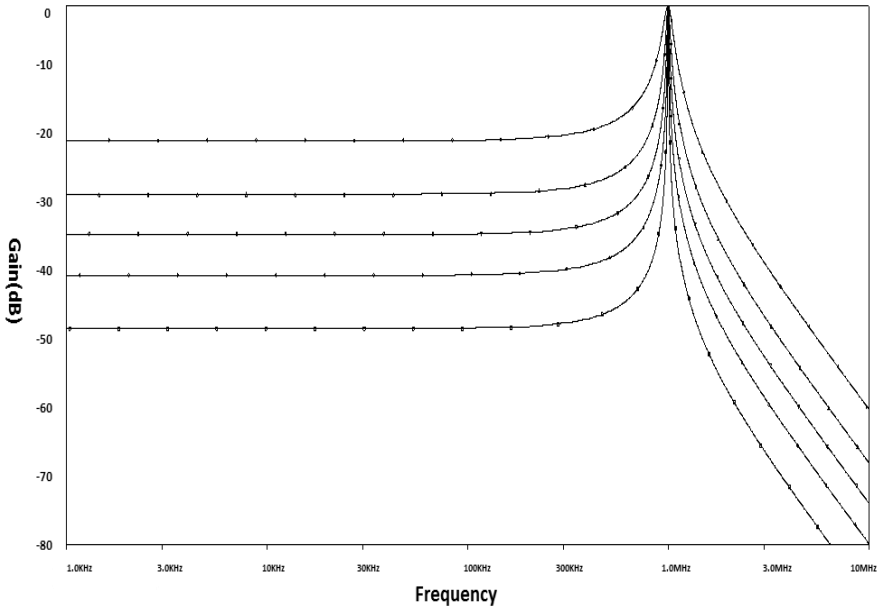

Figure 2.9 Gain spectra of the filter in Fig. 2.5 under the low-pass filtering and damping factor tunability test.

Test Setup	Ifc (A)	500u	500u	500u	500u	500u
	IQ (A)	2u	5u	10u	20u	50u
Test Results	Passband gain	0.004	0.010	0.020	0.040	0.100
	Overshooting peak	0.990	0.996	0.998	0.999	1.001

Table 2-3 Measurement data from the low-pass filtering and damping factor tuning test on the filter in Fig. 2.5.

Observation

The gain spectra above explicitly verify the low-pass filtering function of the filter. According to the particular current source setup, the low-pass filter damping factor is expected to be 1/500, 1/200, 1/100, 1/50 and 1/20 during the sweep of I_Q. The measured passband gain is proportional to the ratio of I_Q to I_{fc}, which agrees well with what is suggested by the transfer function in eqn. (2.17). As the damping factor of the lowpass filter is smaller than unity in each case, overshoot is expected before the roll-off of the gain spectra. The location and value of the overshooting peak remain approximately the same during the tuning of I_Q as long as I_{fc} is unchanged. Measurement shows that the peak is consistently located at the center frequency of the bandpass filter, with a constant gain close to unity.

2. Test on the non-unity gain filter in Fig. 2.6

1) Tunability of the peak gain

Setup

Input: ac=1, dc offset $= 500$u. Output: $\mathrm{I_{out}} = \mathrm{Y\_bp}$

Current sources setup: Ifc=500u. IQ sweeping: 2u, 5u, 10u, 20u, 50u.

Simulation Results

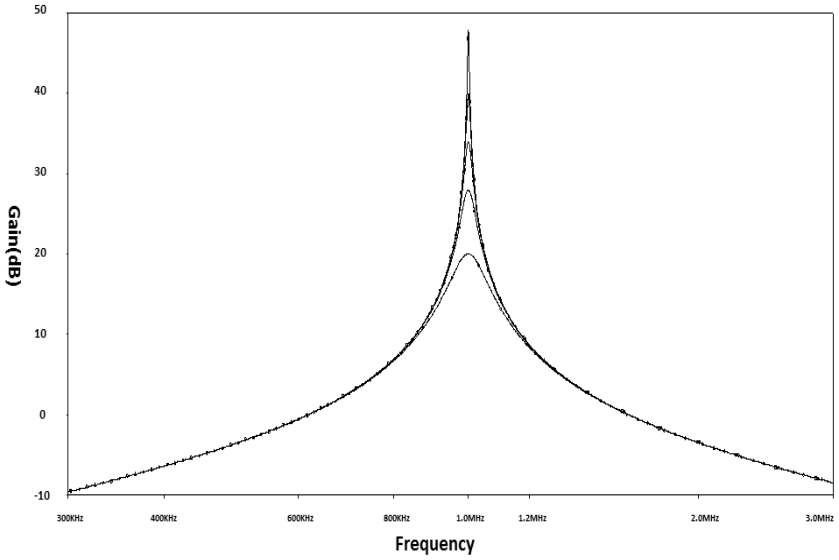

Figure 2.10 Gain spectra of the bandpass filter in Fig. 2.6 under the Q factor tunability test

Test Setup	Ifc (A)	500u	500u	500u	500u	500u
	IQ (A)	2u	5u	10u	20u	50u
Test Results	Center Frequency(Hz)	1000.22k	1000.22k	1000.22k	1000.22k	1000.23k
	Quality Factor	**248.083**	**99.836**	**50.018**	**25.034**	**10.019**
	Peak Gain	**247.497**	**99.599**	**49.899**	**24.974**	**9.996**

Table 2-4 Measurement data from the Q factor tunability test on the filter in Fig. 2.6.

Observation

This particular design implements a bandpass filter whose peak gain equals the quality factor Q ideally, as indicated by eqn. (2.18). When I_Q is tuned with I_{fc} fixed, the quality factor Q is expected to be inversely proportional to I_Q while the center frequency fc stays the same. In the test above, fc was set and fixed at 1MHz, and Q is expected to be 250, 100, 50, 25 and 10 as IQ gets swept from 2uA to 50uA. The measured data agrees well with our expectations: a constant center frequency, a tunable quality factor, and a peak gain that tracks Q and inversely proportional to I_Q.

Transient test

A transient test was run on both designs to test the integrity of the output current signals. Related parameters are as: $\mathrm{I_{dc}} = 0.5\mathrm{mA}, \mathrm{I_{fc}} = 0.5\mathrm{mA}, \mathrm{I_Q} = 10\mathrm{uA}$, C=3.076nF. Based on the setup, the center frequency of the bandpass filter is 1MHz and the quality factor is 50, so the bandwidth of the filter is 20kHz.

1. Test on the unity-gain filter in Fig. 2.5

AM input: $I_{in} = I_{AM} + I_{os} = (0.1m)\sin(2\pi \cdot 1Meg \cdot t)\,[1 + 0.5\sin(2\pi \cdot 10K \cdot t)] + 0.5m$

A more explicit expression of the input, in the form of the sum of sinusoids of different frequencies, could be derived by applying a trig identity to the equation above:

$$I_{in} = (100u)\sin(2\pi \cdot 1Meg \cdot t) + (25u)cos(2\pi \cdot 0.99Meg \cdot t) - (25u)cos(2\pi \cdot 1.01Meg \cdot t) + 0.5m$$

Note that the carrier is at 1MHz and the sideband signals are at 0.99MHz and 1.01MHz respectively. As the bandwidth of the filter is 20kHz, we can expect that the amplitude of both input sideband signals experiences an attenuation of approximately 3dB during the signal processing.

Simulation results

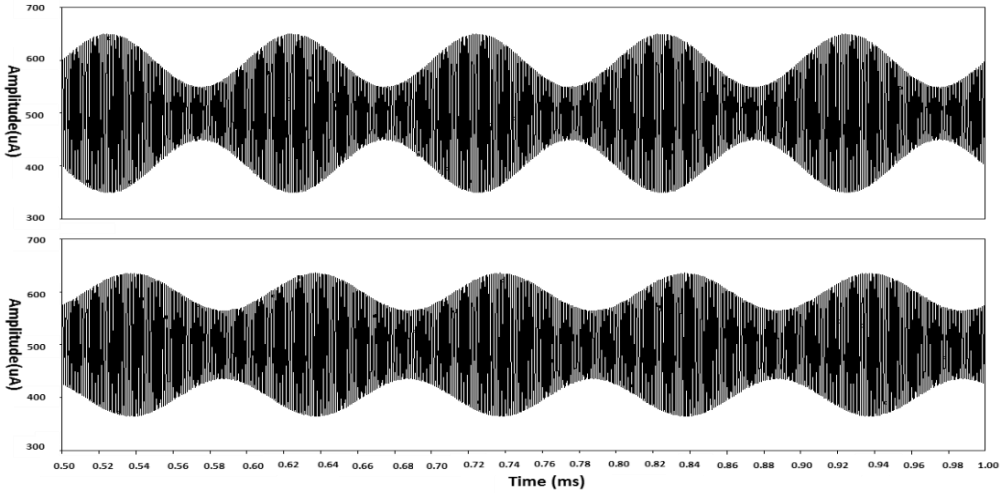

Figure 2.11 Transient plots of the unity-gain bandpass filter input (upper) and output (lower) current signals.

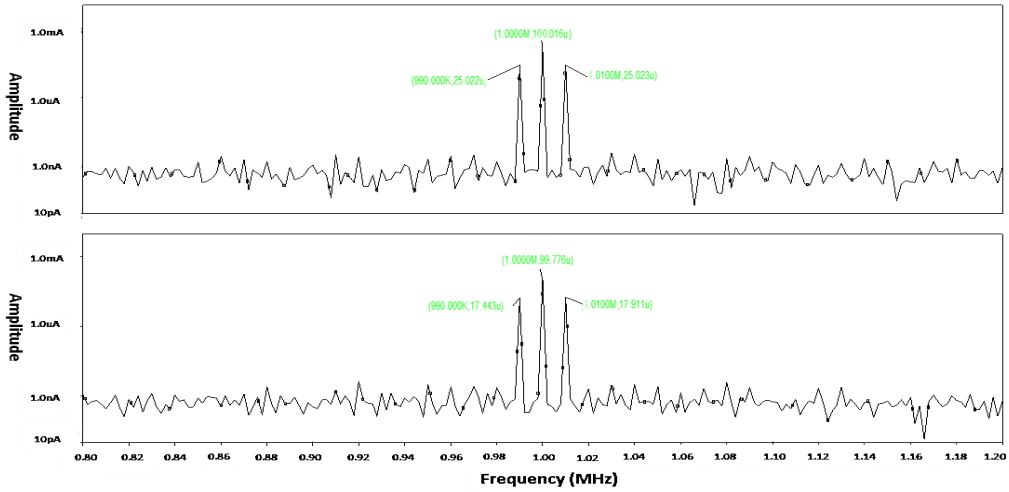

Figure 2.12 FFT spectra of the unity-gain bandpass filter input (upper) and output (lower) current signals.

The above plots show that the designed circuit is capable of generating a distortionless bandpass filtered version of the input current signal. The quality factor of the bandpass filter could be verified by the FFT spectrum of the output signal. Moreover, the output is measured to have the same level of dc offset as the input, which is not labeled out in the figure.

2. Test on the non-unity gain filter in Fig. 2.6

The transient test on the second design is mainly to verify the realization of the non-unity peak gain of the bandpass filter that tracks the filter's quality factor. The same parameter setup for current sources and capacitors was used, which suggests that a peak gain of 50 should be implemented. The amplitude of ac components in the original AM input is scaled by 1/50 to avoid distortion in the process of small signal filtering and amplification. With this setup, the successful implementation of a bandpass filter whose peak gain equals the quality factor is easily verified if the output signal from this test is close to that from the above test.

Input: $I_{in} = (2u)\sin(2\pi \cdot 1Meg \cdot t) + (0.5u)cos(2\pi \cdot 0.99Meg \cdot t) - (0.5u)cos(2\pi \cdot 1.01Meg \cdot t) + 0.5m$

Simulation results

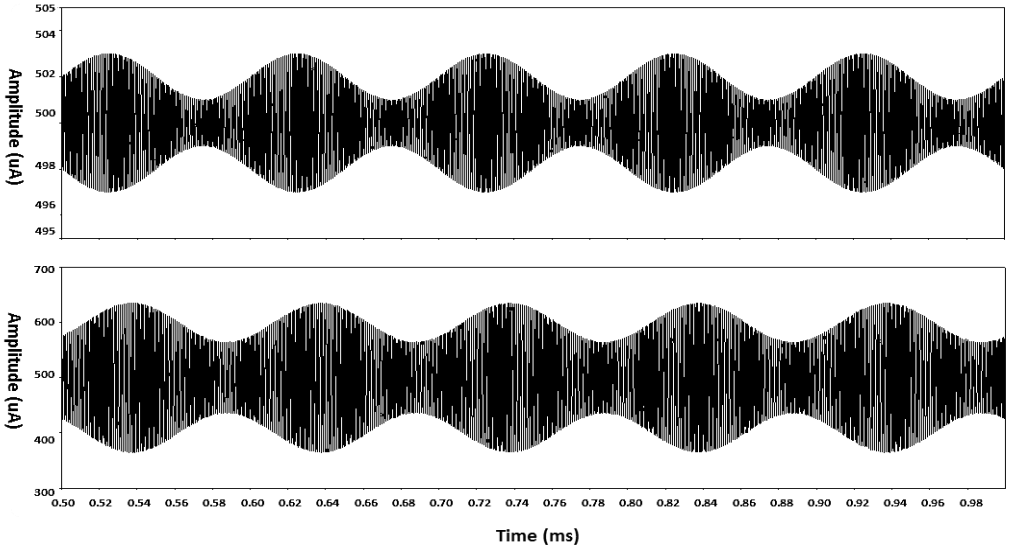

Figure 2.13 Transient plots of the non-unity gain bandpass filter input (upper) and output (lower) current signals.

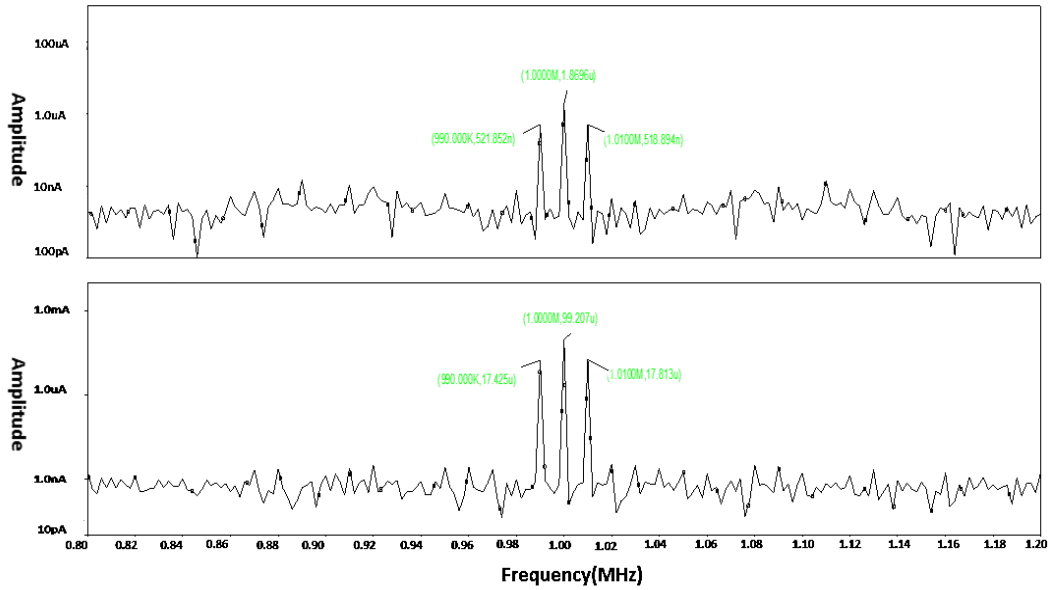

Figure 2.14 FFT spectra of the non-unity gain bandpass filter input (upper) and output (lower) current signals.

As shown in Fig. 2.14 and Fig. 2.15, the simulation results perfectly agree with our expectation.

2.4 AM mode Synchronous Bandpass Filter and Related Feedback Filtering System

2.4.1 The Mathematical Model

It has been introduced in Chapter 1 the derivation and generic state space representation of AM mode synchronous filtering, we now modify the unity-gain bandpass filter discussed above into a synchronous filter of this mode. First, we utilize the transformation approach introduced in Chapter 1 to transform the mathematical model of the standard biquad bandpass filter, given by eqn. (2.19), into a new version that corresponds to a companding system.

$$\begin{vmatrix} \dot{x}_1 \\ \dot{x}_2 \end{vmatrix} = \begin{vmatrix} -\frac{w_0}{Q} & -w_0 \\ w_0 & 0 \end{vmatrix} \begin{vmatrix} x_1 \\ x_2 \end{vmatrix} + \begin{vmatrix} \frac{w_0}{Q} \\ 0 \end{vmatrix} u \ , \qquad y = |1 \quad 0| \begin{vmatrix} x_1 \\ x_2 \end{vmatrix} \tag{2.19}$$

Define the new set of state variables as $\bar{w} = p(t)\bar{x}$, where $p(t)$ is always positive, then an alternate state space representation of the bandpass filter is derived as:

$$\begin{vmatrix} \dot{w}_1 \\ \dot{w}_2 \end{vmatrix} = \begin{vmatrix} -\frac{w_0}{Q} + \frac{\dot{p(t)}}{p(t)} & w_0 \\ -w_0 & \frac{\dot{p(t)}}{p(t)} \end{vmatrix} \begin{vmatrix} w_1 \\ w_2 \end{vmatrix} + \begin{vmatrix} \frac{w_0}{Q} \\ 0 \end{vmatrix} p(t)u \ , \qquad y = \frac{1}{p(t)} |1 \quad 0| \begin{vmatrix} w_1 \\ w_2 \end{vmatrix} \tag{2.20}$$

The above dynamical equation set could be associated with a system that has a core filter with time-varying Q factor and amplitude modulators at both ends. Although internally time variant, the system is externally time invariant and it implements a transfer function identical to that of the original bandpass filter. So if the impulse response of the bandpass filter is $h(t)$, then the output of the derived system to input $u(t)$ could also be expressed as:

$$y(t) = u(t) * h(t) \tag{2.21}$$

where symbol "*" denotes convolution. The block diagram of the derived synchronous filter is shown in Fig. 2.15.

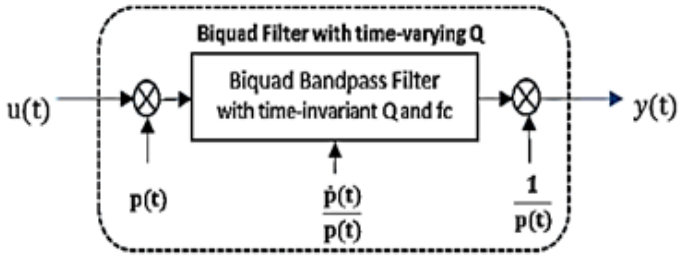

Figure 2.15 Block diagram of an AM mode synchronous BPF specified by eqn. (2.20).

Interestingly, if we take the modified core filter as an independent system and $u(t) \cdot p(t)$ its input, as shown in Fig. 2.16, then the system output could be expressed as $y(t) \cdot p(t)$ or $[u(t) * h(t)] \cdot p(t)$, which is the product of a bandpass filtered $u(t)$ and the original $p(t)$. Suppose $u(t)$ is a carrier and $p(t)$ a properly offset baseband information signal that is always positive, also suppose we were able to generate the ideal $\frac{\dot{p}(t)}{p(t)}$ and alter the core filter into one that corresponds to the state matrix in eqn. (2.20). According to the analysis above, when receiving an AM signal $u(t) \cdot p(t)$, the derived system would apply the bandpass filtering specified by $h(t)$ only to the carrier $u(t)$ and produce the product of the processed carrier and the original information signal as output. If the center frequency of the core filter has been tuned to the carrier frequency w_0, then the frequency component w_0 in the carrier could pass through the modified filter unchanged while other components in the carrier will be attenuated. Therefore, the useful sideband signals in the AM input would ideally stay intact during the signal processing. It leads to an appealing advantage of the system when processing noisy AM input signals: the original time-invariant bandpass filter centered at w_0 could in principle be tuned as sharp as needed to suppress the undesired components near w_0, and the useful input sideband signals would be maintained regardless of the core filter's original Q factor. In

this sense, the system in Fig. 2.16 is capable of producing an output with noticeably improved SNR compared to a standard second-order bandpass filter with the same Q factor. The noise performance of such a system will be discussed in detail in Chapter 4.

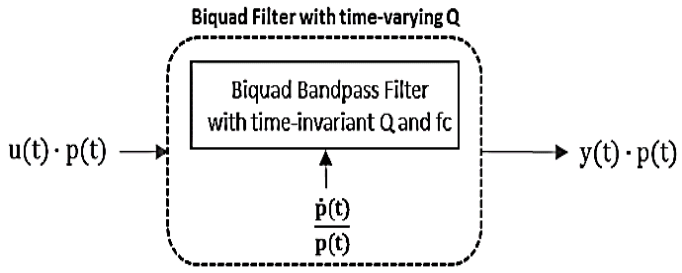

Figure 2.16 Another perspective of the AM mode synchronous BPF: a filter with time-varying Q factor processing an AM input signal, which has the potential of producing an output with very high SNR.

2.4.2 The Filter with a Time-varying Q Factor

In this section, we will implement the filtering block in Fig. 2.16 that has a time-varying Q factor by modifying the log domain unity-gain bandpass filter in Fig. 2.5. The input AM current is particularly set up as:

$$I_{in} = u(t)p(t) + I_{os} \qquad (2.22)$$

where $u(t) = sin(2\pi \cdot 1Meg \cdot t)$, $p(t) = (0.1m)[1 + 0.5sin(2\pi \cdot 10K \cdot t)]$, $I_{os} = 0.5m$. Note that the state matrix in eqn. (2.20) is the sum of $\begin{vmatrix} -\frac{w_0}{Q} & w_0 \\ -w_0 & 0 \end{vmatrix}$ and $\begin{vmatrix} \frac{\dot{p(t)}}{p(t)} & 0 \\ 0 & \frac{\dot{p(t)}}{p(t)} \end{vmatrix}$, where the former matrix is the state matrix for the original time-invariant bandpass filter and the latter specifies the Q factor variation, so the new filter could be realized by respectively injecting the current corresponding to $\frac{\dot{p(t)}}{p(t)}w_1$ and $\frac{\dot{p(t)}}{p(t)}w_2$ to the associated capacitors in the original filter. As $p(t)$ is always positive, it could be realized by the collector current of a BJT and be expressed as $p(t) = I_s exp(\frac{v_p}{v_t})$, where v_p is the base-

emitter voltage difference of the BJT with collector current p(t), and it follows that $\frac{\dot{p(t)}}{p(t)} = \frac{\dot{v}_p}{v_t}$. To realize $\frac{\dot{p(t)}}{p(t)} w_i$(i=1 or 2), we first transform the term the same way as we transform the state equations of the bandpass filter, namely, multiplying it with $C\frac{v_t}{w_i}$. The product could then be simplified as $C\dot{v}_p$, where C is the capacitance of the capacitors in the core filter. The physical meaning of $\frac{\dot{p(t)}}{p(t)} w_i$ has become explicit at this point: the current flowing in the capacitor C when it's applied with voltage v_p. The conceptual implementation of $\frac{\dot{p(t)}}{p(t)} w_i$ is given in Fig. 2.17, where an ideal current source kp(t), an ideal npn transistor and two ideal CCCSs are used. The two branches of output current are respectively injected into the capacitors in the core filer to implement the filter with a time-varying Q factor in Fig. 2.16.

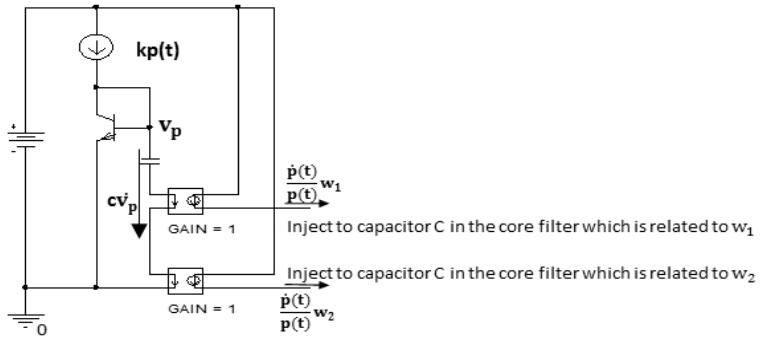

Figure 2.17 Schematic for implementing the time-variant quality factor.

A transient test was run on the resulting time-variant filter to test its performance. For comparison, the output of the original time-invariant bandpass filter corresponding to the same input was also plotted. The core filter was centered at 1MHz and its original Q factor was set to be 50. The input signal is the amplitude modulation result of an offset 10kHz sine wave and a carrier at 1MHz. It's expected that the original bandpass filter

produces an output with sideband signals attenuated by approximately 3dB while the modified filter produces an output almost identical to the intput. Simulation results in Fig. 2.18 demonstrate that the sideband signals of the AM input sent to the modified filter experience very little phase shift or ampitude attenuation, expect that some intermodulation noise components of negligible size were observed. Besides the particular test presented here, simulation was also run on the system set up with other original Q factors and $p(t)$ frequencies, it was consistently observed that the modified system is always able to produce an output signal very similar to the input. Therefore, the function of the filtering block in Fig. 2.16 does agree with our expectation developed from the system mathematical model.

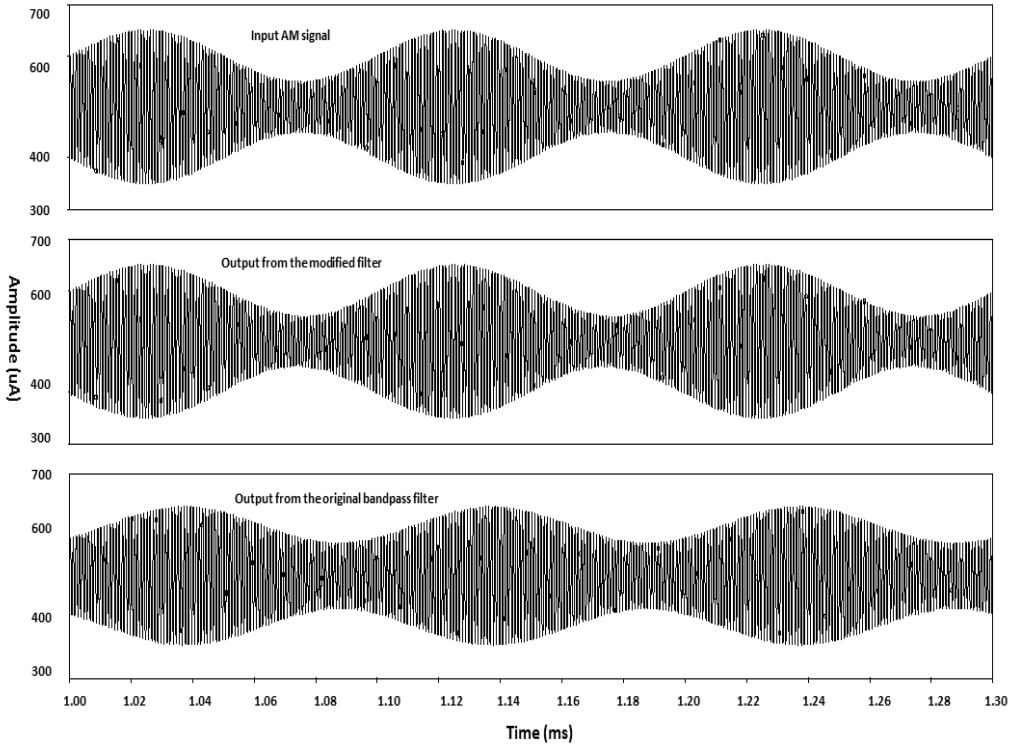

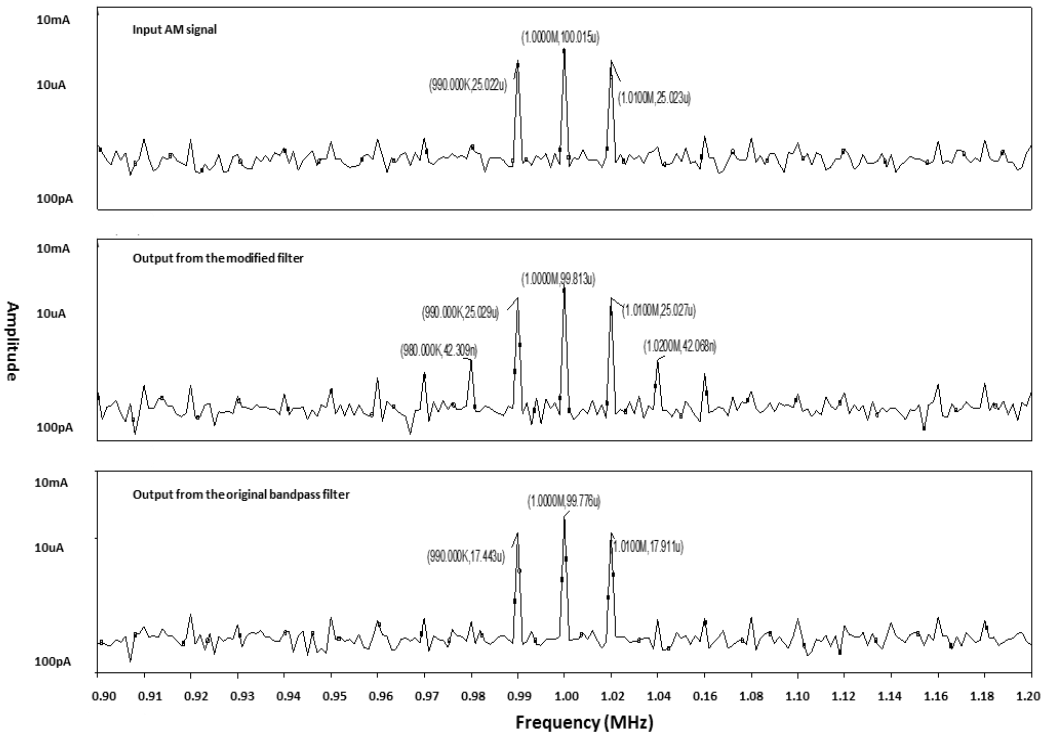

Figure 2.18 Transient plots and corresponding FFT spectra of the input and output signals in the test on the original bandpass filter with a constant Q factor and the ideally modified filter with a time-variant Q factor, where the core filter was centered at 1MHz and the original Q factor was tuned to 50.

2.4.3 A Feedback Bandpass Filter Inspired by AM Mode Synchronous Filtering

In practice, generating the Q factor control signal $\frac{\dot{p(t)}}{p(t)}w_i$ is very challenging, as we usually do not have the baseband information signal $\mathrm{p(t)}$ at the receiver end and have to recover it from the received AM signal. As any demodulator inevitably introduces phase shift to the received AM signal, the recovered baseband signal $\hat{\mathrm{p}}(\mathrm{t})$ always lags the original $\mathrm{p(t)}$ hence doesn't seem to be a proper source for generating the Q factor control signal. In this section, we will explore the possibility of constructing a feedback filtering system with the demodulated input AM signal, shown in Fig. 2.19, and compare its performance to that of the ideally modified filter in Fig. 2.16.

The first task is to design a special demodulator, or envelope detector, to recover $\hat{p}(t)$ from the core filter output with as little introduced phase shift as possible, considering that the ideal $\hat{p}(t)$ is expected to be in phase with the original p(t). Recall that in a conventional AM receiver, as shown in Fig. 2.20, the output of the bandpass filter is mixed with a local oscillator output and the resulting signal is lowpass filtered to recover the useful information, so the phase of the recovered signal is mainly influenced by two blocks: the bandpass filter and the lowpass filter. Since the phase shift results from the bandpass filtering is typically inevitable, we can focus on developing a demodulation module that recovers the information signal with possible minimum phase shift.

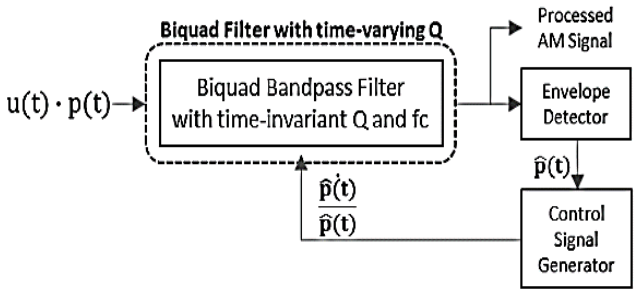

Figure 2.19 Block diagram of the proposed feedback AM-mode filtering system

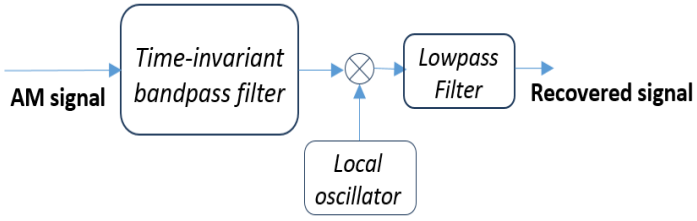

Figure 2.20 Block diagram of a basic conventional AM receiver.

Based on the above analysis, we devised a demodulator that employs a sample-and-hold block (S/H), instead of the mixer-lowpass filter module, to recover the information signal

from the bandpass filtered AM input. The switch of the S/H block is controlled by a pulse train at the carrier frequency and with extremely small duty cycle. According to the sampling theory, the frequency-domain representation of an ideally sampled signal is:

$$F_{\text{ideally\_sampled}}(w) = e^{-j0.5Tw} \cdot \text{sinc}(0.5Tw) \cdot \sum_{n=-\infty}^{n=+\infty} F(w - nw_0) \quad (2.23)$$

where $F(w)$ is the Fourier transform of the signal to be sampled, which in our case is the bandpass filtered AM signal, w_0 is the sampling frequency, T is the sampling period, and n is a integer. For a sampling rate that equals the carrier frequency of the AM input, the phase shift introduced to the baseband components in the S/H output, i.e. $-\frac{w}{w_0}\pi$ ($w \ll w_0$), would be very small. And since the repeating patterns of $F(w)$ over the frequency axis are weighed by function $\text{sinc}(0.5Tw)$, the patterns that are not in the baseband (corresponding to $n \neq \pm 1$) would be scaled to a negligible level compared to those in the baseband (corresponding to $n = \pm 1$). Some analysis would convince readers that the S/H block is able to extract the input signal's envelope with very small error.

Although the phase shift introduced in the lowpass filtering stage in a traditional demodulator could be avoided by utilizing the S/H block, the reconstructed baseband signal $\hat{p}(t)$ still lags the original $p(t)$, due to the preceding bandpass filtering. Therefore, it's still unclear whether $\hat{p}(t)$ could be used to generate the Q-factor control signal. To answer this question and evaluate the performance of the feedback filtering system in Fig. 2.19, a Gm-C system model has been implemented and simulated in PSpice, as shown in Fig. 2.21, where all the sources and blocks are ideal. The system could be divided into two parts: the voltage-mode bandpass filter with a time-invariant Q factor

and the feedback path that consists of an S/H demodulator and a Q-factor control signal generator. The core filter implementation becomes very straightforward after we transform the state space equations in eqn. (2.21) into the following form:

$$\begin{vmatrix} \dot{w}_1 C \\ \dot{w}_2 C \end{vmatrix} = \begin{vmatrix} g_{11} & g_{12} \\ g_{21} & 0 \end{vmatrix} \begin{vmatrix} w_1 \\ w_2 \end{vmatrix} + \begin{vmatrix} g_{u1} \\ 0 \end{vmatrix} p(t)u + \begin{vmatrix} \frac{\dot{\hat{p}}(t)}{\hat{p}(t)} C & 0 \\ 0 & \frac{\dot{\hat{p}}(t)}{\hat{p}(t)} C \end{vmatrix} \begin{vmatrix} w_1 \\ w_2 \end{vmatrix}, \quad y = \begin{vmatrix} 1 & 0 \end{vmatrix} \begin{vmatrix} w_1 \\ w_2 \end{vmatrix} \tag{2.24}$$

where $g_{11} = -\frac{w_0}{Q} C$, $g_{12} = -w_0 C$, $g_{21} = w_0 C$, $g_{u1} = \frac{w_0}{Q} C$.

The original bandpass filter with time-invariant Q factor is explicitly associated with the Gm-C network in Fig. 2.21, where the input is a voltage signal and all the transconductors are modeled by ideal voltage-controlled-current-sources (VCCSs). The core filter is followed by an envelope detector which is modeled as a switch in series with a capacitor. The on and off status of the switch is controlled by an impulse train. Notate the recovered voltage signal as $\hat{p}(t)$ and apply it to a capacitor with one end grounded, then the capacitor current equals $C\dot{\hat{p}}(t)$. A feedback connection control circuitry is included to prevent the Q-factor control signal being sent back before $\hat{p}(t)$ steps into steady state, in order to avoid convergence problem in the simulation.

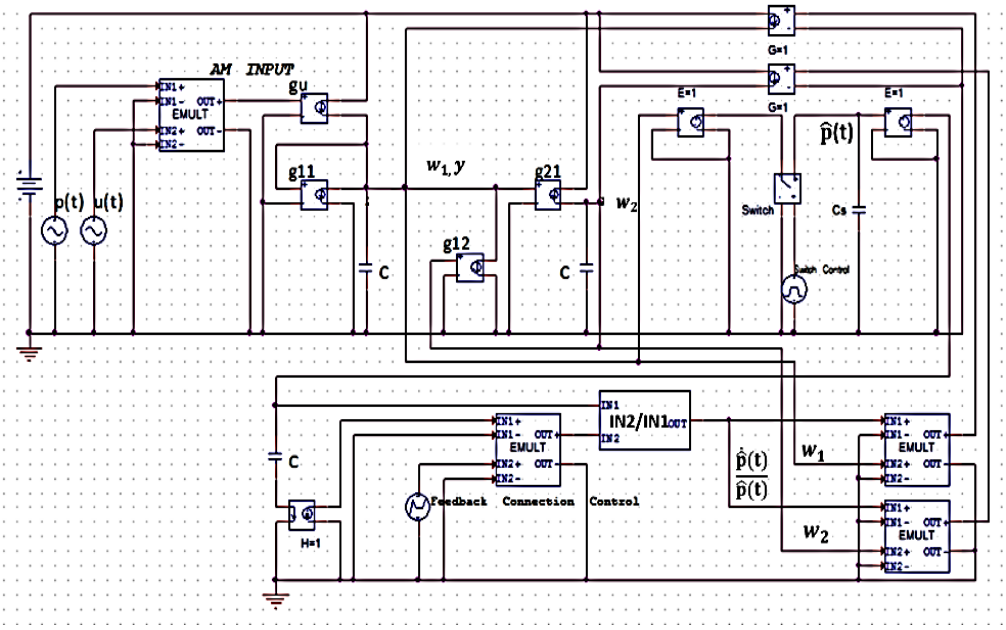

Figure 2.21 Ideal Gm-C model for the feedback filter in Fig. 2.20.

To test the performance of the above system, we set up a simulation as follows:

Input AM voltage signal:

$$p(t)\cdot u(t) = \left[1m + (0.5m)\sin(w_p t)\right]\sin(w_{carrier} t),\ w_p = 2\pi\cdot 10K,\ w_{carrier} = 2\pi\cdot 1Meg;$$

Capacitors and VCCSs:

C=3.075n, Cs=100n, g10=g11=386.416u, g12=g21=19.321m;

S/H impulse train:

TD=250ns, PW=1ns, PER=1000n; *Switch*: RON=1e6, ROFF=1e-3;

Feedback connection control:

From t=0 to 1.5ms, the loop is open; from t=1.5ms to 2ms, the switch is partially on and starting from t=2ms, the switch is completely turned on, 100% of the feedback current is injected into the core filter.

The setup for the filtering capacitors C and the VCCSs implements a center frequency of 1MHz and an original Q factor of 50 for the core filter. So it is easy to

predict that before the loop is closed, the reconstructed baseband signal $\hat{p}(t)$ is 3dB lower than p(t) and 45 degrees lagging in phase. A transient test was run on the feedback bandpass filtering system and the system with a core filter modified by the ideal $\frac{\dot{p}(t)}{p(t)}$.

The blue plot in Fig. 2.22 shows the recovered signal $\hat{p}(t)$ from the system in Fig. 2.21 in the open-loop stage (0ms to 1.5ms), partially closed-loop stage (1.5ms to 2ms) and completely closed-loop stage (2ms to 3ms). It's apparent that the phase and amplitude of $\hat{p}(t)$ in the three stages are different, and with higher percentage of $\frac{\dot{\hat{p}}(t)}{\hat{p}(t)}$ sending back to the core filter, the recovered signal $\hat{p}(t)$ from the feedback system bears stronger resemblance to the original p(t), and when 100% of $\frac{\dot{\hat{p}}(t)}{\hat{p}(t)}$ feeds back, $\hat{p}(t)$ almost overlaps with $p(t)$. The corresponding FFT spectra quantitatively verifies that $\hat{p}(t)$ from the feedback system has most of its energy concentrating at dc and 10kHz, and the respective signal size is very close to its counterpart in the original $p(t)$. Moreover, the size of the undesired harmonics in $\hat{p}(t)$ is at a negligible level compared to that of the information component. The simulation results suggest that it is possible to replace $p(t)$ with $\hat{p}(t)$ to generate a Q-factor control signal for the standard biquad bandpass filter and further develop it into a feedback filtering system. When processing ideal AM signals, the feedback filtering system is capable of recovering a baseband signal that bears remarkable resemblance to the original information signal $p(t)$ in both amplitude and phase.

Finally, it was discovered through varying the AM input bandwidth that to ensure the given feedback system to produce negligible output harmonic distortion, the

bandwidth of the input AM signal needs to be limited in a range which is constraint by the original sharpness of the core filter, while the filter modified by the ideal $\dot{p}(t)/p(t)$ is not subject to such an issue. Table 2.5 provides some measurement data to demonstrate this observation. The discovery could also be interpretted as that unlike the ideally modified filter in Fig. 2.17 of which the original Q factor could in principle be tuned extremely high, the highest original Q factor for the feedback filtering system to generate an output with negligible harmonic distortion is constraint by the bandwidth of the input signal. To better demonstrate this observation, we stuck with the same AM signal tested above (bandwidth of 20kHz) and swept the origianl Q factor of the core filter (centering at 1MHz) over 80, 100, 200, 500 for both systems to compare their performance. Spectra of the steady state recovered signals from the two systems are plotted on the same graph for each Q factor tested, as shown in Fig. 2.23.

Core Filter	Input	Feedback Filtering System		Ideally Modified Filter	
Static BW (KHz)	$f_{p(t)}$ (KHz)	$A_{fundamental}$ (uV)	$A_{2nd\_order\_harmonic}$ (uV)	$A_{fundamental}$ (uV)	$A_{2nd_{order}\_harmonic}$ (uV)
20	1	500.019	0.009	499.966	<0.001
	10	502.737	0.803	499.88	<0.01
	20	511.012	3.496	499.63	~0.01

Table 2-5 Measurement on the fundamental and 2nd-order harmonic in the recovered signals from the feedback filtering system and the ideally modified filtering system when they process noiseless AM signals with different bandwidths.

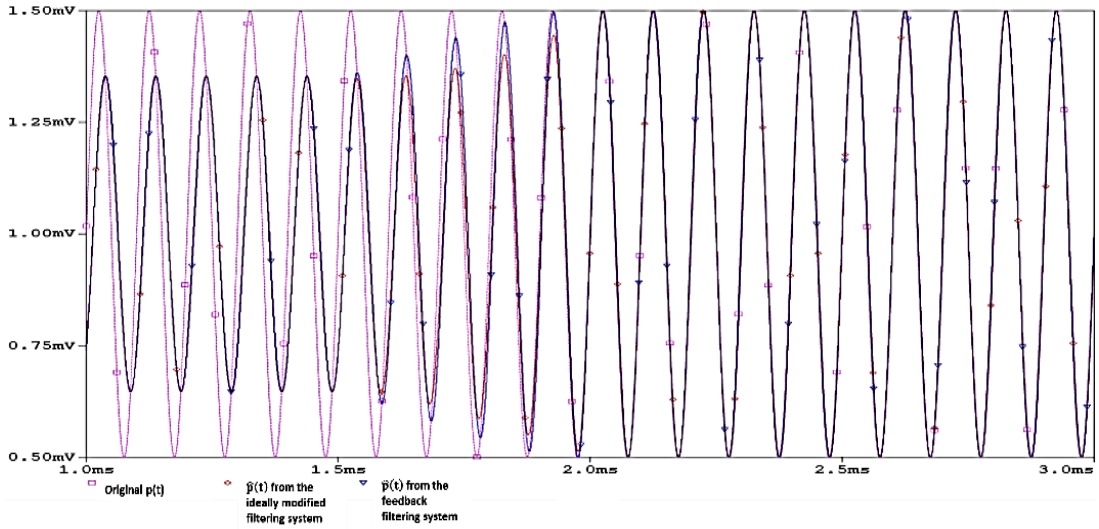

(a) Transient plots

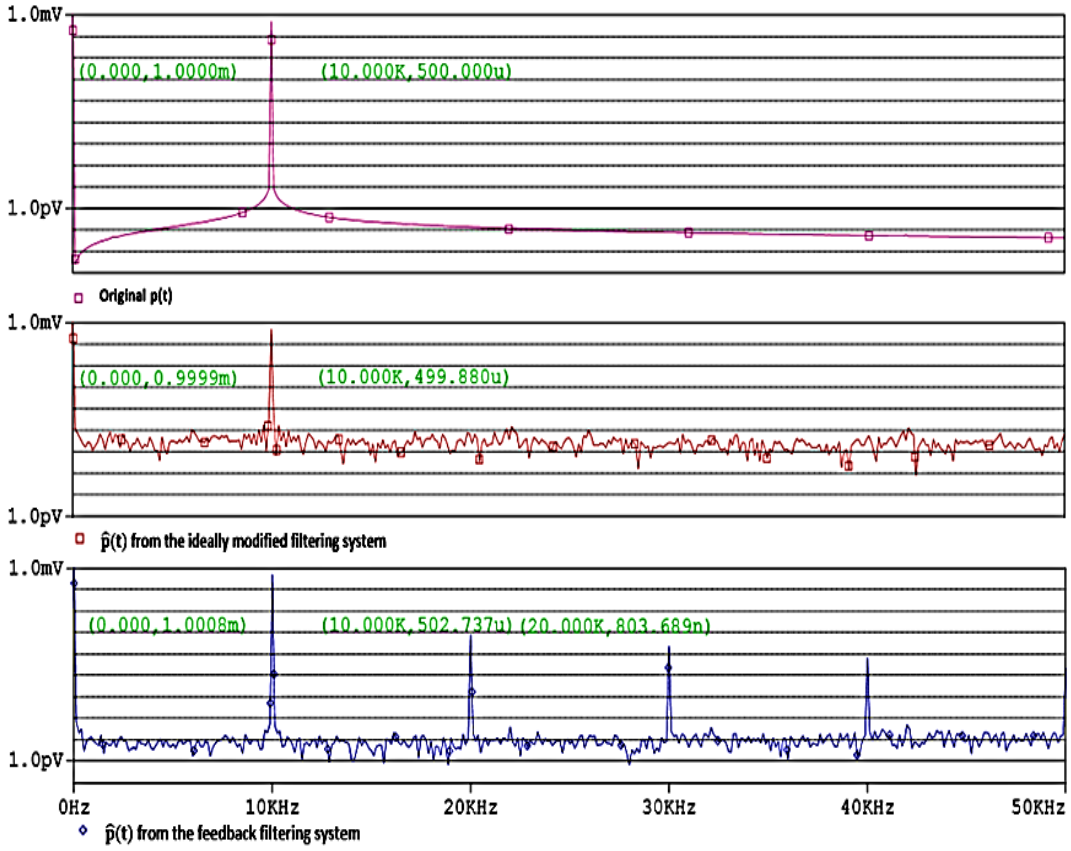

(b) FFT spectra of the plots in (a)

Figure 2.22 The original $p(t)$ and the recovered signal $\hat{p}(t)$ from the feedback filtering system (blue plot) and the system with a core filter modified by the ideal $\dot{p}(t)/p(t)$ (red plot).

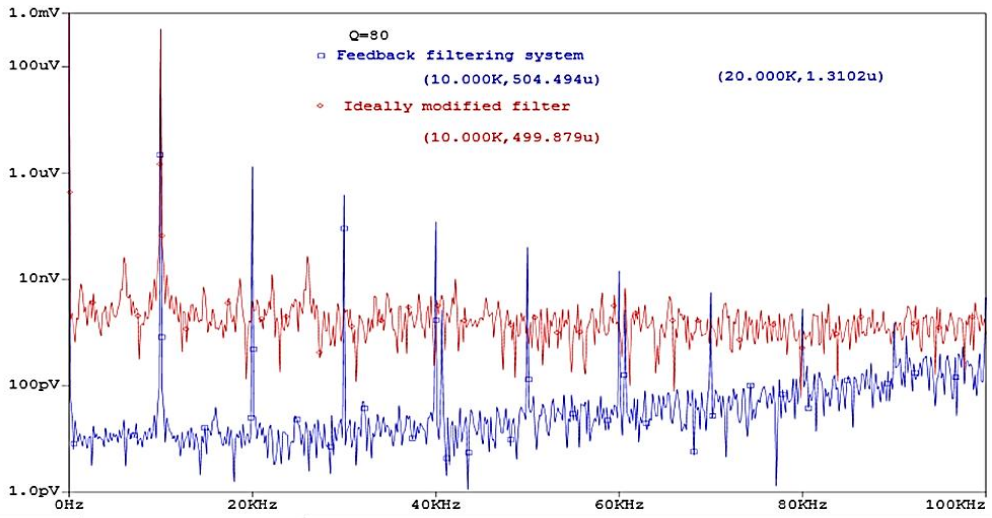

(a) Q=80

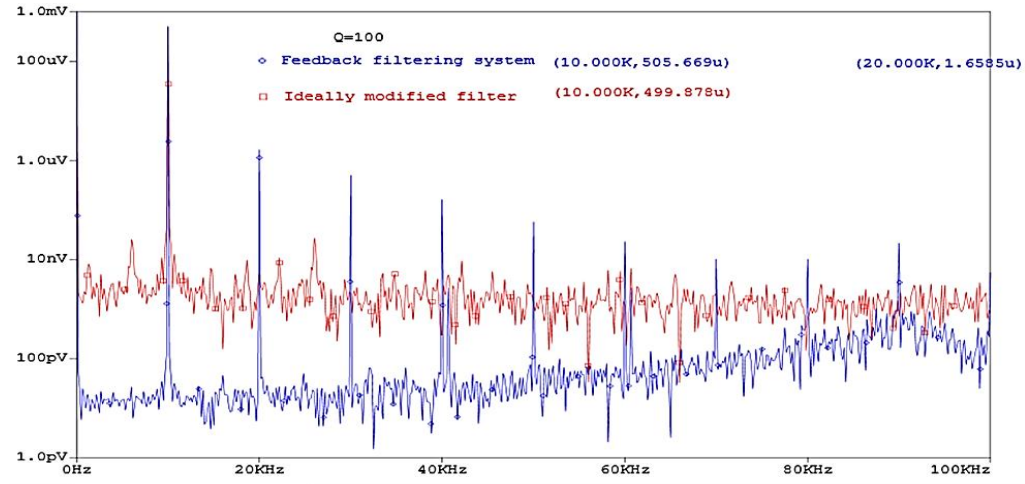

(b) Q=100

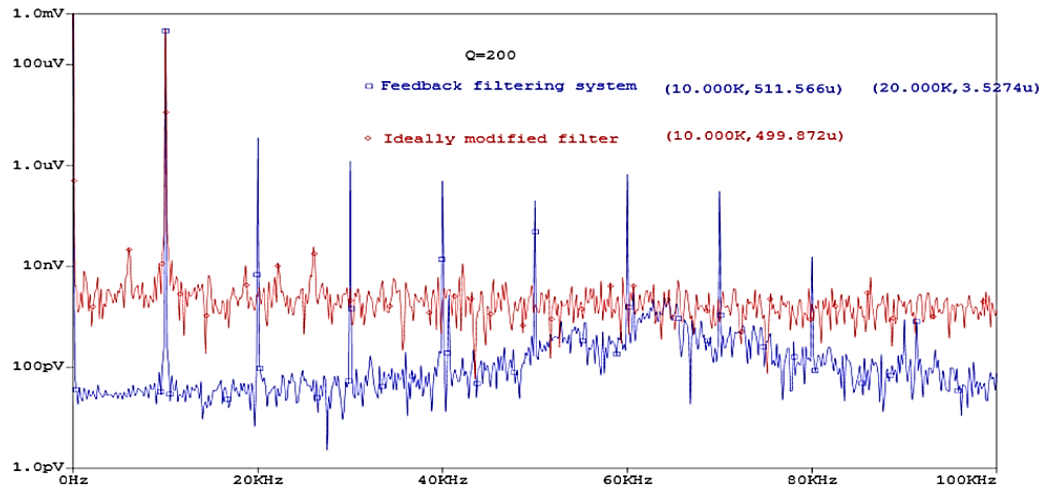

(c) Q=200

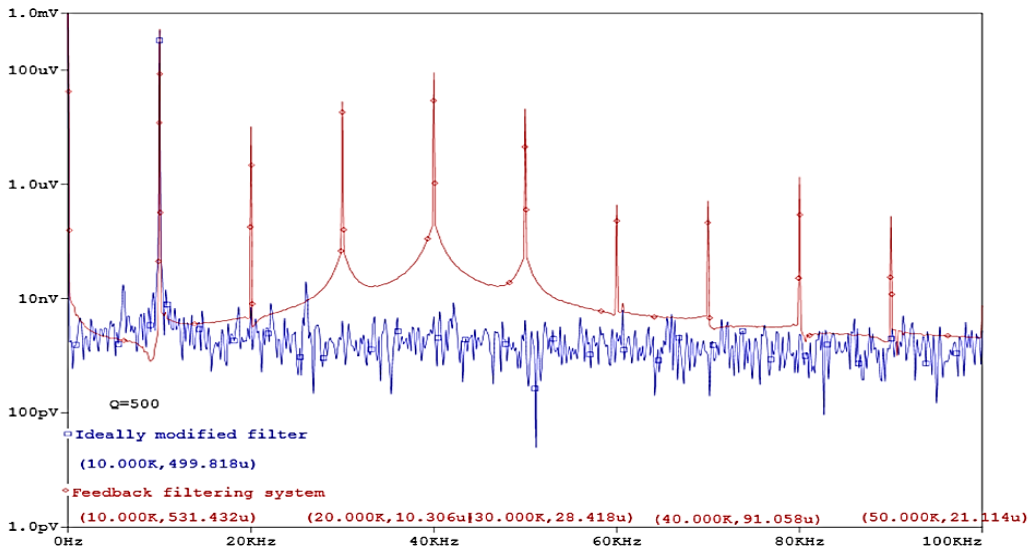

(d) Q=500

Figure 2.23 FFT spectra of the steady state recovered signals from the ideally modified filter and the feedback filtering system with same original bandwidth, under the Q factor sweeping test.

The above test result suggests: 1. For the ideally modified bandpass filter, raising its original Q factor does not result in any undesired harmonic distortion. 2. For the feedback bandpass filter, as the original Q factor increases, the output harmonic distortion rises too. 3. If the original bandwidth of the feedback filter is too narrow compared to the bandwidth of the input signal, large-sized harmonic distortion will be generated so the output SNR is noticeably degraded. 4. Suppose the input signal has a bandwidth of BW_{in}, to ensure the second order harmonic distortion in the feedback bandpass filter output to be lower than 1/300 of the fundamental component size, it's recommended that the minimum original bandwidth of the core filter to be $0.5BW_{in}$, which sets an upper limit for the feedback system's original Q factor. Therefore, it's only under certain circumstances that the feedback bandpass filter produces an output similar to its ideally modified bandpass filter counterpart.

2.5 Summary

Log-domain biquad bandpass filters, with unity peak gain or peak gain proportional to the Q factor have been implemented at the transistor level. Upon verifying their tunability and function, we proposed in Fig. 2.15 an AM mode synchronous filtering system based on the transformed state space representation of a standard biquad bandpass filter. Moreover, we deleted the back end modulator and turned the system into a new one which could be viewed as a double-sideband AM signal being processed by a bandpass filter with time-variant Q factor, shown in Fig. 2.16. Mathematical analysis suggests that in principle the ideal system is able to suppress the input noise as hard as desired while keeping the phase and amplitude of the useful input sideband signals unchanged. It, hence, provides a compromising approach to improving the SNR of a biquad bandpass filter when dealing with noisy AM signals. The implementation of such a system with log-domain circuitries has been discussed and tested. Considering the challenge in generating the ideal Q-factor control signal, a novel feedback AM mode bandpass filter inspired by the system in Fig. 2.16 was proposed and implemented as the ideal Gm-C network model in Fig. 2.21. Surprisingly, when the bandwidth of the AM input is no wider than two times the original core filter bandwidth, the filter modified by the feedback Q-factor control signal is able to maintain the size and phase of the AM input. As the input bandwidth increases, however, harmonic distortion of noticeable size emerges in the output. Therefore, the performance of the feedback system is dependent on the match between the bandwidth of the input and the original bandwidth of the system core filter, while the ideally modified system does not have this issue. The noise performance of both systems will be discussed in Chapter 4.

Chapter 3 FM mode-synchronous-filtering Related Complex Filters

In Chapter 2, the synchronous filtering approach that includes amplitude modulation as part of the signal processing was applied to the implementation of a biquad bandpass filtering system. In this chapter, we will focus on the application of another type of synchronous filtering that performs frequency modulation in some stages of the signal processing and could be viewed as FM mode synchronous filtering. Specifically, we will implement a biquad high-Q high-center frequency complex filter with both static and dynamic synchronous filtering approaches. In the static FM mode synchronous complex filter, the core filter center frequency and the terminal modulating frequencies are time invariant. Due to the front end modulation, the input signal is shifted into a much lower frequency band, so the following signal processing only requires a filter with lower center frequency and Q factor. The back end modulation brings the processed signal back into the original frequency band; hence, the overall system maintains the input-output function of the target filter. Such an architecture relieves the challenge posed by the performance limitation of available components at high frequencies, and makes possible the monolithic realization of a high-center frequency high-Q complex filter. The dynamic FM mode synchronous complex filter, besides making use of the above advantageous architecture, has a time-varying core filter center frequency and end modulating frequencies. The internally time-variant externally time-invariant system is capable of suppressing noise components in a certain frequency range and producing an output of higher SNR, which will be demonstrated in Chapter 4.

3.1 Design of a Static FM Mode Synchronous Complex Filter

Take the design of a subheterodyne synchronous complex filter for instance.

First of all, we reproduce the state space equations specifying the filter and the system block diagram introduced in Chapter 1, by eqn. (3.1) and Fig.3.1. In this section, we will utilize the mathematical model given by eqn. (3.1) and the technique for synthesizing log-domain filters to design a current mode high-center frequency high-Q factor complex filter that incorporates front end and back end modulators and a low-center frequency low-Q factor core filter. The system will be realized with BJTs of high β value, ideal current sources and capacitors. The design and implementation detail of each block will be discussed, followed by functional verification with PSpice simulation.

$$\begin{vmatrix} \dot{w}_1 \\ \dot{w}_2 \end{vmatrix} = \begin{vmatrix} -\frac{\widehat{w_0}}{2\hat{Q}} & -w_{\hat{A}} \\ w_{\hat{A}} & -\frac{\widehat{w_0}}{2\hat{Q}} \end{vmatrix} \begin{vmatrix} w_1 \\ w_2 \end{vmatrix} + \sqrt{2}(w_0/Q) \begin{vmatrix} sin(w_M t) \\ cos(w_M t) \end{vmatrix} u \qquad (3.1)$$

$$y = \sqrt{2}/2 \, |\sin(w_M t) \quad \cos(w_M t)| \begin{vmatrix} w_1 \\ w_2 \end{vmatrix}$$

where $w_{\hat{A}} = w_A - w_M$, w_A is the carrier frequency of the received AM signal u,w_M is the front/back end modulating frequency; $\widehat{w_0} = w_{\hat{A}}/\sqrt{1-(1/2\hat{Q})^2}$, $\widehat{w_0}$ is the center frequency and $\hat{Q}$ is the quality factor of the core filter. Note that for a high $\hat{Q}$, $w_{\hat{A}} \approx \widehat{w_0}$.

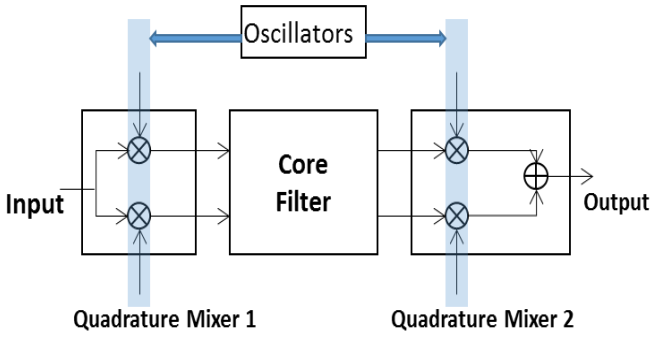

Figure 3.1 Embodiment of a FM mode synchronous complex filter.

3.1.1 The Front End Mixer

Design detail

Note that since the front end and back end modulators have similar block diagrams, they could be implemented together with similar circuitry. Start with the design of the front end quadrature mixer which modifies the frequency spectrum of the input signal. Specifically, the received RF signal is mixed with two channels of quadrature sinusoids generated by a local oscillator, and the mixer outputs are two channels of modulated signal that have the same magnitude spectrum but quadrature phase angle. Synthesis of this block is based on the translinear loop theory, which is commonly utilized in monolithic four-quadrant multipliers to achieve small error over a wide frequency range. The principle is briefly explained with the circuit shown in Fig. 3.2 where all the transistors are assumed to be perfectly matched and have negligible base current, and the current flow in each branch doesn't change direction. Using KVL and the constitutive law of a forward biased ideal PN junction, it is straightforward to formulate:

$$V_{BE3} - V_{BE4} = V_{BE1} - V_{BE2} \quad (3.2)$$

$$i_3/i_4 = i_1/i_2 \quad (3.3)$$

where V_{BEi} represents the base-emitter voltage difference of transistor Q_i. It follows that

$$(i_3 - i_4)/i_4 = (i_1 - i_2)/i_2 \quad (3.4)$$

$$(i_3 + i_4)/i_4 = (i_1 + i_2)/i_2 \quad (3.5)$$

Divide (3.4) with (3.5) and multiply both sides of the resulted equation with "$(i_1 + i_2)$":

$$i_3 - i_4 = (i_1 - i_2)(i_3 + i_4)/(i_1 + i_2) \quad (3.6)$$

Eqn. (3.6) suggests that the circuit in Fig. 3.2 could be used in the design of a multiplier. Strictly speaking, the difference between collector current i_3 and i_4 is a scaled product of the sum of i_3, i_4 and the difference between collector current i_1, i_2. Typically, $i_1 + i_2$

and $i_3 + i_4$ are constants and they are realized as two current sources in the circuit. Note that a proper dc offset is required to ensure all the transistors are consistently working in active region.

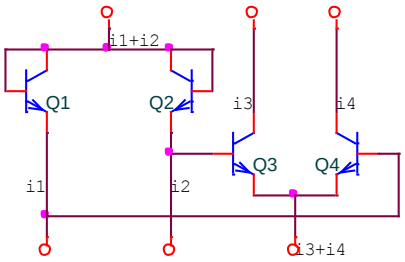

Figure 3.2 A translinear circuit example.

Circuit realization of the front end mixer is shown in Figure 3.3, where all the ac current sources are offset with I_{dc}. In the circuitry enclosed by the broken line, a three-diode drop bias is generated for the transistor pair hosting the received RF current and its differential signal. The circuit configuration in the two solid-line boxes is identical and the circuitry implements two parallel four-quadrant multipliers. Each multiplier consists of two differential pairs connected to a current mirror, a dc current source and an output transistor. The greyish part in the mixer could be taken as a one-stage operational amplifier, which is employed to improve the accuracy of the current mirror by reducing Early effect. The output signals of this block are collector currents labeled as I_{out} and I^*_{out}. They are a scaled product of ac component in I_{RF} and ac component in the quadrature pair I_{LO1}, I^*_{LO1} respectively. Both output signals are offset with I_{dc} in the design to guarantee a consistent direction of the current flows, and they can be formulated as:

$$I_{out} = \frac{2(I_{RF}-I_{dc})(I_{OL1}-I_{dc})}{I_{dc}} + I_{dc}\,, \quad I^*_{out} = \frac{-2(I_{RF}-I_{dc})(I^*_{OL1}-I_{dc})}{I_{dc}} + I_{dc} \qquad (3.7)$$

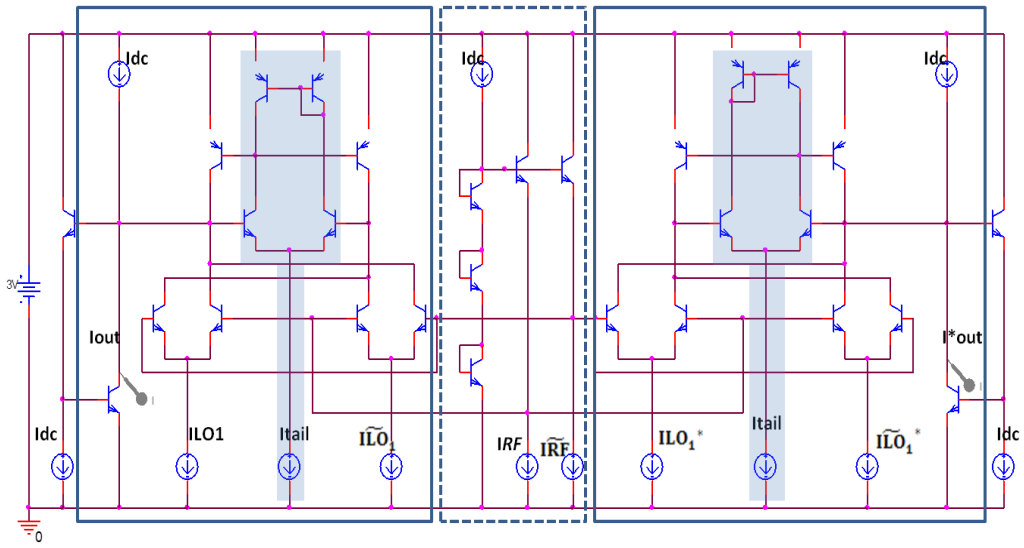

Figure 3.3 Schematic of the front-end mixer. The notation Idc, IRF, ILO1 and Iout represents the system dc offset current, the received RF current offset with Idc, the local oscillator output offset with Idc and the block output. Symbols '∼' and '∗', respectively, stand for the differential and quadrature counterpart of a signal.

Simulation setup and results

Unless otherwise mentioned, ideal sources and transistors with $\beta = 10k$ are used in PSpice simulation for all designed circuits in this chapter. The particular set of current sources used in the test is listed below:

$$I_{dc} = 500u,\ I_{tail} = 50u$$

$$I_{RF} = 500u + 400u \times \sin(2\pi \cdot 5Meg \cdot t),\ \widetilde{I_{RF}} = 500u - 400u \times \sin(2\pi \cdot 5Meg \cdot t)$$

$$I_{LO1} = 500u + 200u \times \sin(2\pi \cdot 4Meg \cdot t),\ \widetilde{I_{LO1}} = 500u - 200u \times \sin(2\pi \cdot 4Meg \cdot t)$$

$$I_{LO1}{}^{*} = 500u - 200u \times \cos(2\pi \cdot 4Meg \cdot t),\ \widetilde{I_{LO1}}{}^{*} = 500u + 200u \times \cos(2\pi \cdot 4Meg \cdot t)$$

Therefore, the two channels of output currents are expected to be:

$$I_{out} = 160u \times \cos(2\pi \cdot 1Meg \cdot t) - 160u \times \cos(2\pi \cdot 9Meg \cdot t) + 500u$$

$$I_{out}{}^{*} = 160u \times \sin(2\pi \cdot 1Meg \cdot t) + 160u \times \sin(2\pi \cdot 9Meg \cdot t) + 500u$$

In the derived output signals, frequency component 1MHz in $I_{out}{}^{*}$ lags that in I_{out} by 90°, while frequency component 9MHz in $I_{out}{}^{*}$ leads that in I_{out} by 90°. The phase

angle relationship is well verified by Fig. 3.4. On the other hand, by measuring the magnitude of 1MHz and 9MHz components in the output FFT spectra (as labeled in Fig. 3.5) and comparing the data to the ideal values above, we are further convinced that the modulator in Fig. 3.3 implements a quadrature mixer as expected.

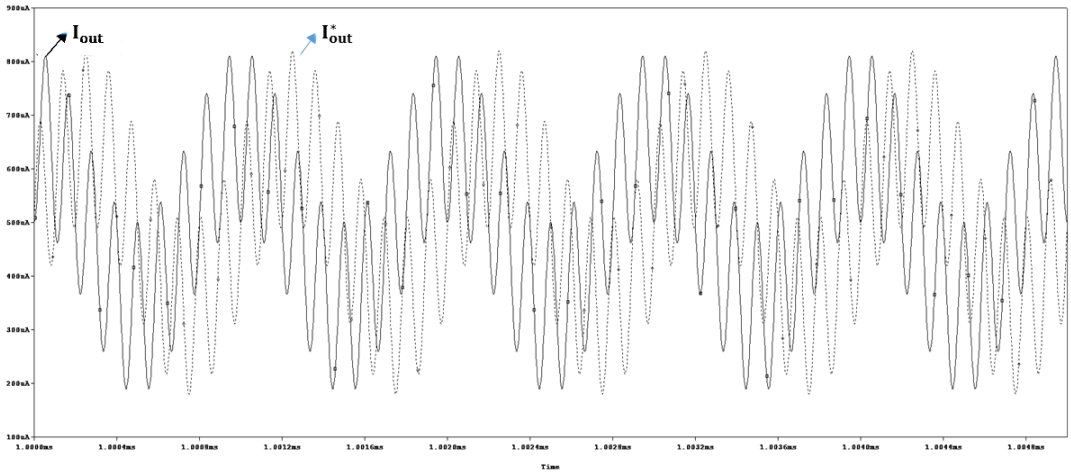

Figure 3.4 Transient plots of I_{out} and I_{out}^*.

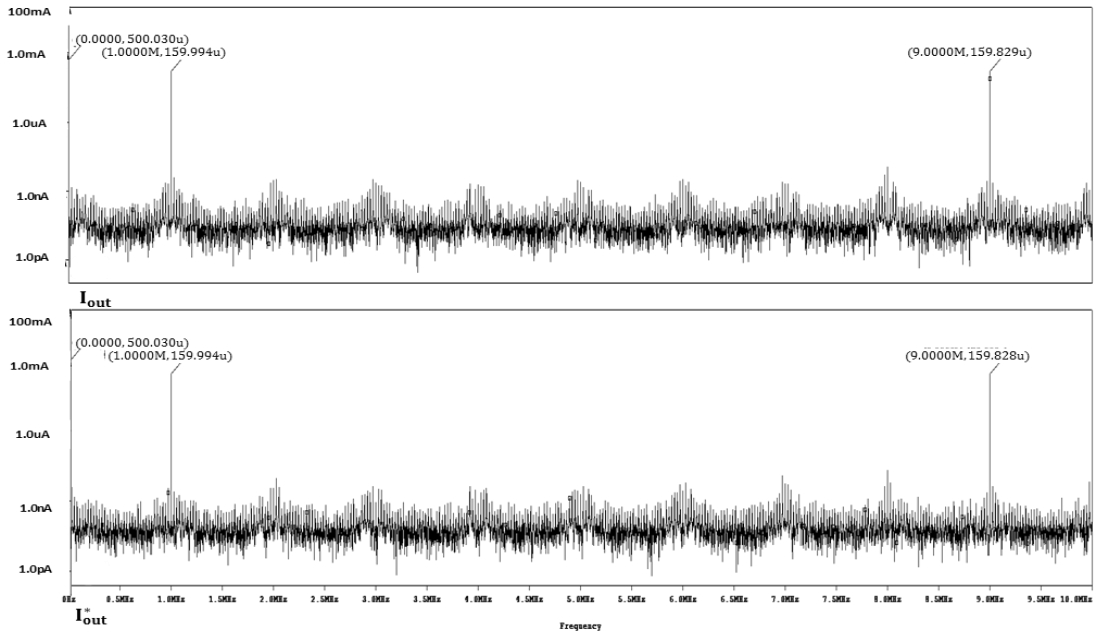

Figure 3.5 FFT spectra of I_{out} and I_{out}^*.

3.1.2 The Core Filter

Design detail

For the sake of argument, we made a little modification to the system dynamical equations given by (3.1) and focused on the input-output characteristic of the core filter:

$$\begin{vmatrix}\dot{w}_1\\ \dot{w}_2\end{vmatrix} = \begin{vmatrix}-\frac{\widehat{w_0}}{2\hat{Q}} & -w_{\hat{A}}\\ w_{\hat{A}} & -\frac{\widehat{w_0}}{2\hat{Q}}\end{vmatrix}\begin{vmatrix}w_1\\ w_2\end{vmatrix} + \frac{\widehat{w_0}}{\hat{Q}}\begin{vmatrix}u_{M1}\\ u_{M2}\end{vmatrix}, \quad y = \begin{vmatrix}w_1\\ w_2\end{vmatrix} \tag{3.8}$$

where $w_{\hat{A}} = w_A - w_M$, w_A is the carrier frequency of the input AM signal,w_M is the front end modulating frequency; $\widehat{w_0} = w_{\hat{A}}/\sqrt{1-(1/2\hat{Q})^2}$, $\widehat{w_0}$ is the center frequency and $\hat{Q}$ is the quality factor of the core filter. Note that for a high $\hat{Q}$, $w_{\hat{A}} \approx \widehat{w_0}$. u_{M1} and u_{M2} are input signals to the filter. In the synchronous complex filtering system they are generated by the preceding mixer and are two channels of quadrature modulated current with the same dc offset. We started the design with the development of an ideal Gm-C filter that only deals with small signals and provides a block-level perspective of the core filer. First, define $w_1 = v_{C1} = y_1$, $w_2 = v_{C2} = y_2$, where both state variables are ac voltages without offset. Eqn. (3.8) is now rewritten as:

$$C\dot{v}_{C1} = (-C\widehat{w_0}/2\hat{Q})v_{C1} - Cw_{\hat{A}}v_{C2} + (Cw_0/Q)u_{M1} \tag{3.9}$$

$$C\dot{v}_{C2} = Cw_{\hat{A}}v_{C1} + \left(-C\widehat{w_0}/2\hat{Q}\right)v_{C2} + (Cw_0/Q)u_{M2} \tag{3.10}$$

We then make another definition to introduce the transconductors:

$$g_{11} = -C\widehat{w_0}/2\hat{Q},\ g_{12} \approx -C\widehat{w_0},\ g_{u1} = Cw_0/Q,\ g_{21} \approx -C\widehat{w_0},\ g_{22} = -C\widehat{w_0}/2\hat{Q},\ g_{u2} = Cw_0/Q$$

It follows that the electrical network in Fig. 3.6 provides a straightforward implementation of the core filter, of which both input and output are voltage signals. The schematic suggests that the core filter can be realized with a pair of capacitors and circuits demonstrating positive or negative transconductance.

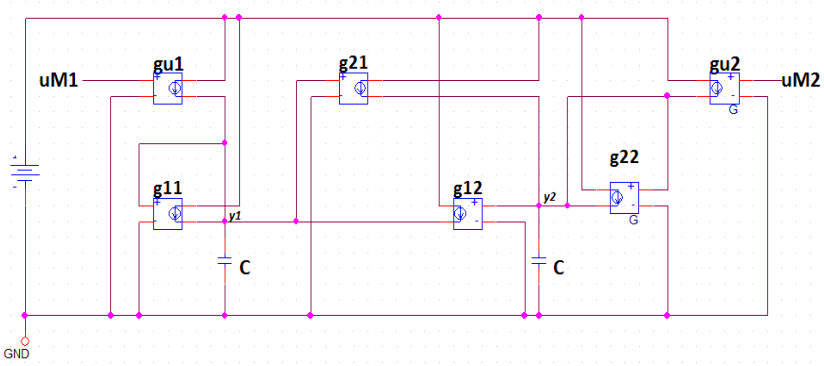

Figure 3.6 An ideal Gm-C model of the core filter.

To design a transistor-level log-domain filter, exponential mapping was first applied to the state-space description in eqn. (3.8) to derive an equation set that could be associated with an electrical network. Utilizing the synthesis technique introduced in Chapter 2, we define the system state variables as:

$$w_1 = I_s \exp\left(\frac{v_1 - v_{I_{dc}}}{v_t}\right) = y_1 , \quad w_2 = I_s \exp\left(\frac{v_2 - v_{I_{dc}}}{v_t}\right) = y_2 \qquad (3.11)$$

where v_1 and v_2 are two-diode drop voltages, $v_{I_{dc}}$ representing the base-emitter voltage drop of a BJT carrying current I_{dc}.The state equations are correspondingly converted into:

$$C\dot{v}_1 = -\frac{I_{fc}}{2Q} - I_s \exp\left(\frac{v_2 - v_1 + v_{I_{fc}}}{v_t}\right) + I_s \exp\left(\frac{v_{u_{M1}} - v_1 + v_{I_Q}}{v_t}\right) \qquad (3.12)$$

$$C\dot{v}_2 = I_s \exp\left(\frac{v_1 - v_2 + v_{I_{fc}}}{v_t}\right) - \frac{I_{fc}}{2Q} + I_s \exp\left(\frac{v_{u_{M2}} - v_2 + v_{I_Q}}{v_t}\right) \qquad (3.13)$$

where related definitions are listed as follows:

$$I_{fc} = \widehat{w_0} C v_t = I_{dc}, \quad v_{I_{fc}} = v_t \ln\left(\frac{I_{fc}}{I_s}\right) = v_{I_{dc}},$$

$$v_{M_1} = v_t \ln\left(\frac{u_{M1}}{I_s}\right) + v_t \ln\left(\frac{I_{dc}}{I_s}\right), v_{M_1} = v_t \ln\left(\frac{u_{M2}}{I_s}\right) + v_t \ln\left(\frac{I_{dc}}{I_s}\right), I_Q = \frac{I_{fc}}{Q}, \; v_{I_Q} = v_t \ln\left(\frac{I_Q}{I_s}\right).$$

The resulting equation set could be taken as nodal equations for a pair of interconnected capacitors, with one end grounded and the other end connected to a node of v_i ($i =$

1 or 2) volts. The left-hand side of each equation represents a current flowing into the related capacitor, generated by the variation in v_i, and the right-hand side is the sum of other current flows from surrounding circuitry to balance the left-hand side current. From this perspective, the core filter is implemented as shown in Fig. 3.7. For the circuit to work properly, a stable dc operating point of two-diode drop across both capacitors has to be forced. The circuitry enclosed with a dotted line is designed for this purpose. Moreover, for design simplicity, terms "v_{I_Q}" in eqn. (3.12) and (3.13) were actually implemented as $v_{0.5I_Q} = v_t\, ln(0.5I_Q/I_s)$. This modification only lowers the gain of the core filter by 0.5 and has no other influence on the transfer function.

The current sources in the circuit could be categorized based on their function: 1) Current sources "I_{fc}" that in conjunction with the capacitors set the filter's center frequency to be $\widehat{w_0} = I_{fc}/cv_t$. 2) Current sources that influence the quality factor are labeled as I_Q, and Q $\approx I_{fc}/2I_Q$. 3) Auxiliary current sources "I_{dc}" that help generate a proper dc operating point for the circuit. 4) Input currents u_{M1} and -u_{M2} that are both offset with I_{dc}. 5) If the circuit works properly, both output currents y_1 and $y_2$would have the same offset I_{dc}.

Tuning $\widehat{w_0}$ and Q of this filter is simple. For example, by changing the value of all the current sources labeled as "I_{fc}", the filter's center frequency will be tuned while its bandwidth remains the same. Similarly, varying the value of all the "I_Q" sources will change the bandwidth of the filter without affecting the filter's center frequency.

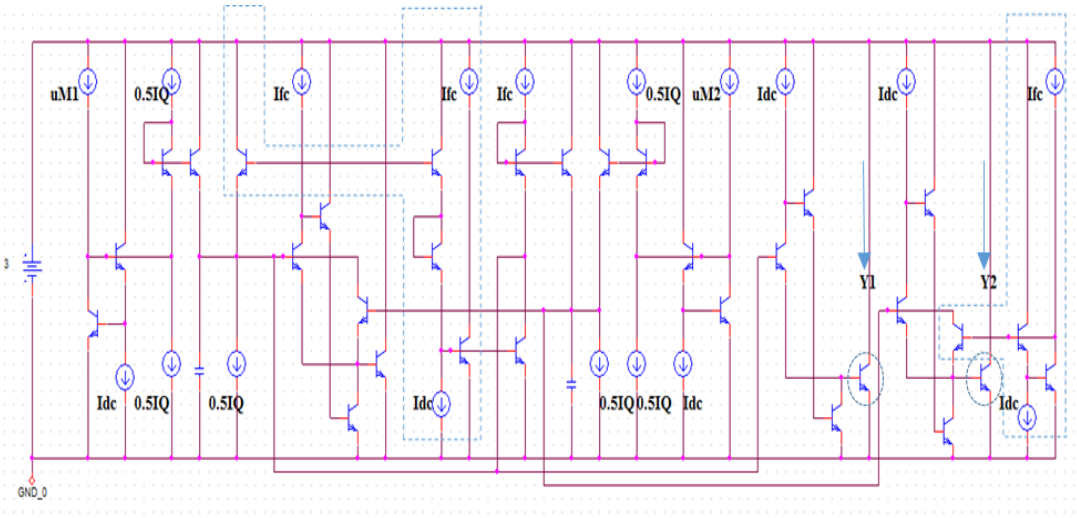

Figure 3.7 A log-domain complex filter implemented with the state-space exponential mapping technique.

Simulation setup and results

We simulated the transistor level log-domain complex filter above with PSpice to test its function and properties. The tests include: 1) Generating Bode plots to verify the bandpass filtering function and the electronic tunability in both center frequency and quality factor. 2) Transient test on the combination of the filter and its preceding modulator, to check out signal integrity and verify the image rejection capability of the filter.

Test 1: Transfer function verification

The state space equation set corresponding to the design in Fig. 3.7 is a little different from eqn. (3.8) in the input matrix, which only halves the gain of the resulting filter. The equation set is formulated as below:

$$\begin{vmatrix}\dot{w}_1\\ \dot{w}_2\end{vmatrix} = \begin{vmatrix}-\frac{\widehat{w_0}}{2\hat{Q}} & -w_{\hat{A}}\\ w_{\hat{A}} & -\frac{\widehat{w_0}}{2\hat{Q}}\end{vmatrix}\begin{vmatrix}w_1\\ w_2\end{vmatrix} + \frac{\widehat{w_0}}{2\hat{Q}}\begin{vmatrix}u_{M1}\\ u_{M2}\end{vmatrix}, \qquad y = \begin{vmatrix}w_1\\ w_2\end{vmatrix} \qquad (3.14)$$

To estimate the performance of the core filter, all the transfer functions relevant to eqn. (3.14) were derived and listed below:

$$H_{11} = \frac{w_1}{u_{M1}} = \frac{(s+\frac{\widehat{w_0}}{2\hat{Q}})\frac{\widehat{w_0}}{2\hat{Q}}}{s^2+\frac{\widehat{w_0}}{\hat{Q}}s+w_{\hat{A}}{}^2+(\frac{\widehat{w_0}}{2\hat{Q}})^2} \quad (u_{M2}=0),\ H_{21} = \frac{w_2}{u_{M1}} = \frac{-(\frac{\widehat{w_0}}{2\hat{Q}})w_{\hat{A}}}{s^2+\frac{\widehat{w_0}}{\hat{Q}}s+w_{\hat{A}}{}^2+(\frac{\widehat{w_0}}{2\hat{Q}})^2} \quad (u_{M2}=0)$$

$$H_{12} = \frac{w_1}{u_{M2}} = \frac{(\frac{\widehat{w_0}}{2\hat{Q}})w_{\hat{A}}}{s^2+\frac{\widehat{w_0}}{\hat{Q}}s+w_{\hat{A}}{}^2+(\frac{\widehat{w_0}}{2\hat{Q}})^2} \quad (u_{M1}=0),\ H_{22} = \frac{w_2}{u_{M2}} = \frac{(s+\frac{\widehat{w_0}}{2\hat{Q}})\frac{\widehat{w_0}}{2\hat{Q}}}{s^2+\frac{\widehat{w_0}}{\hat{Q}}s+w_{\hat{A}}{}^2+(\frac{\widehat{w_0}}{2\hat{Q}})^2} \quad (u_{M1}=0)$$

(3.15)

To verify the above transfer functions are successfully implemented, the core filter center frequency was tuned to 1MHz and the quality factor was tuned to be 50. Therefore, $\frac{\widehat{w_0}}{2\hat{Q}}$ is two orders of magnitude lower than $\widehat{w_0}$, and $w_{\hat{A}}$ would be very close to $\widehat{w_0}$. The setup also suggests that the magnitude spectra of H_{11} and H_{22} would be similar to that of a bandpass filter whose center frequency is close to 1MHz and peak gain is about -6dB. Also, H_{21} and H_{12} are expected to have magnitude spectra similar to that of a second-order lowpass filter, with a pass-band gain of -40dB, an overshoot peak at 1MHz and a rolloff slope of -40dB/dec, approximately. To plot H_{11} and H_{21}, u_{M2} was set up as Idc and u_{M1} was an ac current offset with Idc. We switched the setup for u_{M1} and u_{M2} to generate the Bode plot of H_{12} and H_{22}. All the plots generated, as shown in Fig. 3.8 and Fig. 3.9, agree with our expectation. Note that the minus sign in H_{12} indicates an introduced phase shift of 180 degrees, which is verified by the phase spectrum of H_{12}.

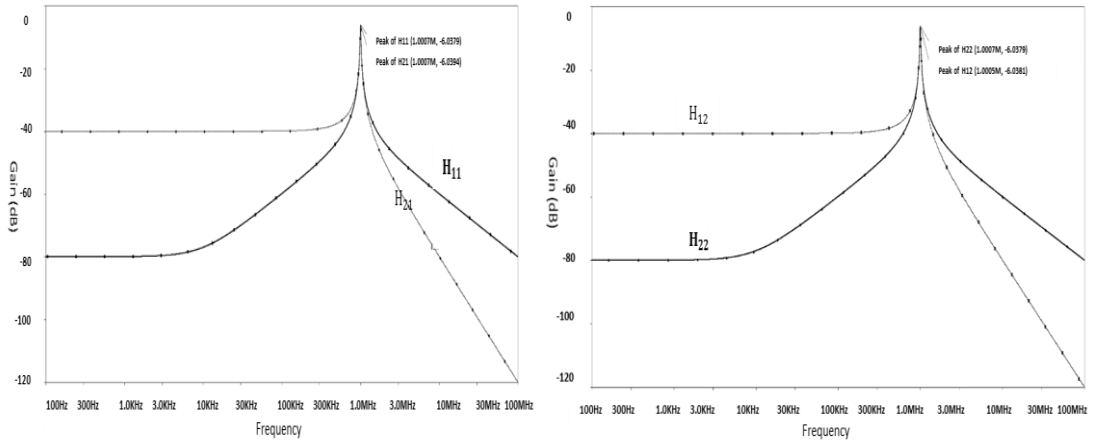

Figure 3.8 Magnitude spectra of H_{11}, H_{21}, H_{12}, H_{22} for a complex filter with fc=1MHz, Q=50.

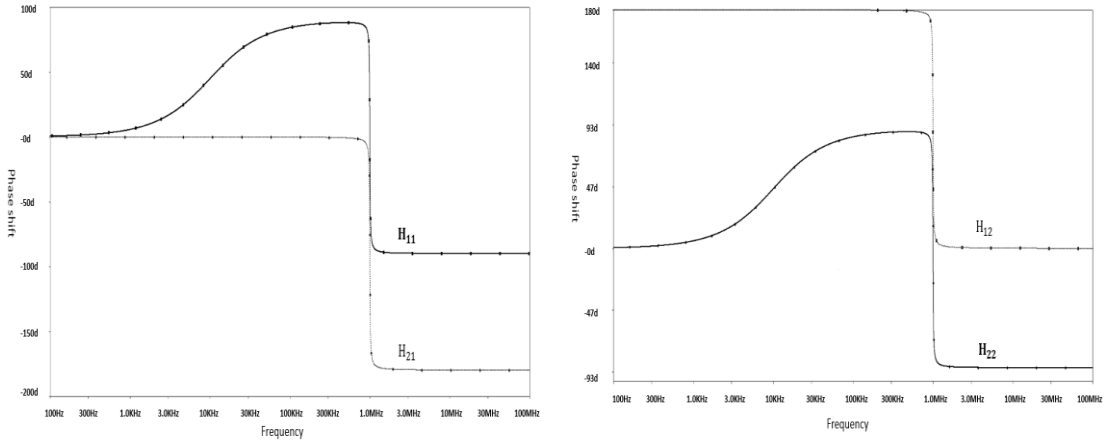

Figure 3.9 Phase spectra of H_{11}, H_{21}, H_{12}, H_{22} for a complex filter with fc=1MHz, Q=50.

Test 2: Image rejection capability

Typically, a complex filter takes a pair of quadrature signals as input and it is capable of distinguishing one frequency component from its image with respect to the center frequency. Therefore, the core filter should be able to attenuate the input quadrature signal pair in certain phase relationship (u_{M1} leads/lags u_{M2} by 90 degrees) to a negligible level while letting the quadrature pair in the opposite phase relationship (u_{M1} lags/leads u_{M2} by 90 degrees) pass through. Dual-channel ac input was set up in the following simulation to test the image rejection capability of the designed filter.

Specifically, u_{M1} was set up to lead and lag u_{M2} by 90 degrees respectively. As shown in Fig. 3.10, the magnitude and phase spectra suggest that input quadrature pairs with u_{M1} lagging u_{M2} by 90 degrees will be attenuated heavily, while the input quadrature pairs in the opposite phase relationship will be bandpass filtered in the frequency range near 1MHz. The magnitude spectra also indicate that the peak image rejection ratio of the filter about -50dB.

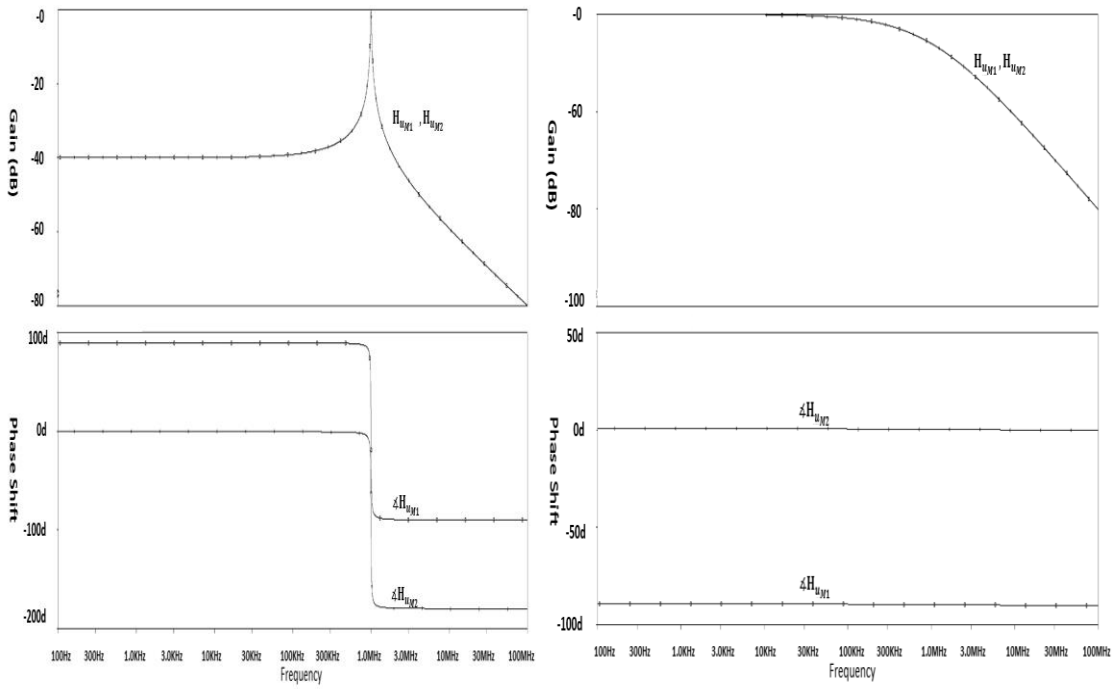

(a) (b)

Figure 3.10 Gain and phase spectra of the quadrature input signals corresponding to (a) u_{M1} leading u_{M2} by 90 degrees and (b) u_{M1} lagging u_{M2} by 90 degrees.

Test 3: Center frequency and quality factor tunability

Due to the particular implementation technique we used, the resulting filter is supposed to be electronically tunable in both center frequency and quality factor with great convenience. In this section, we generated gain and phase spectra of the input quadrature signals while sweeping either I_{fc} or I_Q over certain range.

Test 3.1 Center frequency tunability

Current sources setup: IQ=5u (Q=50), Ifc: 320u, 410u, 500u, 660u, 720u.

Test results:

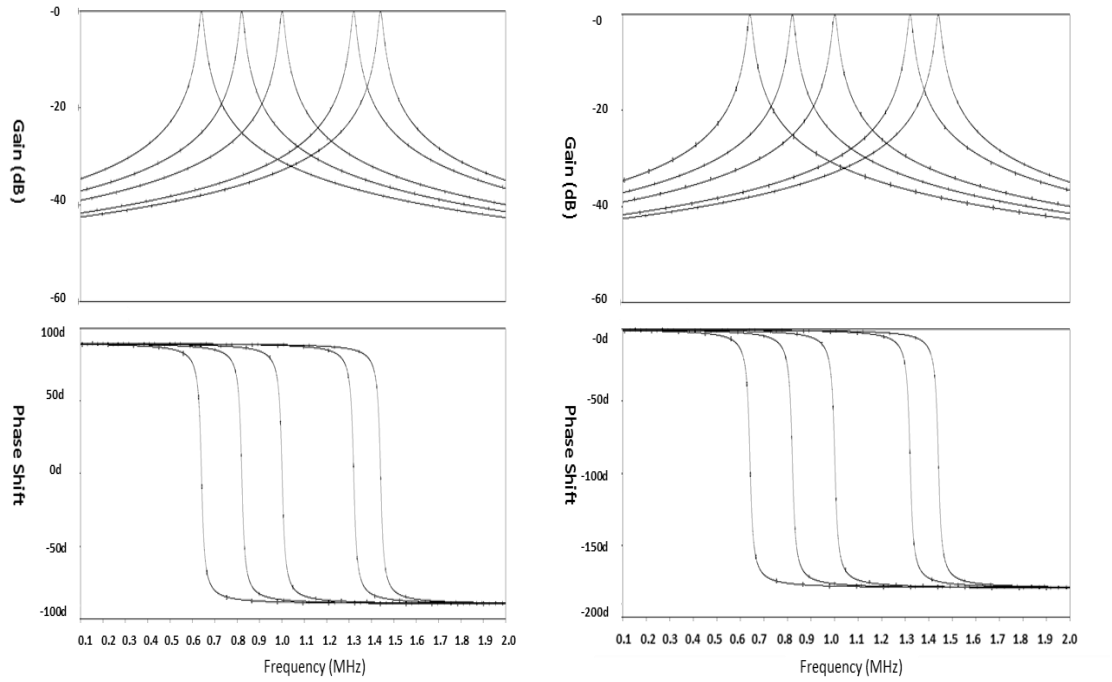

(a) (b)

Figure 3.11 Gain and phase spectra of (a) the leading input and (b) the lagging input in the center frequency tunability test.

Current Setup	Ifc	320u	410u	500u	660u	720u
	IQ	5u	5u	5u	5u	5u
Center Frequency (Hz)	u1	**640.279k**	**820.396k**	**1.001meg**	**1.321meg**	**1.441meg**
	u2	**640.279k**	**820.396k**	**1.001meg**	**1.321meg**	**1.441meg**
Quality Factor	u1	32.031	41.024	50.024	65.979	71.962
	u2	32.031	41.024	50.024	65.979	71.962
Bandwidth (Hz)	u1	**19.990k**	**19.998k**	**20.005k**	**20.017k**	**20.021k**
	u2	**19.990k**	**19.998k**	**20.005k**	**20.017k**	**20.021k**
Peak Gain (dB)	u1	-0.011	-0.014	-0.018	-0.023	-0.025
	u2	-0.011	-0.014	-0.018	-0.023	-0.025

Table 3-1 Measurement result from Test 3.1 (u1: the leading input; u2: the lagging input).

The test results above explicitly verify that the filter's center frequency is proportional to I_{fc}, the bandwidth is proportional to I_Q and the Q factor is determined by the ratio of

I_{fc} to I_Q. Varying I_c while maintaining I_Q changes the filter's center frequency and Q factor but barely affects its bandwidth.

Test 3.2 Quality factor tunability

Current sources setup: Ifc =500u (fc=1MHz), IQ sweeping: 1u, 2u, 5u, 10u, 20u.

Test results:

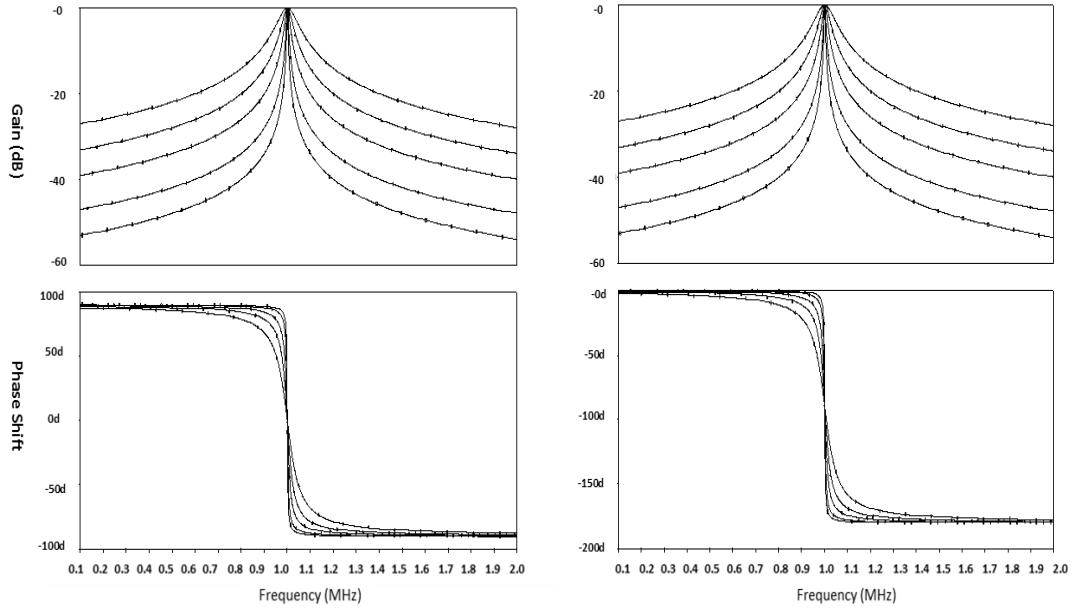

(a) (b)

Figure 3.12 Gain and phase spectra of (a) the leading input and (b) the lagging input in the Q factor tunability test.

Current Setup	Ifc	500u	500u	500u	500u	500u
	IQ	1u	2u	5u	10u	20u
Center Frequency (Hz)	u1	**1.001meg**	**1.001meg**	**1.001meg**	**1.000meg**	**1.000meg**
	u2	**1.001meg**	**1.001meg**	**1.001meg**	**1.000meg**	**1.000meg**
Quality Factor	u1	**247.538**	**124.489**	**50.009**	**25.006**	**12.502**
	u2	**247.538**	**124.489**	**50.009**	**25.006**	**12.502**
Bandwidth (Hz)	u1	4.042k	8.037k	20.006k	40.004k	79.966k
	u2	4.042k	8.037k	20.006k	40.004k	79.966k
Peak Gain (dB)	u1	-0.096	-0.046	-0.018	-0.009	-0.004
	u2	-0.096	-0.045	-0.018	-0.009	-0.004

Table 3-2 Measurement result from Test 3.2 (u1: the leading input; u2: the lagging input).

According to measurement results, Q factor of the filter is inversely proportional to IQ. In the tuning of the Q factor, the center frequency stays at 1MHz and the filter's peak gain is consistently close to unity.

Test 4: Transient tests

The first transient test run on the combination of the front end modulator and the complex filter was to evaluate the signal integrity during the modulation and filtering process. In the following image rejection test, another AM signal was generated, which is the image of the input signal used in the first test with respect to the core filter's center frequency. The specific test setup, important plots and observation are given below.

Test 4.1 Front end modulation and complex filtering

The transient plots and corresponding FFT spectra of the original AM signal, modulator output and filter output are plotted. The system input is an AM current signal generated by mixing an offset 10kHz sine wave with a 5MHz carrier, plus a dc offset. Main components of the input include dc, 4.99MHz, 5MHz and 5.01MHz, as shown in Fig. 3.13. The front end modulating frequency was set to be 4MHz, as the designed modulator performs sub-heterodyning and the following filter is centered at 1MHz. After the modulation, ac components in the received AM signal will be shifted to the sum and difference of 5MHz and 4MHz and the dc component will be shifted to 4MHz. Fig. 3.14 and Fig. 3.15 respectively show the left channel input/output and right channel input/output signals of the core filter. According to the core filter setup (fc=1MHz, Q=50), it is expected that the filter attenuates frequency components far away from 1MHz to a negligible level, suppresses the sideband signals at 0.99MHz and 1.01MHz by approximately 3dB and provides unity gain to the components at 1MHz.

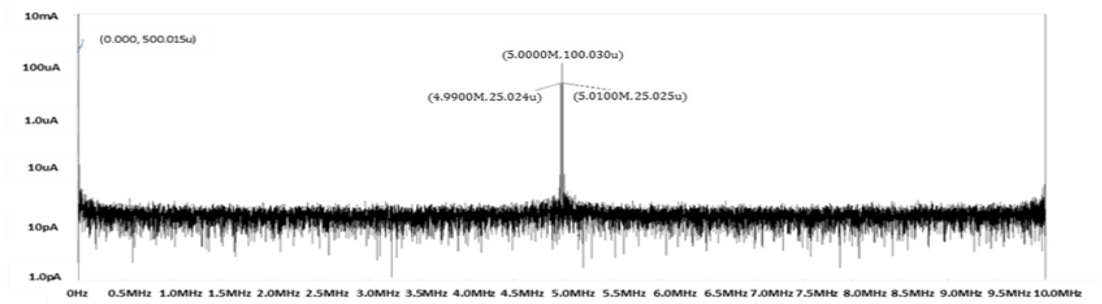

Figure 3.13 FFT spectrum of the input AM signal

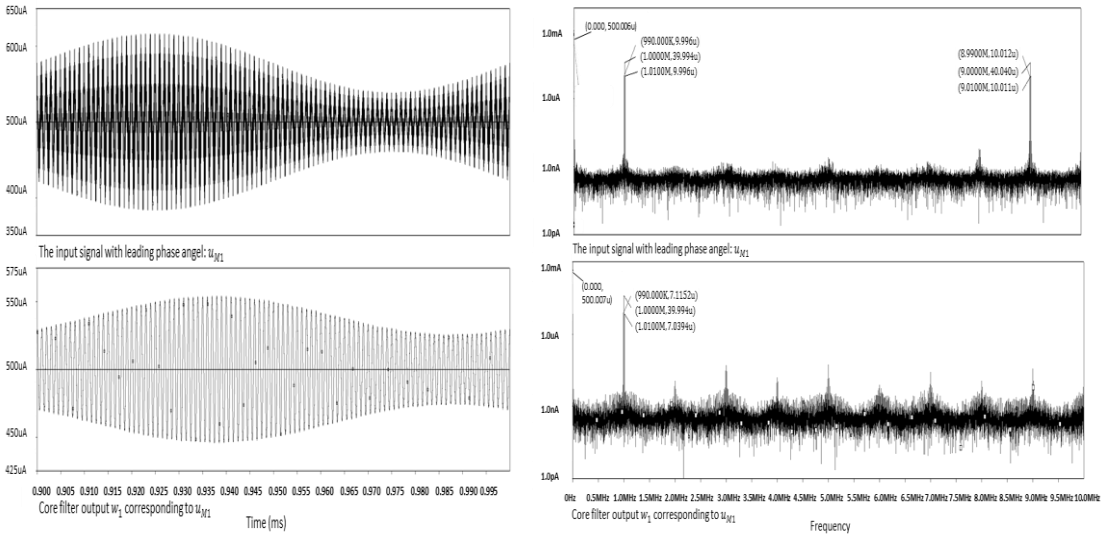

Figure 3.14 Transient plots and FFT spectra of the left channel input u_{M1} and the corresponding output w_1.

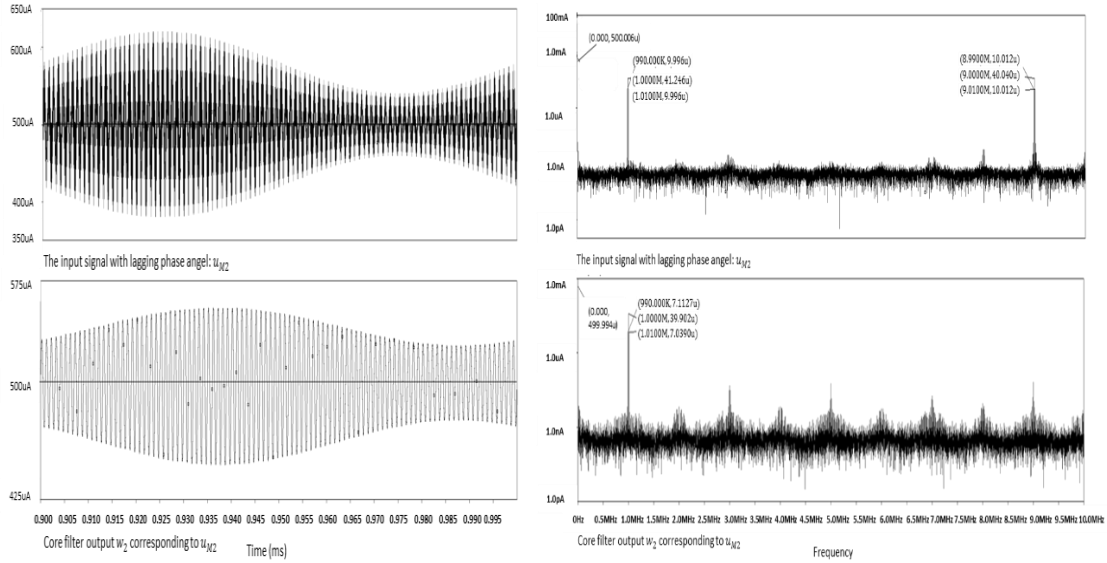

Figure 3.15 Transient plots and FFT spectra of the right channel input u_{M2} and corresponding output w_2.

The figures above show that the modulator generates a pair of quadrature signals from the AM input and the filter processes the quadrature signals exactly as expected. No distortion is observed in the transient plots. Comparing the spectra of the input and corresponding output, the average noise level is a little higher after filtering. The introduced noise is of a negligible size and mainly distributes near harmonics of 1MHz, which might be the computation noise generated by the simulator.

Test 4.2 Image rejection

To generate the image counterpart of the above input AM signal, the carrier was switched from 5MHz to 3MHz, which is the image of the original carrier with respect to 4MHz. The new system input is represented by the FFT spectrum below. The AM signal is then processed by the front end modulator, which yields two channels of quadrature signal, both containing components at dc, 0.99MHz, 1MHz, 1.01MHz, 6.99MHz, 7MHz and 7.01MHz. It's expected that the bandpass filtering function of the complex filter (centering at 1MHz) attenuates the components at 6.99MHz, 7MHz and 7.01MHz to a negligible level. On the other hand, due to the particular respective phase relationship between the components at 0.99MHz, 1MHz and 1.01MHz in the the two channels, all of them are supposed to be attenuated heavily. Therefore, both output channels of the filter should ideally have no ac component. Fig. 3.17 and Fig. 3.18 respectively show the left channel and right channel input, and their corresponding output from the filter. The image rejection capability is verified by comparing the output signals in Fig. 3.17 and Fig. 3.18 to that in Fig. 3.14 and Fig. 3.15.

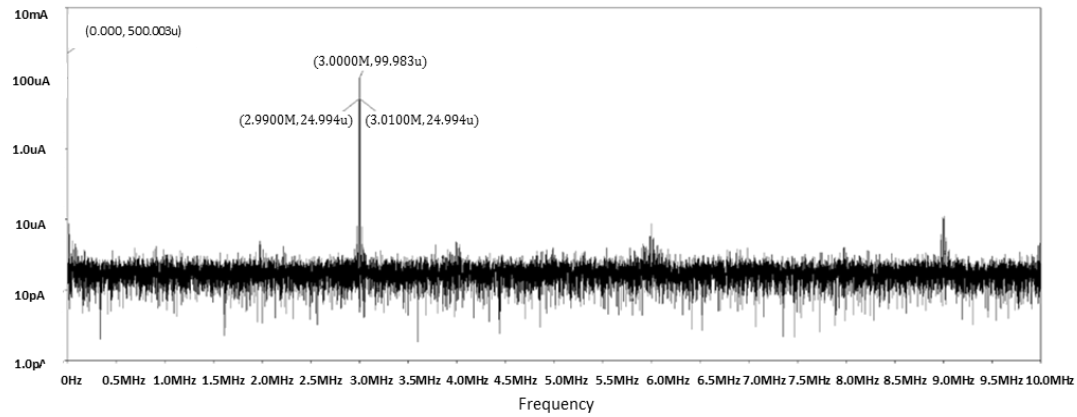

Figure 3.16 FFT spectrum of the input AM signal for the image rejection test, which is the image of the input AM signal in Fig. 3.13 about 4MHz.

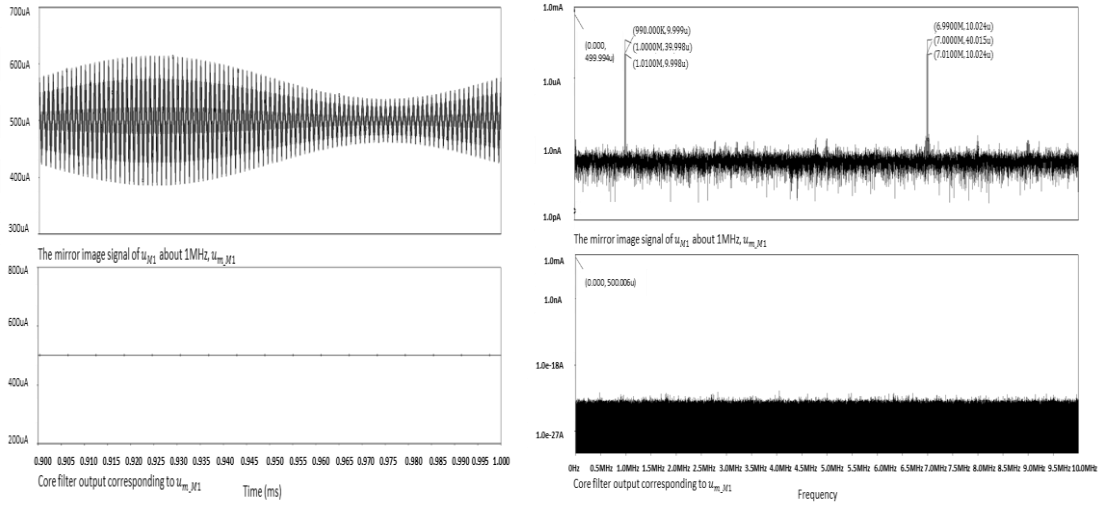

Figure 3.17 Transient plots and FFT spectra of u_{m_M1}, the image signal of u_{M1} and its corresponding core filter output.

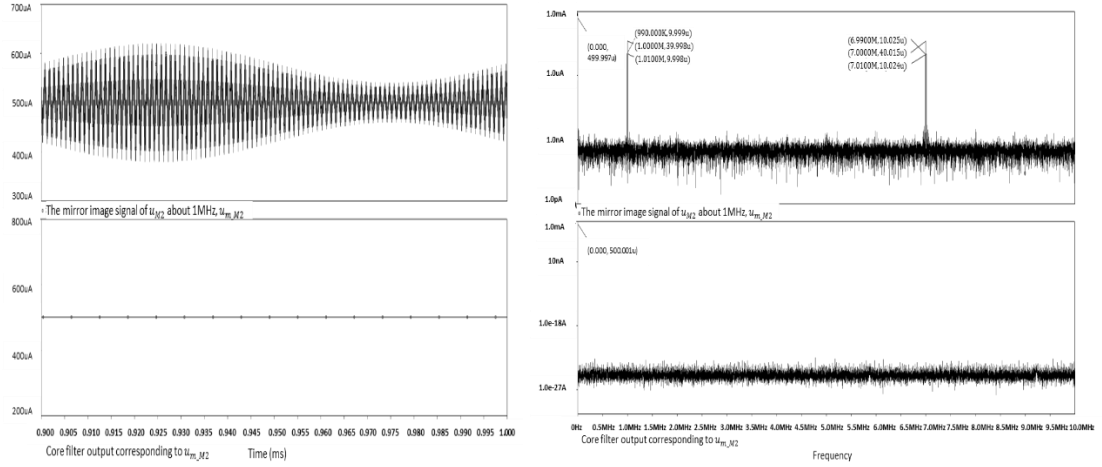

Figure 3.18 Transient plots and FFT spectra of u_{m_M2}, the image of u_{M2} and its corresponding core filter output.

3.1.3 The Back End Modulator

Design detail

This block applies frequency shifting to the core filter output. It consists of an interface circuit, a pair of mixers and a current subtractor. The interface acts as both a voltage-current converter and a differential signal generator. Connecting the base of the output transistors in Fig. 3.7(the two circled transistors) to the base of the two input transistors of the interface circuit, the output currents of the core filter are directly 'copied' to the interface circuit. As both input currents have the same dc offset I_{dc}, two current sources of $2I_{dc}$ are used to generate the differential of the input, which is needed in the subsequent modulation. The following circuitry is similar to the front end modulator and it is able to perform either up conversion or down conversion, depending on the setup of local oscillators. Specifically, if I_{LO2} has the same frequency as I_{LO1} in the front end modulator, the backend modulator would generate an up-converted output signal, so the system is equivalent to a complex filter. If I_{LO2} oscillates at a frequency that equals the core filter's center frequency, then the system is capable of recovering the baseband information carried by the received AM signal. Note that the quadrature and differential current sources eed to be carefully set up in order to implement the expected conversion. Schematic of the modulator is shown in Fig. 3.19, where the output is labeled as IOUT and could be expressed as:

$$I_{OUT} = \frac{2I_{LO2\_ac} \cdot y_{1\_ac}}{I_{dc}} - \frac{2\widetilde{I_{LO2}}^{*}_{\_ac} \cdot y_{2\_ac}}{I_{dc}} + I_{dc} \qquad (3.16)$$

where I_{LO2_ac}, y_{1_ac}, $\widetilde{I_{LO2}}^{*}_{\_ac}$, y_{2_ac} are ac components in signal I_{LO}, y_1, $\widetilde{I_{LO2}}^{*}$, y_2.

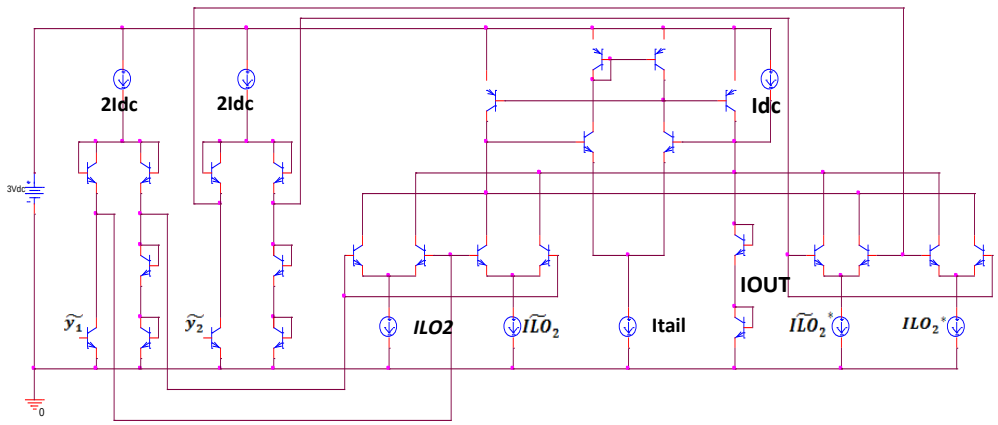

Figure 3.19 Schematic of the back end modulator. The notation y1and y2, ILO2, IOUT means the two channels of input current, the current generated by local oscillator and offset with Idc, and the block output. The symbols '∼' and '∗', respectively, stand for the differential and quadrature counterpart of a signal.

Simulation setup and results

Transient simulation was run to test both up-conversion and down-conversion performance of the modulator. In the up conversion test, the back end modulating frequency was set to be 4MHz, and I_{OUT} is expected to be a bandpass filtered version of the input AM signal. Fig. 3.20 shows the transient plots and FFT spectra of the system's input and output. Comparison between the transient plots shows that the introduced phase shift to the input sideband signals is approximately 45 degrees. Also, according to the parameter setup, the gain contributed by the front end and back end modulators together is 0.64. Measurement results labeled on the spectra suggest that the core filter in the system provides a peak gain of unity to the components equal or very close to 5MHz, the gain drops by 3dB at 4.99MHz and 5.01MHz. That is to say, the center frequency of the overall system is approximately 5MHz and the quality factor is about 250. Simulation results from the down conversion test are shown in Fig. 3.21, in which the back end modulating frequency was tuned to 1MHz and the phase of all the back end

modulating signals was accordingly adjusted. In the spectrum of the recovered baseband signal, most energy concentrates at dc and 10kHz, harmonic distortion at a negligible level is observed.

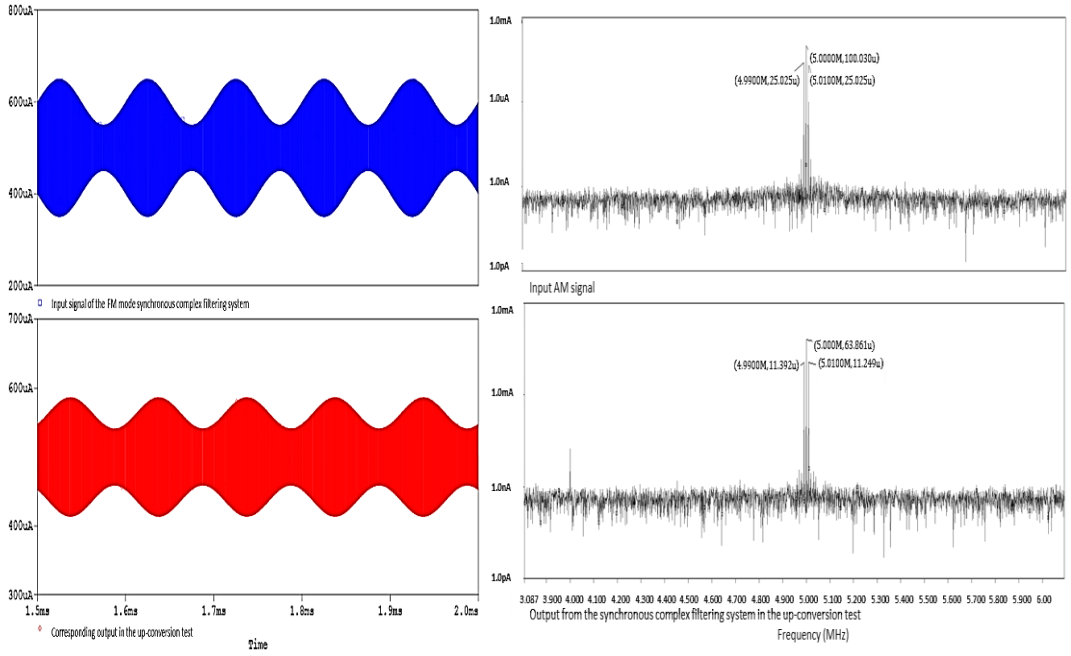

Figure 3.20 Transient plots and FFT spectra of the input and output current signals of the static synchronous complex filtering system in the up conversion test.

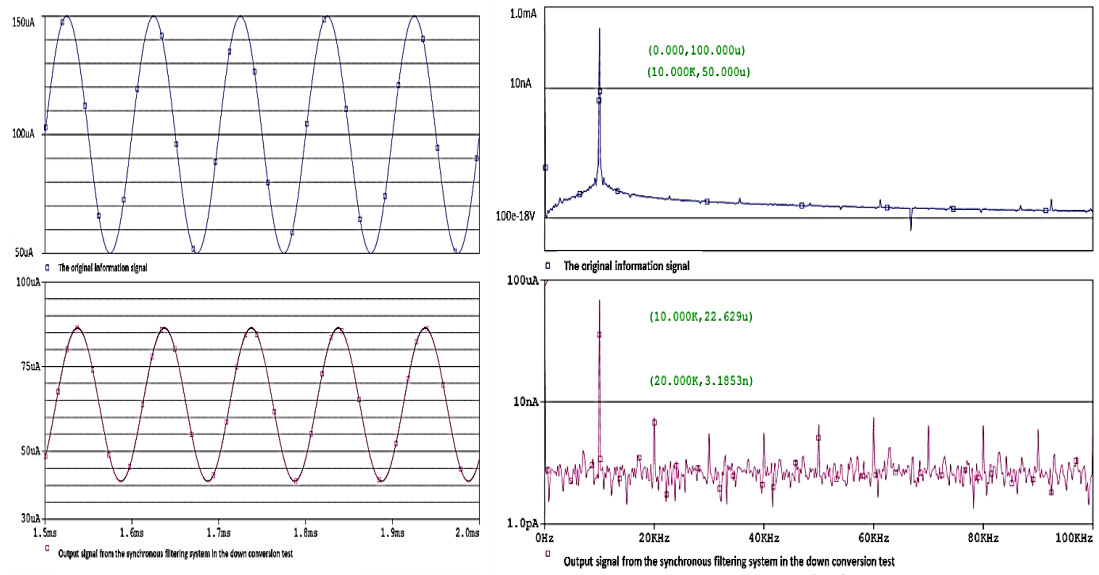

Figure 3.21 Transient plots and FFT spectra of the original modulating signal and the output signal from the synchronous complex filtering system in the down conversion test.

3.1.4 Overall System Test

Gain spectrum

To verify that the synchronous filtering system designed above, when performing up conversion in the back end, implements the input-output function of a complex filter, we plotted its gain spectrum over certain frequency range. Specifically, the system core filter was set up with $f_c = 1\text{MHz}$ and $Q = 50$, whose gain spectrum is plotted in Fig. 3.22(a); the carrier frequency of the system's AM input was 5MHz and a series of baseband signals ranging from dc to 50kHz were used as the information signal. In the superheterodyne mode, both the front end and back end modulating frequencies were set to be 6MHz; in the subheterodyne mode, they were tuned to 4MHz. The gain spectra generated in both modes were plotted in Fig. 3.22(b), and they almost overlap. Compared to the spectrum in Fig. 3.22(a), it's obvious that the synchronous complex filter has higher center frequency and higher Q factor. Moreover, the magnitude spectrum of the transfer function of a biquad complex filter with $f_c = 5\text{MHz}$ and Q=250 was plotted too. The strong resemblance between the three plots in Fig. 3.22(b) clearly proves the functional equivalence between the synchronous filtering system with a low-Q low-center frequency core filter ($f_c = 1\text{MHz}$ and $Q = 50$) and a complex filter with high-Q high-center frequency($f_c = 5\text{MHz}$ and Q=250).

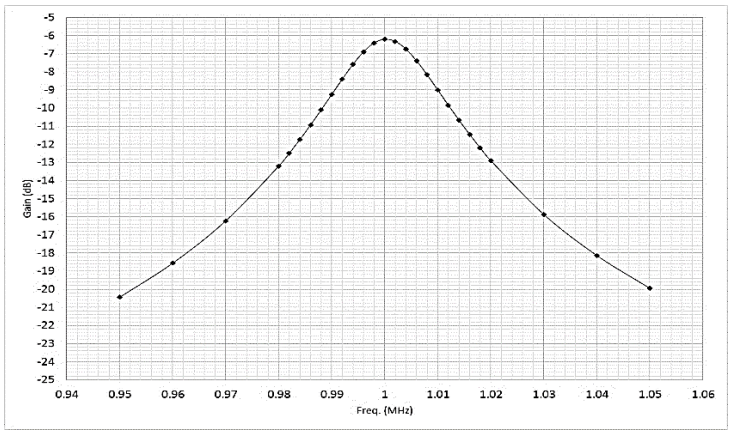

(a)

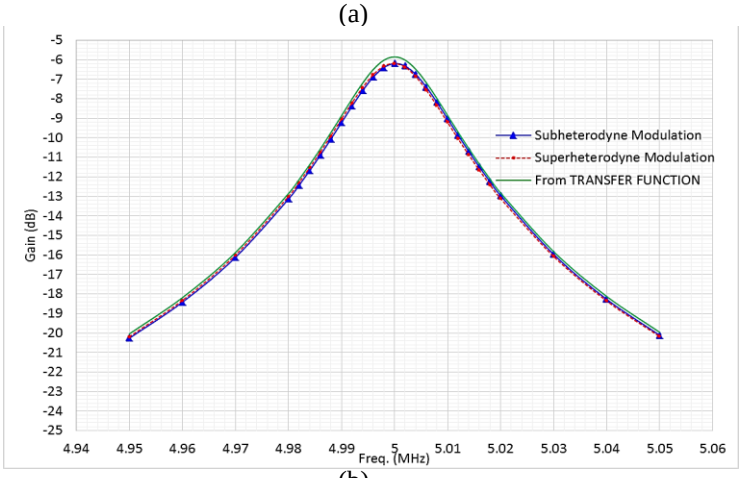

(b)

Figure 3.22 The gain spectrum of (a) a biquad complex filter with $f_c = 1\text{MHz}$ and $Q = 50$, (b) a static synchronous complex filter developed with the core filter specified by (a), in both subheterodyne mode and superheterodyne mode. The magnitude spectrum of the transfer function of a complex filter given by H_{11} (H_{22}) in eqn. 3.15, with $w_{\hat{0}} = w_{\hat{A}} = 5\text{MHz}$ and $Q = 250$, is also plotted in (b) as a reference.

Image rejection

A synchronous complex filter in the subheterodyne mode was tested first. The front end and back end modulating frequency was set to be 4MHz. The input currents were generated by mixing a baseband information signal at 10kHz with carriers at 5MHz and 3MHz respectively, so that they form an image pair with respect to 4MHz. Plots in Fig. 3.23(a) and (b) suggest that the synchronous filtering system is able to suppress the input signal carried by 3MHz to approximately 45dB lower than the filtered version of

the input carried by 5MHz. The filter was then modified into superheterodyne mode and its end modulating frequency was still 4MHz. Simulation results in Fig. 3.23 (c) and (d) show that the new filter lets the input signal carried by 3MHz pass through while heavily suppresses the signal carried by 5MHz, which is excatly opposite to the performance of the subheterodyne mode system. Therefore, a synchronous complex filter in either mode maintains the image rejection capability, and the subheterodyne synchronous complex filter shows slightly stronger image suppression capability.

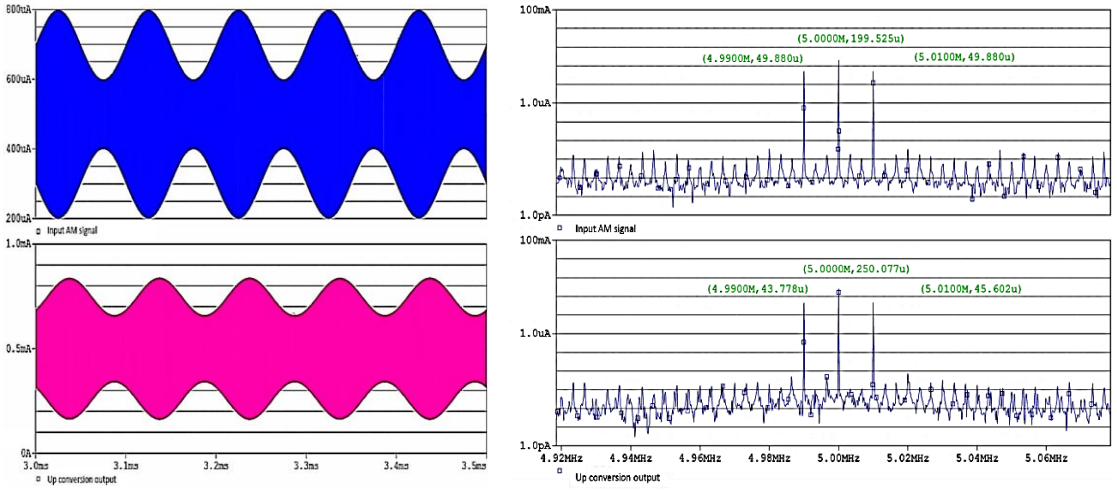

(a) The AM input carried by 5MHz and the up conversion output from a subheterodyne synchronous complex filter

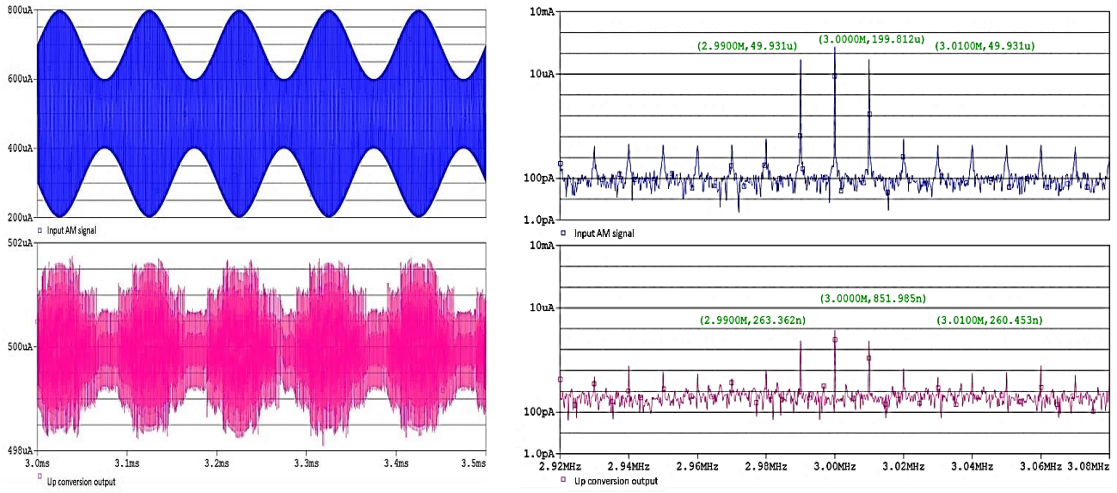

(b) The AM input carried by 3MHz and the up conversion output from a subheterodyne synchronous complex filter

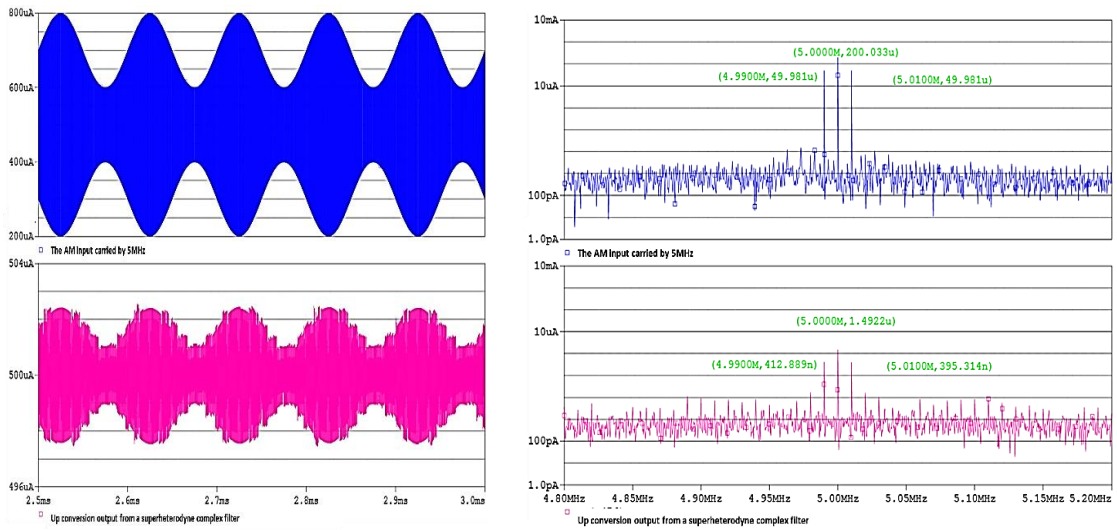

(c) The AM input carried by 5MHz and the up conversion output from a superheterodyne synchronous complex filter

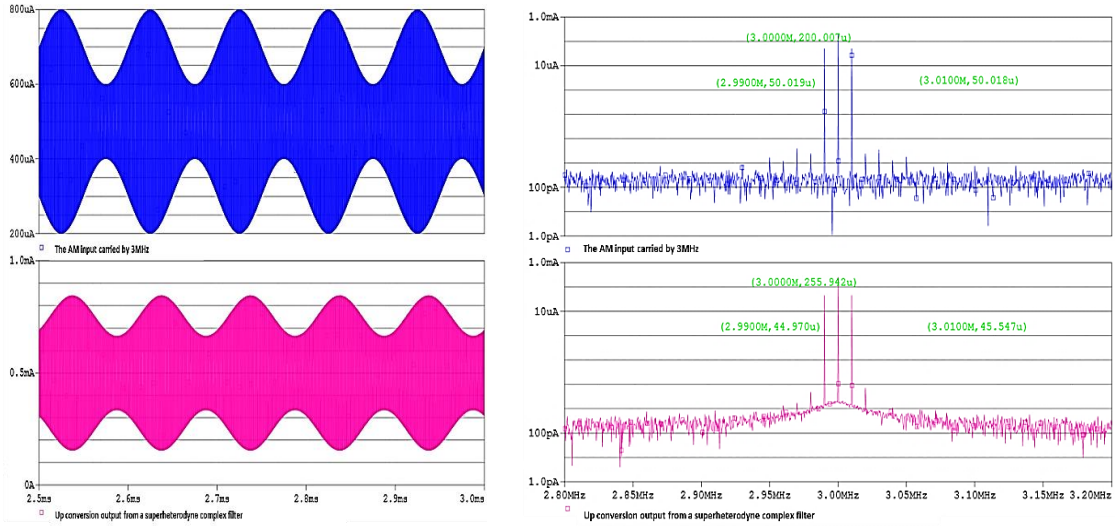

(d) The AM input carried by 3MHz and the up conversion output from a superheterodyne synchronous complex filter

Figure 3.23 Results from the image rejection test on a static synchronous complex filter with front end and back end modulating frequency at 4MHz, in either subheterodyne or superheterodyne mode.

3.2 Design of a Dynamic FM Mode Synchronous Complex Filter

3.2.1 The Mathematical Model

In this section, we develop a more sophisticated FM mode synchronous filter, which is in the same architecture as the system implemented above but with time-varying

core filter center frequency and both end modulating frequencies. A dynamic synchronous complex filter could be represented by either eqn. (3.17) or eqn. (3.18), depending on the front end modulation mode.

$$\begin{vmatrix}\dot{w}_1\\ \dot{w}_2\end{vmatrix} = \begin{vmatrix}-\widehat{w_0}/2\widehat{Q} & -w_{\widehat{A}}(t)\\ -w_{\widehat{A}}(t) & -\widehat{w_0}/2\widehat{Q}\end{vmatrix}\begin{vmatrix}w_1\\ w_2\end{vmatrix} + \sqrt{2}(\widehat{w_0}/\widehat{Q})\begin{vmatrix}\sin(\phi(t))\\ \cos(\phi(t))\end{vmatrix} u$$

$$y = \sqrt{2}/2|\sin(\phi(t)) \quad \cos(\phi(t))|\begin{vmatrix}w_1\\ w_2\end{vmatrix} \qquad (3.17)$$

$$\begin{vmatrix}\dot{w}_1\\ \dot{w}_2\end{vmatrix} = \begin{vmatrix}-\widehat{w_0}/2\widehat{Q} & -w_{\widehat{A}}(t)\\ w_{\widehat{A}}(t) & -\widehat{w_0}/2\widehat{Q}\end{vmatrix}\begin{vmatrix}w_1\\ w_2\end{vmatrix} + \sqrt{2}(\widehat{w_0}/\widehat{Q})\begin{vmatrix}\cos(\phi(t))\\ \sin(\phi(t))\end{vmatrix} u$$

$$y = \sqrt{2}/2|\cos(\phi(t)) \quad \sin(\phi(t))|\begin{vmatrix}w_1\\ w_2\end{vmatrix} \qquad (3.18)$$

where $\widehat{w_0}$ is the dc offset of the time-varying core filter center frequency, $\widehat{Q}$ is the dc offset of the time-varying quality factor, while $\widehat{w_0}/\widehat{Q}$ is time invariant; $w_{\widehat{A}}(t)$ is the time-varying center frequency of the core filter; eqn. (3.17) represents a subheterodyne mode system, where $d\phi(t)/dt = w_A - w_{\widehat{A}}(t)$; eqn. (3.18) represents a superheterodyne mode system, and $d\phi(t)/dt = w_A + w_{\widehat{A}}(t)$; w_A is the carrier frequency of system input u. In principle, a dynamic synchronous complex filter maintains the function of the targeted complex filter as long as $d\phi(t)/dt = w_A - w_{\widehat{A}}(t)$ (subheterodyne) or $d\phi(t)/dt = w_A + w_{\widehat{A}}(t)$ (superheterodyne), but some particular variation patterns for $w_{\widehat{A}}(t)$ are preferable if they have the following properties: 1) the associated phase angle $\phi(t)$ in the modulating signals is simple, implementable and conveniently tunable; 2) the synchronized variation of the core filter center frequency and the modulating frequencies makes the system superior to its static counterpart in noise performance. Taking these concerns into consideration, two types

of $w_{\hat{A}}(t)$ are proposed here. One pattern of our interest is the sinusoidal waveform. Recall that the core filter center frequency is proportional to the center frequency control current "I_{fc}", so to realize the sinusoidal center frequency specified by eqn. (3.19), we only need to set up the control currents as given by eqn. (3.20). The phase angle $\phi(t)$ of the modulating signals is accordingly derived as eqn. (3.21).

$$w_{\hat{A}}(t) = w_0 + \Delta w_0 \sin(w_{var} t) \quad (3.19)$$

$$I_{fc}(t) = I_{os} + (\frac{\Delta w_0}{w_0}) I_{os} \sin(w_{var} t) \quad (3.20)$$

$$\phi(t) = w_M t - (\frac{\Delta w_0}{w_{var}}) \cos(w_{var} t) \quad (3.21)$$

where w_0 is the offset component in the time-varying center frequency, Δw_0 represents the center frequency variation range, w_{var} is the variation rate; $I_{os} = CV_T w_0$ and C is the value of the capacitors in the filter.

The other proposed pattern of $w_{\hat{A}}(t)$ is the square waveform. Suppose that the dc offset of the core filter's time-varying center frequency is w_0, the variation range is $w_0 \pm \Delta w_0$ and the switching rate is w_{var}, then the control current $I_{fc}(t)$ should be a square waveform at frequency w_{var}, with peak value of $(\frac{\Delta w_0}{w_0}) I_{os}$ and an offset of I_{os}. The phase angle $\phi(t)$ in synchronization with $w_{\hat{A}}(t)$ is derived as the sum of $w_0 t$ and a triangle waveform at frequency w_{var} with peak-to-peak value of $(\pi \Delta w_0)/w_{var}$. Moreover, an offset component, ϕ_0, may be added to $\phi(t)$ to specify the phase angel initial condition.

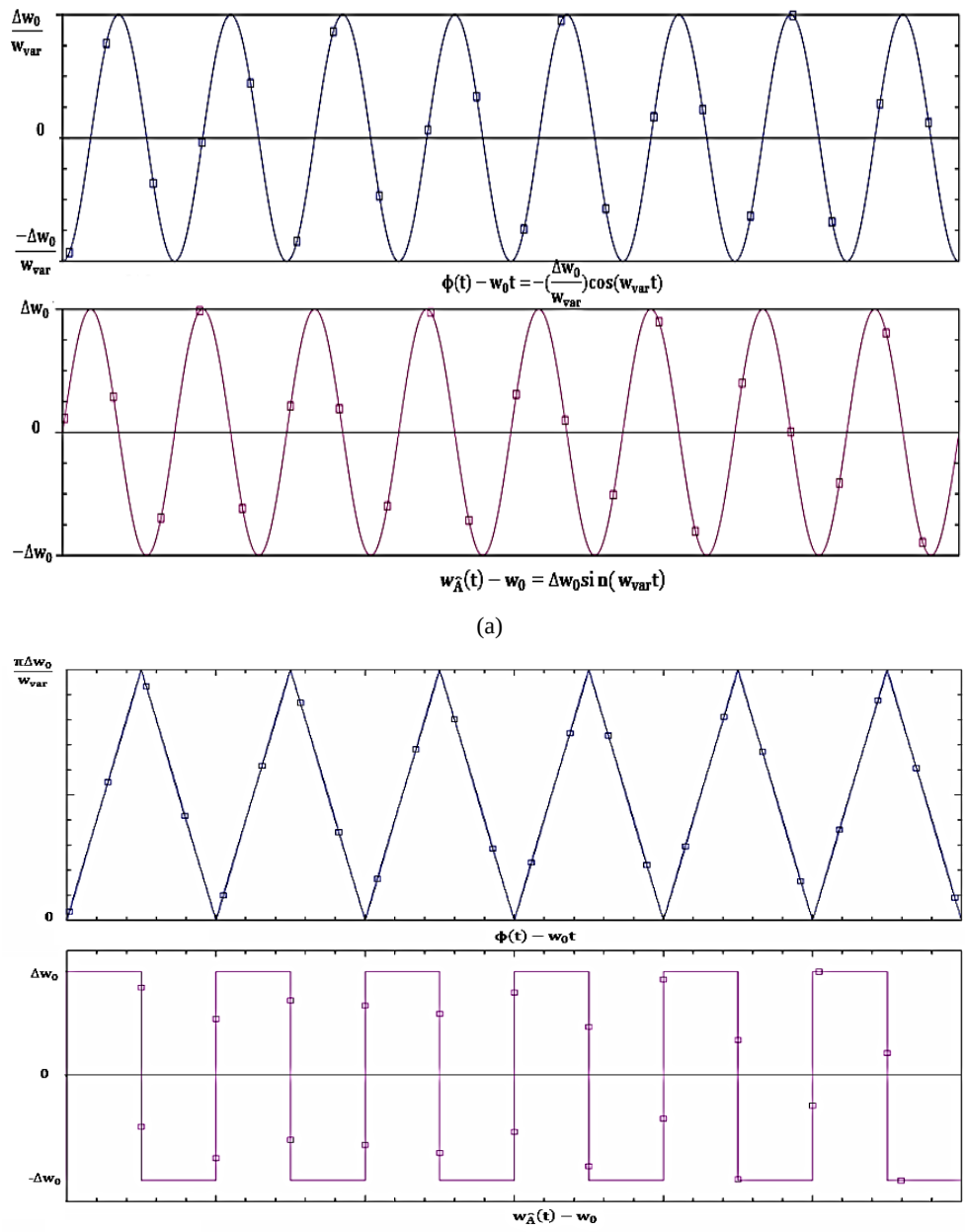

Figure 3.24 Graphical representation of the modulating signal phase angle and the core filter center frequency in a dynamic synchronous complex filter. (a) The sinusoidal variation pattern. (b) The square waveform variation pattern.

3.2.2 Overall System Test

Dynamic synchronous complex filters with core filter center frequency varying in both patterns were set up in Pspice, where ideal programmable blocks were used to

implement the time-varying center frequency for the core filter and the time-varying modulating frequencies. The following tests were run to evaluate the system up/down conversion performance, image rejection capability and input-output function in certain frequency range.

Up/down conversion

Take a dynamic synchronous complex filtering system in subheterodyne mode for instance. The system was tested with different center frequency variation rate and variation range. Table 3.3 lists the specific test setup. Fig. 3.25 shows the output signal spectra from the up conversion test and Fig. 3.26 gives both transient plots and FFT spectra of the down conversion system output. A static subheterodyne synchronous complex filtering system was simulated too, to provide a reference to evaluate the performance of the dynamic systems.

AM input carrier frequency	5MHz (0.1A)	AM input modulating frequency	dc(1mA)+10KHz (0.5mA)
Front end modulating frequency offset	4MHz	Core filter center frequency variation rate	16KHz,80KHz,200KHz
Core filter center frequency offset	1MHz	Core filter Q-factor offset	50
Back end modulating frequency offset	4MHz (up conversion)	Core filter center frequency variation range	1MHz±400KHz
	1MHz(down conversion)		1MHz±800KHz
Gain of the front end modulator	1.6	Gain of the back end modulator	0.8 (up conv.) /1.6(down conv.)

Table 3-3 Parameter setup for the up/down conversion test on a dynamic synchronous complex filtering system.

Simulation results suggest: 1) Regardless of the variation rate and variation range, the amplitude of useful signals in the dynamic system output is very close to its static system counterpart, but the dynamic system output contains more spurious noise due mainly to the intermodulation between the modulated input signal and the time-varying core filter center frequency. 2) When set up with the same variation rate and variation range, a square waveform center frequency variation pattern produces higher

intermodulation distortion than a sinusoidal variation pattern does, which might be due to the periodic instantaneous level transitions in the former pattern. 3) The size of the noise components is related to the variation rate, and it was discovered through sweeping the variation rate that if the core filter's static time constant is τ, then a variation rate lower than $1/\tau$ typically produces an output with higher intermodulation distortion. For example, comparing Fig. 3.25 (b) and Fig. 3.25(c), we found that the intermodulation noise corresponding to the center frequency varying in a sinusoidal waveform at 16kHz is about four times higher than its counterpart corresponding to a rate of 80kHz, which is slightly higher than $1/\tau$ of the system under test; the 200kHz variation rate further lowers the intermodulation distortion, as shown in Fig. 3.25(d). 4) Widening the variation range from $1\text{MHz} \pm 400\text{KHz}$ to $1\text{MHz} \pm 800\text{KHz}$ doubles the size of the intermodulation distortion, so a proper variation range is also critical for the dynamic system to produce a cleaner output.

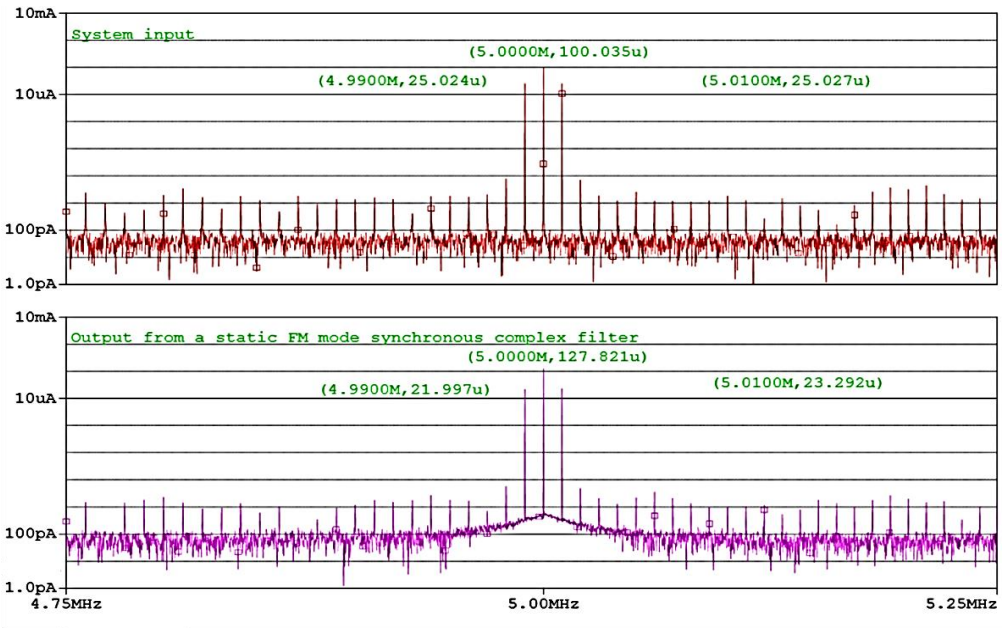

(a) Input signal and the output from a static complex filter

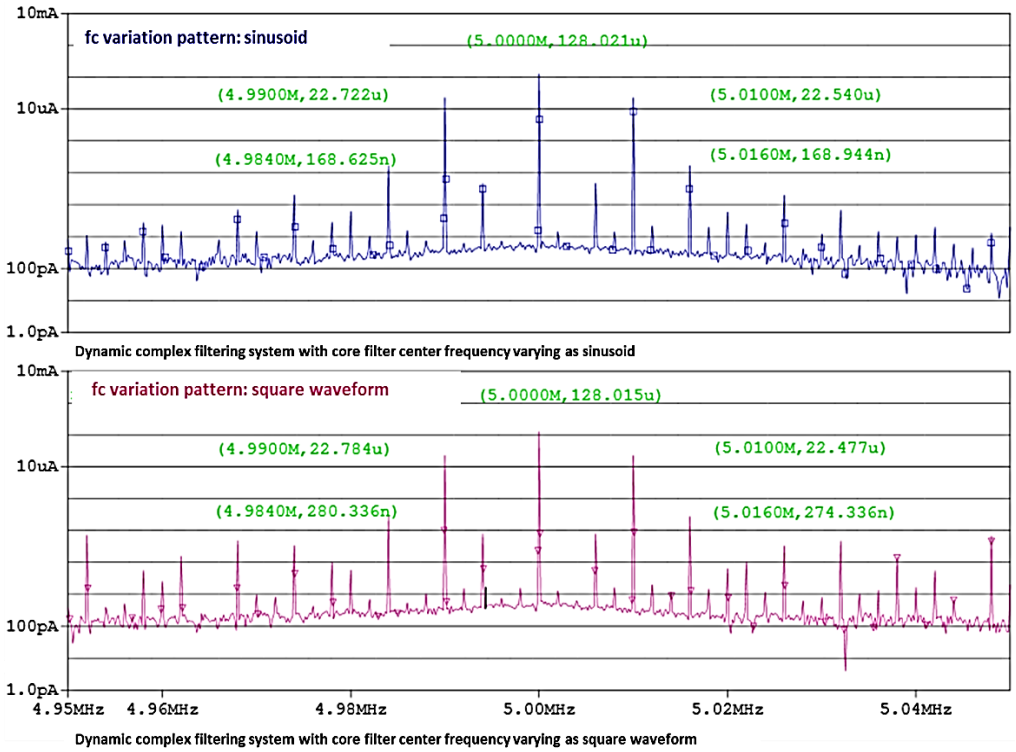

(b) Up conversion output signals from a dynamic system with different center frequency variation patterns but the same variation rate and variation range: $f_{var} = 16KHz$ and $f_{dev} = 400KHz$.

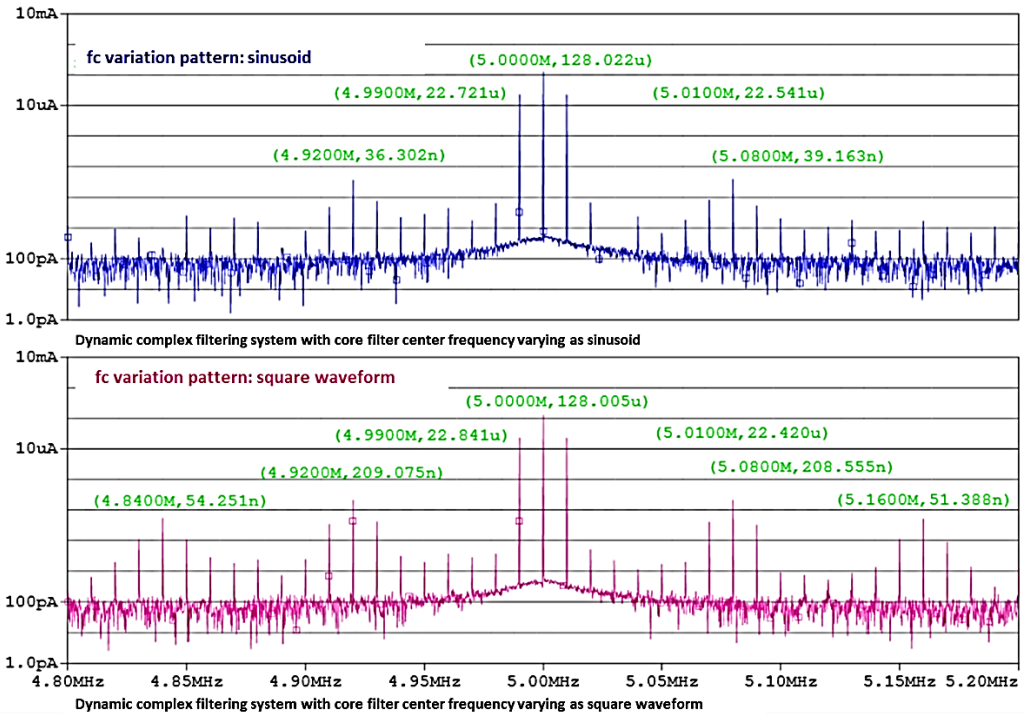

(c) Up conversion output signals from a dynamic system with different center frequency variation patterns but the same variation rate and variation range: $f_{var} = 80KHz$ and $f_{dev} = 400KHz$.

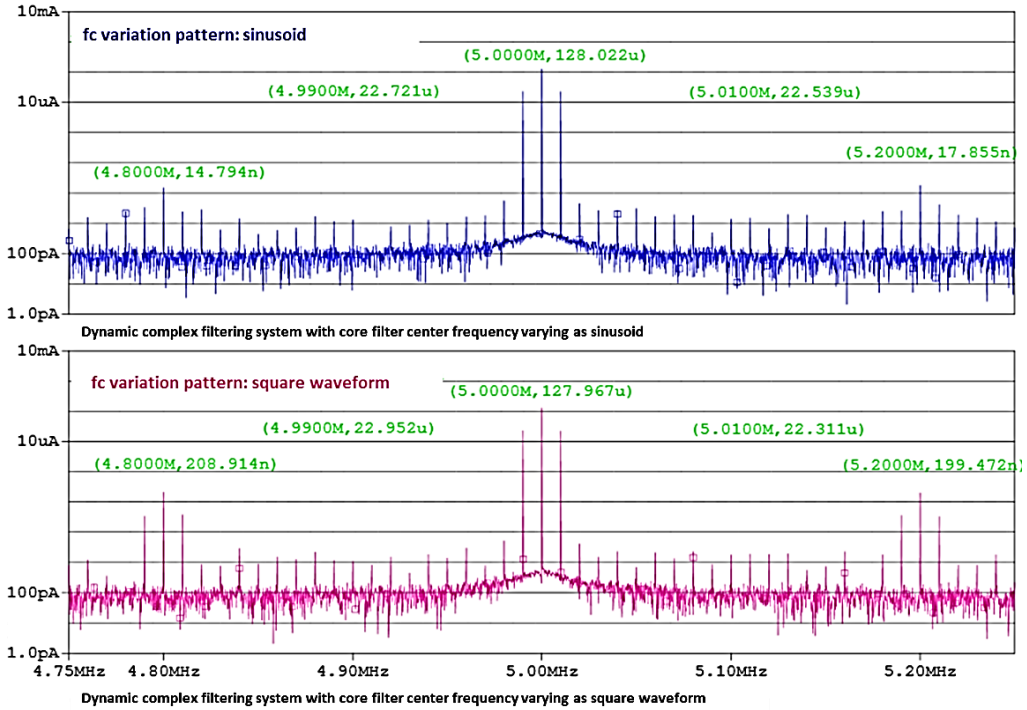

(d) Up conversion output signals from a dynamic system with different center frequency variation patterns but the same variation rate and variation range: $f_{var} = 200\text{KHz}$ and $f_{dev} = 400\text{KHz}$.

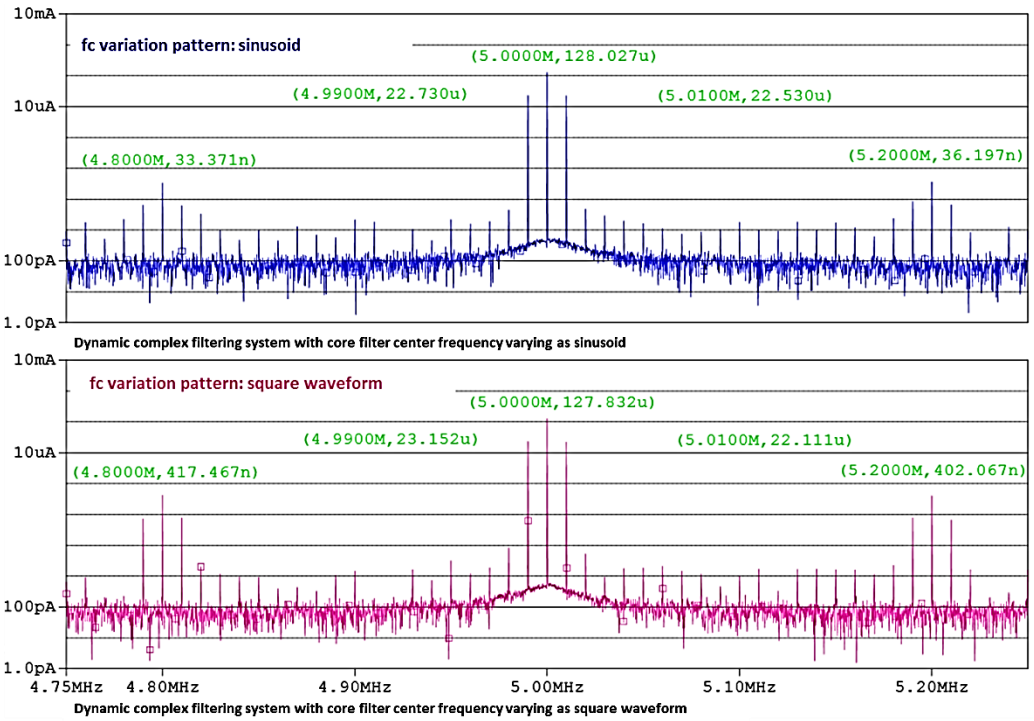

(e) Up conversion output signals from a dynamic system with different center frequency variation patterns but the same variation rate and variation range: $f_{var} = 200\text{KHz}$ and $f_{dev} = 800\text{KHz}$.

Figure 3.25 FFT spectra of output signals from the dynamic synchronous complex filters under test.

For the down conversion test, only the output signals from the dynamic systems with $f_{var} = 16\text{KHz}$ and $f_{dev} = 400\text{KHz}$ are shown in Fig. 3.26, as this setup yields the noisiest output in the up conversion test. The transient plot of the recovered signal from the dynamic synchronous system employing either center frequency variation pattern is almost identical to its static system counterpart. FFT spectra show some intermodulation distortion in the dynamic system output, which is at a negligible level.

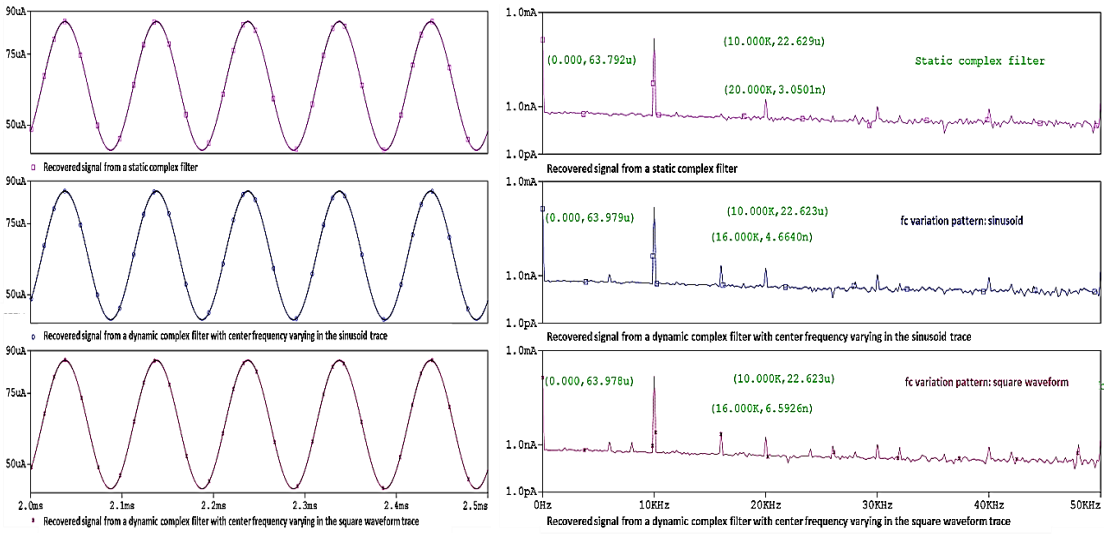

Figure 3.26 Down conversion test output signals from a static complex filter and a dynamic filter with different center frequency variation patterns.

Image rejection

If a subheterodyne mode complex filter has the front end and back end modulating frequency at 4MHz, then any input signal carried by 3MHz will be attenuated heavily due to the filter's image rejection property. To verify that the developed dynamic complex filter also possesses such a capability, a transient test was set up as Table 3.4. We ran the test on both the subheterodyne and superheterodyne mode dynamic synchronous complex filters, with the core filter center frequency varying in sinusoid/square waveform pattern and at different rates. According to the simulation

results in Fig. 3.27, a properly synchronized dynamic complex filter of either mode maintains the capability of suppressing image signals, and a subheterodyne filter has slightly stronger image rejection capability.

AM input carrier frequency	3MHz	AM input modulating frequency	10KHz
Front end modulating frequency offset	4MHz(subht)/2MHz(superht)	Core filter center frequency variation rate	16KHz,200KHz
Core filter center frequency offset	1MHz	Core filter Q-factor offset	50
Back end modulating frequency offset	4MHz(subht)/2MHz(superht)	Core filter center frequency variation range	1MHz±400KHz

Table 3-4 Parameter setup for the image rejection capability test on the dynamic synchronous complex filtering systems.

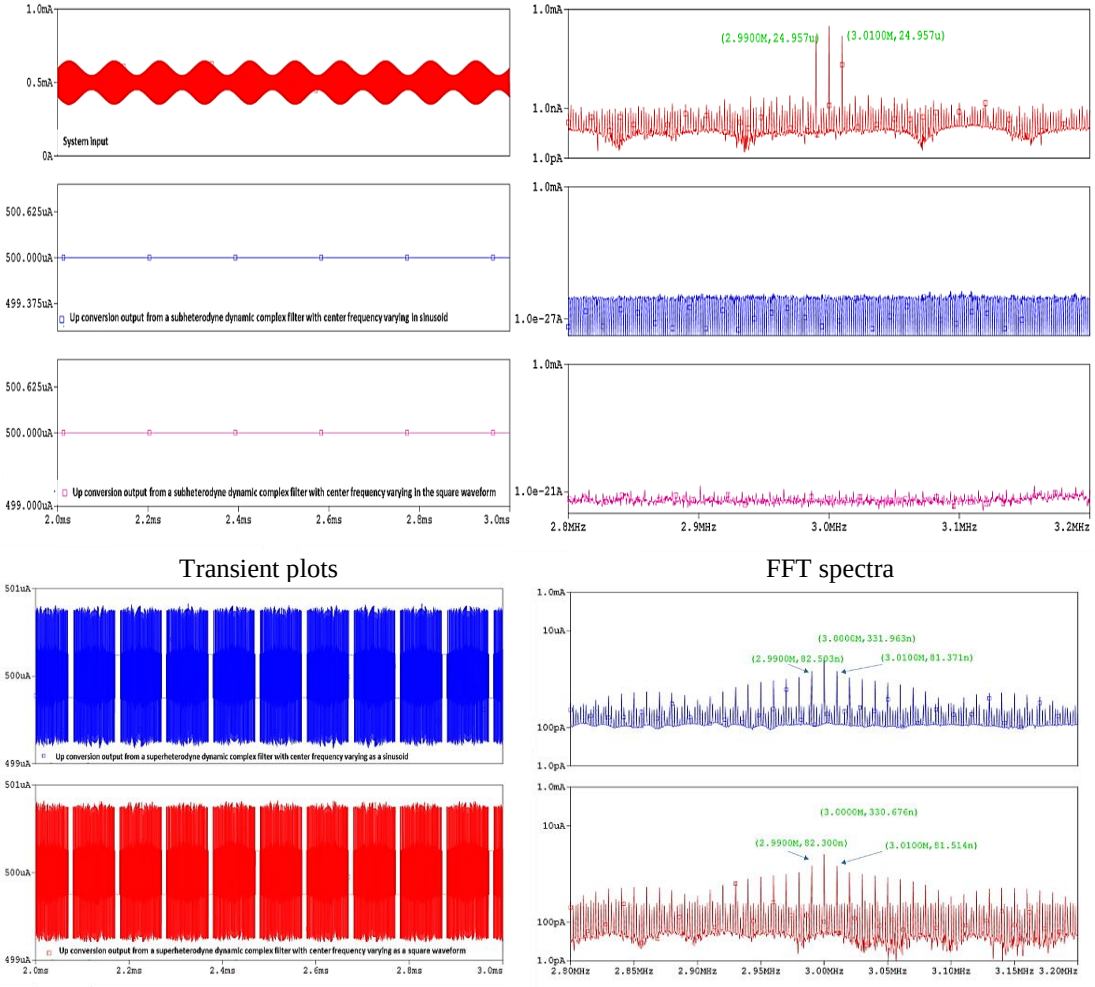

Transient plots FFT spectra

Transient plots FFT spectra

(a) Up conversion result from dynamic complex filters with sinusoid or square waveform center frequency variation pattern both of $f_{var} = 16\text{KHz}$ and $f_{dev} = 400\text{K Hz}$. The output plots in the upper group correspond to a subheterodyne system and those in the lower group correspond to a superheterodyne system. In each group, the blue plot corresponds to the sinusoidal center frequency variation pattern and the red one corresponds to the square waveform center frequency variation pattern.

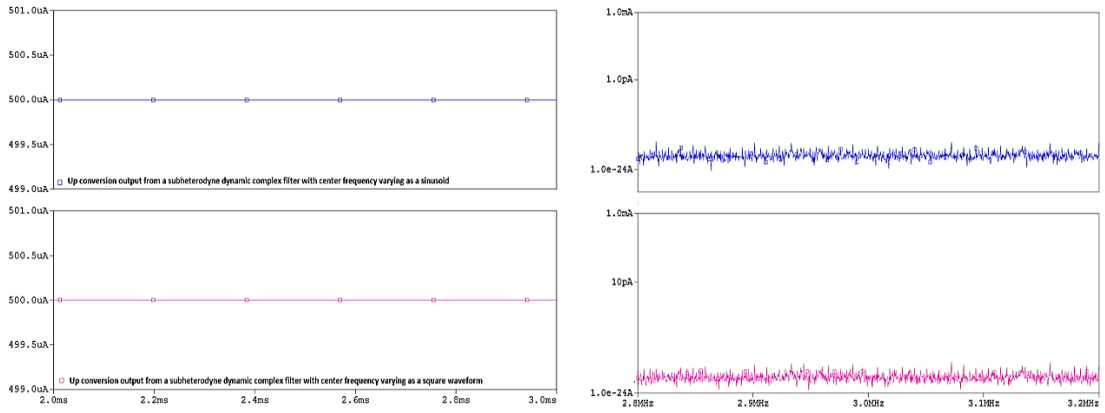

Transient plots FFT spectra

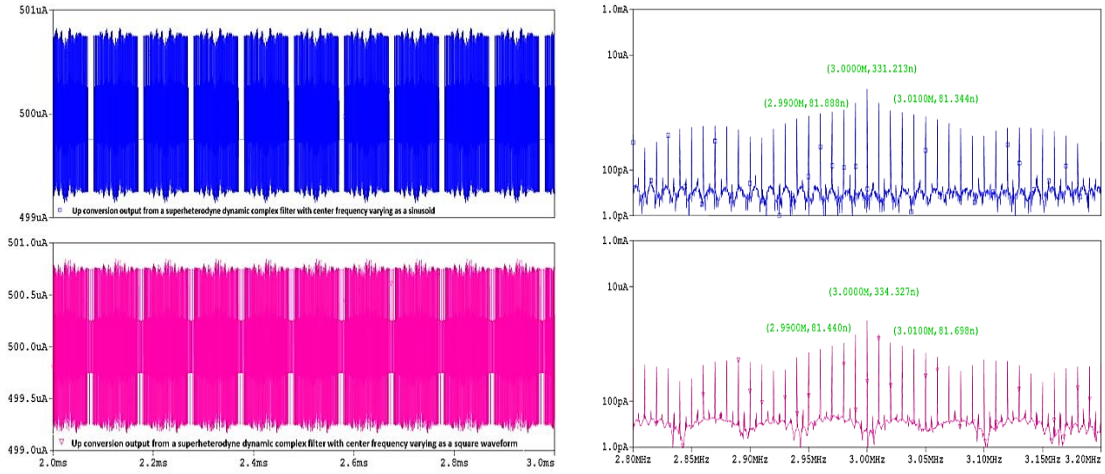

Transient plots FFT spectra

(b) Up conversion result from dynamic complex filters with sinusoid or square waveform center frequency variation pattern both of $f_{var} = 200\text{KHz}$ and $f_{dev} = 400\text{KHz}$. The output plots in the upper group correspond to a subheterodyne system and those in the lower group correspond to a superheterodyne system. In each group, the blue plot corresponds to the sinusoidal center frequency variation pattern and the red one corresponds to the square waveform center frequency variation pattern.

Figure 3.27 Results from the image rejection test on the dynamic synchronous complex filters. The input is the image of the signal shown in Fig. 3.25 (a), about the modulating frequency of 4MHz.

The gain spectra

To show the frequency response of the impelemented dynamic synchronous complex filter, gain spectra of the system in both superheterodyne mode and subheterodyne mode were generated. In each mode, both the sinusoidal center frequency variation pattern and the squae waveform center frequency variation pattern were tested.

Related parameter setup is listed in Table 3.5, where the variation rate and variation range were randomly picked.

Input carrier frequency	5MHz	AM input modulating frequency	0 ~ 50KHz
Front end modulating frequency offset	4MHz(subht)/6MHz(superht)	Core filter center frequency variation rate	120KHz
Core filter center frequency offset	1MHz	Core filter Q-factor offset	50
Back end modulating frequency offset	4MHz(subht)/6MHz(superht)	Core filter center frequency variation range	1MHz±500KHz

Table 3-5 Parameter setup for the frequency test on dynamic synchronous complex filters in different modulation modes and with different center frequency variation patterns.

According to Fig. 3.28, dynamic complex filters of the same mode have almost identical frequency responses regardless of their different center frequency variation patterns. However, when set up with the same variation pattern, the gain spectrum of a superheterodyne mode dynamic filter is a little different from its subheterodyne counterpart, which might be due to the non-ideal synchronization between the modulating frequency and the core filter center frequency. The magnitude spectrum of the transfer function for the target complex filter (fc=5MHz, Q=250) was plotted out as a reference. Interestingly, in lower frequency range, the gain spectra of the subheterodyne systems almost overlap with the reference plot and their superheterodyne counterpart are slightly off; as the frequency approaches 5MHz and gets higher, the opposite scenario is observed. It's possible that the equivalent center frequency of the dynamic complex filter under test was slighly lower than 5MHz when it's in the subheterodyne mode and a little higher than 5MHz when it's in the superheterodyne mode.

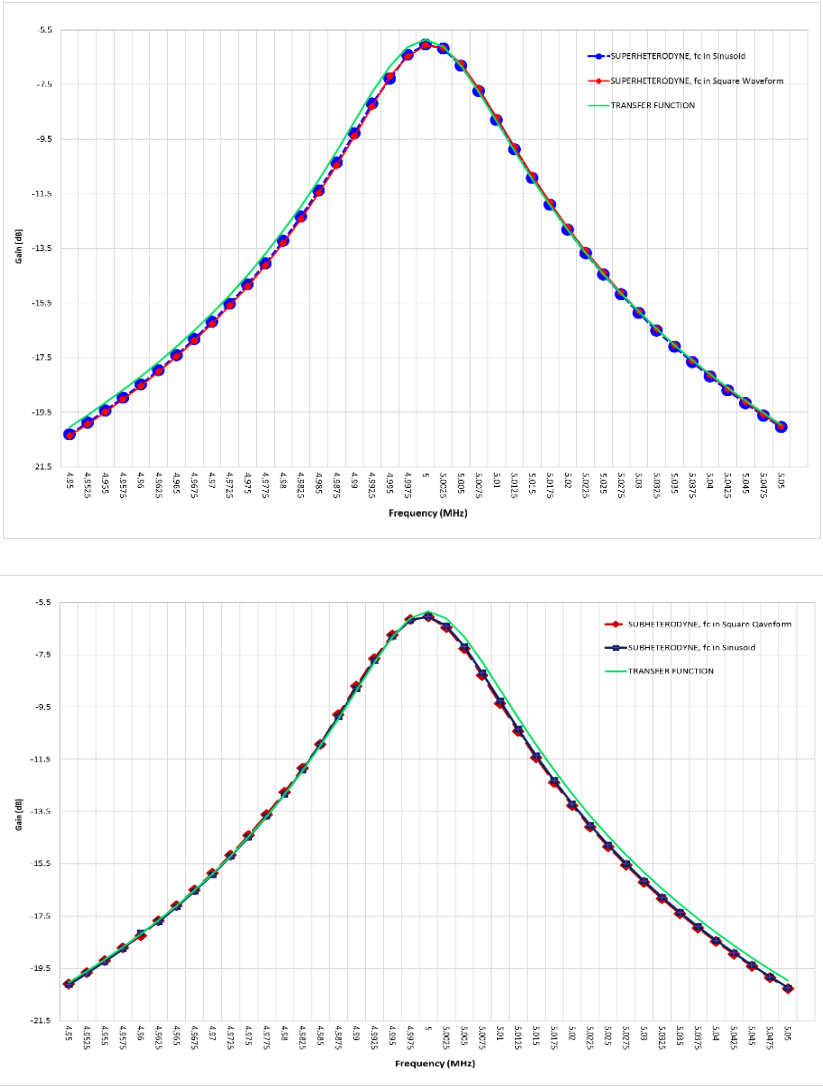

Figure 3.28 Frequency response of the dynamic synchronous complex filters under test

3.3 Summary

This chapter discusses in detail the state space representation, log-domain implementation and function verification of both static and dynamic FM mode synchronous complex filters. An FM mode synchronous filter is either superheterodyne or subheterodyne, depending on the relationship between the input carrier frequency and the system front end modulating frequency. The two types of filters have quadrature

modulating pairs with different relative phase angels as well as frequencies. Table 3.6 lists the ideal modulating signal pairs for FM mode synchronous filters of both types to perform up/down conversion.

Input: p(t)·carrier	$p(t) = 1 + 0.5\cos(w_{sig}t + \emptyset_{sig})$		$carrier = \cos(w_{carrier}t + \emptyset_{carrier})$		
	Front end modulator	Back end modulator			
Superheterodyne	$sin(w_M t)$	Up	$sin(w_M t - \emptyset_{carrier})$	Down	$sin(w_0 t - \emptyset_{carrier})$
$(w_M = w_{carrier} + w_0)$	$-cos(w_M t)$	Conversion	$-cos(w_M t - \emptyset_{carrier})$	Conversion	$-cos(w_0 t - \emptyset_{carrier})$
	Front end modulator	Back end modulator			
Subheterodyne	$sin(w_M t)$	Up	$sin(w_M t - \emptyset_{carrier})$	Down	$-sin(w_0 t + \emptyset_{carrier})$
$(w_M = w_{carrier} - w_0)$	$cos(w_M t)$	Conversion	$cos(w_M t - \emptyset_{carrier})$	Conversion	$cos(w_0 t + \emptyset_{carrier})$
w_M: System front end modulating frequency			w_0: Center frequency of the core filter		

Table 3-6 Ideal front end and back end quadrature modulating signal setup for an FM mode synchronous complex filter to perform up/down conversion.

While the architecture of a static FM mode synchronous complex filter relieves the challenge of implementing complex filters with high Q factor and high center frequency, the dynamic filters in the same architecture and with a time-varying center frequency synchronized by both end modulating frequencies provide a potential solution to reducing the in-filter single-tone noise in a certain frequency range. Both sinusoid and square waveform center frequency patterns of different variation rates and ranges have been tested on a noiseless filtering system in this chapter. It was discovered that a dynamic synchronous complex filter tends to generate some intermodulation distortion due to the periodic variation in the center frequency, so it's a little noisier than its static counterpart in general. Such distortion, fortunately, could be lowered to a negligible level by properly setting up the time-variant center frequency. For a noiseless system, it's preferable to vary the center frequency in a sinusoidal pattern, at variation rates higher than the inverse of the core filter's static time constant and in a range no larger

than one half of the core filter's static center frequency. Take the test results in section 3.2.2 for instance, for the dynamic synchronous complex filter with original center frequency at 1MHz and original Q factor of 50, a sinusoidal center frequency variation pattern at 200KHz and in the range of 1MHz$\pm$400KHz enables the system to generate the lowest intermodulation distortion. Systems with the core filter center frequency varying as a square waveform consistently generate larger intermodulation distortion and the noise size is much less sensitive to the change of the variation rate and range. Noise performance tests on the FM mode synchronous complex filters will be demonstrated in Chapter 4.

Chapter 4 Noise Performance of the Developed Filtering Systems

Previous chapters have discussed the basic idea, state-space representation, circuit implementation and functional verification of synchronous filtering systems in both AM mode and FM mode. Although a synchronous filter is more complicated and harder to implement, it has higher flexibility in the system parameter configuration. For example, there are in principle infinite ways for an AM mode synchronous bandpass filter to vary its core filter Q factor while maintaining its external transfer function and linearity. An FM mode synchronous complex filter could perform either subheterodyne or superheterodyne modulation, with a dynamic FM mode synchronous complex filter having its time dependent core filter center frequency varying in any waveform. Given these freedoms, it's expected that some variation patterns would effectively improve the noise performance of the filtering system. In this chapter, we will focus on exploring noise reduction methodologies in the context of synchronous filtering, utilizing the filters introduced in Chapter 2 and Chapter 3 as research objects. Ideal Gm-C system models will be simulated in the preliminary tests to exclude all the non-idealities in the transistor-level circuits and help us develop a better understanding on the effectiveness of the designs under test. Systems related to AM mode synchronous filtering will be tested first, followed by the tests on the FM mode synchronous complex filters that have higher circuit complexity and more degrees of freedom in the parameter setup.

4.1 Noise Tests on the AM mode Filtering Systems

4.1.1A Review on the Systems under Test

The idea of AM mode synchronous filtering could be generalized as follows: a system specified by eqn. (4.1) implements the same transfer function as the system represented

by eqn. (4.2) does, as long as $p(t)$ is always non-zero.

$$\frac{\mathrm{d}}{\mathrm{dt}}\bar{\mathrm{w}} = \left(\mathrm{A} + \frac{\dot{\mathrm{p}}}{\mathrm{p}}\mathrm{I}\right)\bar{\mathrm{w}} + \bar{\mathrm{b}}\mathrm{pu}, \quad \mathrm{y} = \frac{1}{\mathrm{p}}\bar{\mathrm{c}}^{\mathrm{T}}\bar{\mathrm{w}} \tag{4.1}$$

$$\dot{\bar{\mathrm{x}}} = \mathrm{A}\,\bar{\mathrm{x}} + \mathrm{bu}, \quad \mathrm{y} = \bar{\mathrm{c}}^{\mathrm{T}}\bar{\mathrm{x}} + \mathrm{du} \tag{4.2}$$

Applying eqn. (4.1) to a standard second-order bandpass filter that is represented by eqn. (4.3), we come up with the state space equations in eqn. (4.4).

$$\begin{vmatrix}\dot{\mathrm{x}}_1\\ \dot{\mathrm{x}}_2\end{vmatrix} = \begin{vmatrix}-\frac{\mathrm{w}_0}{\mathrm{Q}} & -\mathrm{w}_0\\ \mathrm{w}_0 & 0\end{vmatrix}\begin{vmatrix}\mathrm{x}_1\\ \mathrm{x}_2\end{vmatrix} + \begin{vmatrix}\frac{\mathrm{w}_0}{\mathrm{Q}}\\ 0\end{vmatrix}\mathrm{u}\,,\ \mathrm{y} = |1 \quad 0|\begin{vmatrix}\mathrm{x}_1\\ \mathrm{x}_2\end{vmatrix} \tag{4.3}$$

$$\begin{vmatrix}\dot{\mathrm{w}}_1\\ \dot{\mathrm{w}}_2\end{vmatrix} = \begin{vmatrix}-\frac{\mathrm{w}_0}{\mathrm{Q}} + \frac{\dot{\mathrm{p}}(\mathrm{t})}{\mathrm{p}(\mathrm{t})} & \mathrm{w}_0\\ -\mathrm{w}_0 & \frac{\dot{\mathrm{p}}(\mathrm{t})}{\mathrm{p}(\mathrm{t})}\end{vmatrix}\begin{vmatrix}\mathrm{w}_1\\ \mathrm{w}_2\end{vmatrix} + \begin{vmatrix}\frac{\mathrm{w}_0}{\mathrm{Q}}\\ 0\end{vmatrix}\mathrm{p}(\mathrm{t})\mathrm{u}\,,\ \mathrm{y} = \frac{1}{\mathrm{p}(\mathrm{t})}|1 \quad 0|\begin{vmatrix}\mathrm{w}_1\\ \mathrm{w}_2\end{vmatrix} \tag{4.4}$$

The block diagrams of the systems corresponding to eqn. (4.3) and eqn. (4.4) are given in Fig. 4.1. In the second block diagram, the core filter modified by $\frac{\dot{p(t)}}{p(t)}$ has a time-variant Q factor. Amplitude modulators that scales the signal at the front end and back end, respectively with $p(t)$ and $\frac{1}{\mathrm{p(t)}}$, work in a synchronized mode with the time-varying Q factor and ensure the overall system to be equivalent to System 1 in the input-output characteristics.

Based on the AM mode synchronous filter functionally equivalent to System 1, we developed System 2 by redefining the system input and output. Specifically, suppose $\mathrm{u(t)}$ is a carrier and $\mathrm{p(t)}$ a properly offset baseband signal that is consistently positive, then the front end modulator output $\mathrm{u(t)p(t)}$ in the synchronous filter could be viewed as an AM signal, which we take as the input of System 2; also, suppose we were able to generate the ideal $\frac{\dot{\mathrm{p}}(\mathrm{t})}{\mathrm{p}(\mathrm{t})}$ to continuously vary the Q factor of the core filter; moreover, if

we intentionally get rid of the back end modulating block and directly take the core filter output as the output of System 2, then according to eqn. (4.4), it could be expressed as $y \cdot p(t)$, which is the product of the bandpass filtered carrier $\mathrm{u(t)}$ and the original baseband signal $p(t)$. It reveals an appealing property of System 2: as long as the core filter is centered at the input carrier frequency, regardless of its Q factor, the sideband signals in the system output would always have amplitude and phase very close to that of the input sideband signals.

However, it's almost impossible to generate the ideal Q-factor control signal $\frac{\dot{\mathrm{p}}(\mathrm{t})}{\mathrm{p}(\mathrm{t})}$ at the receiver end, as we typically have to reconstruct the information signal from the received AM signal. The recovered information signal, call it $\hat{\mathrm{p}}(\mathrm{t})$, always lags the original $\mathrm{p(t)}$ due to the bandpass filtering and lowpass filtering in a conventional AM receiver. In the novel demodulator proposed in Chapter 2, an S/H block performing ideal sampling was utilized to extract the envelope of the bandpass filter output, so as to minimize the phase difference between $\hat{\mathrm{p}}(\mathrm{t})$ and $\mathrm{p(t)}$. Although $\hat{\mathrm{p}}(\mathrm{t})$ still lags $\mathrm{p(t)}$ due to the bandpass filtering, simulation results have shown that when processing a noiseless AM signal, System 3 in Fig. 4.3, of which the core filter bandwidth is controlled by the feedback signal $\frac{\dot{\hat{\mathrm{p}}}(\mathrm{t})}{\hat{\mathrm{p}}(\mathrm{t})}$, could produce an output very similar to what is produced by System 2. The noise performance of such a feedback filtering system is of our great interest.

Considering the challenge in implementing the S/H block that performs ideal sampling in System 3, we created System 4 that provides a much easier way to recover the information signal. Recall that the FM mode complex filtering system discussed in Chapter 3 comprises a core filter and two terminal modulators, of which the back end

modulator could perform either up conversion or down conversion without introducing extra phase shift if the local oscillators were properly set up. As the transfer function of a second-order complex filter is very similar to that of a standard biquad bandpass filter, we believe that a synchronous complex filter could easily be modified into a feedback filtering system as an alternate of System 3, shown in Fig. 4.4. System 4 might have improved noise performance because of its particular demodulator that produces less high-frequency noise components than the S/H block.

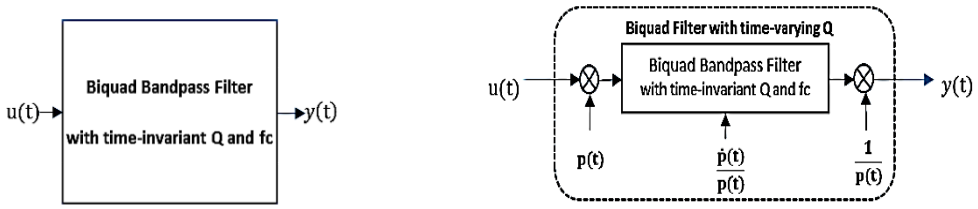

System 1

An AM mode synchronous bandpass filter functionally equivalent to System 1 (p(t)>0 or p(t) <0)

Figure 4.1 Block diagrams of the systems specified by eqn. (4.3) and eqn. (4.4).

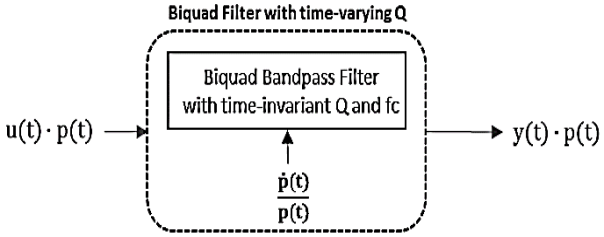

System 2

Figure 4.2 A biquad bandpass filter with time-variant Q factor processing an AM input signal.

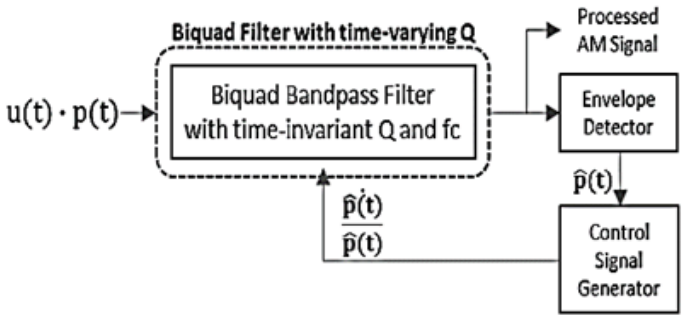

System 3

Figure 4.3 Block diagram of a feedback filtering system inspired by System 2.

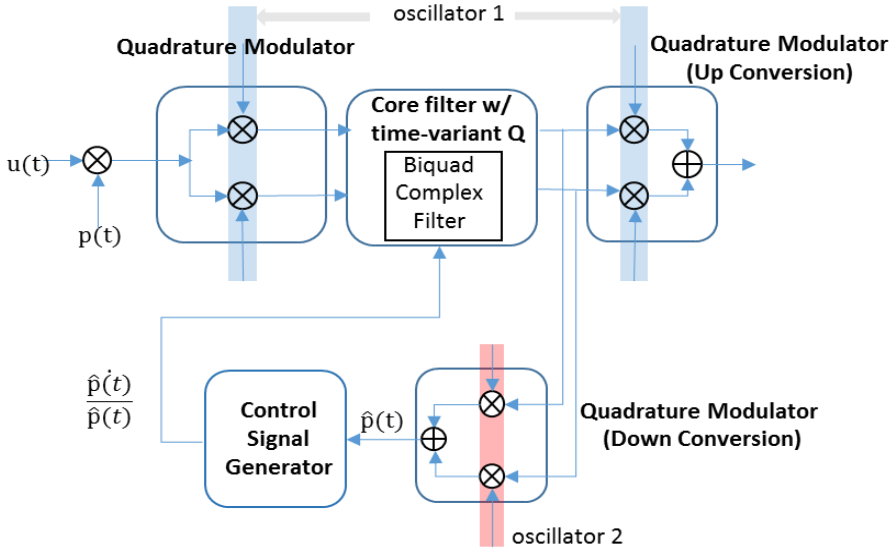

System 4

Figure 4.4 Block diagram of a feedback filtering system developed with a synchronous complex filtering system.

At this point, we have finished reviewing the block diagrams of all the systems related to AM mode synchronous filtering. Their ideal Gm-C models are now produced as follows. Fig. 2.21 in Chapter 2 has given a Gm-C network realization of System 3 based on transforming the modified state space representation of the AM mode synchronous bandpass filter represented by eqn. (4.4). Models for System 1 and System

2 are easily developed by trimming and modifying the design in Fig. 2.21. Fig. 4.5 illustrates the ideal models for System 1, 2 and 3.

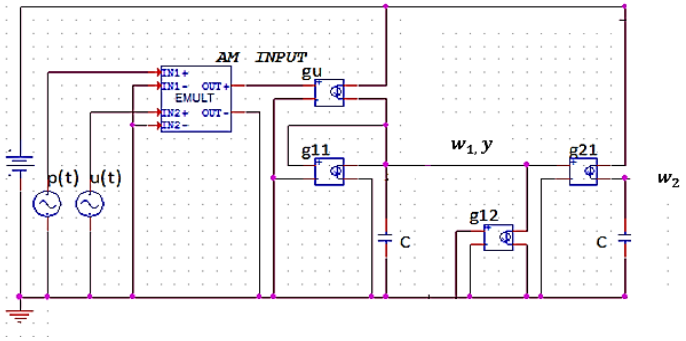

System 1

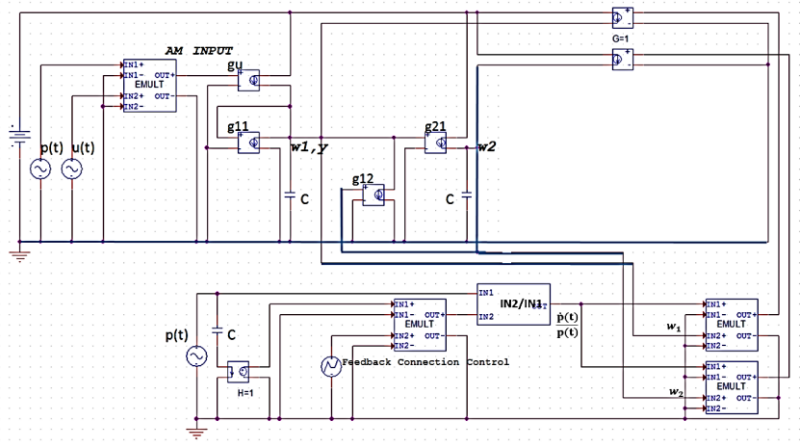

System 2

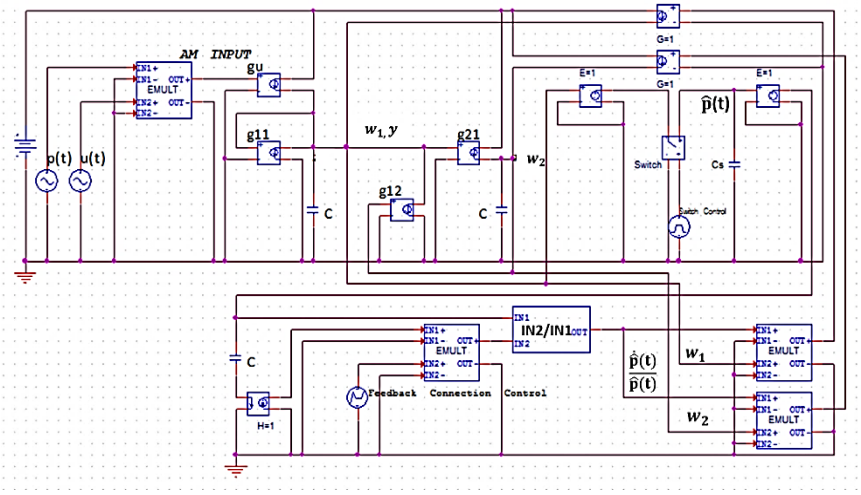

System 3

Figure 4.5 Ideal voltage-mode models for System 1 ~ System 3 with the core filter implemented by a Gm-C network.

The same approach used in implementing System 3 was used to develop the Gm-C model for System 4. Taking a complex filtering system in the superheterodyne mode for instance, the modified core filter is specified in eqn. (4.5). A back end down converter is required so that the output could be taken as the source to generate the Q-factor control signal.

$$\begin{vmatrix} \dot{x_1} \\ \dot{x_2} \end{vmatrix} = \begin{vmatrix} -\frac{w_0}{2Q} + \frac{\dot{\hat{p}}}{\hat{p}} & -w_0 \\ w_0 & -\frac{w_0}{2Q} + \frac{\dot{\hat{p}}}{\hat{p}} \end{vmatrix} \begin{vmatrix} x_1 \\ x_2 \end{vmatrix} + (w_0/Q) \begin{vmatrix} \sin(w_{M1}t) \\ -\cos(w_{M1}t) \end{vmatrix} v \qquad (4.5)$$

$$y_{up_{conversion}} = |\sin(w_{M1}t) \quad -\cos(w_{M1}t)| \begin{vmatrix} x_1 \\ x_2 \end{vmatrix}$$

$$y_{down\_conversion} = |\cos(w_0 t) \qquad \sin(w_0 t)| \begin{vmatrix} x_1 \\ x_2 \end{vmatrix} = \hat{p}(t)$$

where v is the system input and could be represented as $v = u(t) \cdot p(t)$ in our test, with $u(t)$ being the carrier and $p(t)$ the useful information signal; w_{M1} is the front end modulating frequency which is higher than the input carrier frequency for the superheterodyne modulator; w_0 is the center frequency of the core filter which equals the difference between w_{M1} and the input carrier frequency. The reconstruction of the information signal $\hat{p}(t)$ is performed by the down converter specified by the last equation above. Now let us rewrite the state space equations and make relevant definition to associate the core filter with a Gm-C network:

$$\begin{vmatrix} C\dot{x_1} \\ C\dot{x_2} \end{vmatrix} = \begin{vmatrix} g_{11} & g_{12} \\ g_{21} & g_{22} \end{vmatrix} \begin{vmatrix} x_1 \\ x_2 \end{vmatrix} + g_u \begin{vmatrix} \sin(w_{M1}t) \\ -\cos(w_{M1}t) \end{vmatrix} v$$

where $g_{11} = C(-\frac{w_0}{2Q} + \frac{\dot{\hat{p}}}{\hat{p}})$, $g_{12} = C(-w_0)$, $g_{21} = Cw_0$, $g_{22} = C(-\frac{w_0}{2Q} + \frac{\dot{\hat{p}}}{\hat{p}})$, $g_u = C\frac{w_0}{Q}$. A possible implementation of the system is given in Fig. 4.6 where all the components and blocks are ideal. For demonstration simplicity, only the back end down converter is

shown in the figure. The ‘Feedback On/Off Control’ block models a switch that allows us to determine when to send back the Q-factor control signal. When turned off, the system models an open-loop complex filter. Moreover, to implement System 2 with a complex filter, we only need to break the feedback loop at the demodulator output and apply the ideal voltage signal $p(t)$ across the capacitor C.

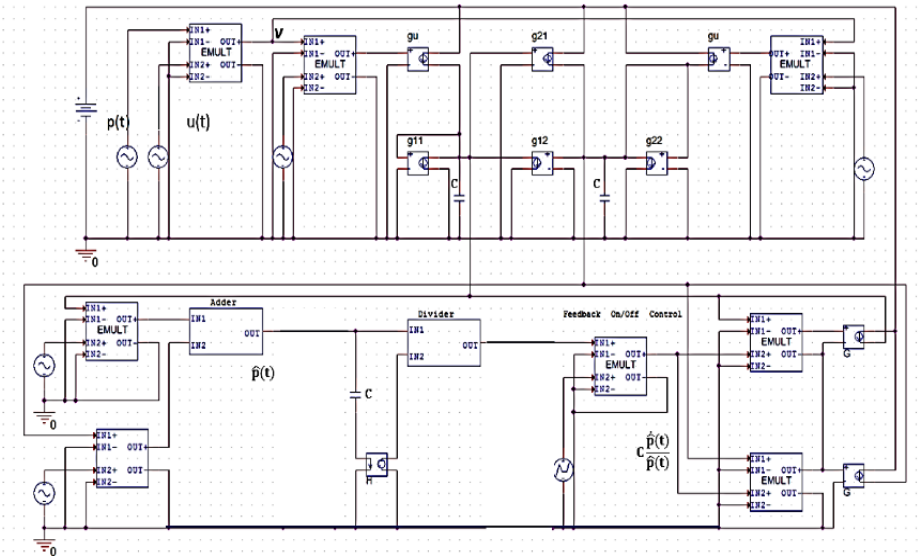

Figure 4.6 Ideal voltage-mode model for System 4 with the core filter implemented by a Gm-C network.

4.1.2 Noise Performance Test

The noise performance of System 1 to System 4 are evaluated by stimulating them with two types of noise sources: the input noise and the in-filter noise.

1. Noisy input and noiseless system

We started off with testing the response of all the systems to a noisy AM input, which was generated by superimposing a white noise voltage signal onto an ideal AM voltage signal. MATLAB was used to generate the data file of the noise, which could be read and converted by PSpice. Test parameters are listed in Table 4-1.

Input (v)	u(t)=p(t)m(t)+noise
	p(t)=1m+(0.5m) sin(2π(10K) t)
	m(t)=sin(2π(1Meg) t)
	White noise: zero mean, 0.2mV RMS
Biquad Bandpass Filter	Q=50 or 500, fc=1MHz
S/H Block	Switching rate=1MHz, ON time=1ns
	ON resistance=1mΩ, OFF resistance=1MegΩ

Table 4-1 Parameter setup for the noise test on the bandpass filters and related AM mode filtering systems.

1) Test on System 1 and System 2

According to the state space representation of System 2, if the center frequency of the core filter is tuned to equal the input carrier frequency, then the ideal Q-factor control signal $\frac{\dot{p}(t)}{p(t)}$ will enable System 2 to suppress the input noise to the same level as System 1 does while maintaining the size and phase of the input sideband signals. To verify this feature of System 2, a noisy AM signal was fed through System 1 and System 2, the core filter output and the S/H output were plotted in Fig. 4.7 and Fig. 4.8. Comparison shows that the noise floor of the core filter output from System 2 almost overlaps that from System 1, while the sideband signals in System 2 output are approximately 3dB higher than their System 1 counterpart. Also, Fig. 4.8 shows that the S/H demodulator output from System 2 nearly overlaps with the original modulating signal $p(t)$. The simulation results suggest that System 2 is capable of suppressing the input noise like a standard biquad bandpass filter while letting the input sideband signals pass through with little attenuation or phase shift, so System 2 yields an output with higher SNR than System 1 does when processing a noisy AM signal. By comparing the

core filter output to the S/H block output, we are convinced that the S/H block is able to reconstruct the baseband signal without introducing extra phase shift or undesired noise, therefore, the baseband noise level of the recovered signal is also a good representation of the core filter output noise level near the center frequency.

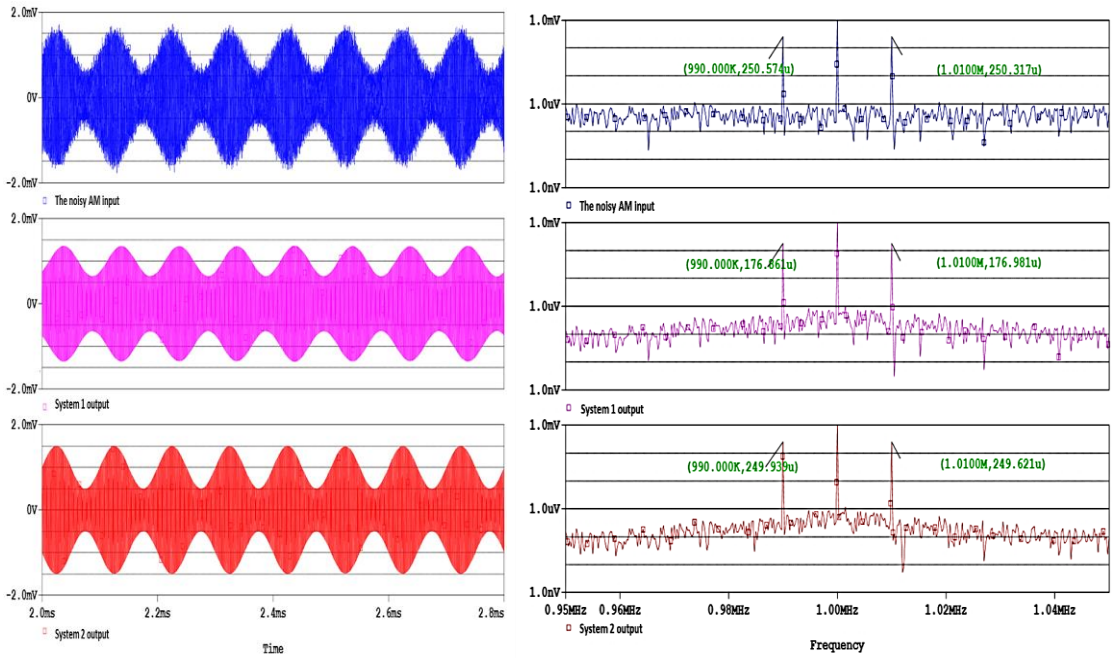

Figure 4.7 Transient plots and FFT spectra of the noisy AM input and the core filter output of System 1 and System2. (Q=50, $f_{center} = 1MHz$ for both core filters)

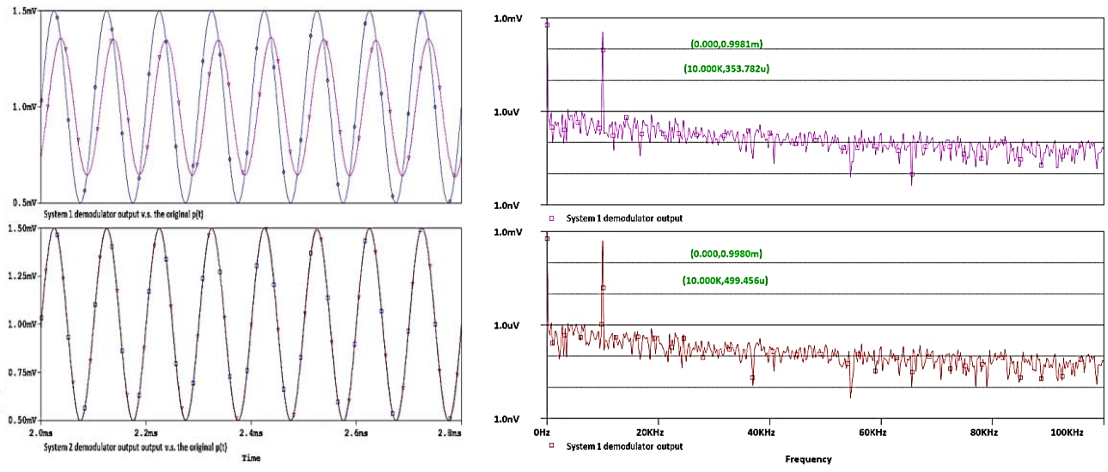

Figure 4.8 Transient plots and FFT spectra of the recovered information signal from System 1 and System2 corresponding to a noisy AM input. (Q=50 for both core filters)

Moreover, according to the derived expression for the output of System 2, the system is expected to have another appealing noise performance: after getting centered at the carrier frequency, the core filter could in principle be tuned as sharp as needed, so that the undesired input noise components will be heavily suppressed; since the amplitude and phase of the useful input sideband signals will be maintained regardless of the core filter's original Q factor, the output SNR will be greatly improved. To verify this expectation, we raised the original Q factor to 500 for the core filters in both systems and drove them with the same noisy AM input. Because of the sharpened core filter, the output noise floors in Fig. 4.9 and Fig. 4.10 are obviously lower than that in Fig. 4.7 and Fig. 4.8. While the useful input sideband signals get heavily attenuated by System 1, they magically pass through System 2 almost unchanged. Therefore, if an ideal Q-factor control signal were available, System 2 could produce an output with very high SNR.

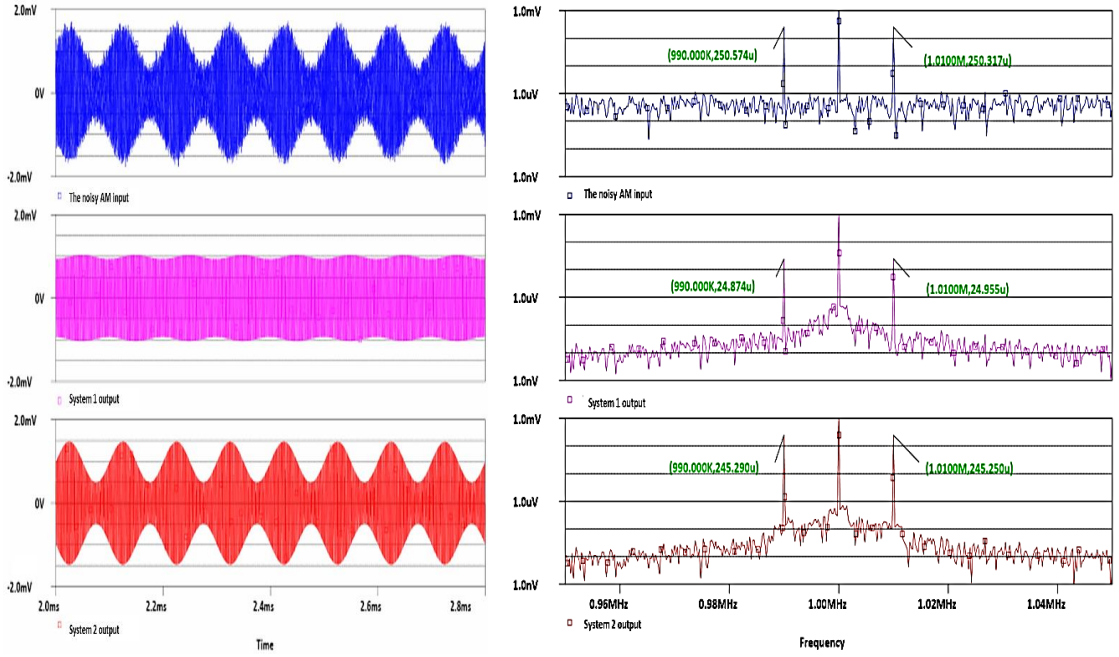

Figure 4.9 Transient plots and FFT spectra of the noisy AM input and the core filter output of System 1 and System2. (Q=500 for both core filters)

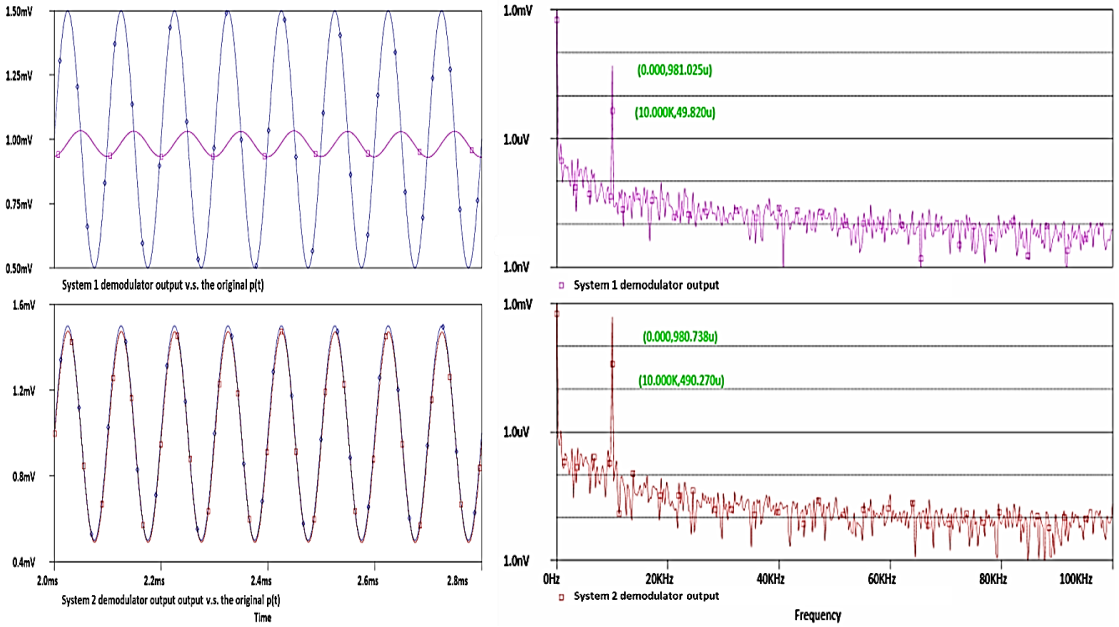

Figure 4.10 Transient plots and FFT spectra of the recovered information signal from System 1 and System2 corresponding to a noisy AM input. (Q=500 for both core filters)

2) Test on System 3

It has been verified in Chapter 2 through simulation that when the AM input is noiseless, System 3 reconstructs a baseband signal which is very similar to the original information signal in both amplitude and phase. However, when receiving a noisy AM signal, the recovered information signal, $\hat{p}(t)$, is noisy too, it is hence unobvious whether the Q-factor control signal generated with the noisy $\hat{p}(t)$ is still capable of yielding a feedback filter which has the noise reduction capability comparable to that of System 2. System 3 with the original Q factor of 50 and 500 was tested with the above noisy AM signal, and related output signals were plotted in Fig. 4.11 and Fig. 4.12.

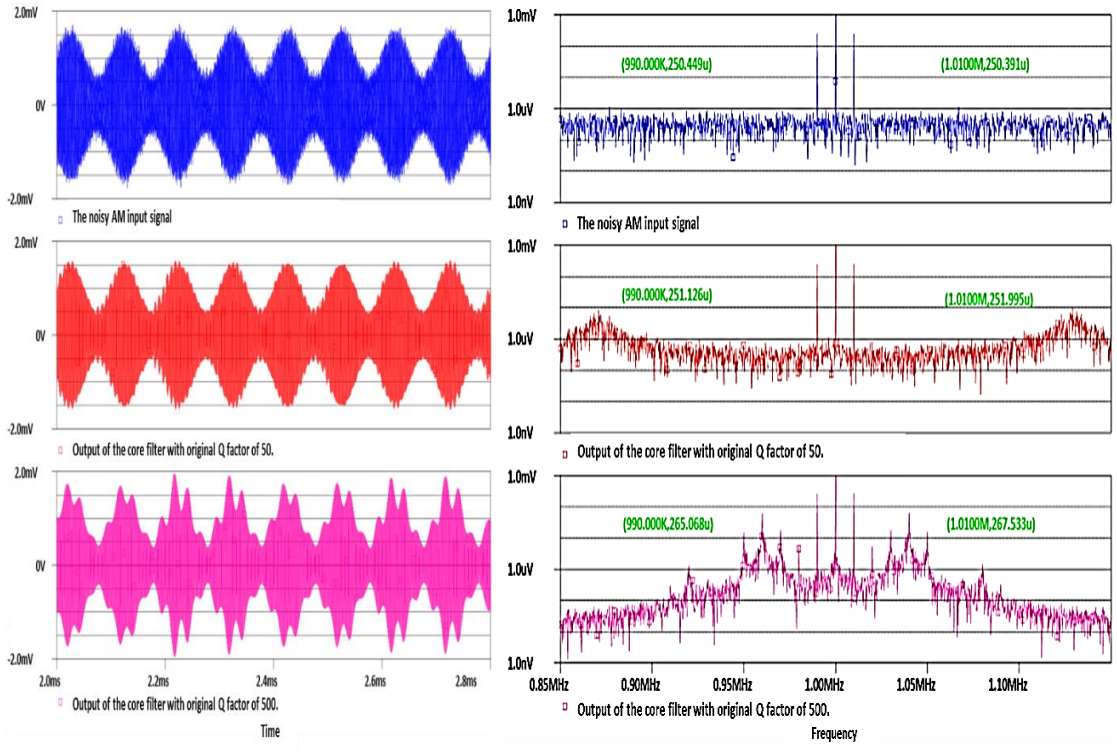

Figure 4.11 Transient plots and FFT spectra of the noisy AM input and the core filter output from System 3. (Q=50 and Q=500)

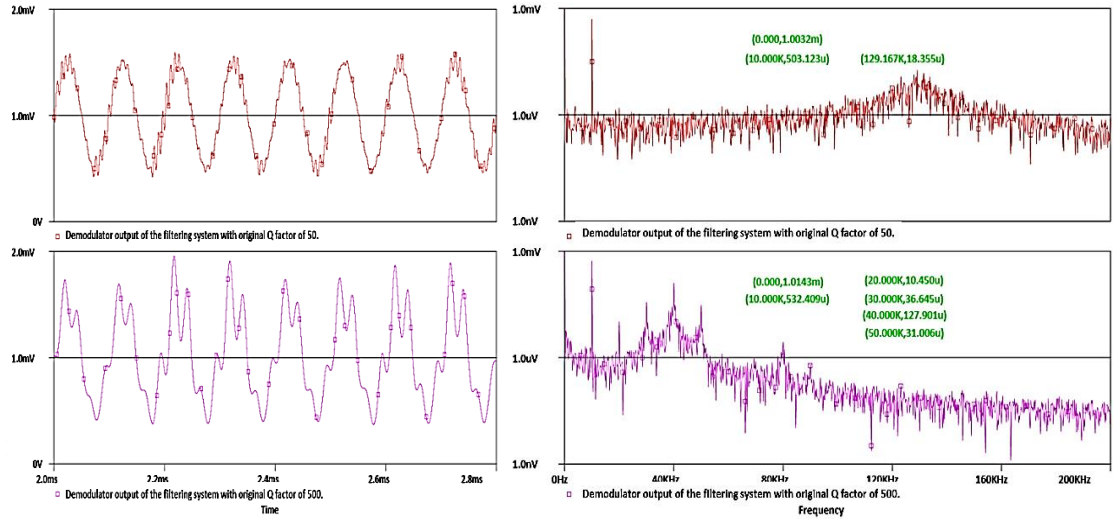

Figure 4.12 Transient plots and FFT spectra of the S/H output from System 3 (Q=50 and Q=500).

FFT spectra of the core filter output suggest: 1) The input noise is not suppressed by System 3 as hard as it is by System 1 and System 2. 2) Noise peaks are observed

appearing in pairs in the core filter output, symmetric about the filter's center frequency. Moreover, the system with a higher original Q factor generates more distortion and higher noise peaks that distribute closer to the center frequency. The noise components near 1MHz in the core filter output are shifted into the base band after demodulation, as shown in Fig. 4.12, which results in a noisy recovered information signal. 3) The core filter in System 3 produces larger-sized sideband signals than the core filter in System 2 does, which might be caused by the noisy feedback signal. The recovered information signal from System 3 has larger amplitude than its System 2 counterpart too. However, due to the introduced large-sized distortion, the output SNR of System 3 is much lower than that of System 2. Moreover, when processing a noisy AM signal, the noise performance of System 3 is even inferior to that of System 1, and a sharper core filter tends to result in more noise in the frequency range of our interest hence further lowers the system output SNR.

As the cause to the noise components in the core filter output is obscure, we did a set of trial-and-error simulation in an effort to search for some solutions to alleviate this situation. Specific setup and test results are given below. The same noise source used above was added to the input signals in all the tests.

Sweeping the frequency of $p(t)$

In this test, we set up the core filter with original Q factor of 500 and center frequency of 1MHz. The input modulating frequencies under test were 500Hz, 1kHz, 5kHz and 15kHz. The FFT spectra in Fig. 4.13 suggest that the noise level and noise peak of the core filter output have very little dependence on the bandwidth of the input

signal. As the modulating frequency increases, the intermodulation noise becomes higher and more noticeable, degrading the output SNR.

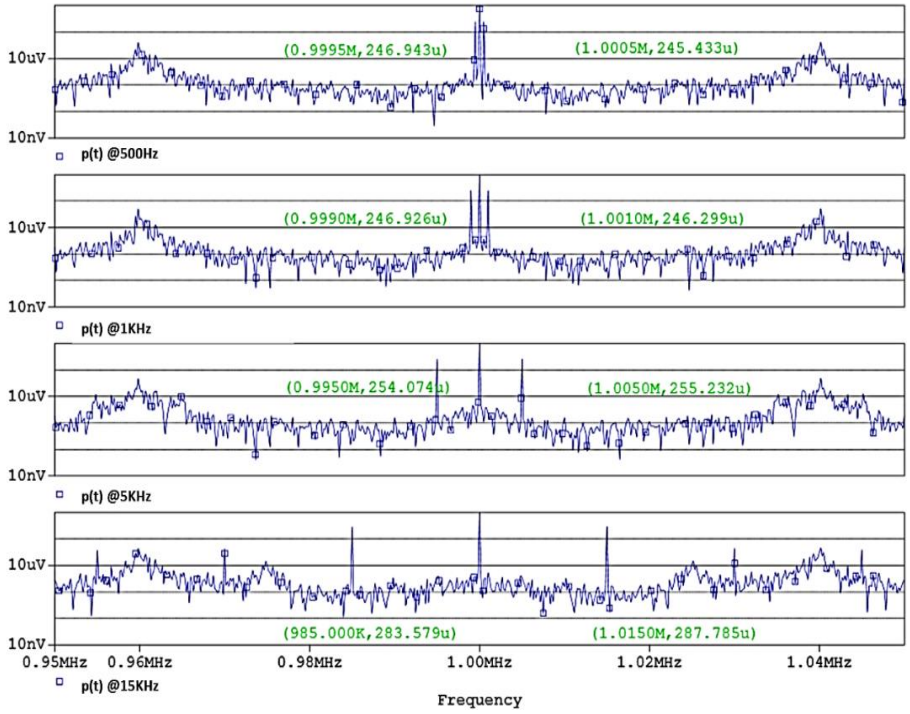

Figure 4.13 FFT spectra of the core filter output from System 3 corresponding to AM input signals of different bandwidths. (Original Q=500)

Varying the original Q factor of the core filter

Having excluded the effect of the input signal bandwidth, we swept the original Q factor of the core filter in this test. The core filter was still centered at 1MHz and the Q factor was tuned to 20, 100 and 200 respectively. The modulating signal of the AM input was set to be 10kHz, so Fig. 4.11 could also be used in the output comparison. The spectra in Fig. 4.14 and Fig. 4.11 reveal that System 3 with a smaller original Q factor produces lower noise peaks that are further away from the center frequency while a high Q factor raises the distortion components and pushes them toward the center frequency. The recovered signal from the system with a sharper original core filter usually has a

higher baseband noise floor hence lower SNR. The test results again indicate that when dealing with a noisy AM input, System 3 does not possess the appealing input noise suppression capability as System 2 does, due mainly to the noisy feedback Q-factor control signal.

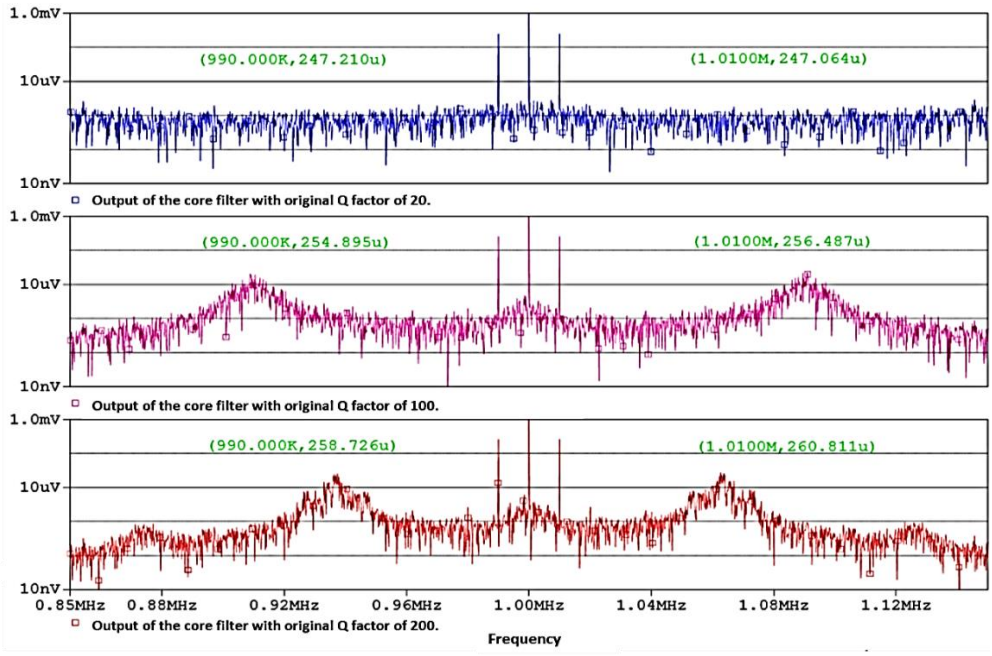

Figure 4.14 FFT spectra of System 3 core filter output (original Q=20, 100, 200).

Adding a lowpass filter behind the S/H block

Furthermore, we tried adding a lowpass filter between the S/H block and the control signal generator, expecting it to attenuate the noise in the recovered signal and make the feedback Q-factor control signal less noisy. The system centering at 1MHz with an original Q factor of 100 followed by a first-order lowpass filter was tested. The filter's cutoff frequency was set to be 20kHz, 50kHz, 100kHz and 500kHz in the test.

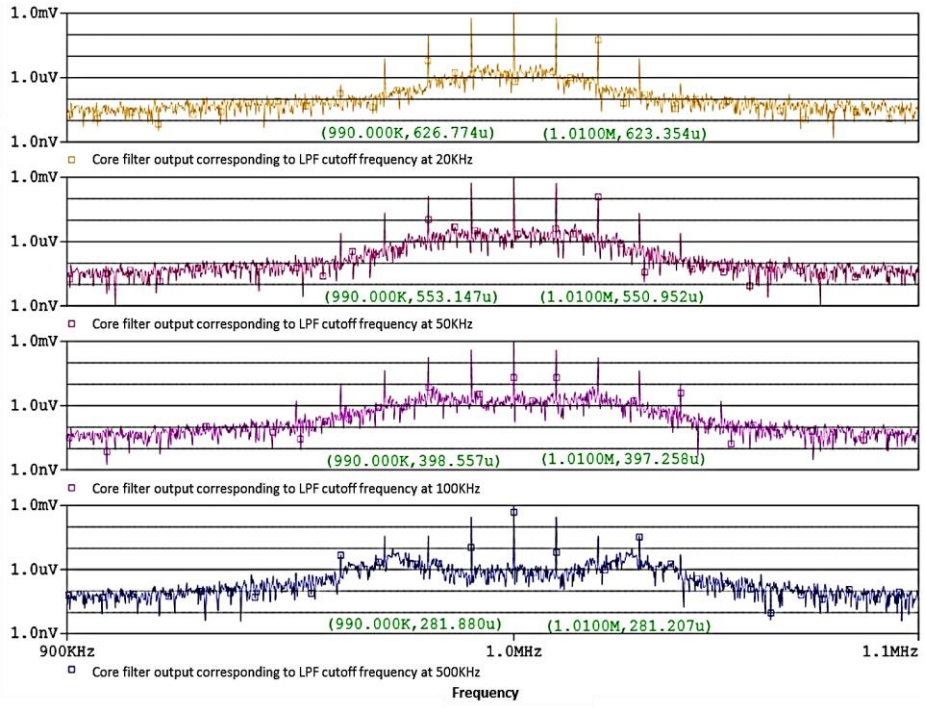

Figure 4.15 FFT spectra of the core filter output from the modified System 3 where a first-order LPF is put behind the demodulator. Cutoff frequencies under test are 20kHz, 50kHz, 100kHz and 500kHz. (Original Q=100)

Comparing the spectra in Fig. 4.15 to the second spectrum in Fig. 4.14, we discovered that the inserted lowpass filter suppresses the core filter output noise floor at the cost of introducing undesired harmonic distortion of large size, and the filter with lower cutoff frequency yields higher in-band noise floor and larger sideband information signals in the core filter output. It might because the Q-factor control signal is very sensitive to the phase change in the baseband signal with which it's generated, any phase shift caused by the lowpass filter deforms the Q-factor control signal and degrades the output SNR. As it is very hard to determine the cutoff frequency to make a good tradeoff between the reduction of output noise and the rise of output harmonic distortion, inserting a lowpass filter in the feedback path does not seem to be an effective way to improve the system noise performance.

Utilizing an assistant bandpass filter

In this experiment, another bandpass filter of the same type as the core filter is employed to help produce a less noisy Q-factor control signal for the core filter. Block diagram and circuit model of the proposed design are given in Fig. 4.16 and Fig. 4.17. In the first test, we utilized a noiseless AM signal as input to explore a proper setup for Q_{core} and Q_{ctrl} so the sideband signals in the core filter output have amplitude close to that of the input sideband signals. As shown in the table below, the system input was an AM signal carried by 1MHz and has a bandwidth of 20kHz, the two filters are both centered at 1MHz. We stuck with $Q_{core} = 50$ while swept the assistant filter's Q factor, and plotted related output signals from each case.

Input (v)	u(t)=p(t)m(t)
	p(t)=1m+(0.5m)sin(2π(10k) t)
	m(t)=sin(2π(1Meg) t)
Core Bandpass Filter	Q_{core}=50, fc=1MHz
Assistant Bandpass Filter	Q_{ctrl}=5, 20, 50, 100, 200 , fc=1MHz

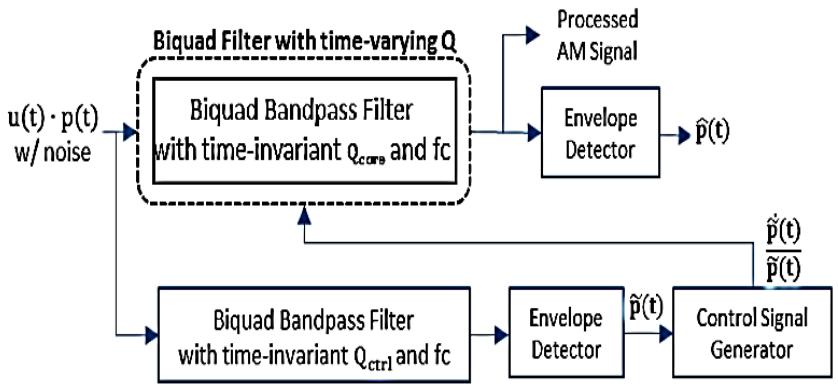

Figure 4.16 A two-filter system derived from the feedback system for processing noisy AM signals.

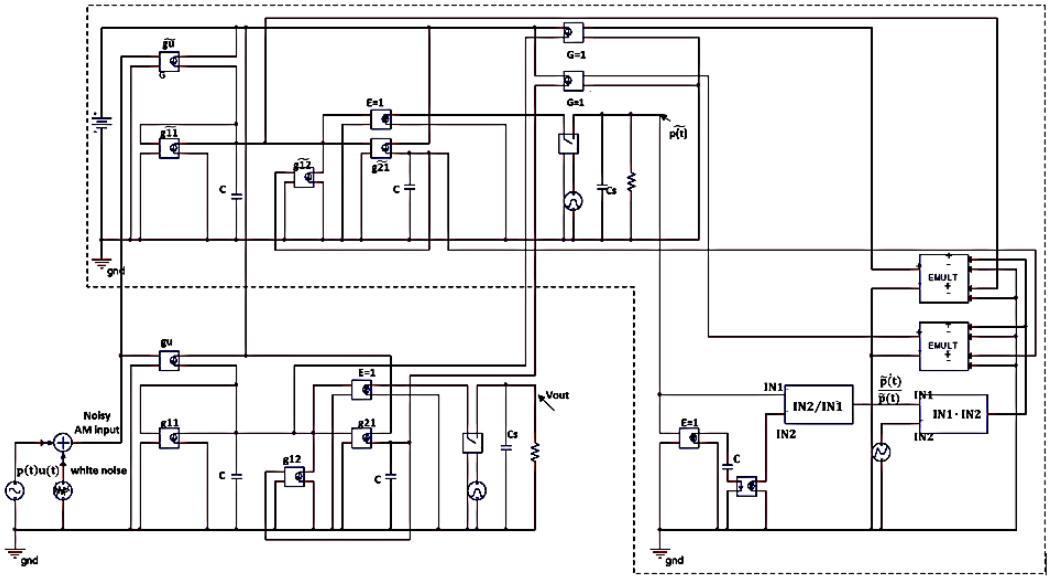

Figure 4.17 Ideal Gm-C model for the two-filter system in Fig. 4.16.

Shown in Fig. 4.18 (a), as the ratio of Q_{core} to Q_{ctrl} decreases from 10 to 0.25, the harmonic distortion in the core filter output consistently drops, however, the amplitude of the output sideband signals increases at first, hitting a peak value even higher than that of the input sideband signals when the ratio is around 2.5, and then consistently decreases. Fig. 4.18(b) suggests that the recovered signal from the two-filter system always lags the original modulating signal regardless of the ratio, and a lower ratio results in a larger phase shift. We screened out the combination of $Q_{core} = 50$ and $Q_{ctrl} = 200$ as it yields an output with sideband signals lower than the input sideband signals. For the rest combinations, the lower the ratio of Q_{core} to Q_{ctrl}, the higher the core filter output SNR is. In the following noisy input test where the AM signal was added with white voltage noise of 0.2mVrms, the system was set up with $Q_{core} = 50\ and\ Q_{ctrl} = 5, 20, 50, 100$ respectively, and the output signals in Fig. 4.19 were compared to evaluate the system noise performance.

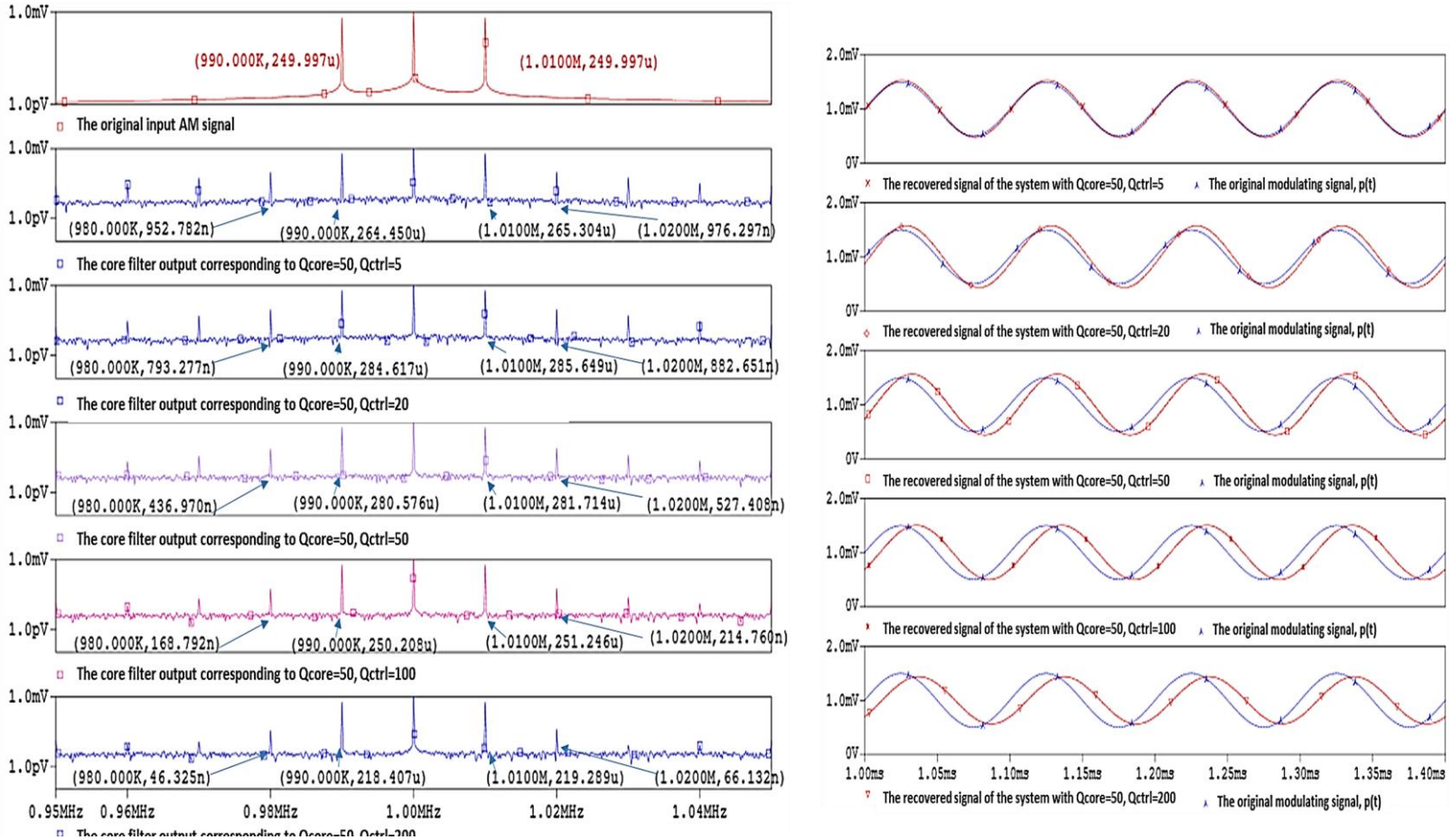

(a) (b)

Figure 4.18 (a) FFT spectra of the core filter output and (b) Transient plots of the recovered signals from the proposed two-filter system in Fig 4.16 with $Q_{core} = 50$ and $Q_{ctrl} = 5,20,50,100,200$ in the noiseless input test.

According to Fig. 4.19(a), the core filter output from the two-filter system does not contain any undesired additional noise components as the feedback filter output does (Fig. 4.12). Different combinations of $\mathrm{Q_{core}}$ and $\mathrm{Q_{ctrl}}$ yield a filtering system with different noise suppression capability, and a rough comparison suggests that the system with higher Q_{ctrl} applies stronger attenuation to the out-band noise. To better evaluate the noise performance of the system, we normalized the 10kHz component in the recovered signals to 0.5m, as shown in Fig. 4.19(b). Comparison between the resulting FFT spectra reveals that the system's capability in suppressing the input white noise depends mainly on the smaller one in $\mathrm{Q_{core}}$ and $\mathrm{Q_{ctrl}}$: when $\mathrm{Q_{ctrl}}$ is lower than $\mathrm{Q_{core}}$, a higher $\mathrm{Q_{ctrl}}$ yields a lower output noise floor; if $\mathrm{Q_{ctrl}}$ is already higher than $\mathrm{Q_{core}}$, tuning $\mathrm{Q_{ctrl}}$ too high would raise the in-band noise floor while only slightly lower the out-band noise floor. To demonstrate this property more clearly, Fig. 4.19(c) gives the FFT spectra of the normalized recovered signal from the systems set up with $\mathrm{Q_{core}} = 50$ and $\mathrm{Q_{ctrl}} = 10, 50, 200, 500$. Fig. 4.19(d) is a zoomed-in version of the spectra in Fig. 4.19(c) (without the one corresponding to $\mathrm{Q_{ctrl}} = 10$) and the FFT spectrum of the normalized recovered signal from an open loop biquad bandpass filter with Q =50. It indicates that a higher $\mathrm{Q_{ctrl}}$ makes the two-filter system with the out-band noise suppression capability closer to that of an open loop biquad bandpass filter with Q factor equals $\mathrm{Q_{core}}$; on the other hand, as $\mathrm{Q_{ctrl}}$ increases, the amplitude of the useful signals in the system output decreases. Considering this tradeoff, setting $\mathrm{Q_{ctrl}} = \mathrm{Q_{core}}$ is appropriate for improving the system output SNR when processing a noisy AM signal.

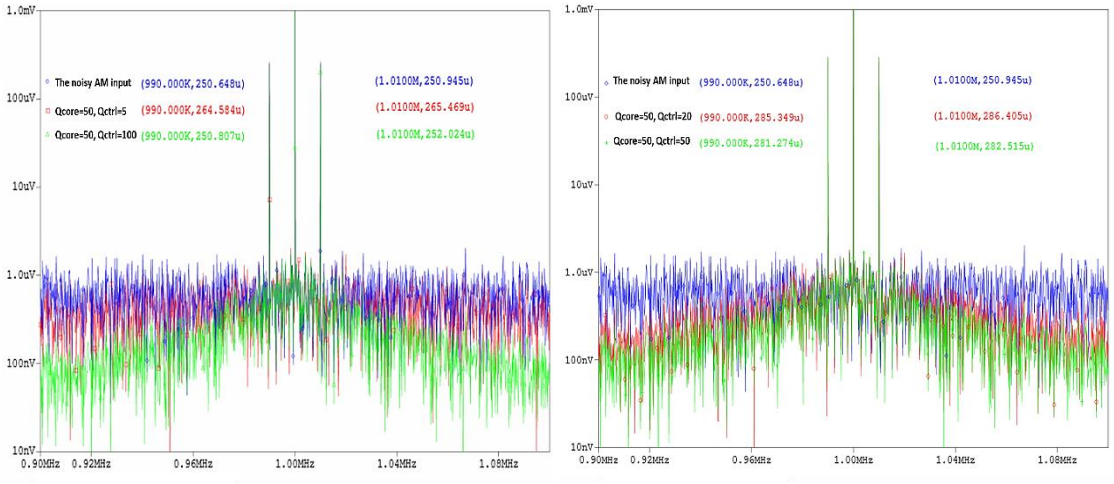

(a) Core filter output from the two-filter system set up with different combinations of Qcore and Qctrl

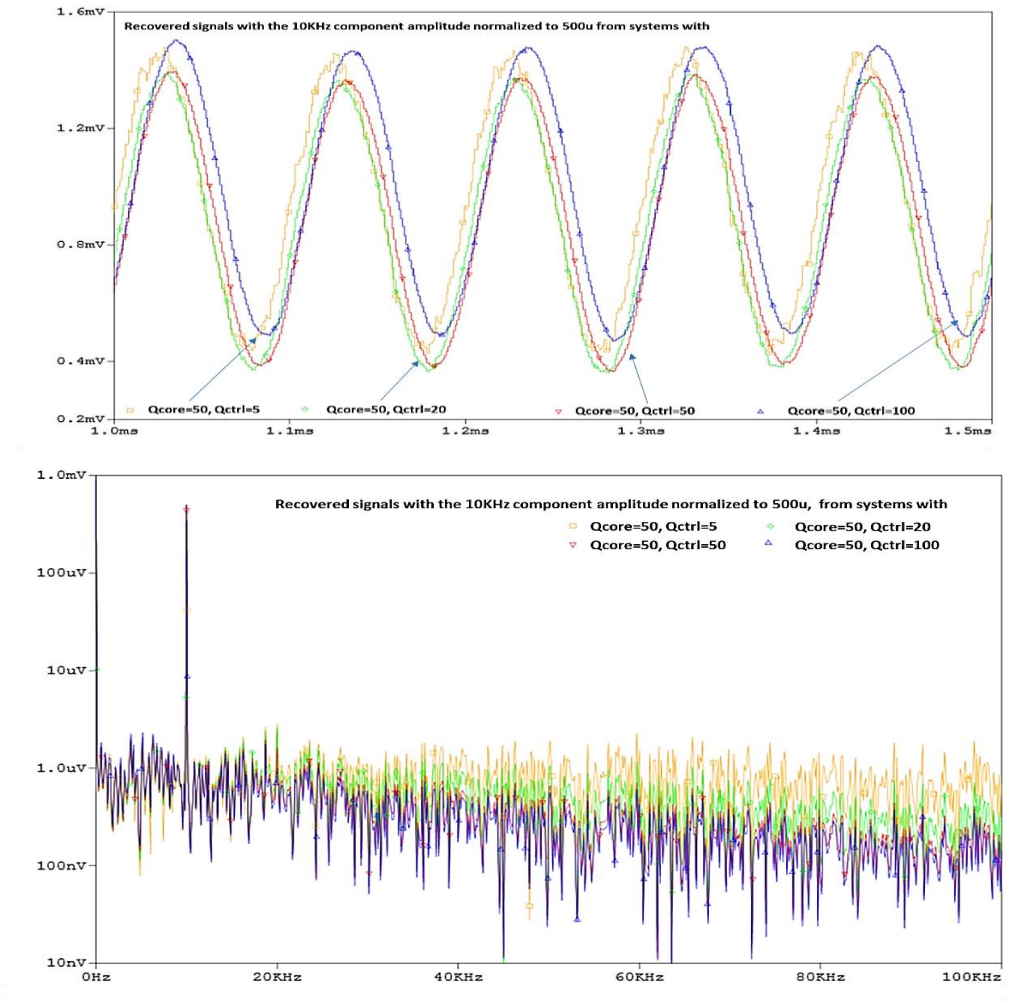

(b) Transient plots and FFT spectra of the recovered signal from the two-filter system set up with different Q factor combinations, with the 10kHz component normalized to 500uV.

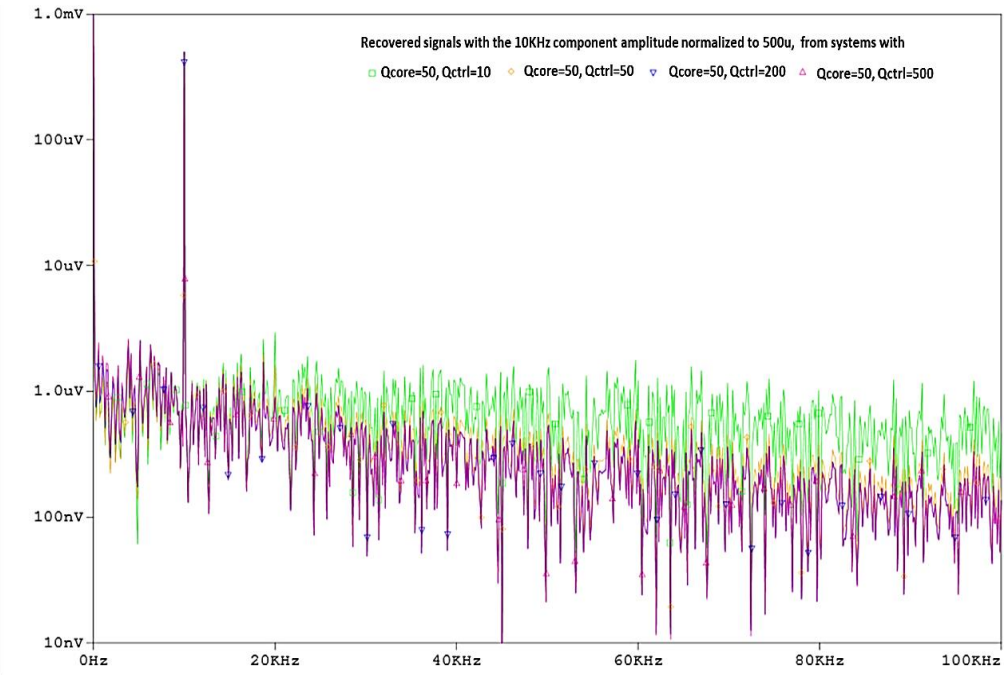

(c) FFT spectra of the recovered signals from the two-filter system set up with different Q factor combinations, with the 10KHz component normalized to 500uV.

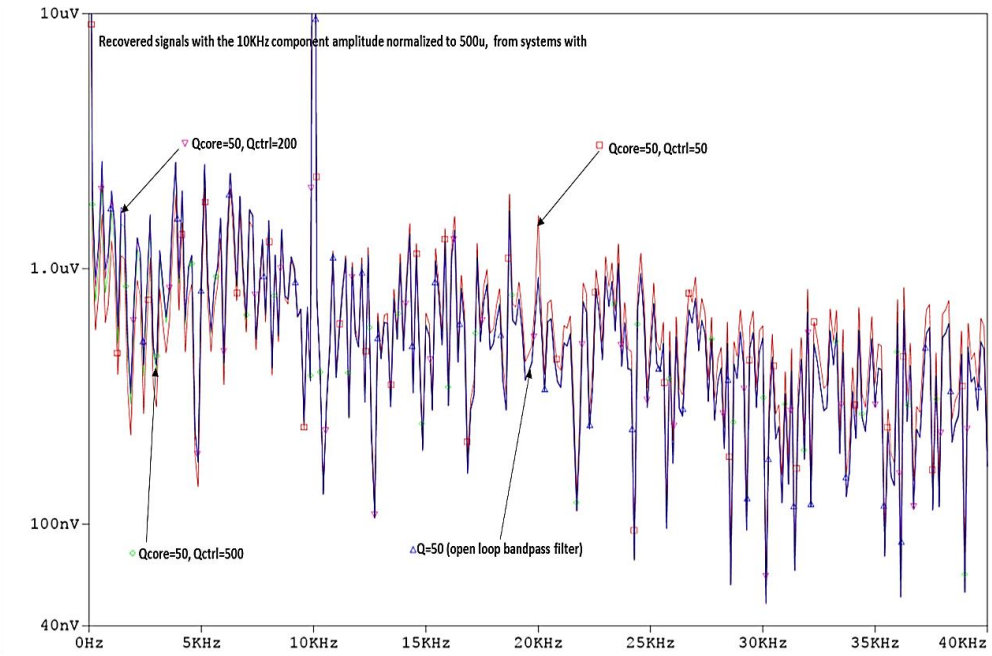

(d) A zoom-in version of the FFT spectra of the recovered signals from the two-filter system set up with $Q_{core} = 50$, $Q_{ctrl} = 50, 200, 500$ and an open loop biquad bandpass filter with $Q = 50$.

Figure 4.19 Results from the noisy input test on the two-filter system in Fig. 4.17.

Finally, we set up the two-filter system with $Q_{core} = Q_{ctrl} = 50$, and $Q_{core} = Q_{ctrl} = 500$, respectively, and compared its noise performance to that of the reference system, the ideally modified bandpass filter shown in System 2. The test results below suggest: 1) Unlike the ideally modified bandpass filter, the two-filter system cannot maintain the amplitude of the useful input components when the filter bandwidth is tuned too narrow compared to the input bandwidth, as shown in Fig. 4.20(a) where the input bandwidth is 20kHz and the bandwidth of all the filters is 2KHz.

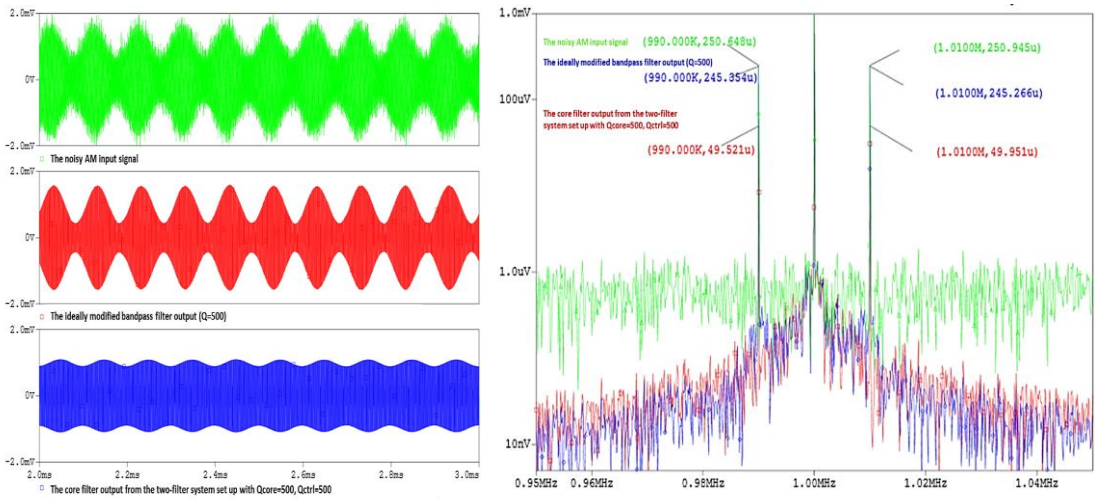

(a) Noisy input test on the two-filter system with $Q_{core} = Q_{ctrl} = 500$ and System 2 with $Q = 500$

2) When there is a good match between the filter bandwidth and the input bandwidth, the useful components in the two-filter system output have an amplitude close to or even higher than that of the original information components. Take the test where the bandwidth of the all the filters and the input signal was 20kHz for instance, the sideband signals in the two-filter system's core filter output have an amplitude of 281uV, while both the input sidebands and the output sidebands from the reference ideally modified filter have an amplitude of 250uV, as shown in Fig. 4.20(b). After normalizing the output sideband components from both systems to 250uV, it's observed in Fig. 4.20(c) that the

output SNR of the two systems are comparable, while the ideally modified bandpass filter demonstrates slightly stronger out-band noise reduction.

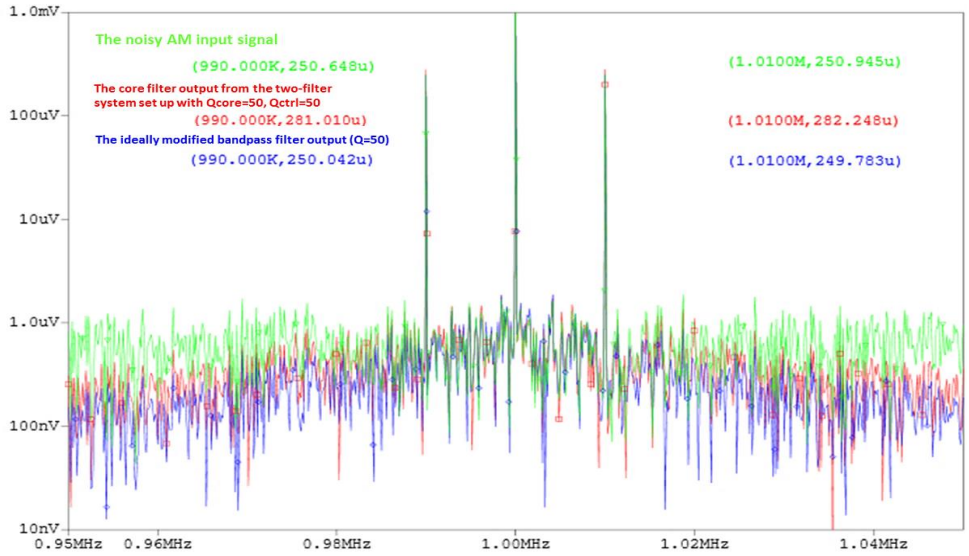

(b) Noisy input test on the two-filter system with $Q_{core} = Q_{ctrl} = 50$ and System 2 with $Q = 50$.

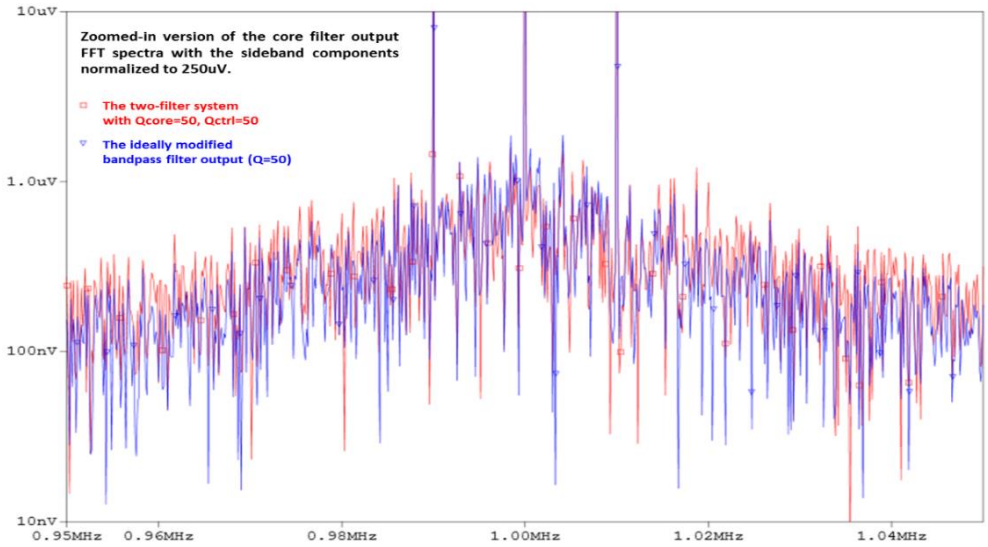

(c) A zoomed-in version of the above output FFT spectra with the sideband components normalized to 250uV.

Trial and error simulation results not shown here suggest that for the core filter output to have sideband signals not smaller than the original input sideband signals, the upper limit for Q_{core} is about $1.4f_0/BW_{in}$, where f_0 is the core filter center frequency

and BW_{in} is the input bandwidth. Take the AM signal of 20kHz bandwidth and carried by 1MHz for instance, when the two-filter system is set up with $Q_{core} = Q_{ctrl} = 70$ and $f_0 = 1MHz$, the core filter output sideband signals have an amplitude very close to that of the input sideband signals. It was also discovered that the two-filter system with $Q_{ctrl} = Q_{core}$ has the input-noise-suppression capability comparable to that of an open loop biquad bandpass filter with Q factor equals $0.7Q_{core}$. As long as the system filter bandwidth is not narrower than $0.7BW_{in}$, the input sideband signals will not be attenuated, although they will always get some negative phase shift.

Based on the above discoveries, we predicted that for noisy AM input signals, the output noise floor of a two-filter bandpass filtering system with $Q_{ctrl} = Q_{core}$ would be very close to that of an ideally modified bandpass filter (System 2) with Q factor equals $0.7Q_{core}$. Therefore, for input AM signals with comparatively narrow bandwidths, the two-filter system is capable of producing an output with very high SNR. The noise performance of the two-filter system and System 2, tested with different Q factors and input bandwidths as shown in Fig. 4.20 (d), agrees well with our expectation.

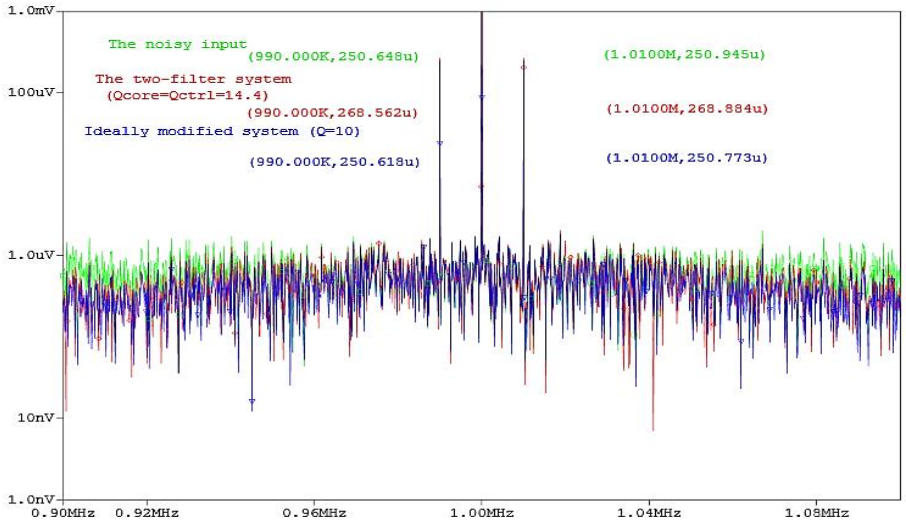

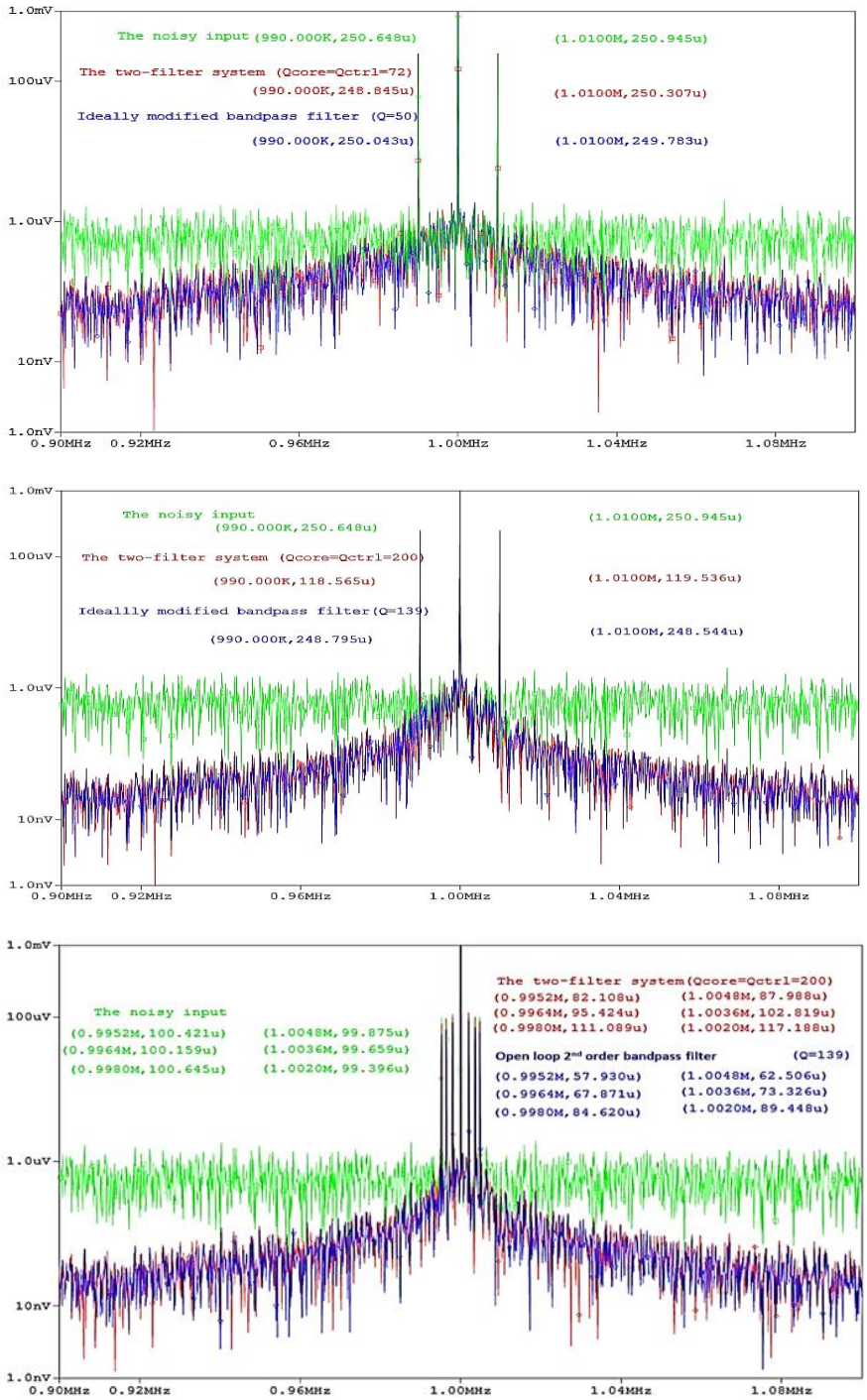

(d) FFT spectra and related measurement of the noisy input signal and the output from the two-filter system with different Q_{core}, Q_{ctrl} setup and the reference ideally modified bandpass filter with a Q factor equals $0.7Q_{core}$.

Figure 4.20 Noise performance test and comparison of the two-filter system with $Q_{core} = Q_{ctrl}$ and the ideally modified bandpass filter with Q factor equals Q_{core} or $0.7Q_{core}$ in dealing with noisy AM input signals.

3) Test on System 4

Note that System 3 utilizes a sample-and-hold block to recover the baseband signal, which has the following drawbacks: 1) In order to minimize the introduced phase shift and noise in the recovered signal, the S/H block is expected to perform ideal sampling at a rate that equals the carrier frequency of the input AM signal. The implementation of such a block is very challenging in practice. For example, the ON resistance of the switch has to be extremely small, SNR of the sampling result is very sensitive to the parasitic resistance of the sampling capacitor, etc. 2) According to the math, the output signal of the S/H block, $\hat{p}(t)$, has components near harmonics of the sampling rate. Although their amplitude is negligible compared to the size of the information signal, they will be responsible for the undesirable high frequency components in the Q-factor control signal $\frac{\dot{\hat{p}}(t)}{\hat{p}(t)}$ and may lower the output SNR of the feedback system. Recall that a synchronous complex filtering system utilizes a mixer module for down conversion, and the recovered signal doesn't contain as many high frequency components as the S/H block output does, System 4 might be superior to System 3 in noise performance.

The test on System 4 is set up as follows: the input is the same noisy AM signal used in the tests on System 1~System 3; the system front end modulating frequency is 2MHz; the core filter center frequency is 1MHz and the original Q factor is 50 or 500; the back end modulating frequency is 1MHz. Moreover, a complex filtering system with its core filter modified by the ideal $\frac{\dot{p}(t)}{p(t)}$ and an open-loop complex filtering system were also tested for comparison.

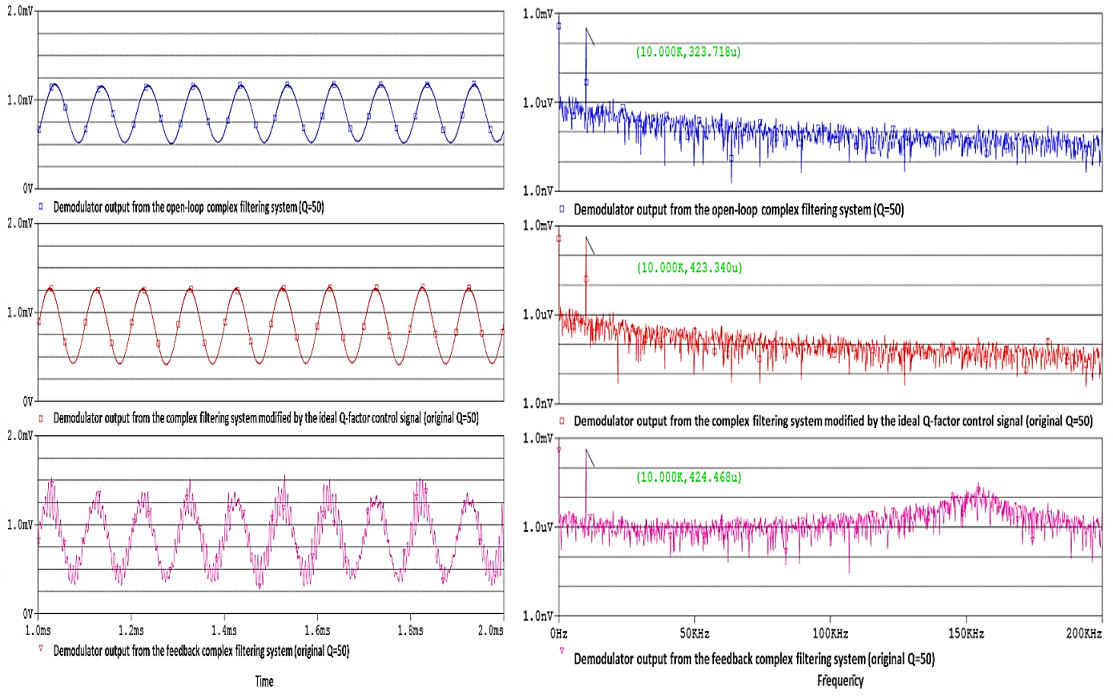

Figure 4.21 Demodulator output from System 4 and two reference complex filtering systems, all with the original Q factor of 50.

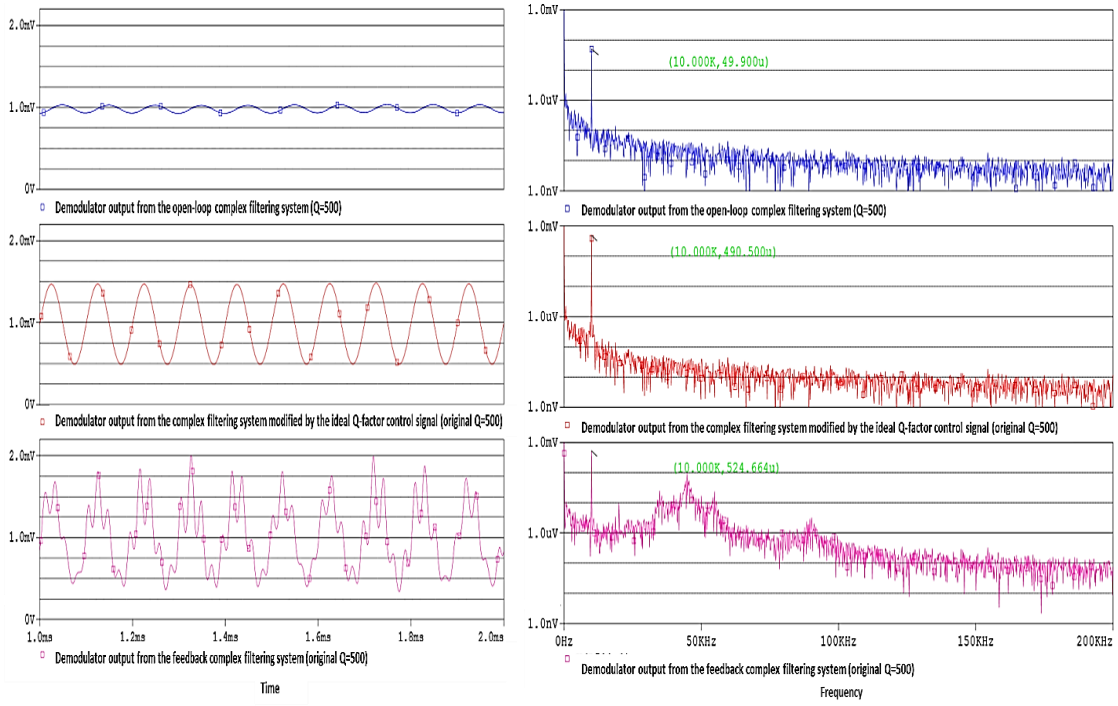

Figure 4.22 Demodulator output from System 4 and two reference complex filtering systems, all with the original Q factor of 500.

In both Fig. 4.21 and Fig. 4.22, the ideally modified complex filtering system produces a recovered signal as if the input noise was processed by an open-loop complex filter with the same Q factor while the input information signal was almost intact. However, the output noise floor of System 4 is obviously higher, and large-sized noise components are observed in a higher frequency range. When the original Q factor is increased to 500, the output noise floor from the feedback complex filtering system does not get further reduction while the noise peak rises and moves into a lower frequency range, which causes the baseband noise floor even higher than it is in the case where Q=50. We tried to alleviate this problem by resetting the input carrier frequency and the front end modulating frequency, to separate their sum and difference further apart, expecting the unwanted high frequency components in front end modulator output to get harder attenuation. Specifically, the carrier frequency was raised to 4MHz from the original 1MHz, and the front end modulating frequency was accordingly increased to 5MHz. Then the front end modulator generates components near 1MHz and 9MHz instead of near 1MHz and 2MHz. Unfortunately, simulation results (not shown here) suggest that although this method lowers the high frequency noise in the output, it barely affects the baseband noise level. Therefore, System 4 is not able to suppress the input noise either, due mainly to the noisy feedback Q-factor control signal.

Finally, we compared the demodulator output of System 3 and System 4 by plotting them on the same graph. Both systems under test have a core filter with an original Q factor of 50 and center frequency of 1MHz. The transient plots in Fig. 4.23 suggest that both systems are able to reconstruct the information component to be in phase with the original modulating signal. According to the FFT spectra, the output noise

floors of both systems are at a similar level in the baseband, and large output noise components are observed near 130KHz for both systems. The recovered signal from System 4 has much less high frequency components due to its signal mixing demodulation approach. As a summary, when dealing with a noisy AM input signal, System 3 and System 4 produce output signals of comparable SNR, and both are noisier than their open loop filter counterpart.

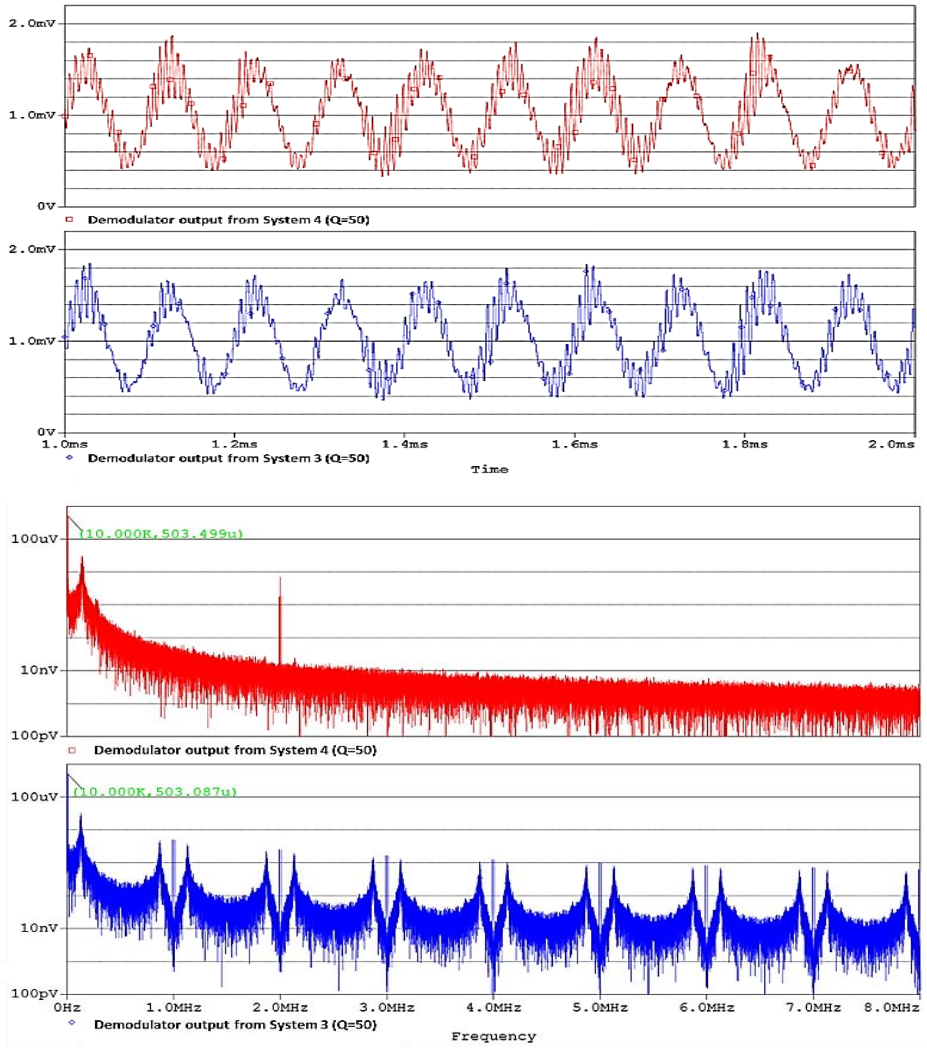

Figure 4.23 Transient plots and wide-range FFT spectra of the recovered signal from System 3 and System 4 when the input is a noisy AM signal. The core filter in both systems has a quality factor of 50.

2. Noiseless input and noisy system

In this section, we focus on the performance of the noisy feedback AM mode filtering systems. Two uncorrelated white noise currents were respectively injected into the capacitors of the core filter to model the in-filter noise.

1) Input-referred noise

First, we verify with simulation that for the open loop counterpart of System 3 and System 4, the same amount of injected noise is equivalent to higher input-referred noise if the core filter has a higher Q factor. The systems were tested with a noisy core filter and the recovered signals were plotted. Since a typical method for evaluating the input-referred noise of an open loop system is to measure the output noise and divide it with the open loop gain, the noise level of the recovered signal could be a good representation of the system's input-referred noise.

Filter in the systems under test	2nd Order Bandpass Filter	2nd Order Complex filter
Filter Q value	50, 200	50, 200
Filter Center Frequency	1MHz	
RMS value of the injected noise	0.1uArms for both uncorrelated currents	
Input AM signal	u(t)=p(t)m(t)	
	p(t)=1m+(0.5m)sin(2π(10k) t), m(t)=sin(2π(1Meg)	

Table 4-2 Parameter setup for the input-referred noise test

As a bandpass filter with Q of 200 has a much narrower bandwidth than the one with Q of 50, it is supposed to apply more attenuation to the input-referred noise in the frequency range of our interest. However, in Fig. 4.24, the recovered signal from the system with Q=200 has even higher baseband noise floor, which suggests that with the same amount of injected noise, a sharper filter tends to have higher input-referred noise. Similar situation was observed in the demodulator output from the open loop complex filtering

systems, which indicates that a complex filter deals with the in-device noise the same way as a standard biquad bandpass filter does.

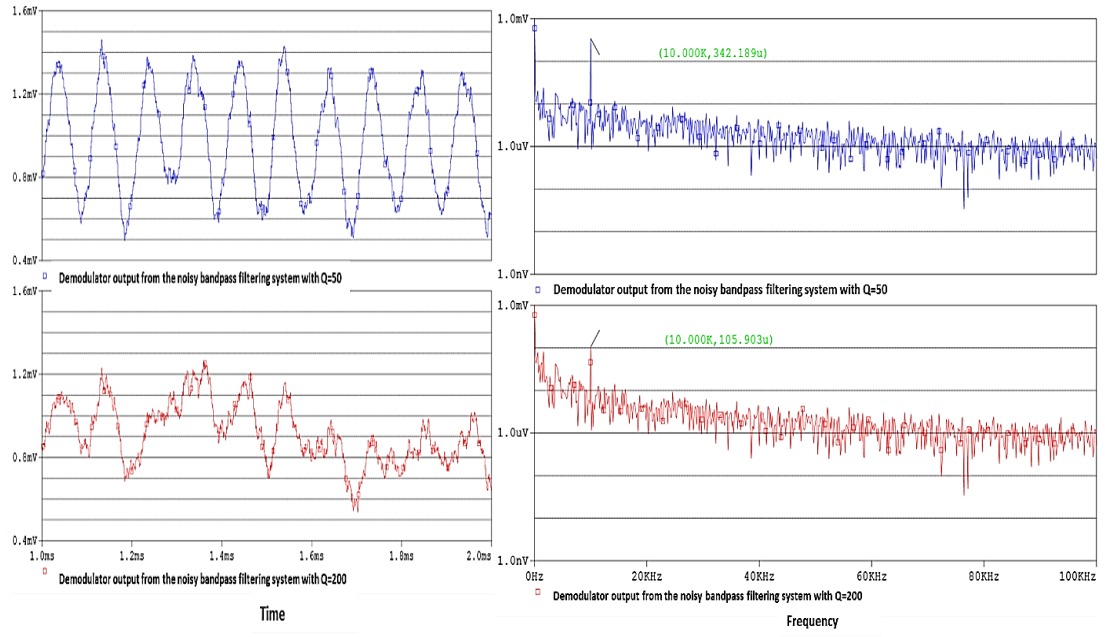

Bandpass filtering system demodulator output

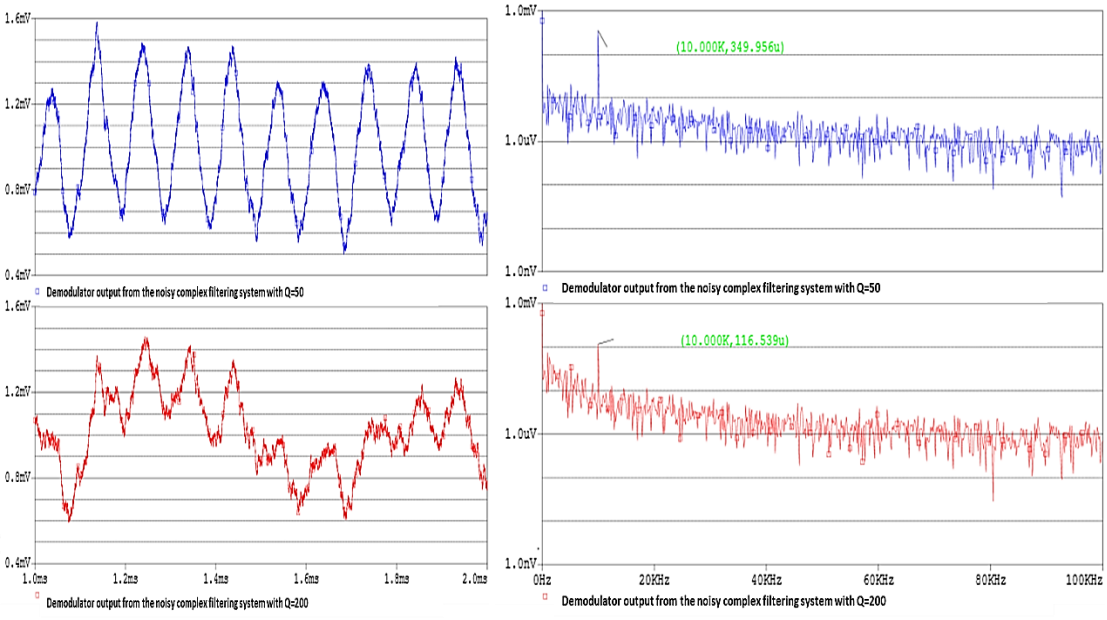

Complex filtering system demodulator output

Figure 4.24 Transient plots and FFT spectra of the recovered signals from the bandpass filtering system and the complex filtering system with a noisy core filter of different Q values.

2) Test on System 3 and System 4

This part focuses on the performance of noisy feedback systems, namely, System 3 and System 4 with a noisy core filter. Reference systems with their core filter modified by the ideal Q-factor control signal were tested too. The spectra in Fig. 4.25 correspond to the recovered signals from the systems under test, all with an original Q factor of 50. The noise suppression capability of the systems controlled by the ideal $\frac{\dot{p}(t)}{p(t)}$ is still comparable to their open loop counterpart, and the recovered information signals are very similar to the original $p(t)$. Unfortunately, both feedback systems again fail to suppress the injected noise as hard as their related open loop filtering systems do, and they generate undesirable noise components in a higher frequency range, hence producing a noisier recovered signal. The recovered information component itself has similar size and phase as that of the original $p(t)$ though. A closer inspection shows that the noise peak appears in a lower frequency range in the output of System 3 while System 4 has a slightly higher output noise floor in the in-band frequency range, so the baseband output noise of System 3 and System 4 has comparable strength.

When raising the original Q factor for both systems to 200, convergence problem was encountered in the simulation, which might be because the input-referred noise was scaled up to a too high level compared to the size of the input AM signal. We hence multiplied the original AM input by 5 and reran the simulation. The demodulator output from the systems under test were shown in Fig. 4.26. Both the noise peak and the baseband noise floor in the demodulator output from System 3 and System 4 became much higher than they were in the case where Q=50. This is due to the scaled up input-

referred noise and the noisier feedback Q factor control signal. Comparing Fig. 4.25 to Fig. 4.26, it was revealed that System 3 and System 4 with a lower original Q factor produce an output with higher SNR when the core filter is noisy.

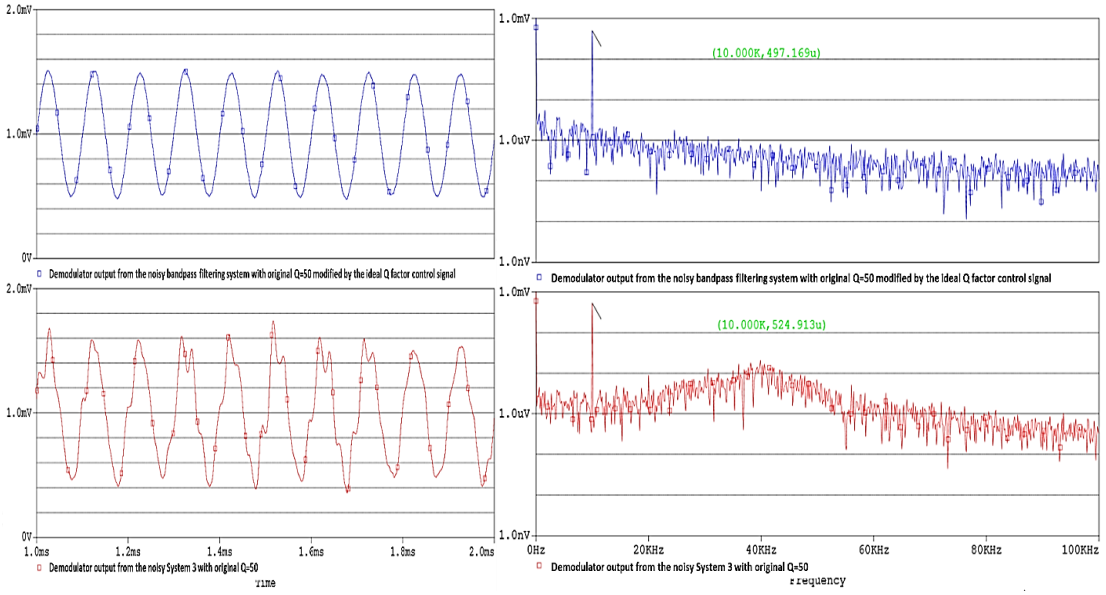

(a)

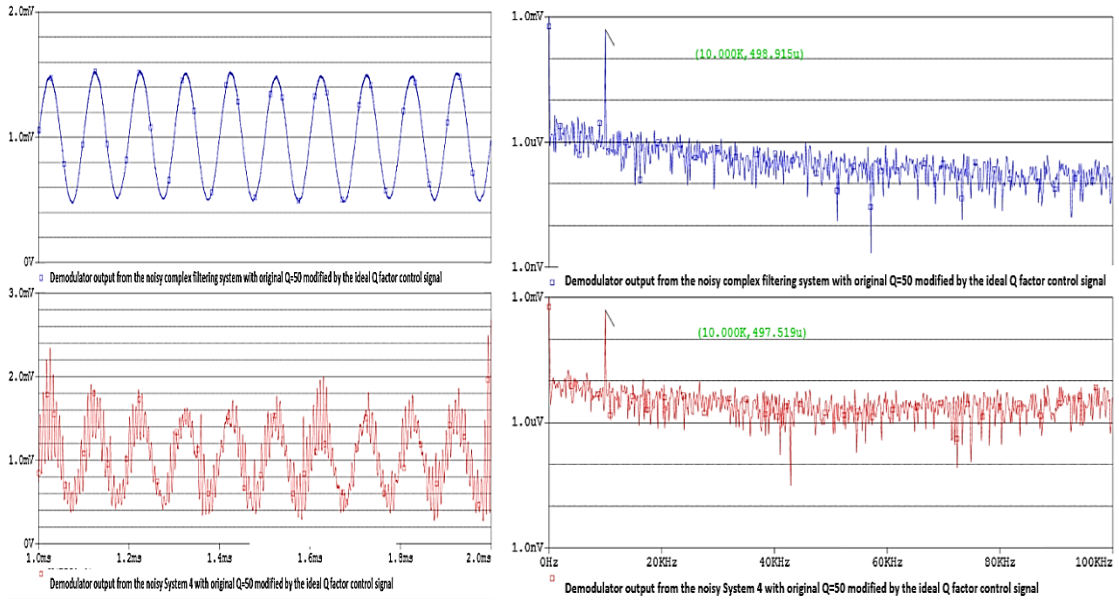

(b)

Figure 4.25 Transient plots and FFT spectra of the recovered signals from the noisy System 3, noisy System 4 and the noisy reference systems modified by the ideal Q-factor control signal. (Original Q=50 for all the systems)

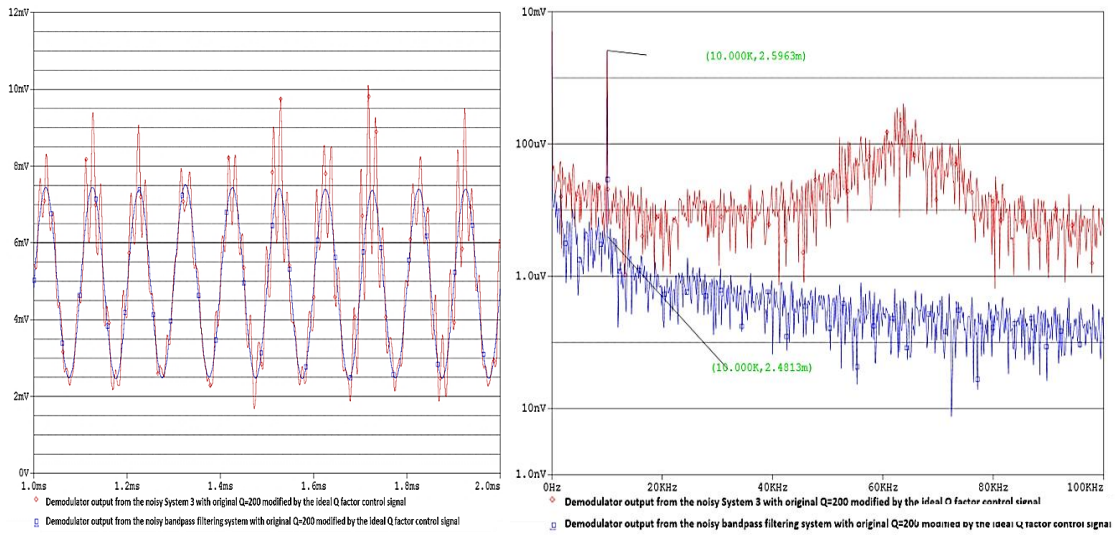

(a)

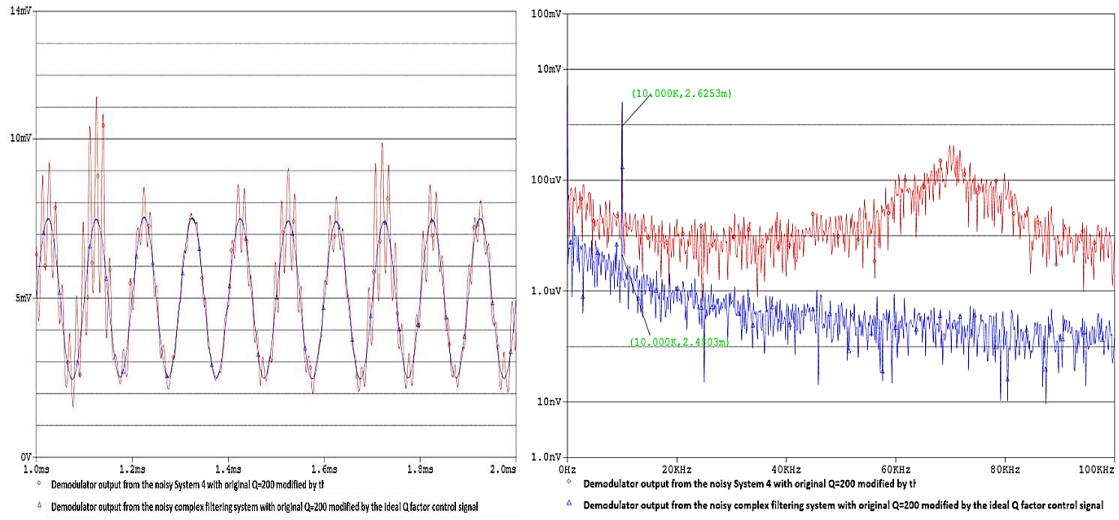

Figure 4.26 Transient plots and FFT spectra of the recovered signals from the noisy System 3, noisy System 4 and the noisy reference systems modified by the ideal Q-factor control signal. (Original Q=200 for all the systems) The input AM signal was set five times larger than it was in the above test to avoid convergence problem in the simulation.

4.2 Noise Tests on the FM Mode Synchronous Filtering Systems

4.2.1 System Review

Dynamic FM mode synchronous filtering systems have been introduced in the last section of Chapter 3. An ideal dynamic synchronous complex filter has external function almost identical to that of its static counterpart, although it has a time-varying

center frequency and accordingly synchronized terminal modulating frequencies. The block diagram below gives a conceptual description on such a system. Two typical variation patterns of the core filter center frequency are sinusoidal waveform and square waveform, as they make the synchronization more straightforward and implementable. An appealing advantage of the dynamic filtering systems is their potential noise suppression capability. Consider a dynamic synchronous complex filter adopts the square waveform pattern, although the overall system performs like a complex filter with a constant center frequency, the core filter center frequency switches between $f_0 \pm \Delta f_0$ at the rate of f_{var} and barely stays at f_0 (f_0 is the dc offset of the core filter center frequency, Δf_0 is the maximum difference between the time-varying center frequency and f_0). Suppose Δf_0 is large and the core filter is sharp enough (the core filter's bandwidth is a constant independent of the center frequency variation), then from intuitive point of view, the system will be able to effectively filter out the noise near f_0 without further attenuating the input sideband signals, hence it is superior to its static counterpart in suppressing the internal noise in a certain frequency range.

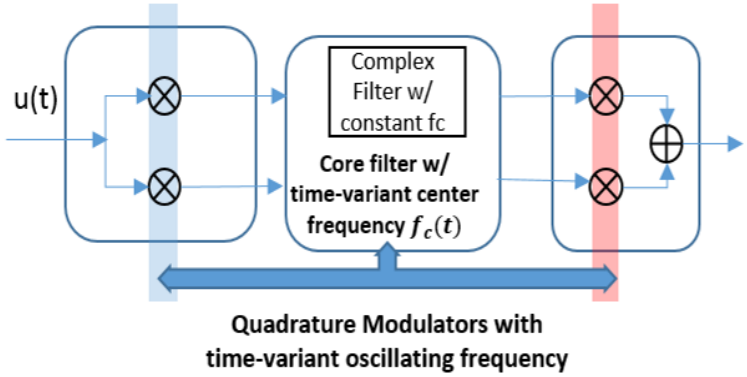

Figure 4.27 The block diagram of a dynamic FM mode sychronous filtering system.

4.2.2 Noise Performance Test

1. Noiseless Input and In-filter Single-tone Noise

Based on the qualitative analysis above, we started off with the test where single-tone noise currents were injected into the core filter while the input signal was noiseless. According to the parameter setup in Table 4-3, the time constant for the complex filter in the static system is about 16us ($\tau = \frac{2Q}{w_0}$), so we swept the switching rate from 80kHz to higher frequencies, as 80kHz corresponds to a switching period a little shorter than the filter's time constant. While sweeping the center frequency variation rate, the variation range was kept to be $1\text{MHz} \pm 400\text{KHz}$ for most tests.

Baseband signal and carrier	$f_{sig} = 10\text{KHz}$ (amplitude: 0.5mA), $f_{carrier} = 5\text{MHz}$(amplitude: 1mA)			
Modulating frequencies	$f_{front\_end} = 6\text{MHz}$ (superheterodyne mode) $f_{back\_end} = 1\text{MHz}$ (down conversion for signal reconstruction) (amplitude of 0.4mA for both ends)			
Complex filter setup	$Q = 50$, $f_0 = 1\text{MHz}$			
Test List	f_0	Δf_0	f_{var}	In-filter noise
Test 1	1MHz	**400kHz**	80kHz	1.003MHz,988kHz (amplitude of 0.5uA for both noise currents)
Test 2			**100kHz**	
Test 3			125kHz	
Test 4			160kHz	
Test 5			200kHz	
Test 6			300kHz	
Test 7		200kHz, **800kHz**	**100kHz**	

Table 4-3 Parameter setup for the in-filter noise immunity test on the FM mode synchronous complex filters.

Plots in Fig. 4.28 to Fig.4.33 represent the demodulated signals from the synchronous complex filtering systems under test. Both sinusoidal and square waveform variation patterns were tested to explore the most effective approach to suppressing the injected single-tone noise. In Fig. 4.28, the demodulator output from a static complex filtering system injected with the same noise is plotted to provide a reference to evaluate the noise performance of the dynamic systems.

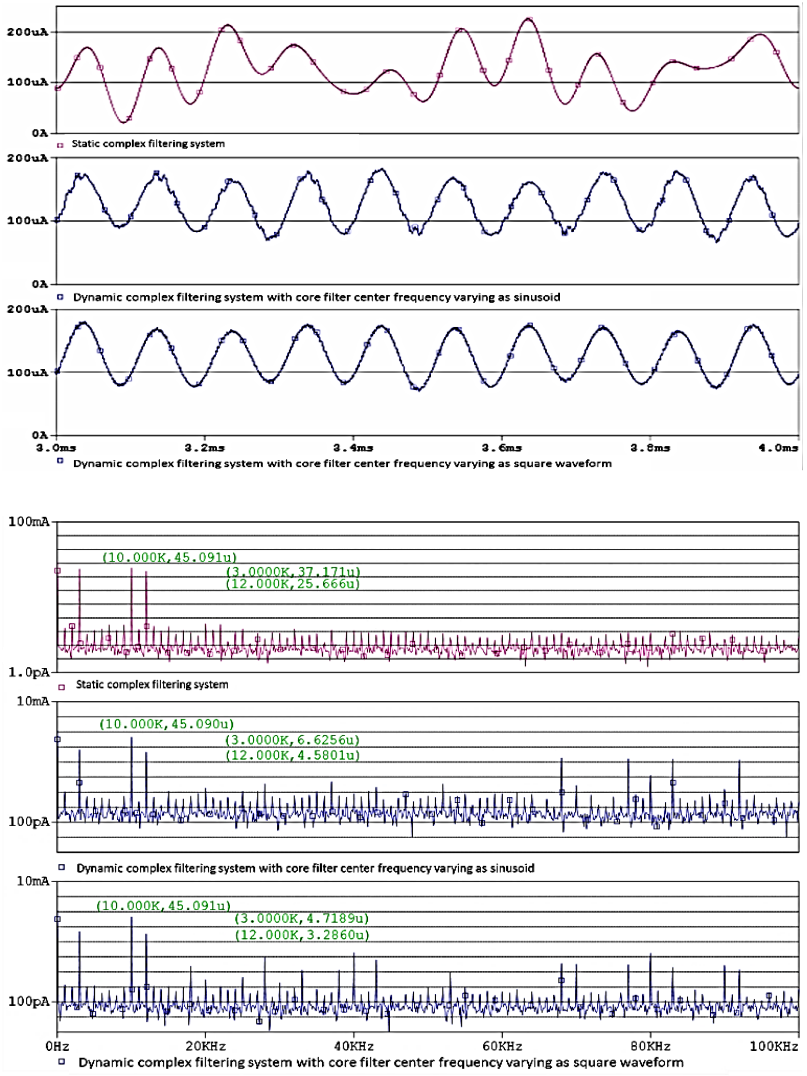

Figure 4.28 Test 1 results: Transient plots and FFT spectra of the down conversion results from a static complex filtering system and dynamic systems of which the core filter center frequency varies in a sinusoidal or square waveform with $f_{var} = 80\text{KHz}$ and $f_{dev} = 400\text{KHz}$.

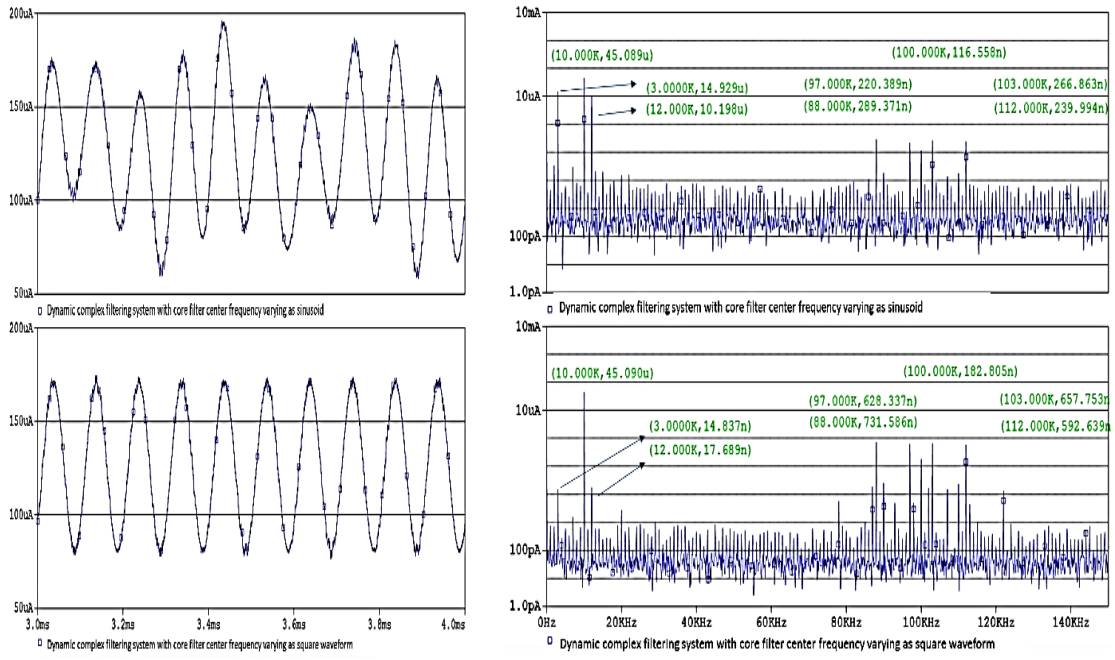

Figure 4.29 Test 2 results: Transient plots and FFT spectra of the down conversion results from a static complex filtering system and dynamic systems of which the core filter center frequency varies in a sinusoidal or square waveform with $f_{var} = 100KHz$, $f_{dev} = 400KHz$.

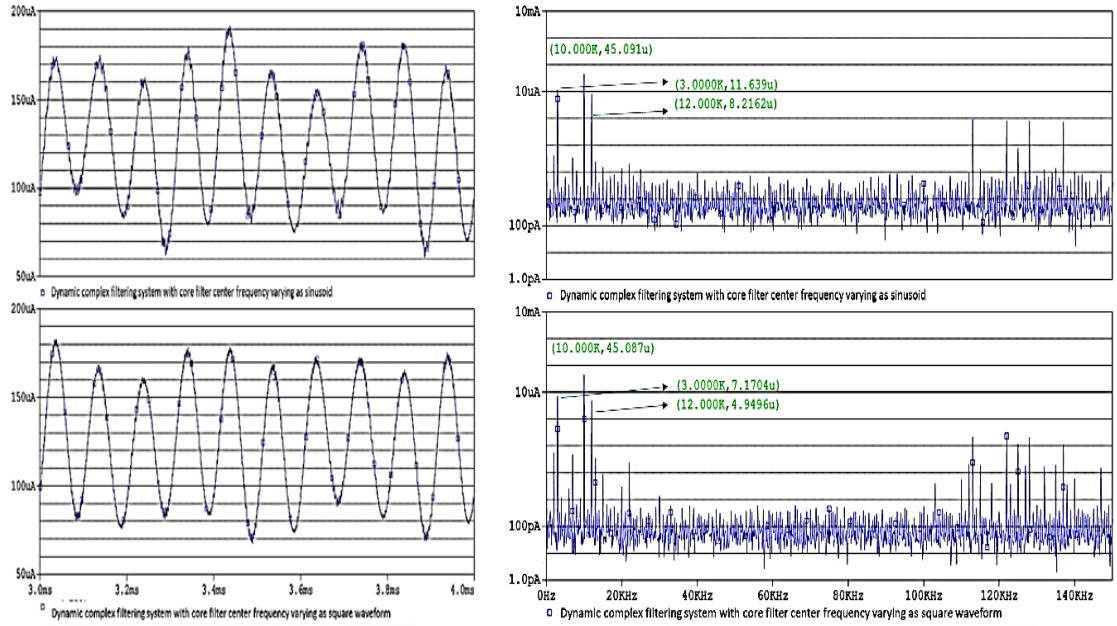

Figure 4.30 Test 3 results: Transient plots and FFT spectra of the down conversion results from a static complex filtering system and dynamic systems of which the core filter center frequency varies in a sinusoidal or square waveform with $f_{var} = 125KHz$ and $f_{dev} = 400KHz$.

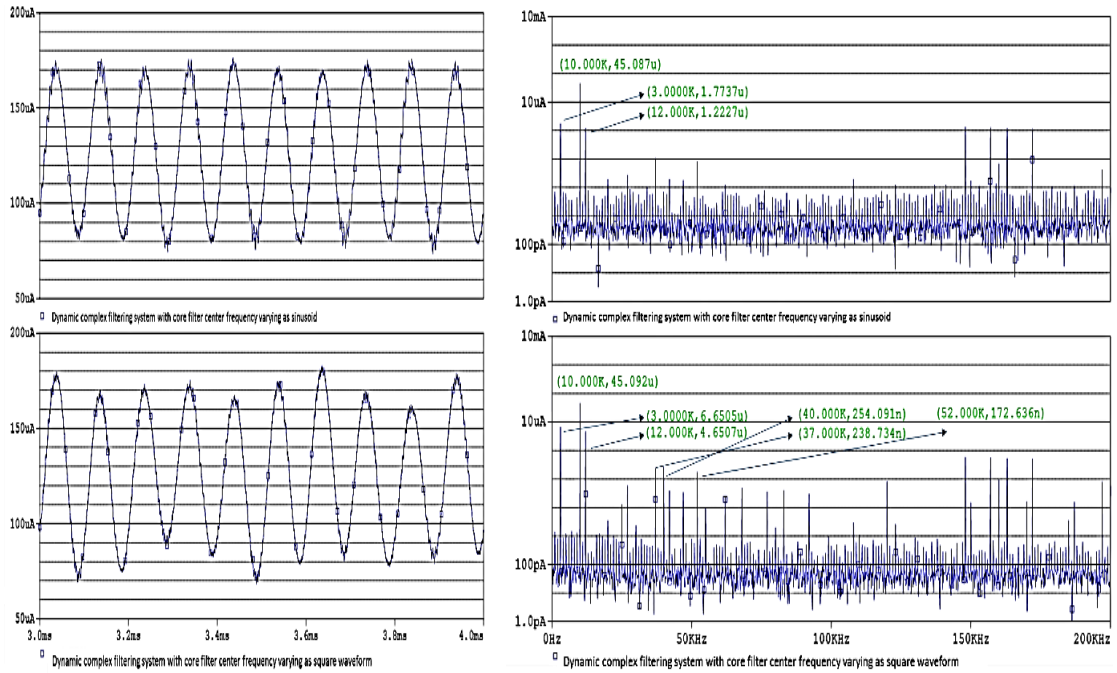

Figure 4.31 Test 4 results: Transient plots and FFT spectra of the down conversion results from a static complex filtering system and dynamic systems of which the core filter center frequency varies in a sinusoidal or square waveform with $f_{var} = 160\text{KHz}$ and $f_{dev} = 400\text{KHz}$.

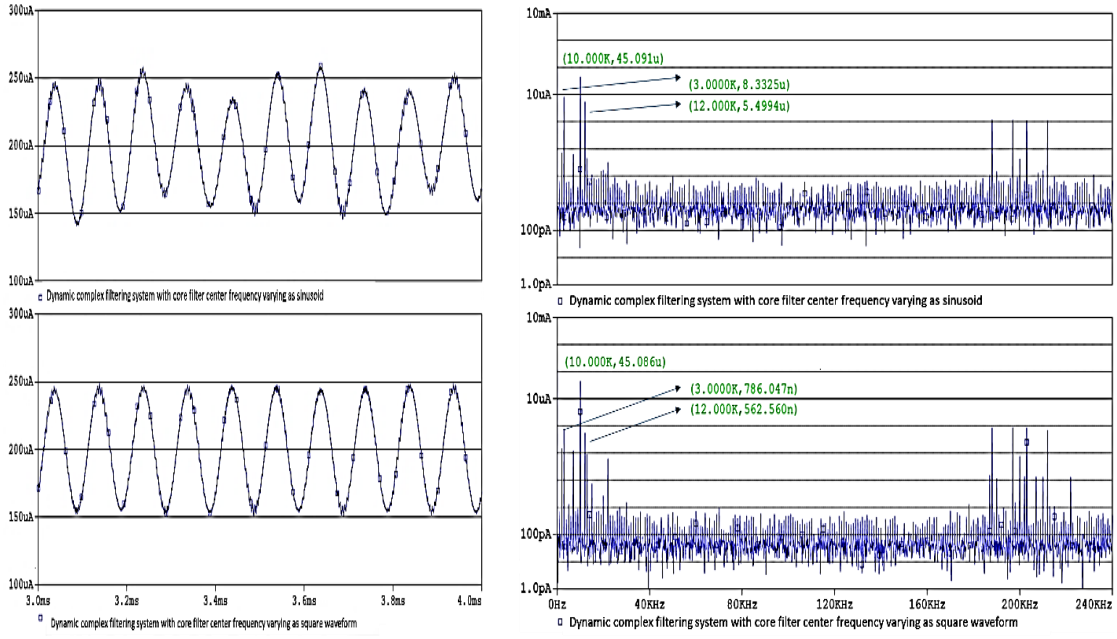

Figure 4.32 Test 5 results: Transient plots and FFT spectra of the down conversion results from a static complex filtering system and dynamic systems of which the core filter center frequency varies in a sinusoidal or square waveform with $f_{var} = 200\text{KHz}$ and $f_{dev} = 400\text{KHz}$.

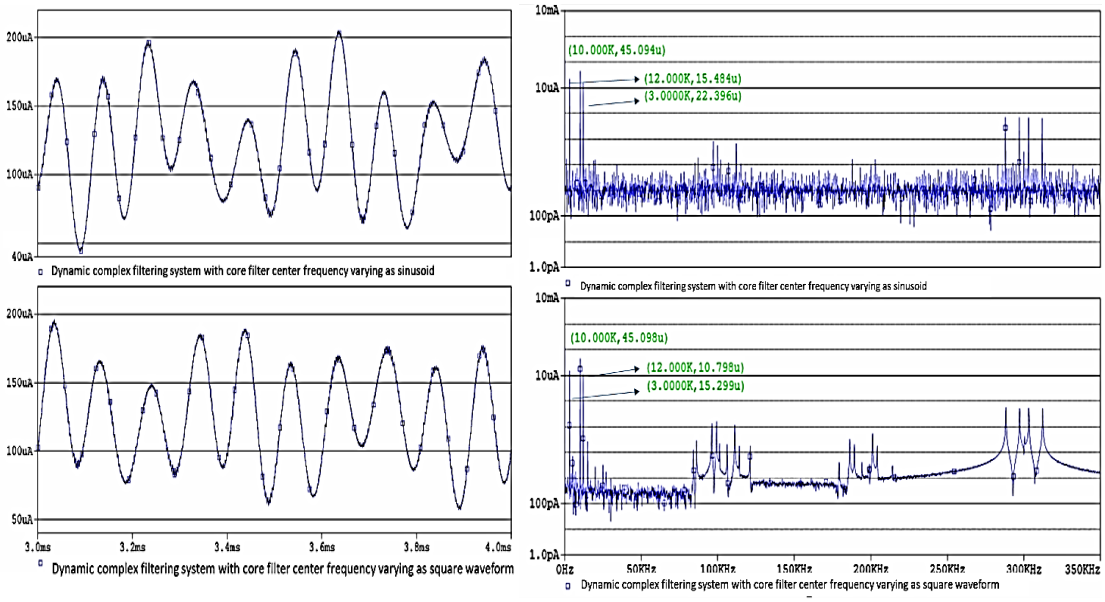

Figure 4.33 Test 6 results: Transient plots and FFT spectra of the down conversion results from a static complex filtering system and dynamic systems of which the core filter center frequency varies in a sinusoidal or square waveform with $f_{var} = 300\text{KHz}$ and $f_{dev} = 400\text{KHz}$.

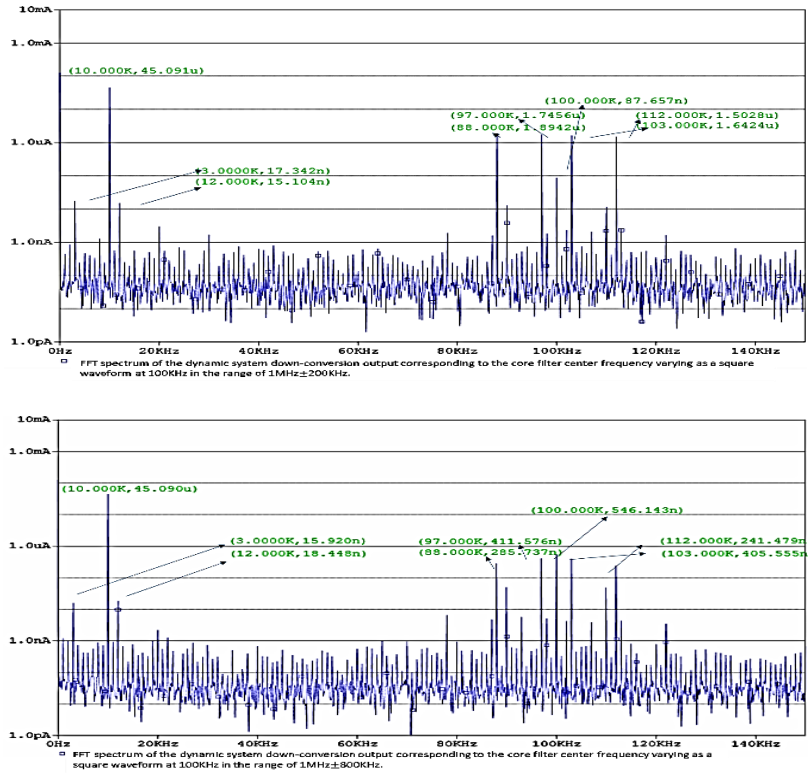

Figure 4.34 Test 7 results: FFT spectra of the down conversion result from a dynamic complex filtering system of which the core filter center frequency varies in a square waveform with $f_{var} = 100\text{KHz}$, $f_{dev} = 200\text{KHz}$ (upper) and 800KHz (lower).

The simulation results suggest: 1) A dynamic system does possess improved capability in suppressing the in-filter noise near the core filter's static center frequency. 2) Square waveform variation patterns are typically superior to sinusoidal patterns in suppressing the in-filter noise, which agrees with the qualitative analysis. 3) Some particular combinations of the variation rate and variation range effectively improve the system noise performance. For example, sticking with the 1MHz$\pm$400kHz variation range, when the center frequency is varied at 100kHz as a square waveform, the system produces an output in which the undesired single-tone noises get suppressed to be more than three orders of magnitude lower than the useful signal (Fig. 4.29). Although noise components of noticeable size are observed near 100kHz in the recovered signal, they could easily be attenuated by the subsequent low pass filtering. Unfortunately, as shown in Fig. 4.28, Fig. 4.30 and Fig. 4.31, a random variation rate other than integer multiples of 100kHz, such as 80kHz, 125kHz and 160kHz, could not suppress the single-tone noises as hard as it could when set to be 100kHz. Not only are the baseband noise components less attenuated, undesired low frequency spurious noise also rises due mainly to the intermodulation and high-frequency noise folding back. 4) A too high variation rate also degrades the system noise performance even it is an integer multiple of 100kHz. Comparing Fig. 4.33 to Fig. 4.28, a variation rate of 300kHz produces an output even noisier than the 80kHz variation rate does; also, comparing Fig. 4.32 to Fig. 4.29, the output baseband intermodulation components corresponding to the square waveform varying at 200kHz are about 50 times higher than those generated by the 100kHz variation rate. 5) Sticking with the square waveform pattern at 100kHz and adjusting the variation range doesn't obviously affect the output baseband spectrum,

while the intermodulation noise components around 100kHz become smaller as the variation range gets wider, comparing the spectra in Fig. 4.34 to the corresponding spectrum in Fig. 4.29. It could be summarized from the above simulation results that for a complex filtering system with original center frequency of 1MHz and Q factor of 50, when the center frequncy varies as a square waveform at 100kHz and in the range of $1\text{MHz} \pm 800\text{kHz}$, the resulting dynamic synchronous system is able to effectively suppress the in-filter single-tone noise without further attenuating the input sidebands.

We continued to test this particular system with AM input of different bandwidths and the injected noise at different frequencies, the test setup is given in Table 4.4. It turned out that in both cases the dynamic system manifests improved performance in suppressing the injected single-tone noise, as shown in Fig. 4.35.

Core Filter	$Q = 50, f_0 = 1\text{MHz}$ Center frequency variation pattern: $\text{square waveform}, \Delta f_0 = 800\text{kHz}, f_{var} = 100\text{kHz}$	
Test List	f_{signal}	Injected noise to the core filter
Test 1	1.5kHz	1.013MHz, 999kHz (both have amplitude of 0.5uA)
Test 2	19.5kHz	

Table 4-4 Parameter setup for the in-filter noise suppression capability tests on a dynamic FM mode synchronous complex filter with a particular center frequency variation pattern.

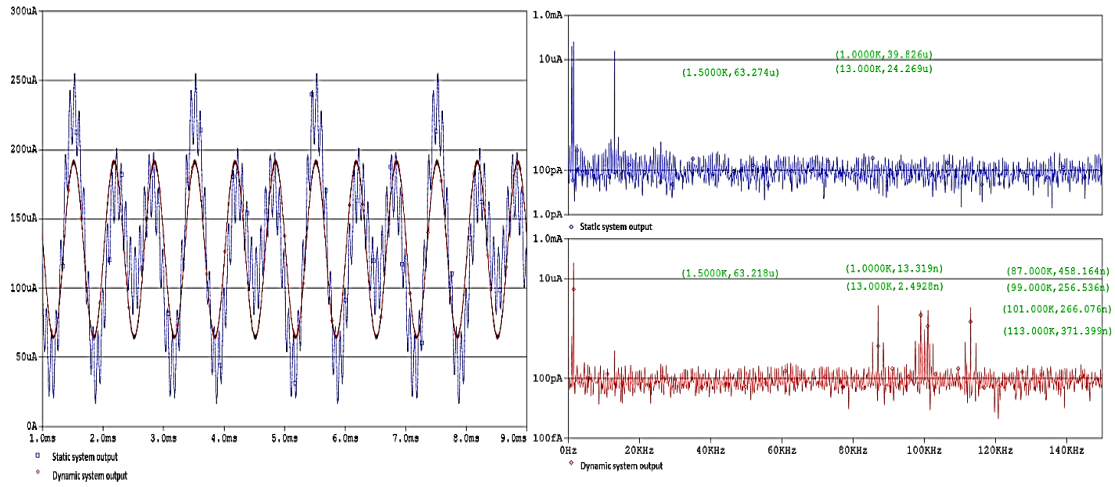

(a)

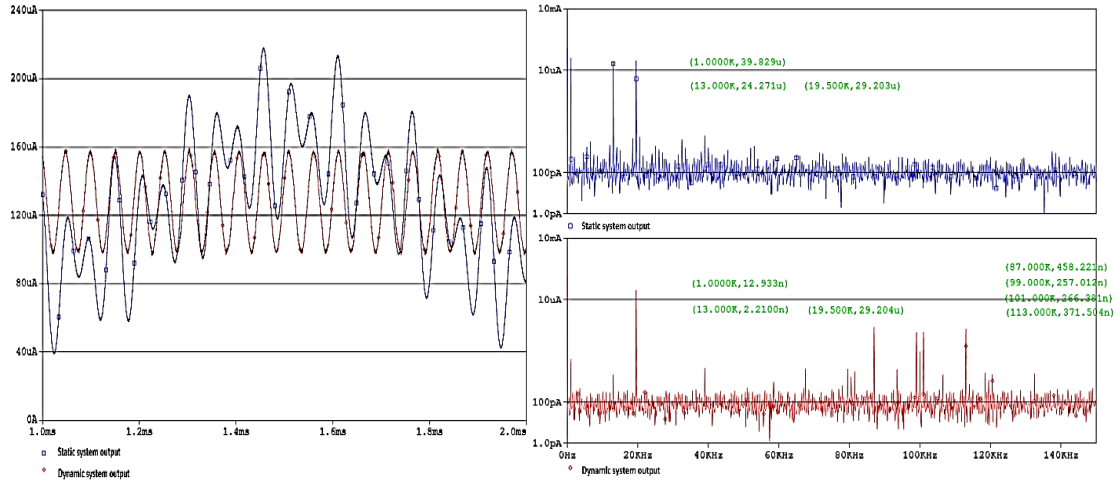

(b)

Figure 4.35 Transient plots and corresponding FFT spectra of the demodulation result from a static complex filtering system and the particular dynamic synchronous filtering system in (a) Test 1 and (b) Test 2.

2. In-filter White Noise and Noiseless Input

Unfortunately, when white noise is injected into the particular dynamic filtering system above, the output noise floor is not lower than that of the reference static filtering system, as shown in Fig. 4.36. This is because the spectrum of white noise determines that no matter where the core filter center frequency is during the variation, there is always same amount of white noise in the frequency range of the instant bandpass

filtering. So an FM mode dynamic synchronous complex filter is not a good candidate to suppress the in-filter white noise.

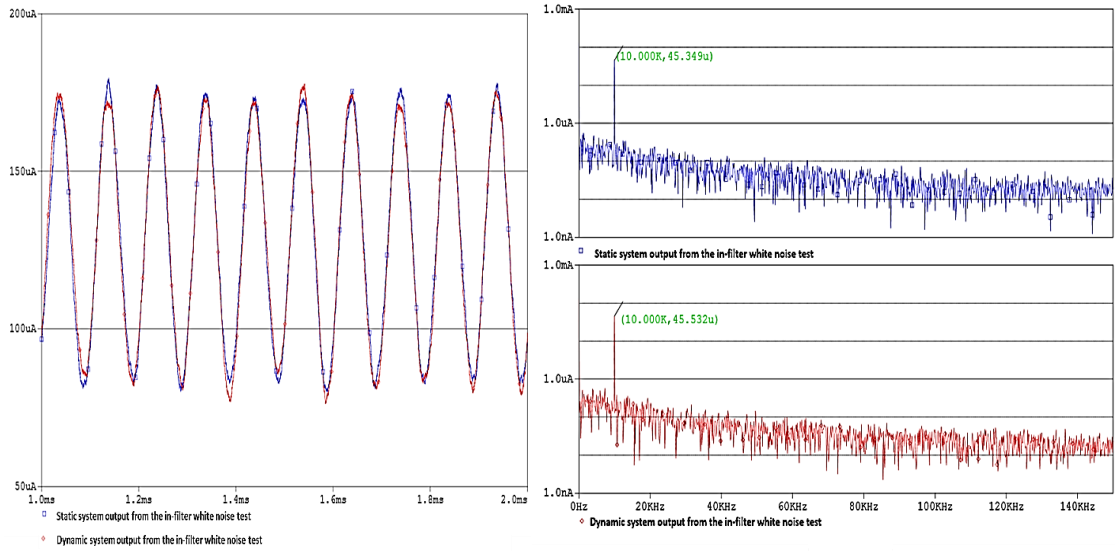

Figure 4.36 Transient plots and corresponding FFT spectra of the demodulation result from both static and dynamic synchronous filtering systems under in-filter white noise test.

3. Noisy Input and Noiseless Filtering System

Finally, a single-tone noise component near 5MHz was added to the original AM input signal and the core filter was set up noiseless for both the static and dynamic sychronous filtering systems under test. The center frequency of the dynamic system was varied as a square waveform at 100KHz in the range of 1MHz$\pm$800KHz . However, according to the test result(not shown here), such a dynamic system is not superior to its static counterpart in suppressing the input noise.

4.3 Summary

Noise performance of some second order filtering systems related to AM mode or FM mode synchronous filtering is tested and compared in this chapter. The two types of noise environment set up for the tests include: an AM signal with white noise

stimulating a noiseless system and a noiseless AM signal driving a system with injected white noise or single-tone noise.

AM mode synchronous filtering related systems

The AM mode synchronous filtering idea is described by eqn. (4.1), and its application in the biquad bandpass filter design is specified by eqn. (4.4) and Fig. 4.1. Eliminating the back end modulator of the AM mode synchronous filter in Fig. 4.1, we discovered an attractive behavior of the yielded system when processing noisy AM signals: according to the derived mathematical expression, the ideal system is able to suppress the undesired input noise as hard as needed while keeping the amplitude and phase of the useful sideband signals. Such a system is illustrated as System 2 in Fig. 4.2. Due to the challenge in generating the ideal Q-factor control signal for System 2, we proposed a feedback filtering system that time varies its Q factor with the signal generated from the system's down conversion result. When dealing with noiseless AM input, the output from this feedback system could be very similar to the output from System 2. System 3 and System 4 are application examples of the feedback system, respectively developed with a standard biquad bandpass filter and a biquad complex filter. Besides the difference in the core filter, they utilize different methods to recover the baseband signal for generating the Q-factor control signal.

Test results

Section 1: Noisy input signal and noiseless filtering systems

System 2 and a standard biquad bandpass filter with Q=50 and Q=500 were tested first. The simulation results agree with our expectation very well and verify that System 2 is capable of suppressing the input noise like a standard biquad bandpass filter

with the same Q factor while letting the input sideband signals pass through with little attenuation or phase shift. Moreover, getting centered at the carrier frequency, the core filter in System 2 could in principle be tuned as sharp as needed to heavily suppress the undesired input white noise without affecting the amplitude and phase of the input sideband signals. Comparing the output of System 2 in Fig. 4.9 and Fig. 4.7, due to the sharpened core filter, the output noise level is apparently suppressed lower but the sideband signals are barely changed. Therefore, System 2 with a sharp core filter could produce an output with very high SNR when processing a noisy AM input signal, as long as the ideal Q-factor control signal is available and the core filter is centered at the carrier frequency.

It has been discovered in Chapter 2 that System 3 could generate an output very similar to the output of System 2 when processing a noiseless AM signal. However, it does not possess the appealing noise performance as System 2 does when processing a noisy AM signal, under any circumstances. The output of System 3 is even noisier than its standard biquad bandpass filter counterpart. Moreover, System 3 with a sharper core filter results in more output noise components of larger size and distributing closer to the center frequency, which further degrades the output SNR. This might be due to the mismatch between the bandwidths of the input white noise and the system core filter introducing new noise with frequency-dependent amplitude through the feedback modulation, which greatly outweighs the filtering capability of the system.

In an effort to improve the noise performance of System 3, we did a few experiments, such as adjusting the input bandwidth, sweeping the system core filter Q factor and inserting a lowpass filter in the feedback path, but didn’t observe anything

exciting. Some interesting discoveries were made through tests on the proposed two-filter design in Fig. 4.17, which is inspired by System 3 and utilizes an auxiliary filtering system of the same type as the main system. We first explored how the setup of $\mathrm{Q_{core}}$ and $\mathrm{Q_{ctrl}}$, the respective Q factor for the main filter and the auxiliary filter, affects the system noise performance. Sticking with $\mathrm{Q_{core}} = 50$ and sweeping $\mathrm{Q_{ctrl}}$ from 5 to 200, it was discovered that the system's capability in suppressing the input white noise mainly depends on the smaller one in the two quality factors: when $\mathrm{Q_{ctrl}}$ is smaller than $\mathrm{Q_{core}}$, a higher $\mathrm{Q_{ctrl}}$ produces a lower output noise floor; if $\mathrm{Q_{ctrl}}$ is already higher than $\mathrm{Q_{core}}$, tuning $\mathrm{Q_{ctrl}}$ to very high does not suppress the out-band noise floor lower than an open loop bandpass filter with $\mathrm{Q_{core}}$ does, moreover, the in-band noise floor gets lifted up and the amplitude of sideband signals drops. Considering this tradeoff, setting $\mathrm{Q_{ctrl}} = \mathrm{Q_{core}}$ is appropriate for improving the two-filter system output SNR when processing a noisy AM signal. Next, we tested whether the system noise performance is constrained by the input bandwidth, or whether the Q factors could be set as high as needed without obviously affecting the output sideband signals. It has been observed: 1) Unlike System 2, the two-filter system cannot maintain the amplitude of the sidebands when the filter bandwidth is tuned too narrow compared to the input bandwidth. 2) For the core filter output to have sidebands with amplitude no smaller than their input level, the upper limit for Q_{core} and Q_{ctrl} is about $1.4f_0/BW_{in}$, where f_0 is the core filter center frequency and BW_{in} is the input bandwidth. 3) The two-filter system with $Q_{ctrl} = Q_{core}$ has the input-noise-suppression capability comparable to that of a biquad open loop bandpass filter with a quality factor of $0.7Q_{core}$. Also, as long as the system filters' bandwidth is not narrower than $0.7BW_{in}$, the input sidebands will not get attenuated, albeit some

inevitable negative phase shift. 4) We hence predicted and verified through simulation that the noise performance of the two-filter bandpass filtering system with $Q_{ctrl} = Q_{core} = Q$ could be very close to that of System 2 with a quality factor of $0.7Q$, when Q is not higher than $1.4f_0/BW_{in}$. Therefore, when driven with noisy narrow-banded AM input signals, the proposed two-filter system is capable of producing an output with very high SNR.

The last test in this section was run on System 4, the feedback system developed with a biquad complex filter. Compared to System 3, the advantage of System 4 lies in its back end down converter which is easier to implement and generates less high frequency components in the recovered signal. Unfortunately, due to the same reason, System 4 is not able to suppress the input noise as the ideally modified system does either. Comparison of the output FFT spectra suggests that when dealing with a noisy AM input signal, System 3 and System 4 have outputs of comparable SNR, and both are noisier than their open loop filter counterpart.

Section 2: Noiseless input and noisy filtering systems

We firstly showed that for both standard biquad bandpass filter and biquad complex filter, the same amount of injected noise generates higher input-referred noise if the filter has a higher Q factor. Next, we tested System 3 and System 4 with Q=50, their ideally modified counterpart and original open loop counterpart. It was observed that the noise suppression capability of the noisy systems controlled by ideal $\frac{\dot{p}(t)}{p(t)}$ is still comparable to that of their open loop counterpart filters, and the recovered information signals from them are very similar to the original $p(t)$. Unfortunately, the feedback

systems, System 3 and System 4, fail to suppress the noise near the center frequency as hard as the reference systems do, and they even generate some undesired components in the output. The recovered information component itself has similar size and phase as that of the original $p(t)$ though. Despite the different spectra, the output baseband noise of System 3 and System 4 has similar strength.

When raising the Q factor for both systems to 200, convergence problem was encountered and it was fixed by scaling up the AM input by a factor of 5. Both the noise peak and the baseband noise floor in the demodulator output from System 3 and System 4 are much higher than they are in the case where Q=50. This is due to the increased input-referred noise and the noisier feedback Q-factor control signal. So when the core filter is noisy, System 3 and System 4 with a lower Q factor would have better noise performance, but still inferior to their open loop counterpart.

FM mode synchronous filtering related systems

The goal of this section is to explore if there are any center frequency variation patterns that would enable a dynamic FM mode synchronous complex filter to effectively suppress the in-filter noise or the input noise. We focused on the sinusoid and square waveform patterns proposed in Fig. 3.24 and sought for a proper setup for the variation rate and range.

Simulation results suggest: 1) A dynamic system does possess improved capability in suppressing the in-filter single-tone noise if it's near the core filter's static center frequency. 2) Square waveform variation patterns are typically superior to sinusoidal patterns in suppressing the in-filter noise, which agrees with the qualitative analysis. 3) Some particular combinations of the variation rate and variation range could

effectively improve the system noise performance. For example, sticking with the 1MHz$\pm$400kHz variation range, when the core filter center frequency is varied at 100kHz in a square waveform, the system produces an output in which the undesired single-tone components get suppressed to be more than three orders of magnitude lower than the useful signal (Fig. 4.29). 4) Unfortunately, when white noise is injected into this particular dynamic filtering system, the output noise floor is not lower than that of the reference static system, as shown in Fig. 4.36. This is because the spectrum of white noise determines that no matter where the core filter center frequency is during the variation, there is always same amount of noise in the frequency range of the instant bandpass filtering. So a dynamic synchronous complex filter is not a good candidate to reduce the in-filter white noise.5) Moreover, a dynamic synchronous complex filter is not superior to its static counterpart in suppressing the input noise of any form.

Chapter 5 A Novel Feedback Filtering System with Improved Noise Performance

5.1 A Q-factor Tuning Approach utilizing the Scaled Feedback Signal

In the exploration of approaches to improving the noise performance of the AM mode feedback filtering system in Fig. 4.3, an interesting discovery was made through varying the feedback scale factor *k* and a new system is developed as shown in Fig. 5.1. Consider a noiseless system at first: when the feedback loop is open, i.e. k=0, the filter output could be expressed as $h(t) * [u(t) \cdot p(t)]$, where $h(t)$ is the impulse response of the core bandpass filter; with 100% feedback of $\frac{\hat{p}(t)}{\hat{p}(t)}$, i.e. k=1, as long as the core filter bandwidth is not too narrow compared to the system input bandwidth, the filter output is very similar to $[h(t) * u(t)] \cdot p(t)$, except that it contains some intermodulation distortion of negligible size. Comparing the sideband signals in the filter output in the above two cases, we could qualitatively say that a scale factor k in the range of 0 to 1 flattens the feedback filter as it approaches 1.

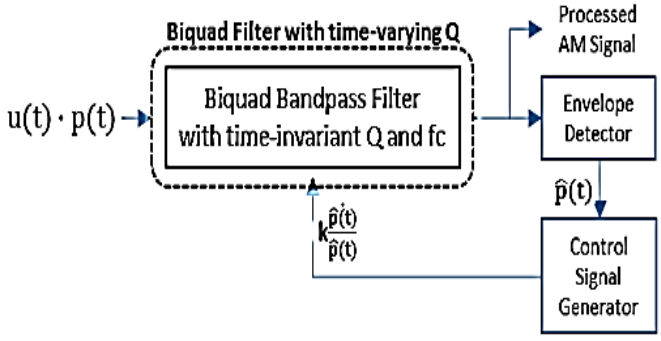

Figure 5.1 A modified version of System 3 in Fig. 4.3 for tuning the filter's equivalent Q factor.

To verify and demonstrate such a property, we ran a sweep simulation on the feedback scale factor k, with a noiseless AM input signal and a feedback filtering system

whose core filter is a standard biquad bandpass filter. Related parameters are listed in Table 5.1. All the demodulation results as shown in Fig. 5.2 contain some undesired harmonic distortion components, which are of negligible size compared to the useful information signal. A larger k consistently yields a larger recovered information signal, which suggests that the resulting feedback filter does become flatter. The dc offset of the demodulated signal in each case remains the same, indicating that the center frequency of the resulting system is independent of the amount of the feedback.

When $k = 0.5$, the recovered 5kHz component is about 3dB lower than the 5kHz component in the original modulating signal, indicating that the equivalent Q factor of the developed filter approximately equals 100. We hence roughly relate the original Q factor of the system's core filter, Q_{core}, the feedback scale factor k and the equivalent Q factor of the feedback system, Q_{eq}, with eqn. (5.1).

$$Q_{eq} \approx (1 - k)Q_{core} \quad (5.1)$$

AM Input (v)	p(t)u(t)
	p(t)=1m+(0.5m)sin(2π·5K· t)
	u(t)=sin(2π·1M·t)
Biquad Bandpass Filter	Q=200, fc=1MHz
S/H Block	Switching rate=1MHz, ON time=1ns
	ON resistance=1mΩ, OFF resistance=1MΩ
Feedback scale factor k	0,0.2,0.5,0.75,1

Table 5-1 Parameter setup for the sweep test on the feedback scale factor k.

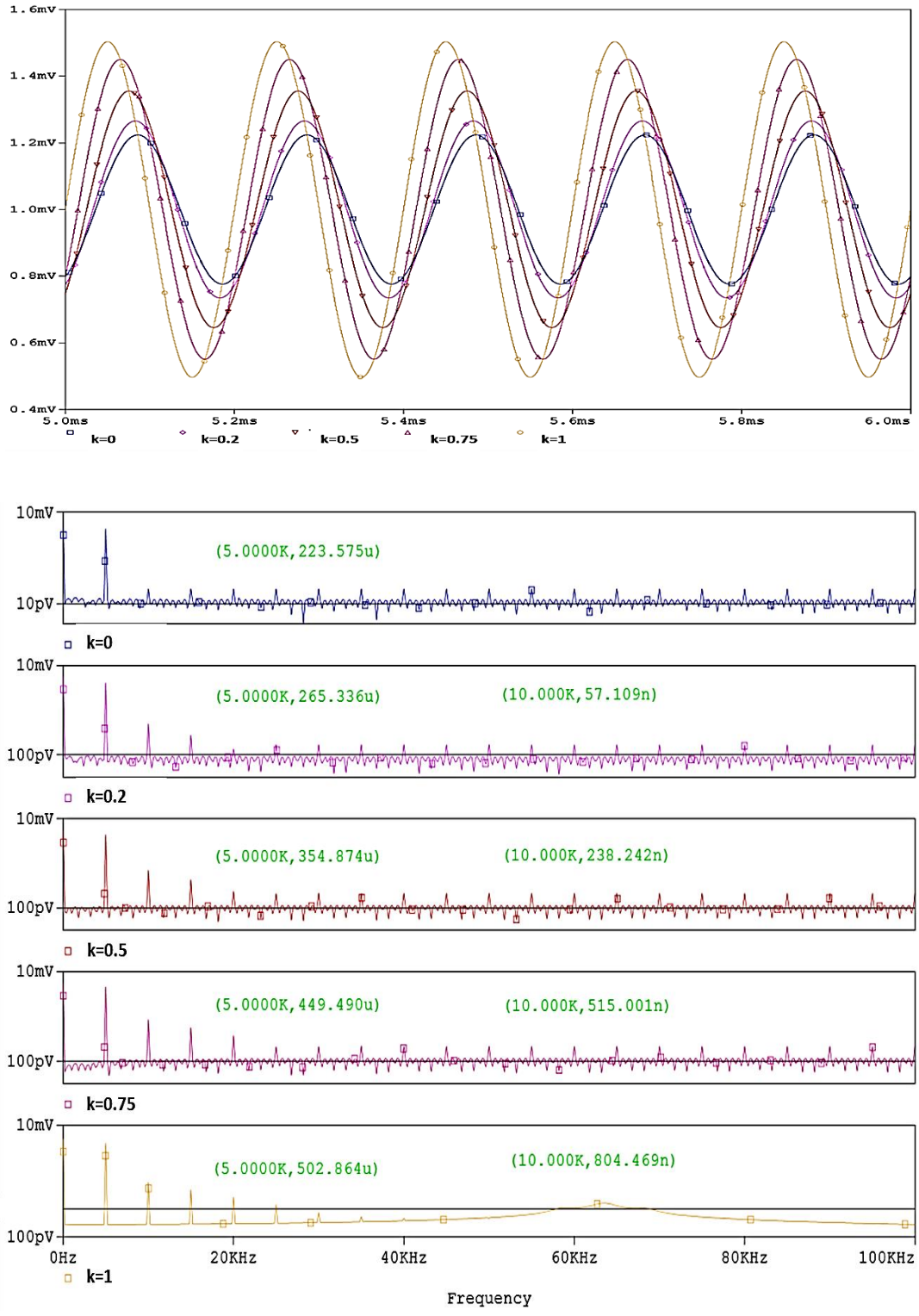

Figure 5.2 Transient plots and FFT spectra of the recovered signal from a feedback bandpass filtering system with different feedback scale factors.

To test the accuracy of eqn. (5.1), we accordingly set up three standard open-loop bandpass filtering systems respectively with Q factor of 160, 100 and 50 and drove them with the same AM input signal used above. The demodulation outputs from the open-loop system and its related feedback system were plotted on the same graph in each test. Shown in Fig. 5.3, the transient plots of the output signals from the open loop system and the feedback system are almost identical, their slight difference is the negligible harmonic distortion that exists in the feedback system output. Therefore, for k in the range of (0,1), eqn. (5.1) provides a proper first order evaluation on the equivalent sharpness of the yielded feedback filtering system for AM input signals.

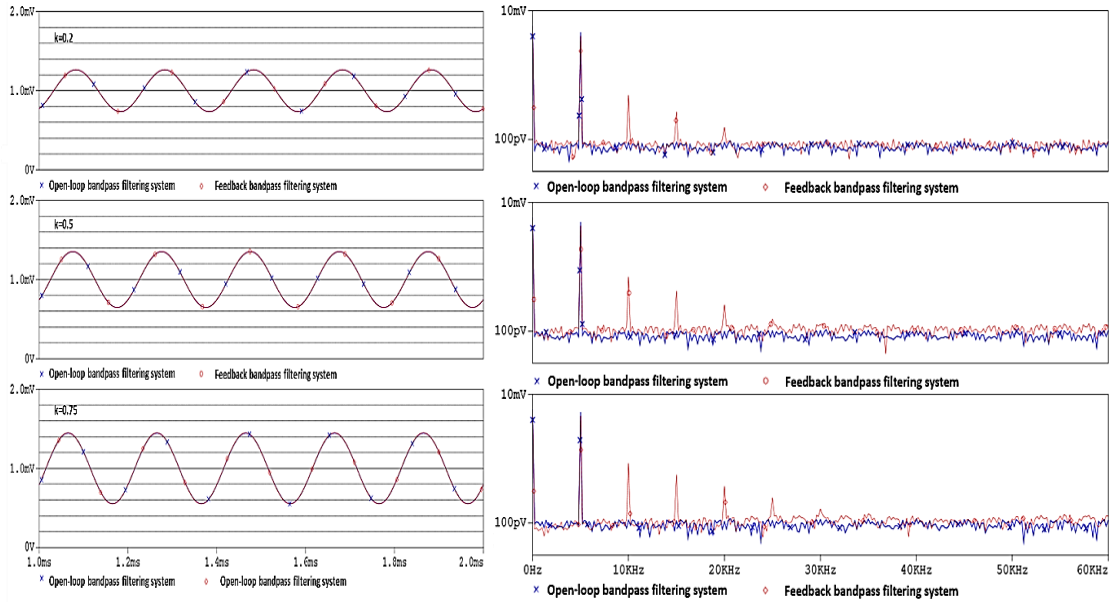

Figure 5.3 Transient plots and FFT spectra of the recovered signal from both feedback system and the corresponding open-loop filtering system for evaluating the accuracy of eqn. 5.1.

Based on the above discovery, we started to question: what would happen if k is negative? Is it possible to sharpen the filter with a negatively scaled feedback signal $\frac{\hat{p}(t)}{\hat{p}(t)}$? A test set up as below was run to figure out the answer.

Input voltage: $p(t) \cdot u(t) = [1m + (0.5m)sin(w_p t)]sin(w_{carrier} t)$,

$where\ w_p = 2\pi \cdot 10k\ , w_{carrier} = 2\pi \cdot 1Meg$

Core filter: $w_0 = w_{carrier} = 2\pi \cdot 1Meg,\ Q = 50$

Feedback scale factor: $k = 0, -0.5, -1, -2, -5$

Simulation results in Fig. 5.4 show that the envelope of the core filter output becomes smaller as the feedback scale factor k gets more negative, indicating that a negatively scaled feedback signal indeed sharpens the filtering system. Measurement data provides some quantitative description on the recovered information signal and its 2nd-order harmonic: their ratio gets smaller as k becomes more negative, which is undesirable; but even the smallest value approximately hits 300, so the harmonic distortion is at a negligible level. Therefore, setting the scale factor k in the feedback system in Fig. 5.1 with negative values provides an approach to implementing a bandpass filter of high equivalent Q factor with a time-invariant low-Q bandpass filter.

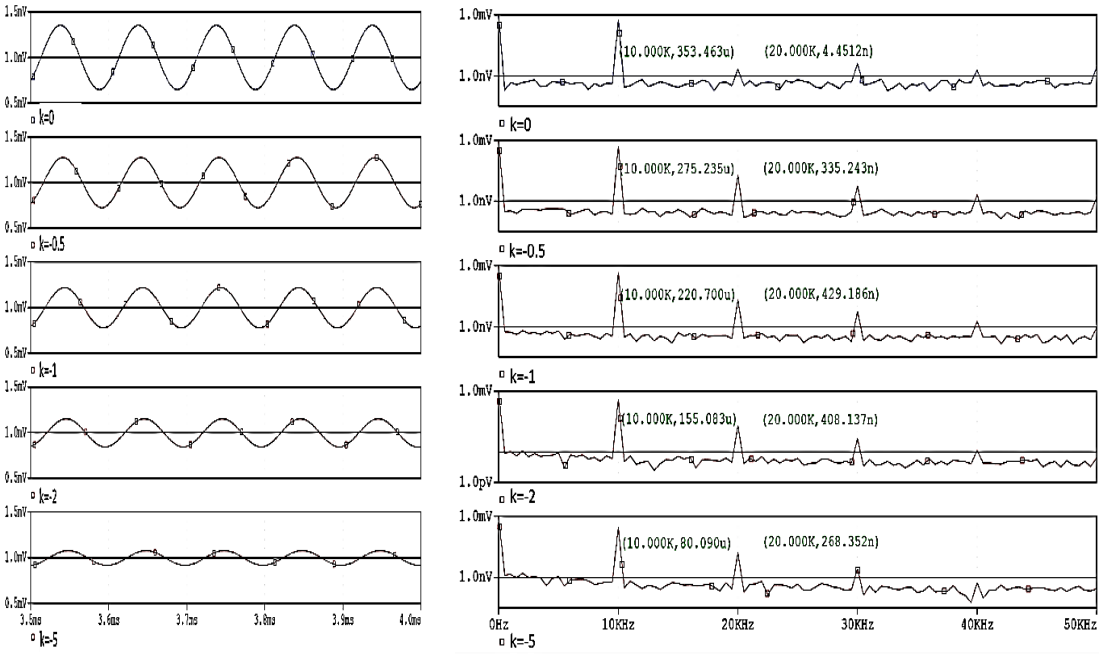

Figure 5.4 Feedback system demodulator output corresponding to different negative k values.

To check out if eqn. (5.1) still holds true for a negative *k*, for each negative *k* above, we swept the frequency of the input modulating signal p(t) over a certain range, maintaining its amplitude and seek for a point at which the recovered modulating frequency component in the demodulator output drops by approximately 3dB from the original amplitude of 0.5mV. Then the equivalent bandwidth of the resulting feedback system is about twice as much that input frequency. Data from Table 5.2 suggests that eqn. (5.1) suits the feedback filtering system with negative k values in the range of [-5, 0) very well.

Core Filter: fcenter=1MHz, Qstat=50					
Parameter	k	fp_tuned (Hz)	Afund_measured(V)	Qeval	Qeval/Qstat
Reference	0	10k	353.5u	50	1
Test 1	-0.5	6.6k	353.4u	76	1.52
Test 2	-1	4.9k	354.4u	102	2.04
Test 3	-2	3.3k	353.1u	152	3.04
Test 4	-5	1.7k	354.2u	294	5.88

Table 5-2 Data from the tests for evaluating the equivalent Q factor of the feedback filter with time-variant bandwidth.

Moreover, the gain spectra of two feedback filtering systems were plotted, as shown in Fig.5.5 (a) and Fig. 5.5 (b). The feedback scale factor for both systems is -9, both core filters are centered at 1MHz and the original Q factors were set to be 5 and 20 respectively. It's clear that both feedback systems are much sharper than the original filters from which they are developed, and they both have an equivalent Q factor comparable to what is estimated by eqn. (5.1), while the equivalent Q factor of the system developed from a sharper core filter fits the equation better. The gain spectra of the feedback filter and its related open-loop filter have strong resemblance but are not identical, so the input-output functions of the two systems are not exactly the same. One

obvious difference, for instance, is manifested by the harmonic distortion generated by the feedback filtering system.

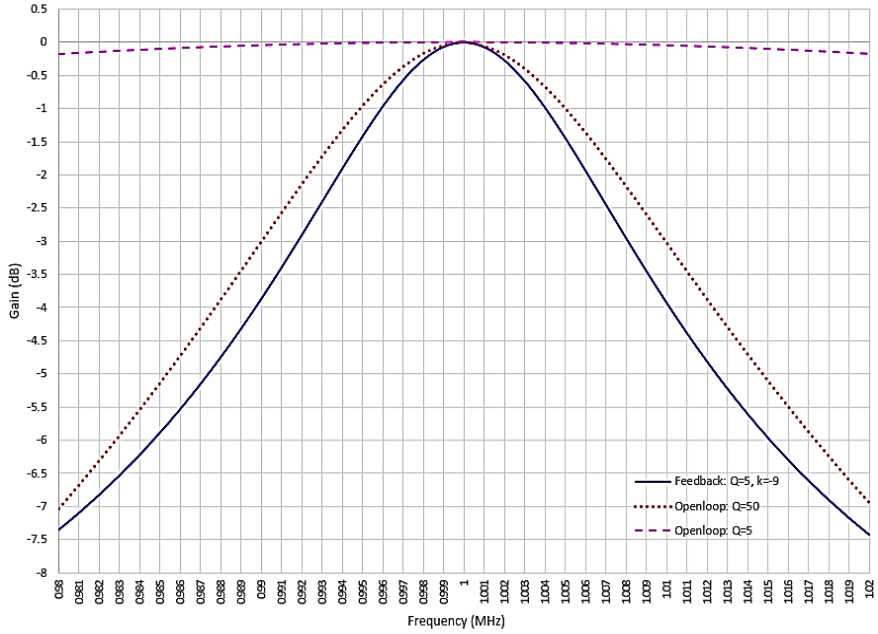

(a)

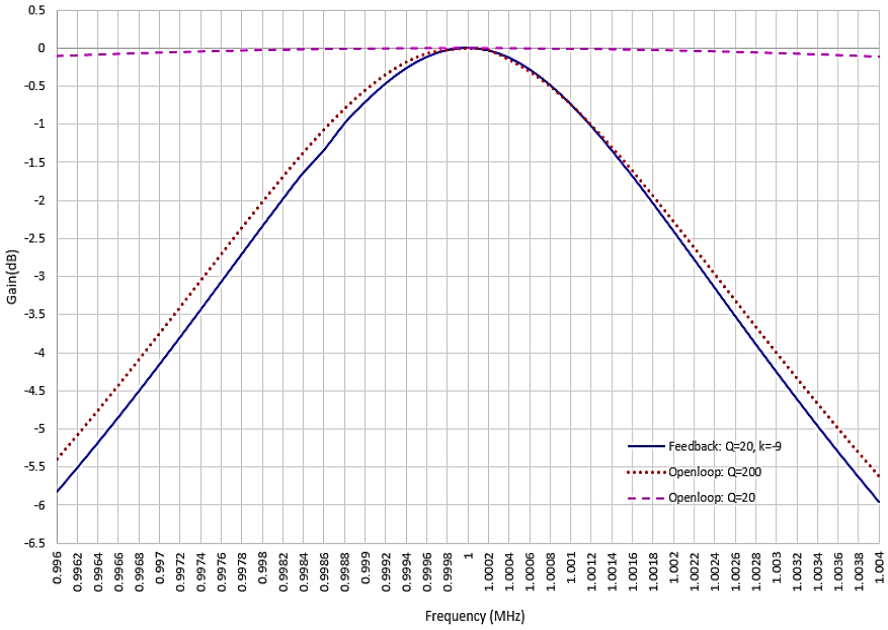

(b)

Figure 5.5 Gain spectra of two feedback filters developed from a core filter with different original Q factors.

Another simulation on the feedback systems with different original Q factors and feedback scale factors shows that the system developed from a sharper original core filter and a less negative feedback scale factor produces an output with higher SNR and behaves more similarly to the open-loop bandpass filter with a Q factor derived by eqn. (5.1) does. In this test, the reference open loop system incorporates a bandpass filter with Q=100, and the feedback systems are set up with Q=50, 20, 10, 5 and k=-1, -4, -9, -19, respectively. Fig. 5.6(a) and (b) show transient plots and FFT spectra of all the system outputs corresponding to the same AM input which is modulated by a sine wave at 5kHz. The output harmonic distortion consistently increases and the amplitude of recovered signal consistently drops as the system's original Q factor decreases. For the systems with Q=10, k=-9 and Q=5, k=-19, the size of harmonic distortion exceeds 1% of the information signal amplitude and the output SNR has been greatly degraded.

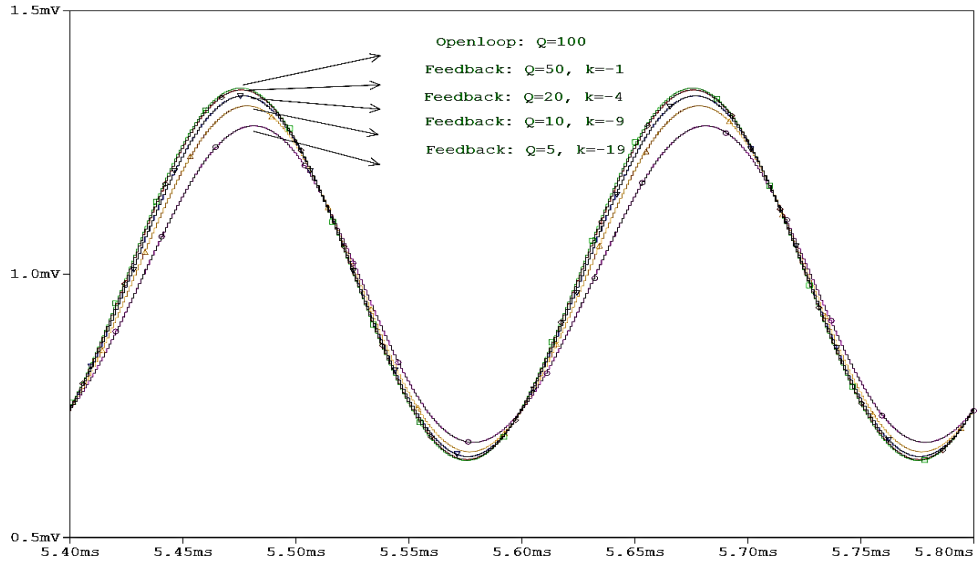

(a)

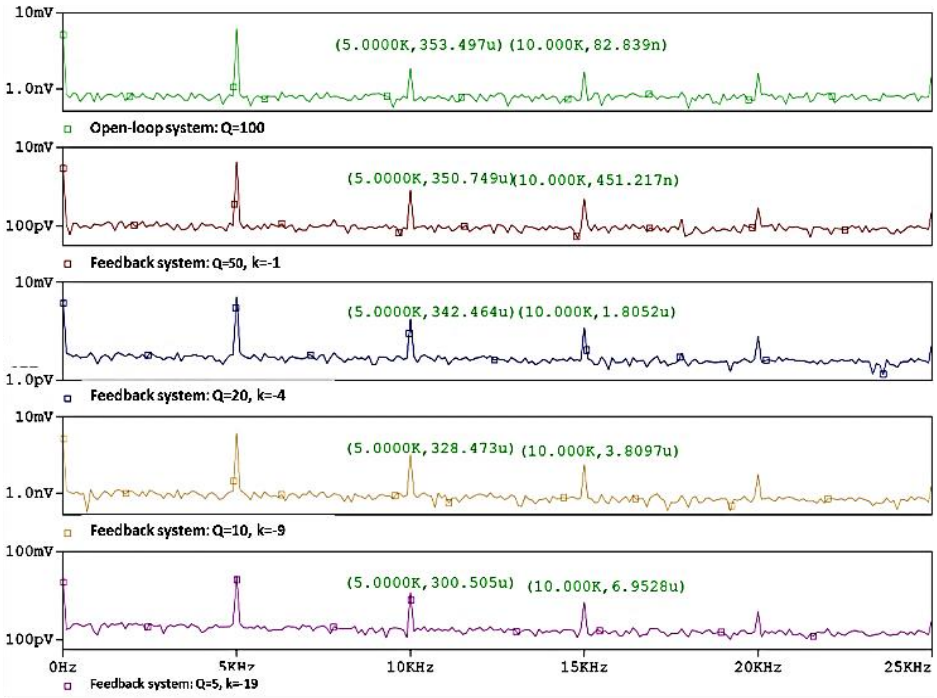

(b)

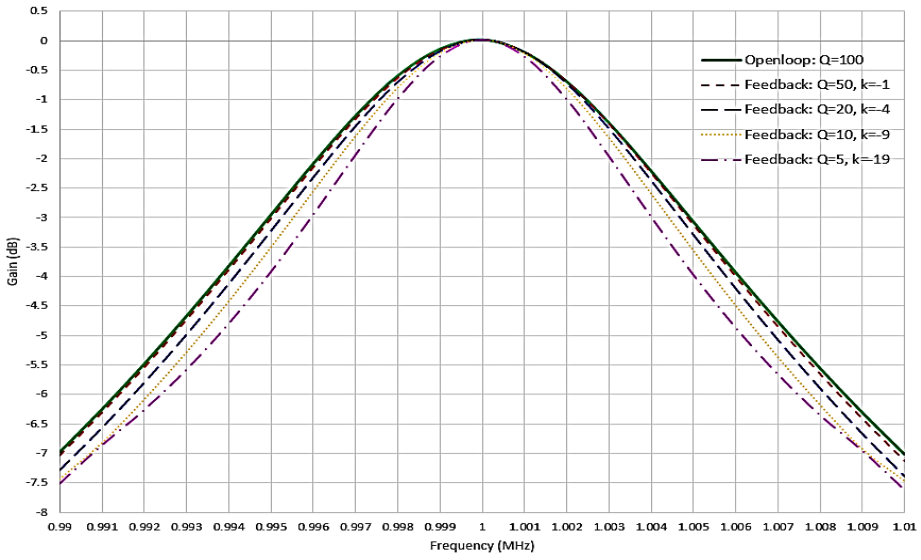

(c)

Figure 5.6 (a), (b) Transient plots and FFT spectra of output signals and (c) gain spectra of the systems under test.

Recall that the FM mode synchronous complex filtering system, System 4 in Fig. 4.4, has very similar function as that of System 3 in Fig. 4.3. One advantage of System 4 over System 3 is its simpler demodulator. As has been introduced in Chapter 3,

implemented only with mixers and a current mirror, the demodulator is able to recover the information signal from the core filter output without introducing additional phase shift. Comparing to the S/H block output from System 3, the recovered signal from System 4 contains less high frequency components. Therefore, it's of our interest if the method discussed above could be used to sharpen the filtering system in Fig. 5.7, a modified version of System 4. In the test where k=-9 and the feedback system was set up with $Q_{core} = 5$, the system steady state output almost overlaps with the output of the open loop complex filtering system with Q=50, and no harmonic distortion is seen in the FFT spectrum, as shown in Fig. 5.8 (a) and (b). Moreover, the gain spectra of the two systems are plotted in Fig. 5.8(c) and they demonstrate higher resemblance in bandwidth and shape than the spectra in Fig. 5.5(a) do. Therefore, the feedback system developed from a low-Q complex filter has input-output function very similar to an open-loop high-Q complex filter, and it produces a less noisy output than the system in Fig. 5.1 developed with a bandpass filter of the same Q_{core} and feedback scale factor k.

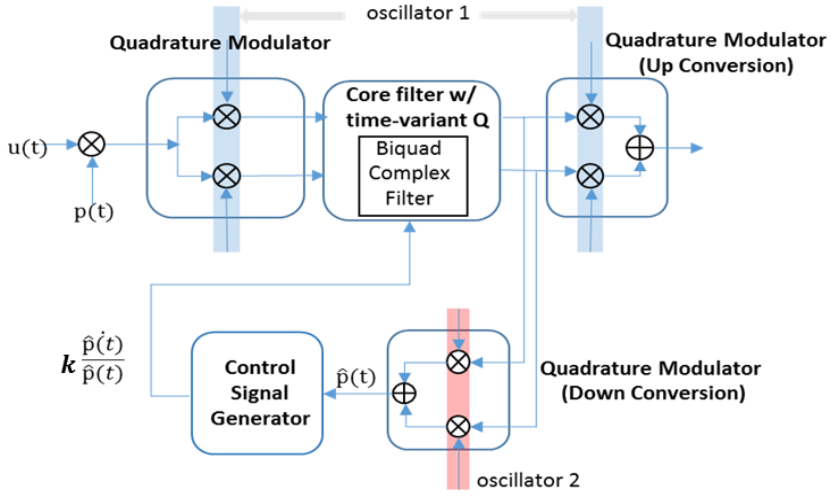

Figure 5.7 A modified version of System 4 in Fig. 4.4 for tuning the complex filter's equivalent Q factor.

To check out if the equivalent Q factor of the system in Fig. 5.7 could also be evaluated by eqn. (5.1), the gain spectra of a set of feedback systems with Q=50, 20, 10, 5 and feedback scale factors of k=-1, -4, -9, -19 were plotted in Fig. 5.9, together with that of the reference open loop system in which the complex filter Q factor equals 100. According to the measurement data, all the feedback systems have similar bandwidths close to that of the reference complex filter, indicating that the relationship between Q_{eq} of a feedback complex filtering system and the original Q_{core} fits eqn (5.1) better than its bandpass filtering system counterpart does.

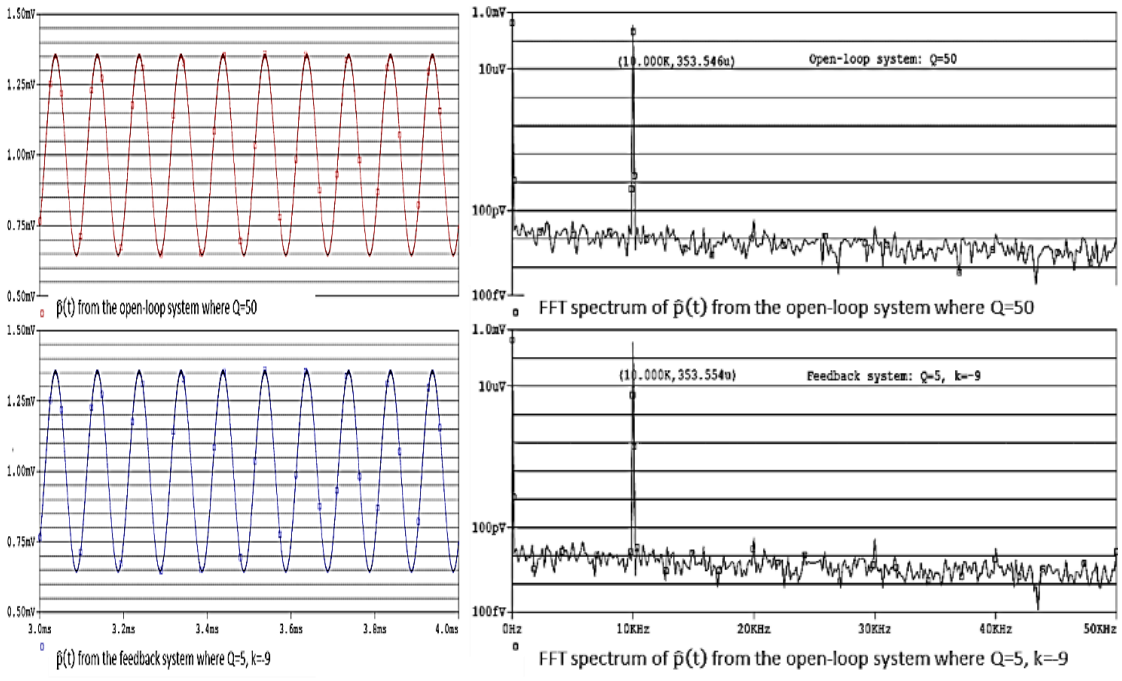

(a) (b)

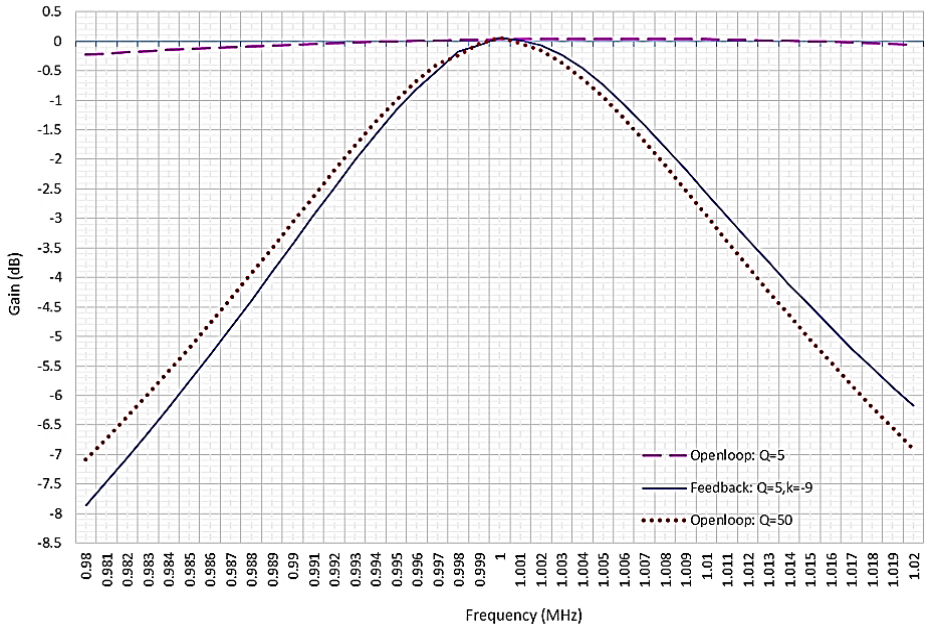

(c)

Figure 5.8 (a), (b) Transient plots and FFT spectra of the output signals from a feedback complex filtering system with $Q_{core} = 5$ and k=-9 and an open-loop complex filtering system with Q=50; (c) Gain spectra of both systems.

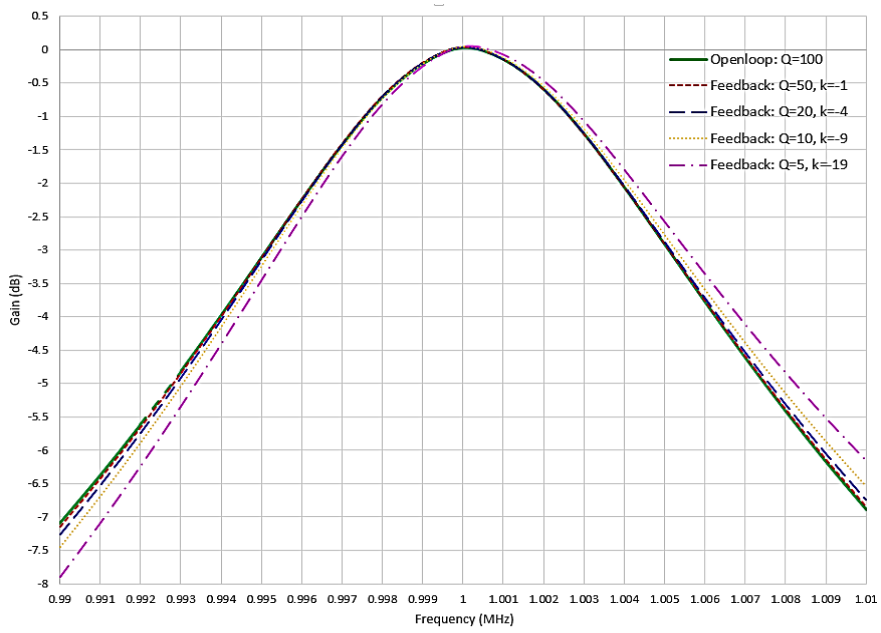

Figure 5.9 Gain spectra of all the feedback complex filtering systems and the reference system under test.

The explanation to the above discoveries is now given as follows. First, consider a simple first order lowpass filter specified by the following differential equation:

$$\dot{y} = -w_0 y + w_0 u \qquad (5.2)$$

where w_0 is the cutoff frequency. Now suppose u is an always non-zero input signal and the gain on the output, y, is modulated in the following way:

$$\dot{y} = \left(-w_0 + k\frac{\dot{y}}{y}\right) y + w_0 u \qquad (5.3)$$

Rearranging the equation to yield the following:

$$(1-k)\dot{y} = -w_0 y + w_0 u \implies \dot{y} = -\frac{w_0}{1-k} y + \frac{w_0}{1-k} u \qquad (5.4)$$

The net result of the modulation of the gain on y in the differential equation is to scale the cutoff frequency of the filter. For $k < 0$, the resulting cutoff frequency is lower than w_0; for $0 \le k < 1$, it is equal to or larger than w_0. For eqn. (5.4) to have physical meaning, k should not exceed 1.

Now consider a pair of lowpass filters of the above type, constituting a second order system that can be written as:

$$\begin{vmatrix}\dot{x}_1\\ \dot{x}_2\end{vmatrix} = \begin{vmatrix}-w_0 & 0\\ 0 & -w_0\end{vmatrix}\begin{vmatrix}x_1\\ x_2\end{vmatrix} + w_0\begin{vmatrix}1\\ -1\end{vmatrix} u \text{ , } y = \frac{1}{2}\begin{vmatrix}1 & -1\end{vmatrix}\begin{vmatrix}x_1\\ x_2\end{vmatrix} \qquad (5.5)$$

It's easy to derive:

$$x_1 = -x_2 = y, \quad \frac{\dot{x_1}}{x_1} = \frac{\dot{x_2}}{x_2} = \frac{\dot{y}}{y}, \quad \dot{y} = -w_0 y + w_0 u$$

Apply the modulation of state variable(s) as introduced in eqn. (5.3):

$$\begin{vmatrix}\dot{x}_1\\ \dot{x}_2\end{vmatrix} = \begin{vmatrix}-w_0 + k\frac{\dot{y}}{y} & 0\\ 0 & -w_0 + k\frac{\dot{y}}{y}\end{vmatrix}\begin{vmatrix}x_1\\ x_2\end{vmatrix} + w_0\begin{vmatrix}1\\ -1\end{vmatrix} u, \qquad y = \frac{1}{2}\begin{vmatrix}1 & -1\end{vmatrix}\begin{vmatrix}x_1\\ x_2\end{vmatrix} \qquad (5.6)$$

It follows that both lowpass filters get their original cutoff frequencies scaled by a same factor, $\frac{1}{1-\mathrm{k}}$, and the system output remains the same as represented by eqn. (5.4). Utilize a time varying matrix, M(t), to transform the above second-order system:

$$\bar{x}(t) \rightarrow \mathrm{M(t)}\bar{x}(t), \text{ where } \mathrm{M(t)} = \begin{vmatrix} \cos(w_M t) & -\sin(w_M t) \\ \sin(w_M t) & \cos(w_M t) \end{vmatrix} \qquad (5.7)$$

Since any state-space transformation with a nonsingular M(t) keeps the system's original input-output characteristics, the system represented by eqn. (5.8) corresponds to the same transfer function as the first order lowpass filter with a scaled cutoff frequency specified by eqn. (5.4) does. The "$\frac{\pi}{4}$" phase angle in all the modulating sinusoids could be removed together without affecting the system's transfer function.

$$\begin{vmatrix} \dot{x}_1 \\ \dot{x}_2 \end{vmatrix} = \begin{vmatrix} -w_0 + \mathrm{k}\frac{\dot{\mathrm{y}}}{\mathrm{y}} & -w_M \\ w_M & -w_0 + \mathrm{k}\frac{\dot{\mathrm{y}}}{\mathrm{y}} \end{vmatrix} \begin{vmatrix} x_1 \\ x_2 \end{vmatrix} + \sqrt{2}w_0 \begin{vmatrix} \sin(w_M t + \frac{\pi}{4}) \\ -\cos(w_M t + \frac{\pi}{4}) \end{vmatrix} u \qquad (5.8)$$

$$\mathrm{y} = \frac{\sqrt{2}}{2} \begin{vmatrix} \sin(w_M t + \frac{\pi}{4}) & -\cos(w_M t + \frac{\pi}{4}) \end{vmatrix} \begin{vmatrix} x_1 \\ x_2 \end{vmatrix}$$

Such a system incorporates a frontend modulator, a second-order core filter and a backend modulator. The input baseband signal is modulated by a pair of quadrature signals at w_M, and the two channels of up converted signals are processed by a biquad core filter that has multiple input and multiple output, the two channels of the filter output are modulated again and summed up to produce the lowpass filtered version of the input. Since the overall system performs like a first order lowpass filter cuts off at $\frac{\mathrm{w_0}}{1-\mathrm{k}}$ and the terminal modulators don't have filtering capability, the biquad core filter could be taken as the lowpass filter being up converted into a higher frequency range,

and it has a bandwidth of $\frac{2w_0}{1-k}$ if $w_M \gg w_0$. The non-zero off-diagonal entries in the state matrix could be interpreted as the up conversion of the lowpass filter, and the bandwidth of the core filter depends only on the diagonal entries.

The above analysis leads to a promising point: when a biquad bandpass filter is processing an AM signal, we might be able to tune its bandwidth (or Q factor) with the approach specified by eqn. (5.8), as long as the filter meets some requirements. First, the biquad bandpass filter could find a state space representation in which the state matrix has identical diagonal entries and opposite off-diagonal entries just like the state matrix in eqn. (5.8). Second, the bandpass filter's magnitude and phase responses to signals at w_0, $w_0 + w_{sig}$ and $w_0 - w_{sig}$ (w_0 is the filter's center frequency, w_{sig} is the baseband information signal frequency, and usually $w_{sig} \ll w_0$) are very similar to that of some first order lowpass filter to signals at dc, w_{sig} and $-w_{sig}$. Third, the bandpass filter has a demodulator which is able to recover the information signal without introducing additional phase shift.

Recall that the state space representations of a standard biquad bandpass filter and a biquad complex filter, respectively given in eqn. (1.30) and eqn. (1.46) (reproduced in eqn. (5.13) and eqn. (5.17)), both have a state matrix in the particular formation. For each bandpass filter, we have proposed and verified an approach to the reconstruction of the information signal from the core filter output, which introduces negligible phase shift in the demodulation process. Therefore, if the magnitude and phase responses of the two bandpass filters meet the second requirement above, when we time vary their bandwidths with $'k\frac{\dot{\hat{p}}}{\hat{p}}'$, where $'\hat{p}'$ is the properly reconstructed baseband signal from their core filter

output, both systems would have a time-varying bandwidth equivalent to $\frac{1}{1-k}$ times their original core filter bandwidth.

The review below, through eqn. (5.9) to eqn. (5.21), formulates the transfer function, the particular state space representation and the frequency response of a standard biquad bandpass filter, a biquad complex filter and a correlated first order lowpass filter.

The first-order lowpass filter cuts off at $\frac{w_0}{2Q}$

- Transfer function: $\mathrm{H}_{LPF}(s) = \frac{\frac{w_0}{2Q}}{s+\frac{w_0}{2Q}}$ (5.9)

- State space representation with the state matrix in the particular formation:

$$\begin{vmatrix}\dot{x}_1\\ \dot{x}_2\end{vmatrix} = \begin{vmatrix}-\frac{w_0}{2Q} & -w_M\\ w_M & -\frac{w_0}{2Q}\end{vmatrix}\begin{vmatrix}x_1\\ x_2\end{vmatrix} + \sqrt{2}w_0\begin{vmatrix}\sin(w_M t)\\ -\cos(w_M t)\end{vmatrix}u$$

$$\mathrm{y} = \frac{\sqrt{2}}{2}|\sin(w_M t) \quad -\cos(w_M t)|\begin{vmatrix}x_1\\ x_2\end{vmatrix}$$

where w_M is the front end and back end modulating frequency. (5.10)

- Magnitude and phase responses:

$$\left|\mathrm{H}_{LPF}(\pm jw_{sig})\right| = \frac{1}{\sqrt{1+(\frac{2\mathrm{Q}w_{sig}}{w_0})^2}},\ \measuredangle \mathrm{H}_{LPF}(\pm jw_{sig}) = \mp\arctan(\frac{2Qw_{sig}}{w_0}) \qquad (5.11)$$

The standard biquad bandpass filter centered at w_0 with a bandwidth of $\frac{w_0}{Q}$

- Transfer function: $\mathrm{H}_{SBPF}(s) = \frac{\frac{w_0}{Q}s}{s^2+\frac{w_0}{Q}s+{w_0}^2}$ (5.12)

- State space representation with the state matrix in the particular formation:

$$\begin{vmatrix}\dot{\mathrm{x}}_1\\ \dot{\mathrm{x}}_2\end{vmatrix} = \begin{vmatrix}-\frac{\mathrm{w}_0}{2\mathrm{Q}} & -\mathrm{w}_\mathrm{A}\\ \mathrm{w}_\mathrm{A} & -\frac{\mathrm{w}_0}{2\mathrm{Q}}\end{vmatrix}\begin{vmatrix}\mathrm{x}_1\\ \mathrm{x}_2\end{vmatrix} + \frac{\mathrm{w}_0}{\mathrm{Q}}\begin{vmatrix}1\\ -1\end{vmatrix}\mathrm{u},\ \ \mathrm{y} = \frac{1}{2\lambda}|(-\gamma+\lambda) \quad -(\gamma+\lambda)|\begin{vmatrix}\mathrm{x}_1\\ \mathrm{x}_2\end{vmatrix}$$

where $\gamma = 1/2Q;\ \lambda = \sqrt{1-(1/2Q)^2};\ w_A = \sqrt{1-(1/2Q)^2}w_0$ (5.13)

- Magnitude and phase responses:

$$\left|\mathrm{H}_{SBPF}(j(w_0 \pm w_{sig}))\right| = \frac{\frac{w_0}{Q}(w_0 \pm w_{sig})}{\left|j\frac{w_0}{Q}(w_0 \pm w_{sig}) + w_{sig}(\mp 2w_0 - w_{sig})\right|} = \frac{\frac{w_0}{Q}}{\sqrt{(\frac{w_0}{Q})^2 + w_{sig}^2\frac{(\mp 2w_0 - w_{sig})^2}{(w_0 \pm w_{sig})^2}}}$$

Assume $w_0 \gg w_{sig}$, $\frac{(\mp 2w_0 - w_{sig})^2}{(w_0 \pm w_{sig})^2} = \frac{(2w_0 \pm w_{sig})^2}{(w_0 \pm w_{sig})^2} \approx \frac{(2w_0)^2}{(w_0)^2} = 2^2$.

It follows that

$$\left|\mathrm{H}_{SBPF}(j(w_0 \pm w_{sig}))\right| \approx \frac{\frac{w_0}{Q}}{\sqrt{\left(\frac{w_0}{Q}\right)^2 + (2w_{sig})^2}} = \frac{\frac{w_0}{2Q}}{\sqrt{\left(\frac{w_0}{2Q}\right)^2 + w_{sig}^2}} = \frac{1}{\sqrt{1+\left(\frac{2Qw_{sig}}{w_0}\right)^2}} \quad (5.14)$$

For $\mathrm{w} = w_0 + w_{sig}$,

$$\begin{aligned}\measuredangle \mathrm{H}_{SBPF}(jw) &= \frac{\pi}{2} - \left[\arctan\left(\frac{\frac{w_0}{Q}w}{{w_0}^2 - \mathrm{w}^2}\right) + \pi\right] = -\frac{\pi}{2} + \arctan\left(\frac{\frac{w_0}{Q}w}{\mathrm{w}^2 - {w_0}^2}\right) \\ &= -\arctan\left(\frac{\mathrm{w}^2 - {w_0}^2}{\frac{w_0}{Q}w}\right) \approx -\arctan\left(\frac{2w_{sig}}{\frac{w_0}{Q}}\right) \end{aligned} \quad (5.15)$$

Similarly, for $\mathrm{w} = w_0 - w_{sig}$, $\measuredangle \mathrm{H}_{SBPF}(jw) \approx \arctan\left(\frac{2w_{sig}}{\frac{w_0}{Q}}\right)$ (5.16)

The biquad complex filter centered at w_0 with a bandwidth of $\frac{w_0}{Q}$

- Transfer function: $\mathrm{H_{CMPLF}(s)} = \frac{(\mathrm{s}+\frac{\mathrm{w_0}}{2\mathrm{Q}})\frac{\mathrm{w_0}}{\mathrm{Q}}}{\mathrm{s}^2+\frac{\mathrm{w_0}}{\mathrm{Q}}\mathrm{s}+{\mathrm{w_A}}^2+(\frac{\mathrm{w_0}}{2\mathrm{Q}})^2}$ (5.17)

- State space representation with the state matrix in the particular formation:

$$\begin{vmatrix}\dot{\mathrm{x}_1}\\ \dot{\mathrm{x}_2}\end{vmatrix} = \begin{vmatrix}-\frac{\mathrm{w_0}}{2\mathrm{Q}} & -\mathrm{w_A}\\ \mathrm{w_A} & -\frac{\mathrm{w_0}}{2\mathrm{Q}}\end{vmatrix}\begin{vmatrix}\mathrm{x}_1\\ \mathrm{x}_2\end{vmatrix} + \frac{\mathrm{w_0}}{\mathrm{Q}}\begin{vmatrix}1\\ -1\end{vmatrix}\mathrm{u},\ \ \mathrm{y} = \frac{1}{2}\begin{vmatrix}1 & -1\end{vmatrix}\begin{vmatrix}\mathrm{x}_1\\ \mathrm{x}_2\end{vmatrix}$$

where $\mathrm{w_A} = \sqrt{1-(1/2\mathrm{Q})^2}\mathrm{w_0}$. (5.18)

- Magnitude and phase responses:

Assume Q is high enough so that ${w_A}^2 \approx {\mathrm{w_0}}^2$,

$$\left|\mathrm{H}_{CMPLF}\left(j(w_0 \pm w_{sig})\right)\right| = \frac{\frac{w_0}{Q}\left|j(w_0 \pm w_{sig}) + \frac{\mathrm{w}_0}{2\mathrm{Q}}\right|}{\left|j\frac{w_0}{Q}(w_0 \pm w_{sig}) + w_{sig}(\mp 2w_0 - w_{sig}) + \left(\frac{\mathrm{w}_0}{2\mathrm{Q}}\right)^2\right|}$$

$$= \frac{\frac{w_0}{Q}\sqrt{\left(\frac{\frac{w_0}{2Q}}{w_0 \pm w_{sig}}\right)^2 + 1}}{\sqrt{(\frac{w_0}{Q})^2 + w_{sig}^2\left(\frac{2w_0 \pm w_{sig}}{w_0 \pm w_{sig}}\right)^2 + \frac{(\frac{w_0}{2Q})^4}{(w_0 \pm w_{sig})^2} + 2w_{sig}(\mp 2w_0 - w_{sig})\left(\frac{\frac{w_0}{2Q}}{w_0 \pm w_{sig}}\right)^2}}$$

Since $\frac{\frac{w_0}{2Q}}{w_0 \pm w_{sig}} \ll 1$, $\left(\frac{\frac{w_0}{2Q}}{w_0 \pm w_{sig}}\right)^2 + 1 \approx 1$ and $\frac{(\frac{w_0}{2Q})^4}{(w_0 \pm w_{sig})^2} \ll (\frac{w_0}{2Q})^2$.

Assume $w_{sig} \ll w_0$, $2w_{sig}(\mp 2w_0 - w_{sig})\left(\frac{\frac{w_0}{2Q}}{w_0 \pm w_{sig}}\right)^2 \approx 2w_{sig}(\mp 2w_0 - w_{sig})\left(\frac{1}{2Q}\right)^2 \approx \mp\frac{w_{sig}w_0}{Q^2}$.

It follows that

$$\left|\mathrm{H}_{CMPLF}\left(j(w_0 \pm w_{sig})\right)\right| \approx \frac{(\frac{w_0}{Q})}{\sqrt{(\frac{w_0}{Q})^2 + 2^2 w_{sig}^2 + \frac{(\frac{w_0}{2Q})^4}{(w_0 \pm w_{sig})^2} \mp \frac{w_{sig}w_0}{Q^2}}}$$

$$\approx \frac{(\frac{w_0}{Q})}{\sqrt{(\frac{w_0}{Q})^2 + 2^2 w_{sig}^2 + \frac{w_0^2}{(2Q)^4} \mp \frac{w_{sig}w_0}{Q^2}}} = \frac{1}{\sqrt{1 + (\frac{2w_{sig}}{\frac{w_0}{Q}})^2 + (\frac{1}{2})^2(\frac{1}{2Q})^2 \mp \frac{w_{sig}}{w_0}}} \approx \frac{1}{\sqrt{1 + \left(\frac{2w_{sig}Q}{w_0}\right)^2}} \quad (5.19)$$

For $\mathrm{w} = w_0 + w_{sig}$, $\measuredangle \mathrm{H}_{CMPLF}(jw) = \arctan\left(\frac{w}{\frac{\mathrm{w}_0}{2\mathrm{Q}}}\right) - [\pi + \arctan\left(\frac{\frac{\mathrm{w}_0}{\mathrm{Q}}\mathrm{w}}{{w_A}^2 + \left(\frac{\mathrm{w}_0}{2\mathrm{Q}}\right)^2 - w^2}\right)]$.

Assume ${w_A}^2 + \left(\frac{\mathrm{w}_0}{2\mathrm{Q}}\right)^2 \approx {\mathrm{w}_0}^2$,

$$\measuredangle H_{CMPLF}(jw) \approx arctan\left(\frac{w}{\frac{w_0}{2Q}}\right) - \pi + arctan\left(\frac{\frac{w_0}{Q}w}{w^2 - {w_0}^2}\right) \approx arctan\frac{w}{\frac{w_0}{2Q}} - \pi + arctan\frac{w_0}{2Qw_{sig}}$$

So $\measuredangle H_{CMPLF}(jw) \approx (\arctan\frac{2\mathrm{Q}w}{\mathrm{w}_0} - \frac{\pi}{2}) - \arctan\frac{2\mathrm{Q}w_{sig}}{\mathrm{w}_0}$, is little less than $-\arctan\frac{2\mathrm{Q}w_{sig}}{\mathrm{w}_0}$.

(5.20)

For $w = w_0 - w_{sig}$, still assume ${w_A}^2 + (\frac{w_0}{2Q})^2 \approx {w_0}^2$,

$$\measuredangle H_{CMPLF}(jw) \approx \arctan\left(\frac{w}{\frac{w_0}{2Q}}\right) - \arctan\left(\frac{\frac{w_0}{Q}w}{{w_0}^2 - w^2}\right) \approx \arctan\left(\frac{w}{\frac{w_0}{2Q}}\right) - \arctan(\frac{w_0}{2Qw_{sig}})$$

$$= \arctan\left(\frac{2Qw}{w_0}\right) - \frac{\pi}{2} + \arctan\frac{2Qw_{sig}}{w_0} \approx \arctan\frac{2Qw_{sig}}{w_0} \quad (5.21)$$

$\measuredangle H_{CMPLF}(jw)$ in this case is a little less than $\arctan\frac{2Qw_{sig}}{w_0}$.

As a summary, the derived magnitude and phase responses suggest:

$$\left|H_{SBPF}(j(w_0 \pm w_{sig}))\right| \approx \left|H_{CMPLF}\left(j(w_0 \pm w_{sig})\right)\right| \approx \left|H_{LPF}(\pm jw_{sig})\right| = \frac{1}{\sqrt{1+\left(\frac{2Qw_{sig}}{w_0}\right)^2}} \quad (5.22)$$

$$\measuredangle H_{SBPF}\left(j(w_0 \pm w_{sig})\right) \approx \measuredangle H_{CMBPF}\left(j(w_0 \pm w_{sig})\right) \approx \left|H_{LPF}(\pm jw_{sig})\right| = \mp\arctan(\frac{2Qw_{sig}}{w_0}) \quad (5.23)$$

At this point, the discoveries we made with the two feedback bandpass filtering systems through sweeping the feedback scale factor $'k'$, as well as eqn. (5.1), get clearly explained. Neglecting the influence of all the undesired high frequency components in the recovered signal, we could formulate rough transfer functions for the two feedback filters when they are processing AM input signals.

$$H_{SBPF_{fb}}(s) = \frac{\frac{w_0}{(1-k)Q}s}{s^2 + \frac{w_0}{(1-k)Q}s + {w_A}^2 + \frac{{w_0}^2}{4(1-k)^2Q^2}} \quad (5.24)$$

$$H_{CMPLF_{fb}}(s) = \frac{\left[s + \frac{w_0}{2(1-k)Q}\right]\frac{w_0}{(1-k)Q}}{s^2 + \frac{w_0}{(1-k)Q}s + {w_A}^2 + \frac{{w_0}^2}{4(1-k)^2Q^2}} \quad (5.25)$$

where $w_A = \sqrt{1-(1/2(1-k)Q)^2}w_0$, as in the original transfer functions $w_A = \sqrt{1-(1/2Q)^2}w_0$. When setting $w_A = w_0$ for analysis and simulation simplicity, $w_A = w_0$ still holds true for the above feedback system transfer functions.

5.2 Noise Performance Test

In this section, we focus on the noise performance of both feedback bandpass filtering systems in Fig. 5.1 and Fig. 5.7, with negative k values. Output signals from the feedback systems and related open loop systems are plotted together for comparison.

5.2.1 The Feedback Bandpass Filtering System

Noiseless input and noisy core filter

The test set up below was run to evaluate the capability of the feedback system in suppressing the white noise injected into its core filter. Demodulated signals from the systems under test were plotted, as their noise floor is a good representation of the core filter output noise level.

Input voltage: $p(t) \cdot u(t) = \left[1m + (0.5m)\sin\left(w_p t\right)\right]\sin(w_{carrier} t)$,

where $w_p = 2\pi \cdot 10k$,$w_{carrier} = 2\pi \cdot 1Meg$

Feedback system: $Qcore = 50,\ k = -4, -9, -19$

Open-loop bandpass filter system: $Q = 250\ , 500, 1000$

Injected noise: two uncorrelated white noise current sources, the RMS value for both is 0.1uA.

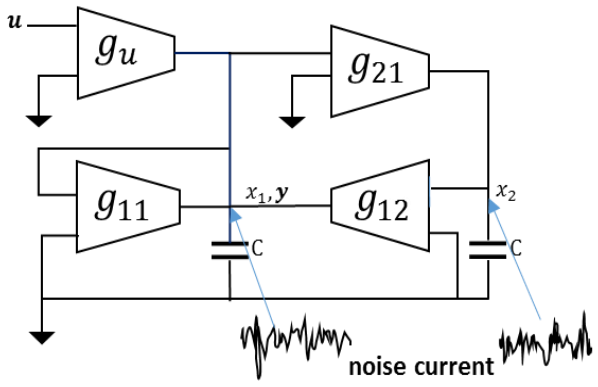

Figure 5.10 A biquad bandpass filter with injected current noise

According to the plots in Fig. 5.11 (a) to Fig. 5.11(c), as the open-loop bandpass filter becomes sharper, the same amount of injected noise yields higher output noise floor. This is due mainly to the transconductance notated by g_u providing a gain of g_u^{-1} to the injected noise, which is proportional to the filter's Q factor and cannot be counter balanced by the system's filtering capability. Therefore, a sharper bandpass filter tends to have higher output noise floor, hence less dynamic range. For all the k values under test, the 10kHz component in the recovered signals from the feedback system and its open-loop reference system is very close in amplitude while the output noise floor of the former is consistently lower. A close inspection reveals that as k becomes more negative, or the equivalent Q factor becomes higher, the feedback filtering system's output noise floor is suppressed to an even lower level, which is in contrast to what was observed in the noise test on the open-loop bandpass filters. This advantageous noise performance of the feedback filtering system is the result of two mechanisms: the input-referred noise of the feedback system depends mainly on the amount of injected noise and the original sharpness of the core filter, and it barely varies with the feedback scale factor k; on the other hand, when k is tuned more negative, the filtering system becomes sharper. When the same amount of input-referred noise gets filtered harder, the output noise floor surely drops to a lower level. Moreover, Fig. 5.11 (d) compares the output signals from two feedback systems set up to implement the same equivalent Q factors. Their original Q factors are 50 and 10, and k values are -3 and -19, respectively. The system with a flatter original core filter produces an output noise level about 1/5 as much as the other system does, but large harmonic distortion and slightly smaller recovered information signal drastically lowers the output SNR. Therefore, the tradeoff between the output noise level,

harmonic distortion and Q_{core} value is an issue worth consideration in tuning a feedback bandpass filter.

As a summary, setting the feedback scale factor k with negative values for the system in Fig. 5.1 provides an approach to implementing with a low-Q bandpass filter a new filtering system that has a time-variant Q factor and equivalent bandwidth comparable to that of a higher-Q bandpass filter; the feedback bandpass filter has improved performance in suppressing the in-filter noise hence a wider dynamic range compared to the open loop bandpass filter of comparable sharpness. Low requirement for the core filter Q factor and the superior in-filter noise suppression capability are two attractive features of the feedback filtering system. However, there is a tradeoff between the output noise level and output harmonic distortion.

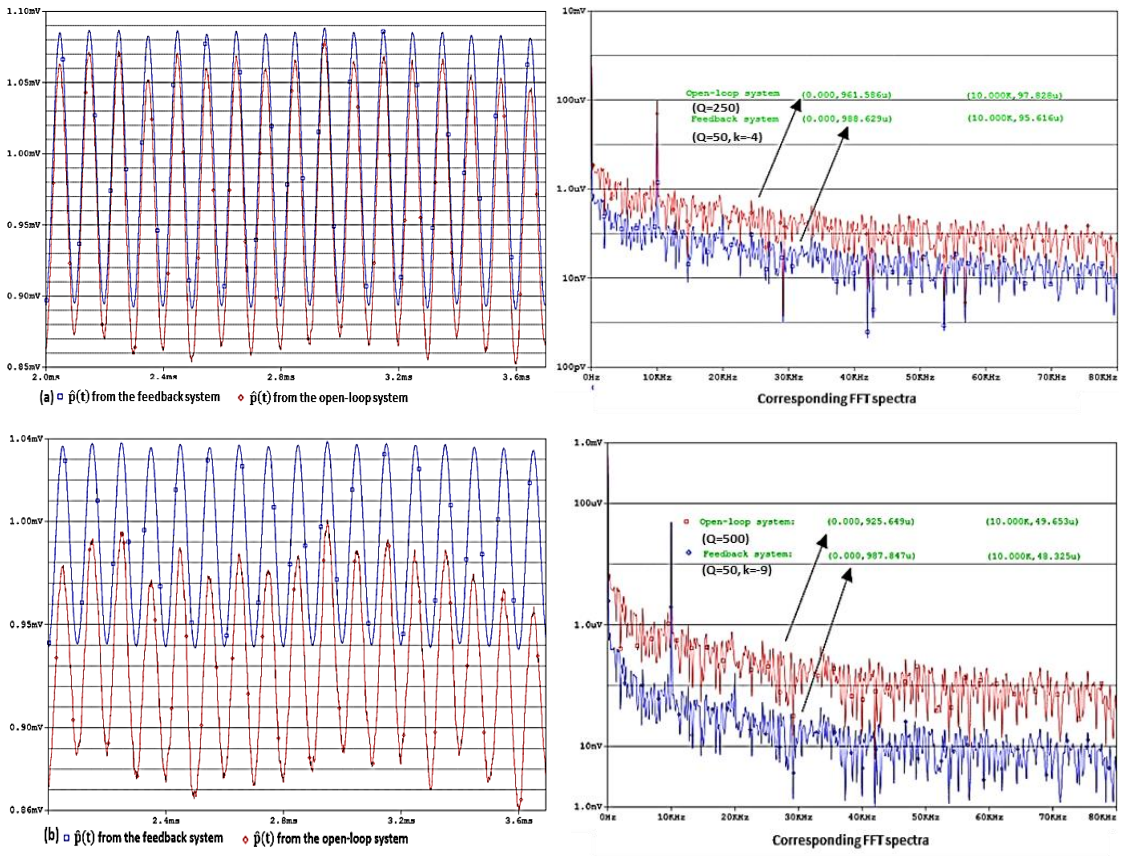

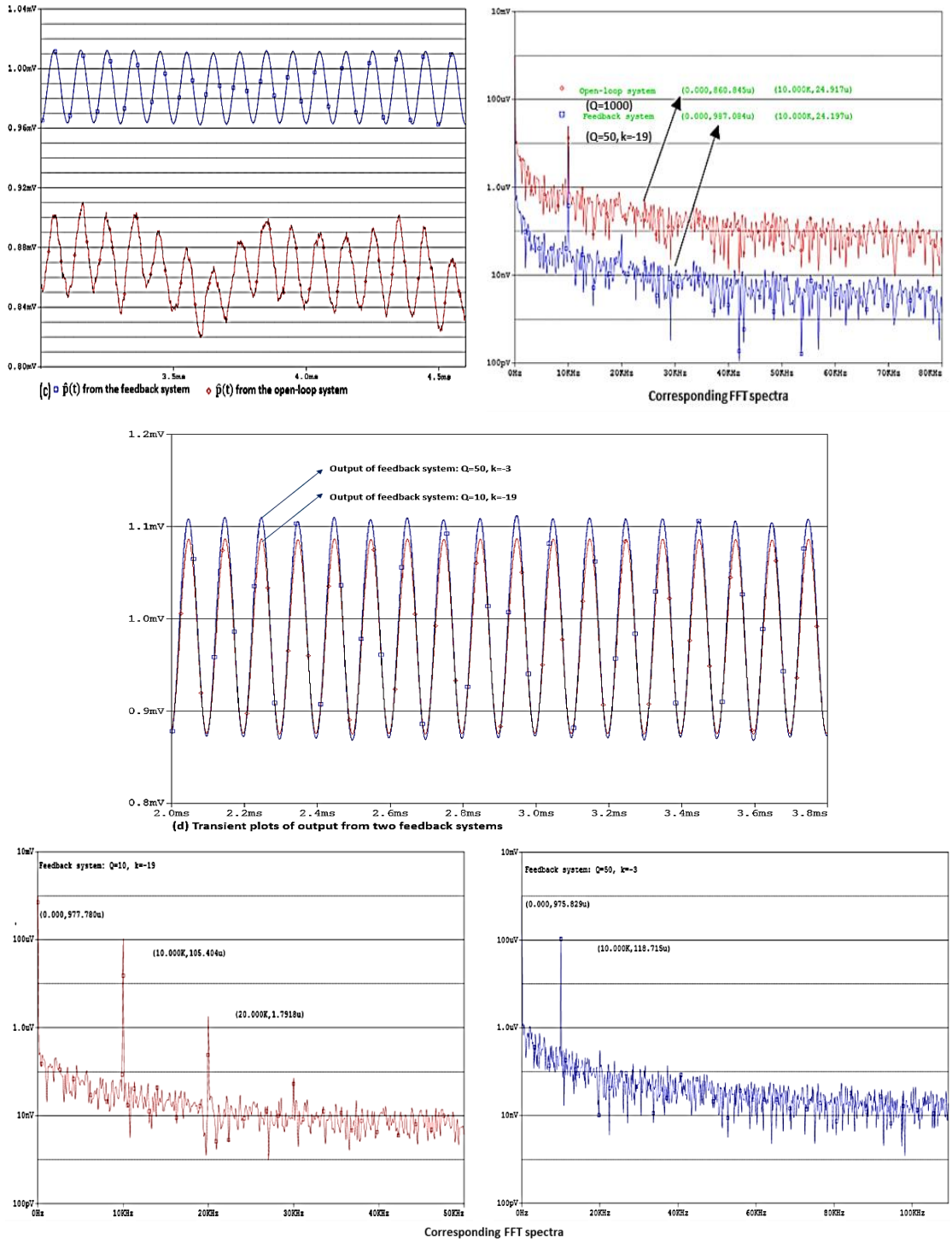

(d)

Figure 5.11 Transient plots and FFT spectra of the recovered signals from systems under the injecting white noise test. (a) Feedback system: Q=50, k=-4. Open-loop bandpass filter Q=250; (b) Feedback system: Q=50, k=-9. Open-loop bandpass filter Q=500; (c) Feedback system: Q=50, k=-19. Open-loop bandpass filter Q=1000; (d) Feedback systems: Q=50, k=-3 and Q=10, k=-19.

Noisy input and noiseless feedback system

Similar setup was used in this test, but the injected current noise was removed and white voltage noise was superimposed onto the system input AM signal:

Input voltage: $p(t) \cdot u(t) = \left[1m + (0.5m)sin\left(w_p t\right)\right]sin(w_{carrier} t\ ) + noise,$

$$where\ w_p = 2\pi \cdot 10k\ , w_{carrier} = 2\pi \cdot 1Meg,\ noise = \ 0.1mVrms$$

Feedback system: $Qcore = 50,\ k = -1, -4, -9$

Open-loop bandpass filter system: $Q = 100, 250\ , 500$

As shown in Fig. 5.12, for each k value under test, the noise floor in the output of both the feedback filtering system and the reference open loop system almost overlap, and the recovered information signals have very similar amplitude, except that the feedback system output contains noticeable harmonic distortion in the baseband. Therefore, the feedback bandpass filtering system is not superior to the open-loop bandpass filter with comparable sharpness in suppressing the input noise.

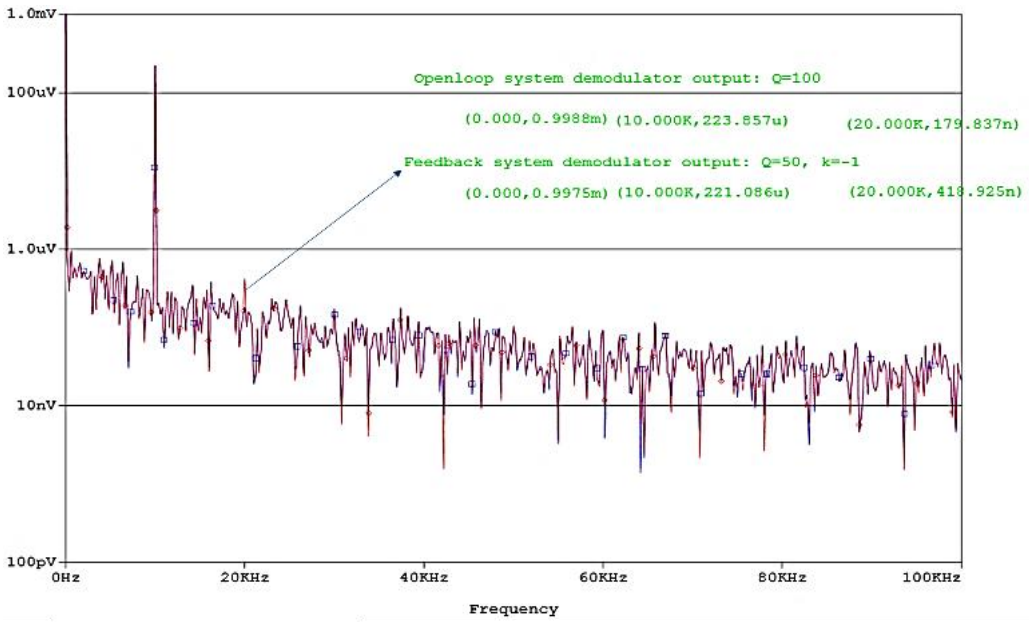

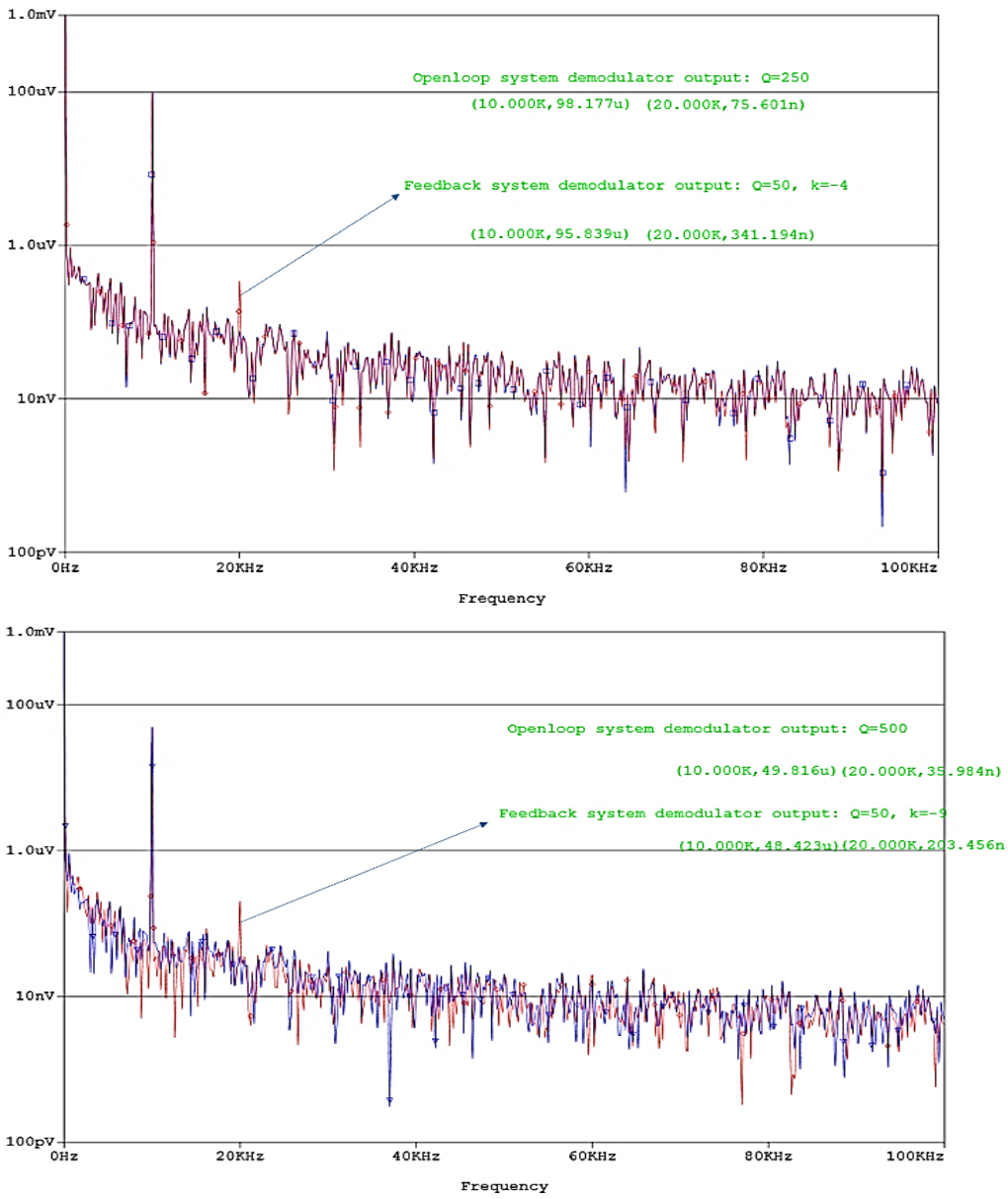

Figure 5.12 FFT spectra of the recovered signals from the feedback system with different k values and from the reference open-loop system in the noisy input test.

5.2.2 The Feedback Complex Filtering System

From the above test, we discovered that when the core filter is noisy, the feedback bandpass filtering system with negative k values produces a less noisy output than the open loop bandpass filtering system of comparable sharpness does, but it fails to more effectively suppress the input noise. We hence only focused on the in-filter noise

suppression capability of the feedback complex filtering systems here. Large amount of simulation in Chapter 4 has shown that a synchronous complex filter behaves similarly to a synchronous bandpass filter, so it's predicted that a feedback complex filtering system with negative *k* also has improved immunity to the injected noise.

Both the feedback system and the reference open-loop system under test were injected with white noise current of 0.1uArms. The original Q factor of the feedback system was set to be 50 and the scale factor *k* was -9. As shown in Fig. 5.13(a), the noise floor in the recovered signal from the reference open-loop system is consistently higher than that from the feedback system in the frequency range of our interest. Lowering k value from -9 to -19 and raising the open-loop complex filter's Q factor from 500 to 1000 accordingly, it's clearly shown by the FFT spectra in Fig. 5.13(b) that a sharper complex filter produces higher output noise floor while the feedback system with higher equivalent Q factor applies stronger attenuation to the injected noise. Finally, to compare the performance of the feedback systems with comparable equivalent bandwidth but different original Q_{core} values, same amount of noise was injected into two systems, with Q_{core}=50, k=-3 and Q_{core}=10, k=-19 respectively. Shown in Fig. 5.13(c), the recovered information signals from both systems have similar amplitude compared to the size of the recovered signal from an open loop complex filter with Q factor of 200, while the feedback system with smaller Q_{core} produces a much lower output noise floor. Moreover, no noticeable harmonic distortion is seen in the output spectra of either feedback system, therefore, the feedback complex filtering systems are superior to the feedback bandpass filtering systems in dealing with the in-filter noise.

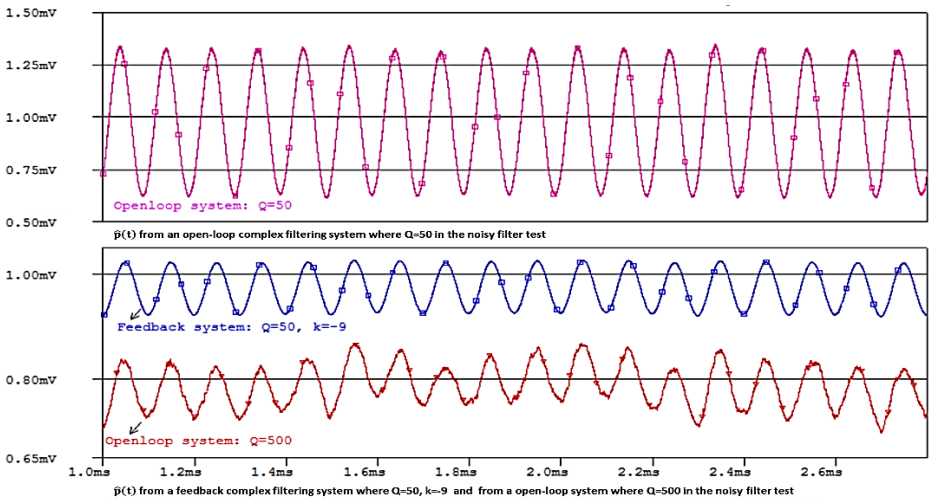

$\tilde{p}(t)$ from an open-loop complex filtering system where Q=50 in the noisy filter test

$\tilde{p}(t)$ from a feedback complex filtering system where Q=50, k=-9 and from a open-loop system where Q=500 in the noisy filter test

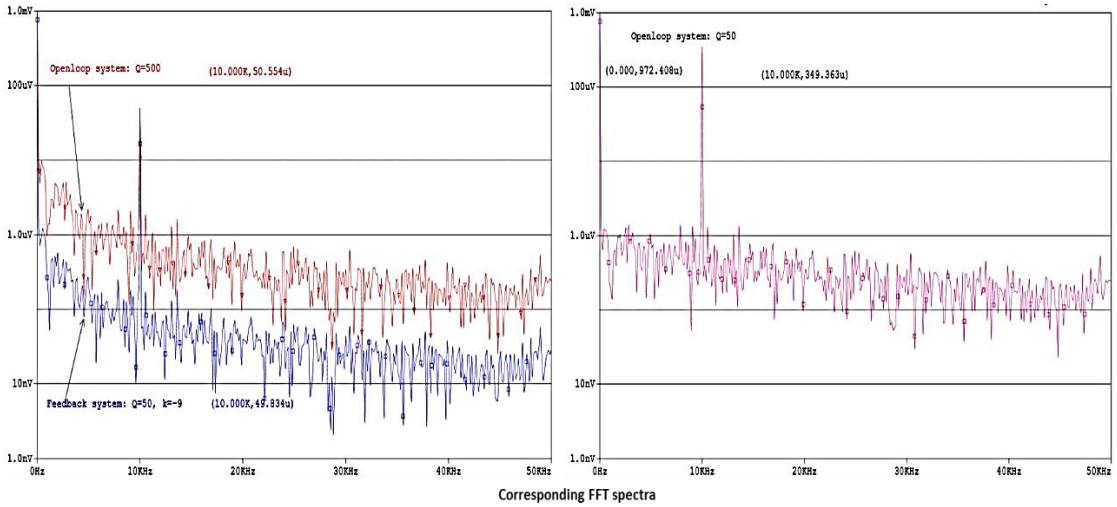

Corresponding FFT spectra

(a)

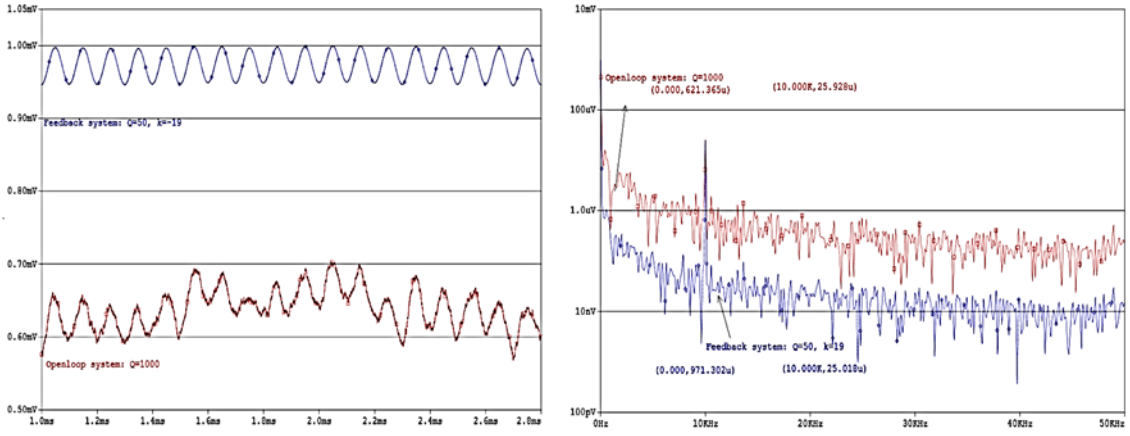

$\tilde{p}(t)$ from a feedback complex filtering system where Q=50, k=-19 and from a open-loop system where Q=1000 in the noisy filter test

Corresponding FFT spectra

(b)

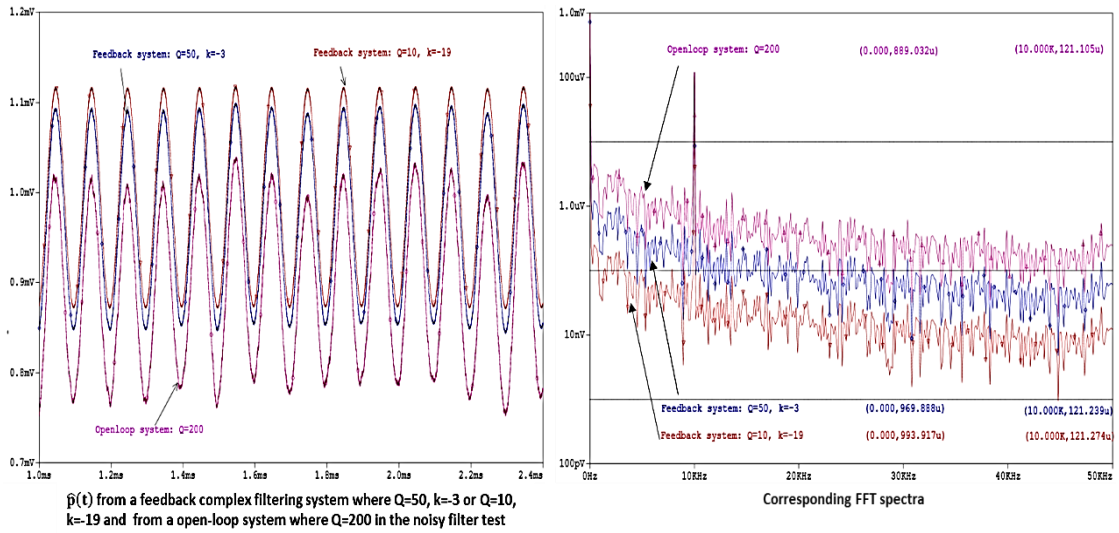

(c)

Figure 5.13 Transient plots and FFT spectra of the recovered signals from systems under the noisy core filter test. (a) Feedback complex filtering system with core filter of Q=50 and k=-9, and the reference open-loop complex filtering system with core filter of Q=500 and 50. (b) Feedback system with core filter of Q=50 and k=-19, and the reference open-loop system with core filter of Q=1000. (c) Feedback systems with Q=50, k=-3 and Q=10, k=-19, and the reference open loop system with Q=200.

5.2.3 A Noisy Feedback Complex Filtering System Model

In this section, we propose and test a more practical Gm-C network model for the feedback complex filtering system where all the transconductors are noisy. In such a situation, the recovered signal $\hat{p}(t)$ is noisier than its ideal model counterpart, and it's of our interest whether the noisy feedback filtering system still has the improved noise performance compared to the reference open loop filtering system.

A brief review on the noisy transconductor model is given as follows. The block schematic shown in Fig. 5.14 illustrates a generic transconduator's noise model [34-36]. Regardless of its type (with differential pair or with second generation current conveyor) and technology realization (bipolar, CMOS), any transconductor may be represented by an active noiseless device with the equivalent noise sources. In the model from Fig.5.14,

$\overline{dv_{ieq}^2}$ is the mean squared value of the equivalent input noise voltage source and $\overline{di_{ieq}^2}$ is the mean squared value of the input noise current source. Depending on the resistance of the circuitry that drives a transconductor, the dominating noise source is different. When the source resistance is comparatively low ($R_s \ll R_{Gm\_in}$), the transconductor could barely divide any current from the input-referred noise current generator, so the equivalent input noise voltage source is dominant. If the source resistance is high ($R_s \gg R_{Gm\_in}$), then the transconductor takes most of the current from the input-referred noise current generator and almost no voltage from the input-referred noise voltage generator, so it's the input current noise source mainly contributes to the transconductor output noise in this situation. For finite and not-null values of R_s, both input noise generators need to be taken into consideration.

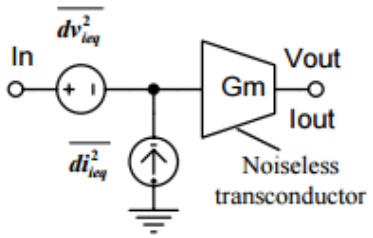

Figure 5.14 Noise model of a transconductor.

Power density of the equivalent input noise current and voltage of a transconductor stage (in bipolar or CMOS technology) can be expressed as follows [37]:

$$\overline{dv_{ieq}^2} = \gamma_v \frac{kT}{\pi G_m} dw, \quad \overline{di_{ieq}^2} = \gamma_i \frac{kTG_m}{\pi G_m} dw \qquad (5.26)$$

where γ_v and γ_i coefficients are the noise voltage and current factors of the transconductor, G_m– the transconductance value of the circuit, k – Boltzmann's constant, and T – absolute temperature. An important difference between a CMOS and a bipolar

transistor is that usually the base current flows in a BJT cannot be neglected. Shot noise is associated with this current, which gives rise to the equivalent input noise current generator that is not present in a MOSFET. As a result, each BJT virtually has two input noise generators.

To simplify the modeling of the noisy transconductors in our system, we assume that each transconductor has only the input-referred noise voltage source as its dominant noise source while the input-referred noise current source is of little importance. The BJT "tanh" transconductor in Fig. 5.15 for instance, has such a noise property. As analyzed in the literature [38], it has an input-referred noise voltage power density of:

$$\overline{dv_{ieq}^2} = 4\overline{dv_1^2} = 4\frac{kT}{\pi G_m}dw \qquad (5.27)$$

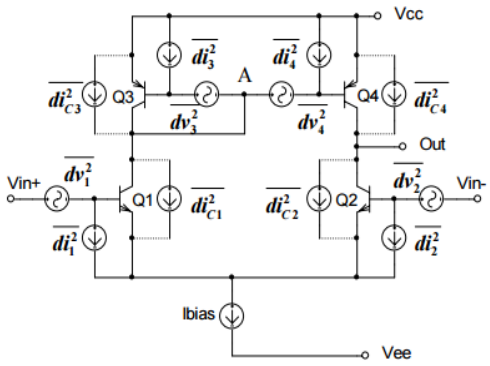

Figure 5.15 "Tanh" transconductor noise sources.

We utilized eqn. (5.27) to determine the amount of white noise voltage to insert in front of each VCCS and developed a noisy system as shown in Fig. 5.16. The specific test setup is listed in Table 5. 3, where the feedback filter has an original Q factor of 50 and a feedback scale factor of -9, and the reference open loop filter has a Q factor of 500. Using filtering capacitors of 3.07nF and a 3.07uF capacitor for generating the feedback signal, we could determine all the transconductors in the system. Take $g_{11} = g_{22} =$

$-192.89uS$ which corresponds to a core filter with center frequency of 1MHz and Q factor of 50 for instance, using eqn. (5.27), the input noise power density is:

$$\overline{dv_{ieq\_Q50}^2} = \frac{8kT}{G_m}df = \frac{8\times 25.85mV\times 1.602\times 10^{-19}A\cdot s}{192.89uAV^{-1}}df \qquad (5.28)$$

As all the white noise sources (uncorrelated) were generated in MATLAB at the rate of 1sample/20ns, the flat noise spectrum has a bandwidth of $\frac{1}{20\times 10^{-9}\times 2} = 25MHz$. Therefore, the rms value of the transconductor's input noise voltage is:

$$v_{ieq\_Q50\_rms} = \sqrt{25MHz\cdot \overline{dv_{ieq\_Q50}^2}} = \frac{8\times 25.85\times 1.602\times 10^{-19}\times 25\times 10^{6}}{0.19289}V = 65.527uV \qquad (5.29)$$

Similarly, the input noise voltage for g_{12} and g_{21} (19.289mS) has an rms value of $6.553uV$. For the transconductor in the feedback path (9mS or 1mS), the input noise rms value is about $9.593uV$ or $30uV$.

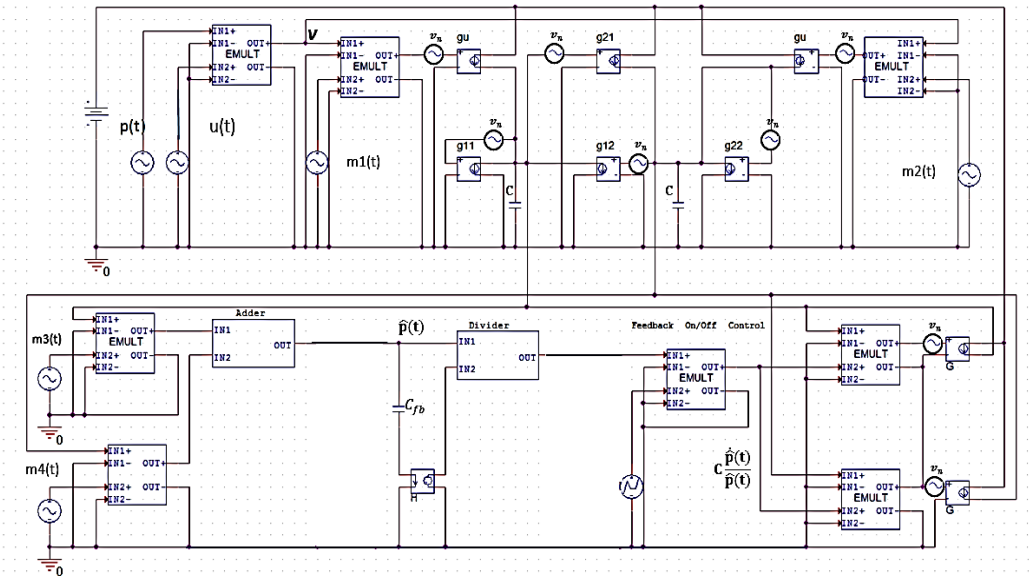

Figure 5.16 A noisy model for the feedback complex filtering system.

Input and modulating signals(V)	p(t)	1m+0.5msin(2π·10K· t)	
	u(t)	sin(2π·4M·t)	m1=2sin(2π·5M· t), m2=-2cos(2π·5M· t), m3=cos(2π·1M· t), m4=sin(2π·1M· t)
Transconductors (S)	**The feedback system core filter (f0=1MHz, Q=50, k=-9 or -1)**: |g11|=|g22|=|gu1|=|gu2|=192.89u, |g12|=|g21|=19.289m, $\|g_{fb}\|=9m/1m$		
	The openloop system core filter(f0=1MHz, Q=500 or 100): |g11|=|g22|=|gu1|=|gu2|=19.289u or 96.445u, |g12|=|g21|=19.289m		
Capacitance (f)	The feedback system: Ccore=3.07n, Cfb=3.07u The openloop system: Ccore=3.07n		
Noise sources(Vrms)	Test1	**The feedback system(k=-9)**: Vin_g11=Vin_g22=Vin_gu1=Vin_gu2=65.5u, Vin_g12=Vin_g21=6.55u, Vin_gfb=10u	
		The openloop system: Vin_g11=Vin_g22=Vin_gu1=Vin_gu2=65.5u, Vin_g12=Vin_g21=6.55u	
	Test2	**The feedback system(k=-1)**: Vin_g11=Vin_g22=Vin_gu1=Vin_gu2=65.5u, Vin_g12=Vin_g21=6.55u, Vin_gfb=29u	
		The openloop system: Vin_g11=Vin_g22=Vin_gu1=Vin_gu2=65.5u, Vin_g12=Vin_g21=6.55u	

Table 5-3 Test setup for comparing the performance of the noisy feedback complex filtering system and the reference noisy open-loop complex filtering system.

For both tests, we intentionally set up the core filter in the open loop system with the same set of input noise voltage sources derived for the core filter with Q=50 in the feedback system, which actually makes the open loop filter less noisy than it is supposed to be. The up conversion and down conversion output signals from the systems under test were plotted in Fig. 5.17. The noisy feedback filter and the noisy reference open loop filter still have comparable sharpness, as their recovered information signals are very close in amplitude. Moreover, the output noise floor of the feedback system is obviously lower than its open loop counterpart. Comparing the results of Test 1 and Test 2, the in-band output noise is apparently higher for the open loop filter with a larger Q factor, while there is barely difference between the in-band output noise levels for the feedback filters with different k value. Therefore, even the transconductors in the Gm-C model are noisy, the feedback complex filter is still able to produce an output with higher SNR than the output from an open loop complex filter of comparable sharpness. Considering that a noisy filter with smaller Q factor usually outputs lower in-band noise but it has very limited filtering capability, the feedback complex filtering system provides an innovative method to effectively sharpen a filter without raising the output noise floor in the interested frequency range.

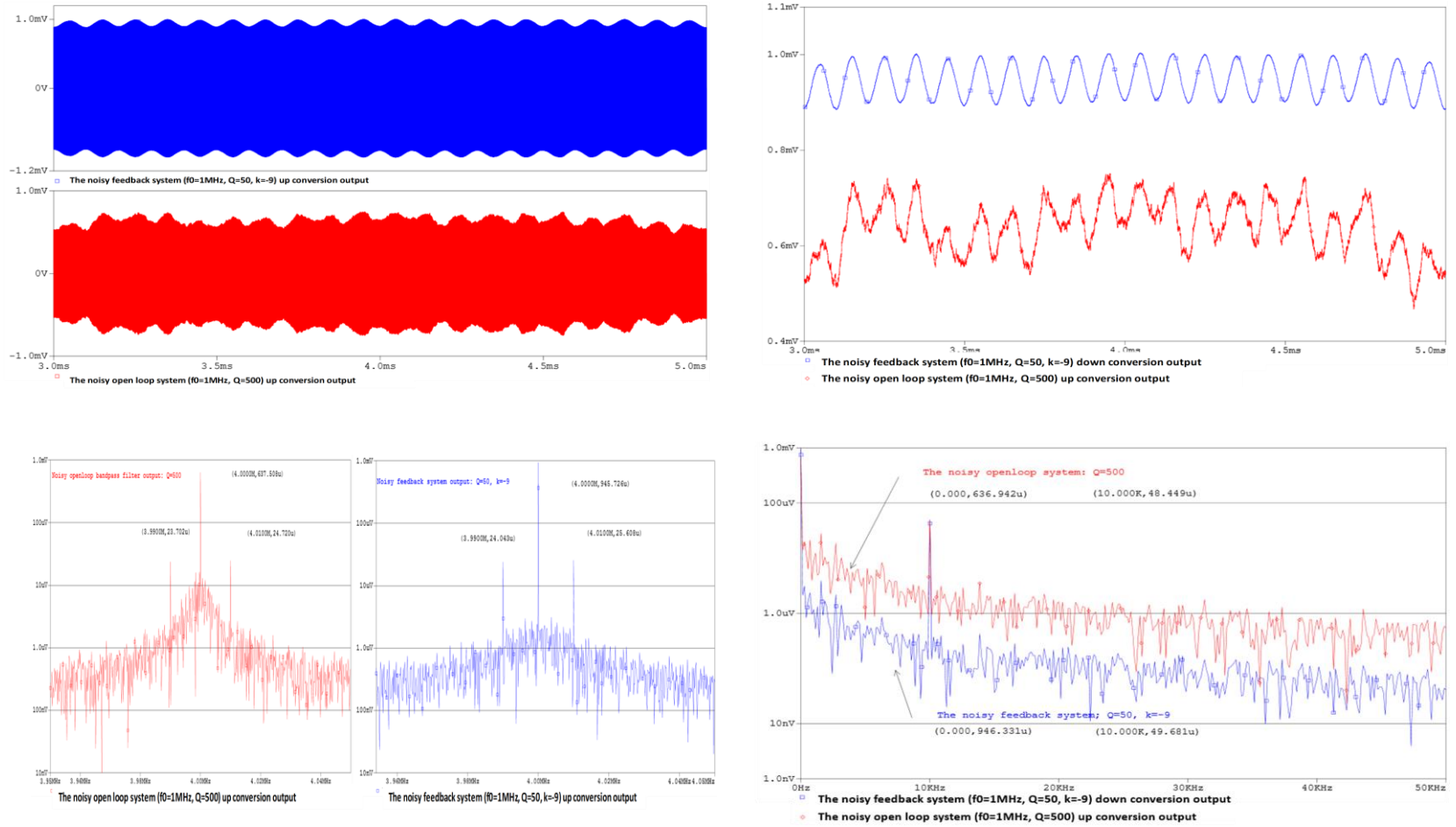

(a)

Left column: Up conversion results from Test 1 Right column: Down conversion results from Test 1

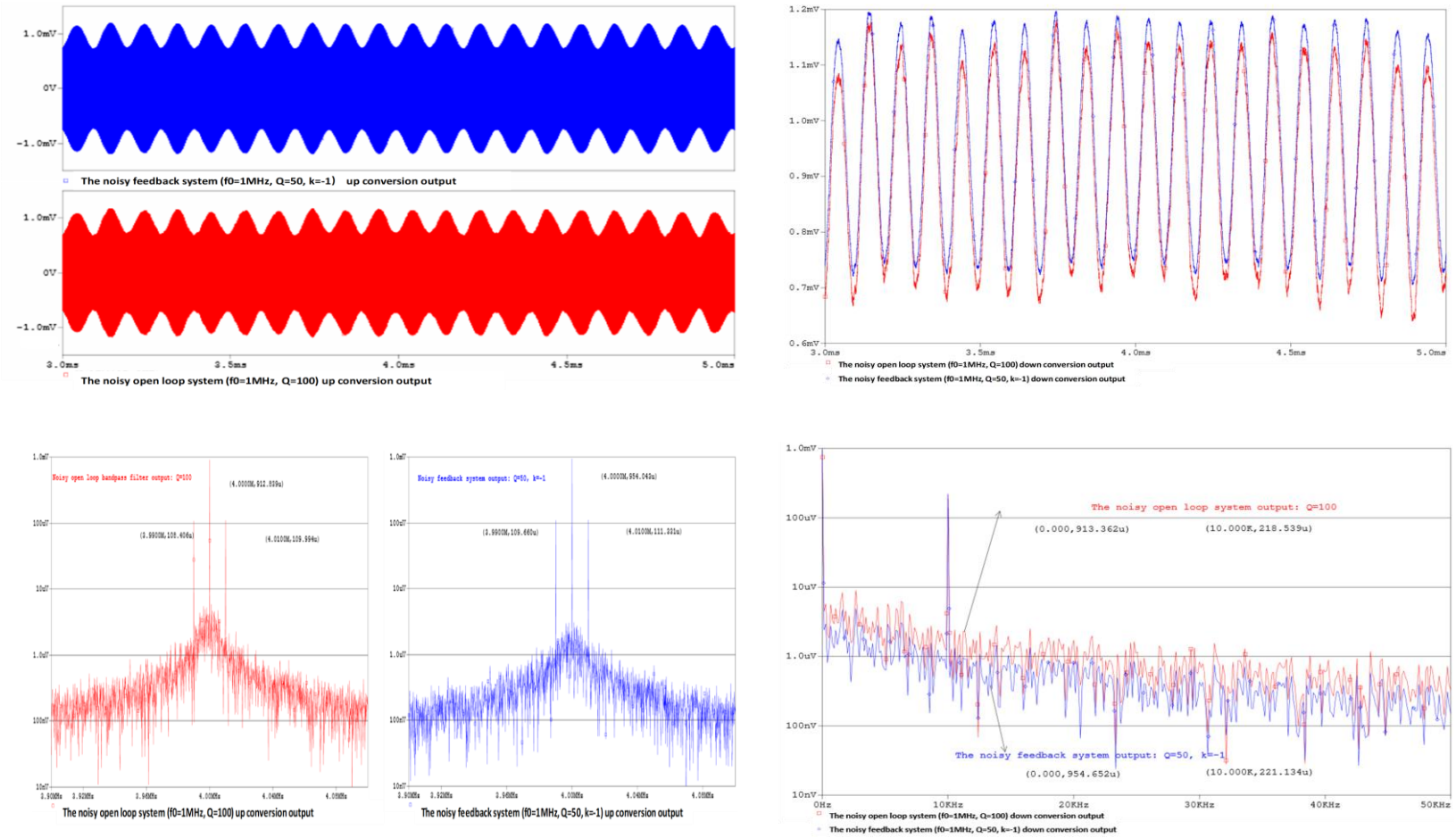

(b)

Left column: Up conversion results from Test 2 Right column: Down conversion results from Tes t2

Figure 5.17 Transient plots and FFT spectra of (a) Test 1 and (b) Test 2.

5.3 The Implementation of a Log-domain Feedback Complex Filtering System

Finally, we propose a transistor-level implementation solution for the feedback complex filtering system that utilizes log-domain filtering circuitries and related technique. We have implemented in Chapter 3 a log-domain open loop synchronous complex filtering system that is able to perform both up conversion and down conversion at the back end stage, and we have verified that the down conversion result, $\hat{p}(t)$, could be used to generate the Q-factor control signal $k\frac{\dot{\hat{p}}(t)}{\hat{p}(t)}$. We now discuss in detail the implementation of the feedback path. The state-space representation of a superheterodyne feedback complex filtering system is reproduced in eqn. (5.30), where $k\frac{\dot{\hat{p}}}{\hat{p}}x_{1,2}$ corresponds to the feedback Q-factor control signal.

$$\begin{vmatrix}\dot{x_1}\\ \dot{x_2}\end{vmatrix} = \begin{vmatrix}-\frac{w_0}{2Q}+k\frac{\dot{\hat{p}}}{\hat{p}} & -w_0\\ w_0 & -\frac{w_0}{2Q}+k\frac{\dot{\hat{p}}}{\hat{p}}\end{vmatrix}\begin{vmatrix}x_1\\ x_2\end{vmatrix} + (w_0/Q)\begin{vmatrix}sin(w_{M1}t)\\ -cos(w_{M1}t)\end{vmatrix} v$$

$$y_{up\_conversion} = |sin(w_{M1}t) \quad -cos(w_{M1}t)|$$

$$y_{down\_conversion} = |cos(w_0 t) \quad sin(w_0 t)|\begin{vmatrix}x_1\\ x_2\end{vmatrix} = \hat{p}(t) \qquad (5.30)$$

In the log-domain complex filtering system, $\hat{p}(t)$ is an always positive current signal which is realized as the current flowing in the output transistor of the back end down converter. For demonstration sake, we express

$$\hat{\mathrm{p}}(t) = I_s \exp(v_{be_o}/v_T) \qquad (5.31)$$

where v_{be_o} is the base-emitter voltage difference of the output transistor. It follows that

$$\dot{\hat{\mathrm{p}}} = \frac{\dot{v_{be_o}}}{v_T}\hat{\mathrm{p}} \rightarrow \frac{\dot{\hat{\mathrm{p}}}}{\hat{\mathrm{p}}} = \frac{\dot{v_{be_o}}}{v_T} \qquad (5.32)$$

Recall that to associate the state space representation with a log-domain circuit, both sides of the state equations are multiplied with $\frac{Cv_T}{\mathrm{x}_{1,2}}$. Terms $\mathrm{k}\frac{\dot{\hat{\mathrm{p}}}}{\hat{\mathrm{p}}}\mathrm{x}_{1,2}$ are correspondingly transformed into:

$$\mathrm{k}\frac{\dot{\hat{\mathrm{p}}}}{\hat{\mathrm{p}}}\mathrm{x}_{1,2}\cdot\frac{Cv_T}{\mathrm{x}_{1,2}}=\mathrm{k}\frac{\dot{\hat{\mathrm{p}}}}{\hat{\mathrm{p}}}Cv_T=kCv_{\dot{be}_o} \qquad (5.33)$$

Eqn. (5.33) reveals the explicit physical meaning of the feedback signal: k times the current flowing in a capacitor of C farads when applied with voltage v_{be_o}. Based on the analysis above, we designed the circuitry in Fig. 5.18 to generate a current signal that approximately equals $kCv_{\dot{be}_o}$ with some offset, using the complex filtering system's down converter output current $\hat{\mathrm{p}}(t)$. The design consists of two log-domain first-order lowpass filters connected by a current mirror. $\hat{\mathrm{p}}(t)$ is sent to LPF1 by connecting the base of the output transistor in the down converter to the emitter of the filter's input transistor. The transfer function of LPF1 is:

$$\frac{I_{OUT}(s)}{I_{IN}(s)}=\frac{w_1}{s+w_1},\ \text{where}\ \mathrm{w}_1=\frac{\mathrm{I}_{\mathrm{LP1}}}{\mathrm{CV}_\mathrm{T}} \qquad (5.34)$$

When w_1 is tuned to be far away from the input information component, the baseband of the filter output current is very similar to that of $\hat{\mathrm{p}}(t)$, so the log version of the output current, i.e. the voltage across the capacitor C notated as $\widehat{\mathrm{v}_{\mathrm{be}_0}}$, has very similar baseband as that of v_{be_o}. Therefore, the current flowing in C approximately equals $Cv_{\dot{be}_o}$. To scale this current, another low-pass filter, LPF2, with tunable peak gain is included, the transfer function of which is:

$$\frac{I_{OUT}(s)}{I_{IN}(s)}=\frac{kw_2}{s+w_2},\ \text{where}\ \mathrm{w}_2=\frac{\mathrm{I}_{\mathrm{LP2}}}{\mathrm{CV}_\mathrm{T}} \qquad (5.35)$$

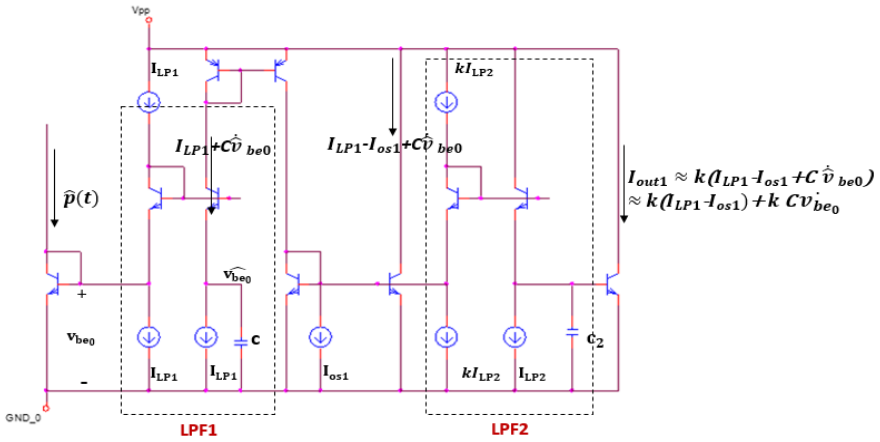

Figure 5.18 Implementation of $kCv_{be_o}^{\cdot}$ with dc offset.

Note that the dc component in the input current of LPF2 will be scaled by k too, it's preferable to adjust it to a low level before the signal processing so that the output dc offset will not be too high. This issue can be fixed by adding a tunable source I_{os1} to pull away some dc current from the current mirror output, so the offset could be tuned conveniently without affecting the cutoff frequency of LPF1. The output current of the overall circuitry, call it I_{out1}, is an offset, low-pass filtered version of $kCv_{be_o}^{\cdot}$. If w_1 and w_2 are high enough, very few phase shift would be introduced to the useful components, so the baseband spectrum of I_{out1} would be very similar to that of $kCv_{be_o}^{\cdot}$ $(k > 0)$. The circuitry in Fig. 5.19 gets rid of the dc component in I_{out1} and reverses the ac components to implement the negative k. The output current I_{out2} approximately equals $-kCv_{be_o}^{\cdot}$ and could be sent back to the core filter to time vary its Q factor. Switches not shown here are used as an interface, with which we could prevent the Q-factor control signal being immediately sent back when it's just generated but close the loop at some point when the transient part in the signal fades to a negligible level. The switches are indispensable for avoiding convergence problem in the simulation.

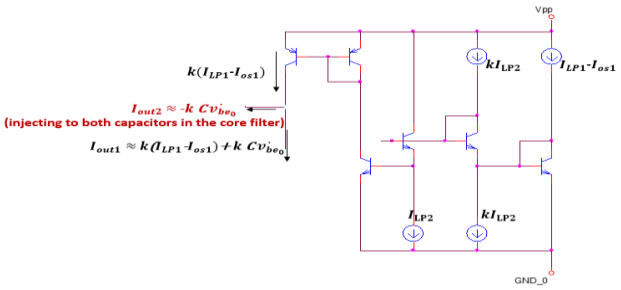

Figure 5.19 Implementation of $-kC\dot{v}_{be_o}$

The trickiest part in the feedback path design lies in eliminating the undesired signals resulted from the interaction between the Q-factor control signal and the quiescent signals in the core filter. Qualitatively, for the feedback system to work as expected, the Q-factor control signal should only interact with the ac components in the core filter and generate signals in the frequency range near the filter's center frequency. However, the log-domain core filter incorporates circuitry that helps establish the dc operating point, which inevitably generates dc signals at some nodes that will be modulated by the feedback signal. Such an undesirable modulation results in ac components in the baseband, which is far away from the filter's center frequency. Considering that the filter output contains ac components near its center frequency and in the baseband as well, the down conversion result is much noisier than expected due to the baseband components being shifted into a higher frequency range. The high frequency noise would lower the SNR of the feedback Q-factor control signal and degrades the performance of the feedback system, which is manifested by the large output harmonic distortion. Lowpass filtering is not an effective solution because the high frequency noise has comparable size as that of the baseband signals, and the feedback system is very sensitive to the phase change in the recovered baseband signal.

To fix the issue, we introduced another core filter, which is exactly the same as the core filter but with no ac input. It's used to model the quiescent part of the original core filter, so when the same Q-factor control signal is injected, it would produce baseband ac components almost identical to the baseband components produced by the modified core filter. Subtracting the output of the modified auxiliary filter from that of the modified core filter, we would be able to get rid of most of the undesired baseband components and recover $\hat{p}(t)$ with much less noise near the back end modulating frequency. The design is illustrated in Fig. 5.20.

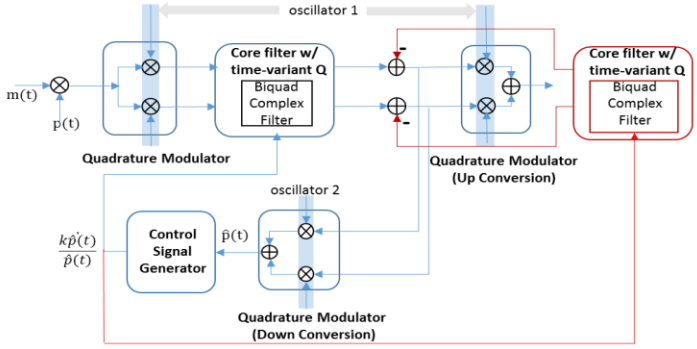

Figure 5.20 Embodiment of the log-domain feedback complex filtering system

The interface between the core filter and the back end modulator in the feedback system is accordingly redesigned to perform current subtraction. Related circuitry is shown in Fig. 5.21. The schematic of the feedback log-domain complex filtering system is shown in Fig. 5.22, where the up converter is omitted. All the BJTs are ideal and have $\beta = 100K$, MbreakN and MbreakP models from the PSpice Breakout library were used to implement the switches. A transient test was run on both the feedback system and its related open loop system. Furthermore, the gain spectra of the particular systems under test were plotted to show their frequency response in a generic way. The specific setup for the transient test is listed in Table 5.4.

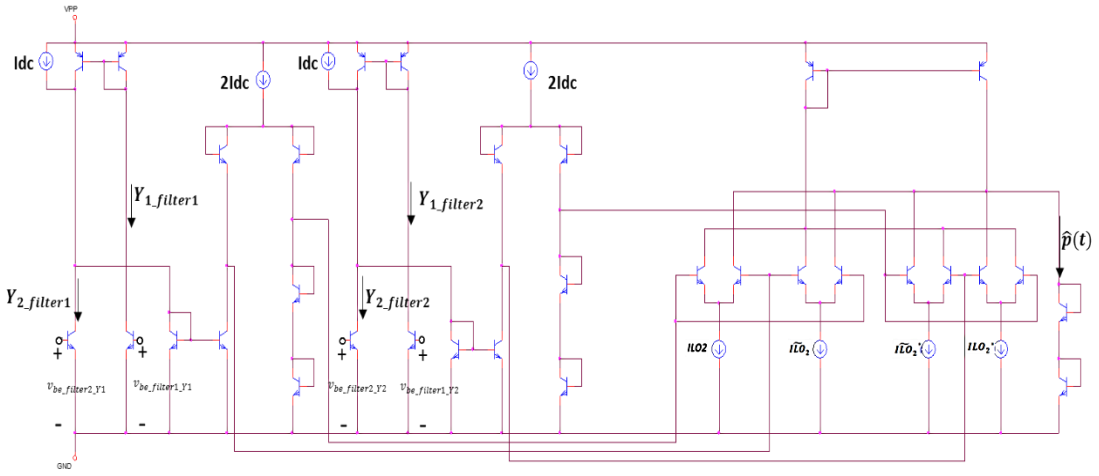

(a)

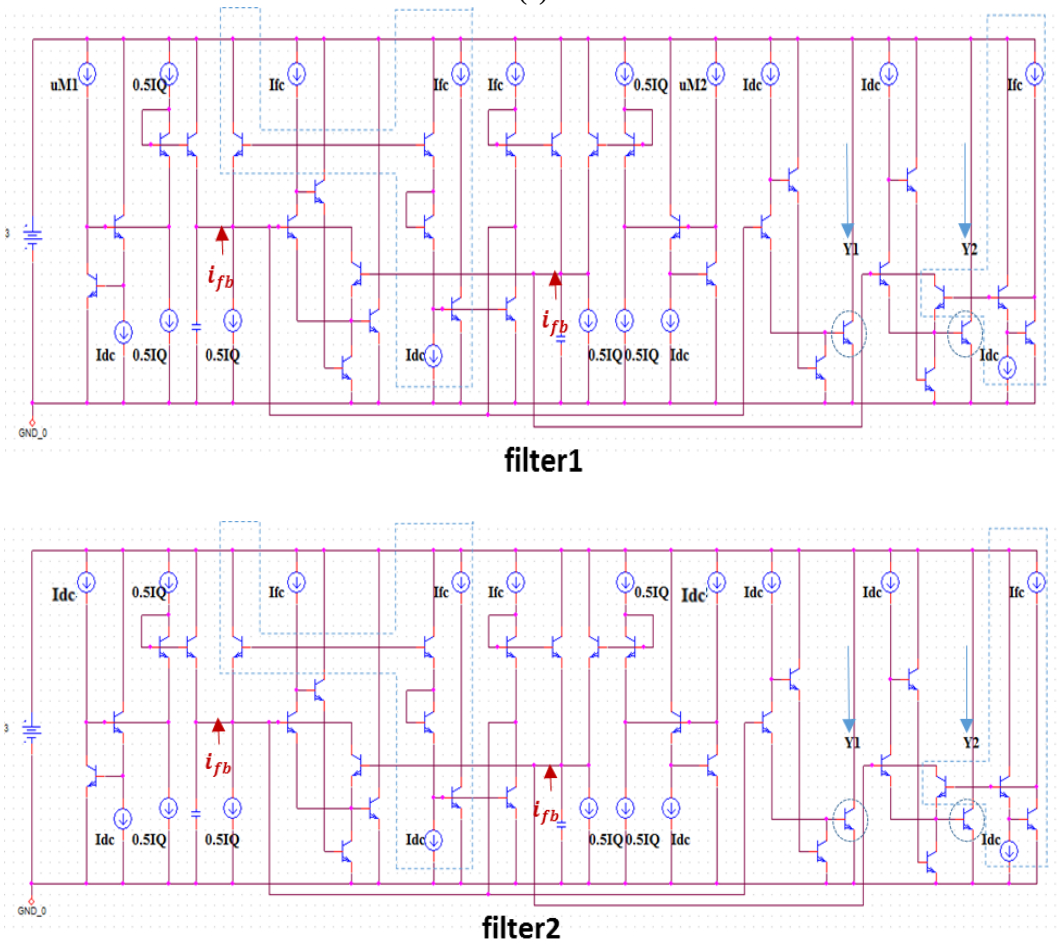

(b)

Figure 5.21 Schematic of (a) the back end stage and (b) the two modified filters in the feedback system.

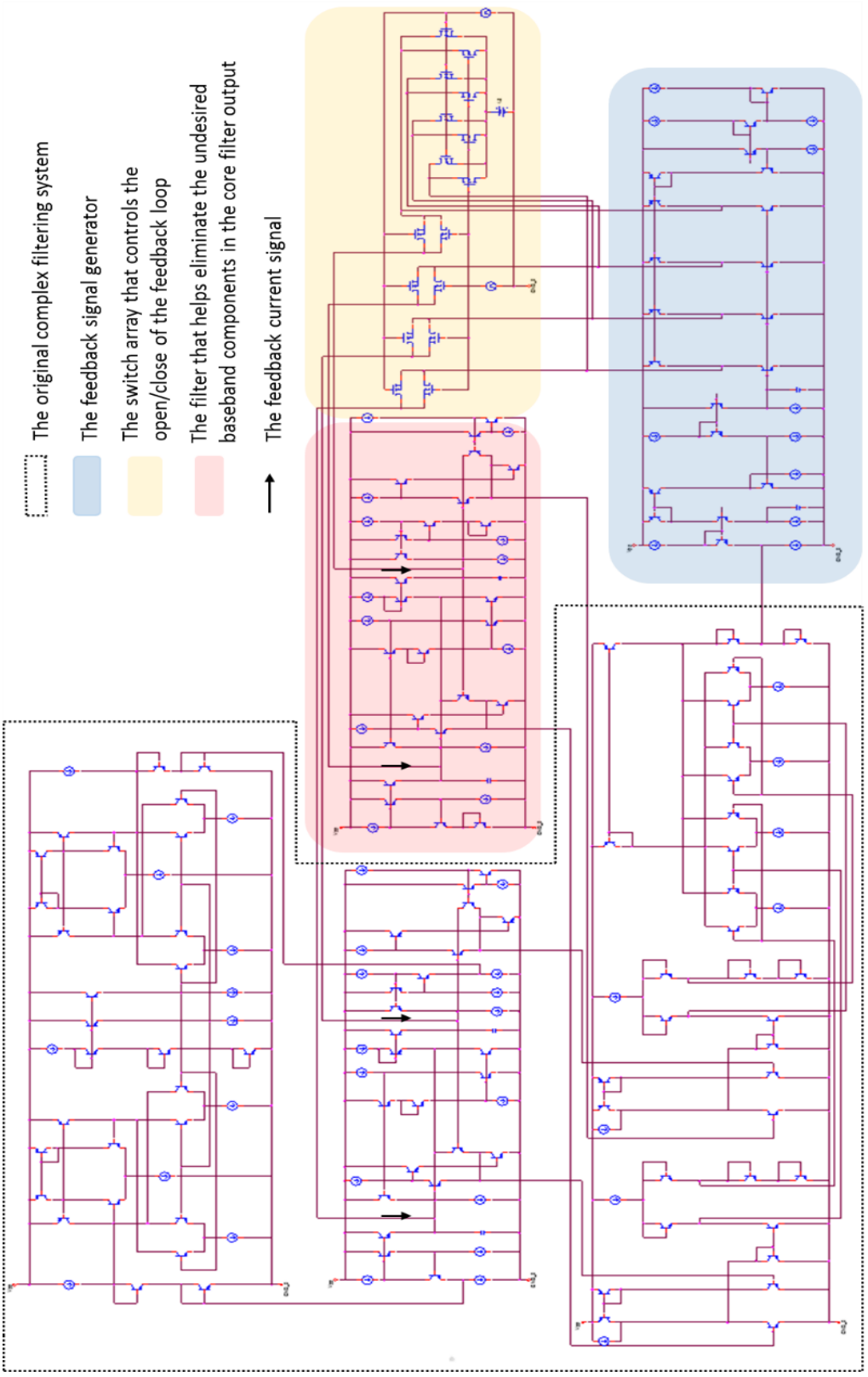

Figure 5.22 The transistor-level implementation of a feedback log-domain complex filtering system

Input and front end modulator (A)	p(t)	1m+(0.2m)[sin(2π·2K· t)+ sin(2π·10K· t)+ sin(2π·16K· t)+sin(2π·25K· t)]								
	carrier(t)	0.2sin(2π·4M·t)	I_{dc}	500u	m_1(t)=1.6sin(2π·5M· t)		m_2(t)=-1.6cos(2π·5M· t)			
Core filter	$I_{dc} = I_{f0}$	500uA	C	3.075nF	I_Q (feedback system)	50uA	I_Q (openloop system)	5uA, 2.5uA		
	(f_0 = 1MHz)				(Q=5)		(Q=50, 100)			
Back end modulator(A)	Down Converter				m_1(t)=1.6cos(2π·1M· t)		m_2(t)=1.6sin(2π·1M· t)		Iout_os=0A	
	Up Converter				m_1(t)=1.6sin(2π·5M· t)		m_2(t)=-1.6cos(2π·5M· t)		Iout_os=500uA	
Feedback signal generator	I_{LP1}	250uA	C	3.07nF	I_{OS1}	200uA	I_{LP2}	50uA	C2	0.6nF
	(f_{LP1}= 0.5MHz)				kI_{LP2}	450uA, 950uA	(k = −9, −19 f_{LP2} = 0.5MHz)			

Table 5-4 Circuit parameters for the feedback log-domain complex filter.

The first set of systems under the transient test include: a feedback complex filtering system with Q=5, k=-9, an open loop system with Q=5 and an open loop system with Q=50. The down conversion results from all the systems are plotted in Fig. 5.23(a). According to the simulation setup, the feedback loop is not closed until t=2ms, so the output signal of the feedback system (k=0) perfectly overlaps with the output from the open loop filter with Q=5 till 2ms, then becomes smaller when the loop is closed and gets in phase with the output of the open loop system with Q=50. FFT spectra of the steady state output signals from the two systems are given in Fig. 5.23(b), measurement results show that they have baseband components of similar respective sizes, but the amplitude difference is a little higher for dc component. It might be due to the feedback filter's peak gain is slightly higher and its actual center frequency is a little off.

In the second set of systems tested, the feedback system is set up with Q=5, k=-19 and the reference open loop system has Q=100. Down converter output signals from the two systems are plotted in Fig. 5.24. Their dc levels have even larger difference, while for the rest components the amplitude difference is at a negligible level. It indicates that a feedback filter with more negative k has a higher peak gain. Moreover, the feedback system output is noisier than its open-loop system counterpart, which is

due to the high frequency components inevitably generated in the down conversion process. As the output noise is in a higher frequency range and at a comparatively low level, it could be attenuated by an additional low-pass filter without affecting the useful baseband components.

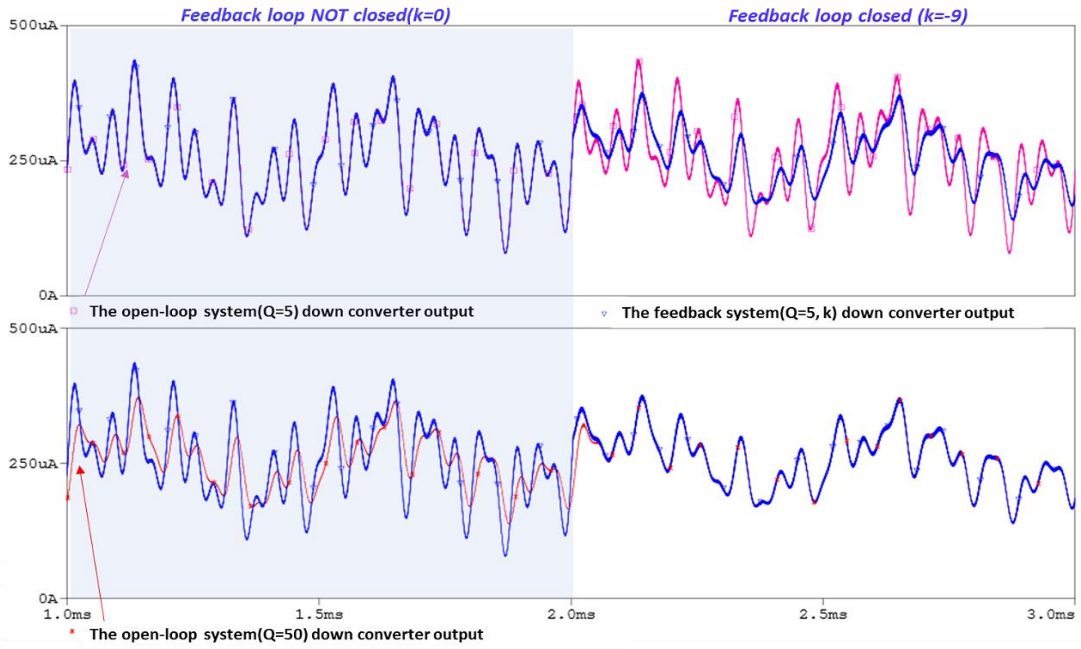

(a)

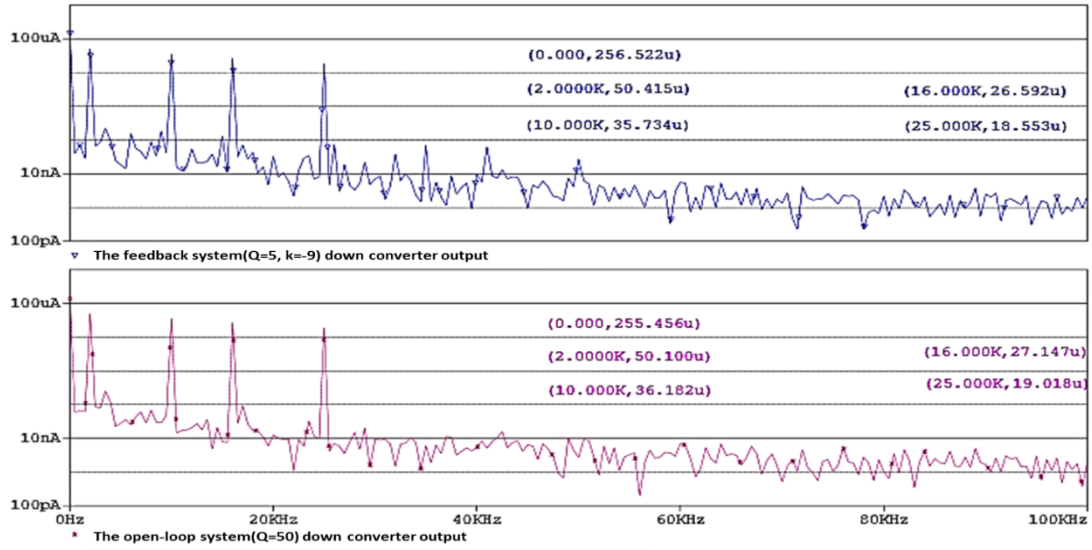

(b)

Figure 5.23 Transient plots and FFT spectra of the recovered signals from the first set of systems

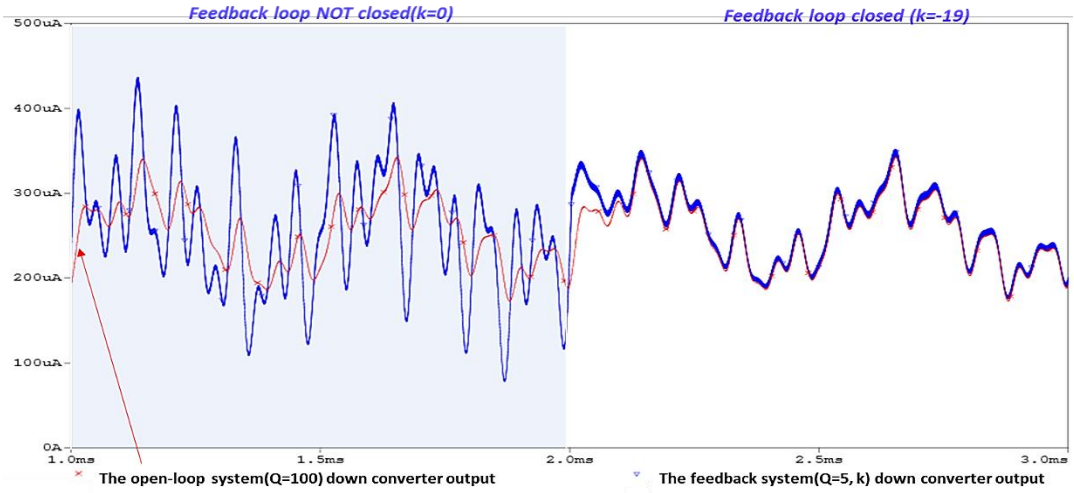

(a)

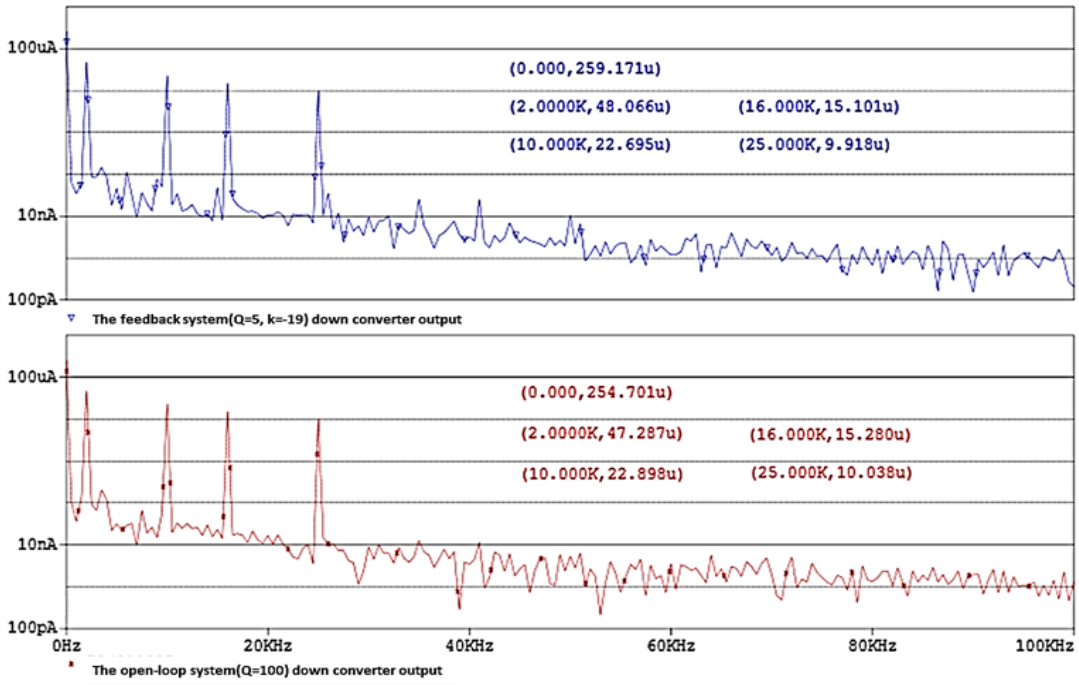

(b)

Figure 5.24 Transient plots and FFT spectra of the recovered signals from the second set of systems

Gain spectra of all the filtering systems under test above are plotted, together with gain spectra of the transfer functions for biquad complex filters with Q=200, f_0=4MHz and Q=400, f_0=4MHz, as shown in Fig. 5.25. High similarity between the

bandwidths of the filters in the same set verifies that the log-domain feedback system with a low-Q core filter is capable of implementing a high Q filtering system when the current sources varying the core filter bandwidth are properly set up. The peak gain of the feedback filter is closer to the ideal value, while the gain spectrum of the open loop filter bears stronger resemblance to the Bode plot of the target transfer function.

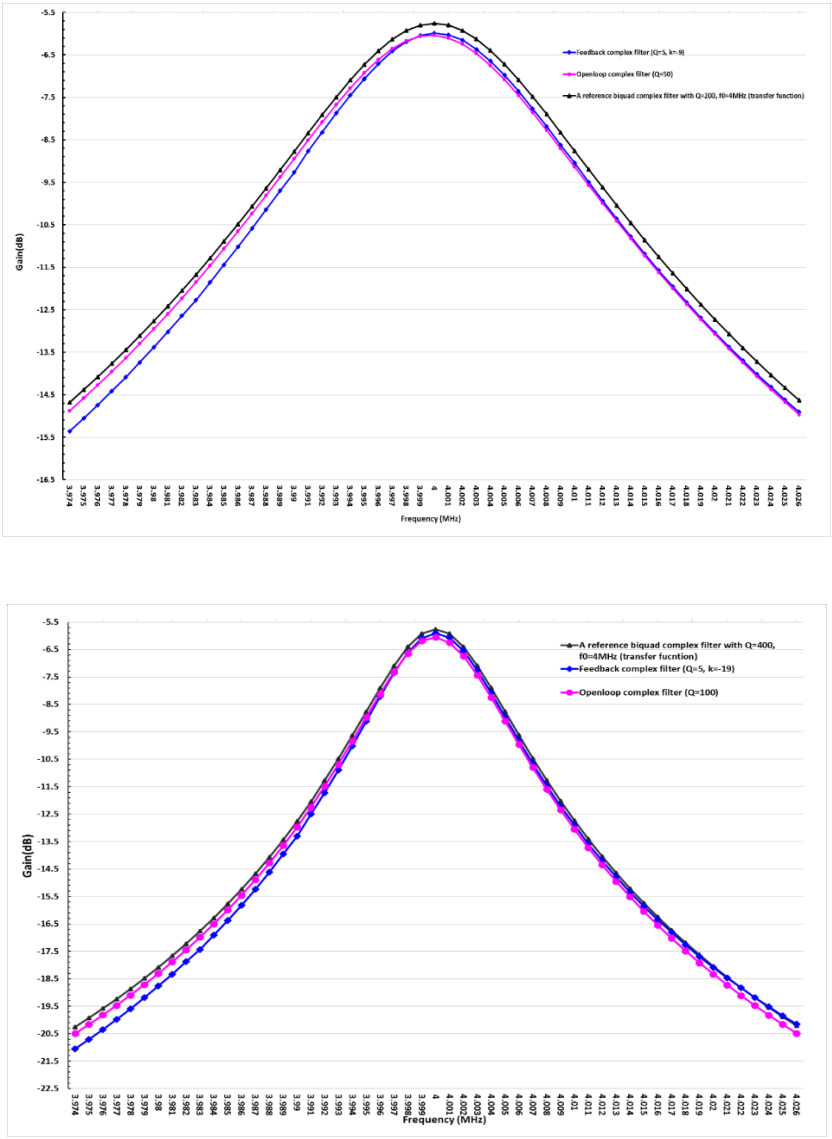

Figure 5.25 Gain spectra of all the log-domain filtering systems under test and the transfer functions of two reference biquad complex filters.

Finally, to compare the capability of the log-domain feedback complex filter in suppressing the internal noise to that of its reference open loop complex filter, white noise currents of 1uArms were injected into the filtering capacitors in the core filter in both systems. The feedback system was set up with $Q_{core} = 5\ and\ k = -19$ and the reference open loop complex filter had Q_{core} of 100. Simulation results in Fig. 5.26 explicitly verify the improved noise performance of the feedback filtering system in dealing with the in-filter noise. Moreover, it was observed that even when the assistant filter in the feedback system is injected with noise currents of the same RMS value, its output SNR is still about one order of magnitude higher than that of the open loop filter in the frequency range of interested. (The test results are not plotted here)

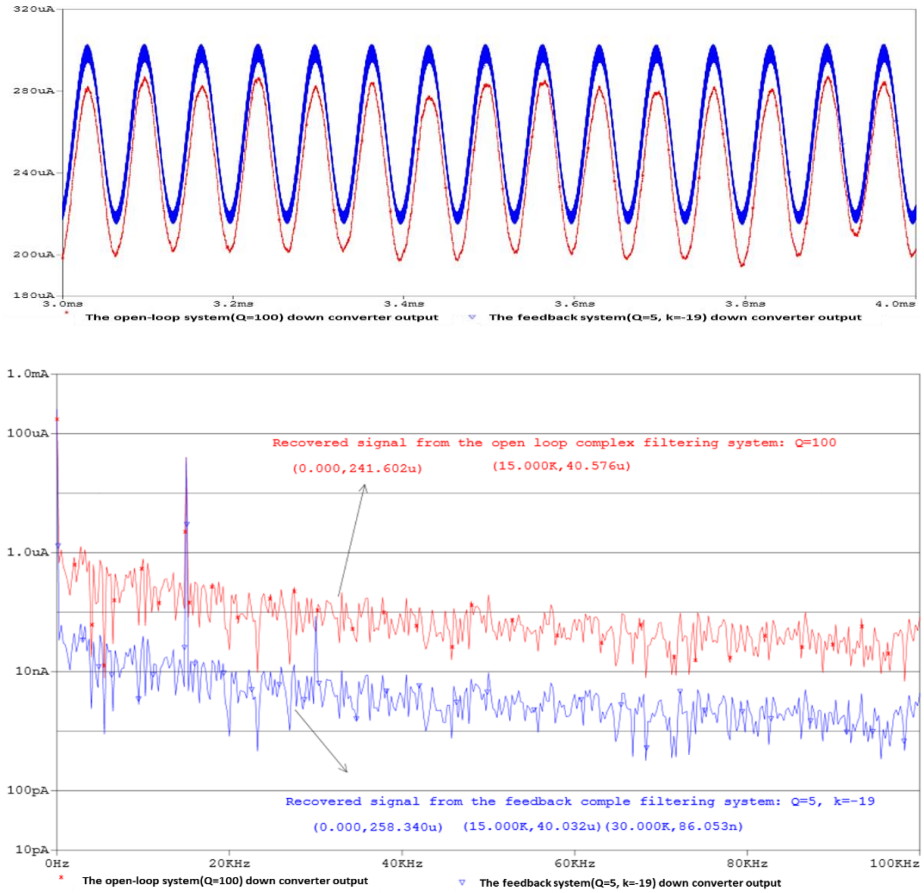

(a)

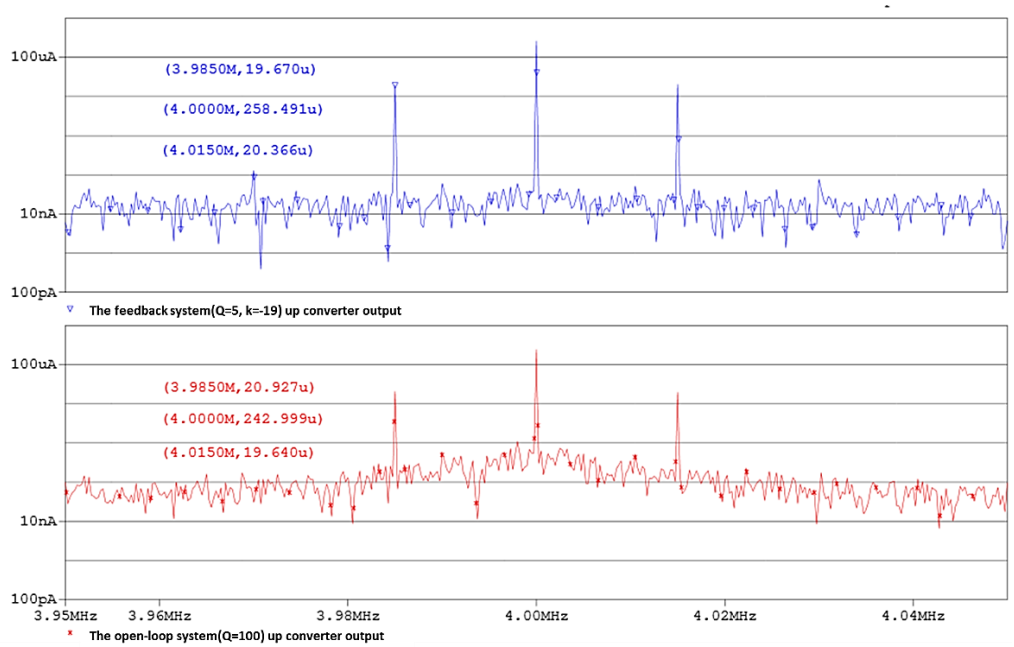

(b)

Figure 5.26 Transient plots and FFT spectra of the interested output signals from the log-domain feedback complex filter (Q=5, k=-19) and the reference open loop complex filter (Q=100) in the in-filter noise test.

5.4 Summary

An innovative approach to tuning the Q factor of a biquad bandpass filter processing AM signals was discovered and mathematically proved. The idea is inspired by the AM mode synchronous filtering and is illustrated in Fig. 5.1. Simply put, by scaling the feedback signal $\frac{\hat{p}(t)}{\hat{p}(t)}$ with k ($k \leq 1$), we would be able to turn the original bandpass filter with quality factor Q_{core} into one with time-variant bandwidth and an equivalent quality factor of $(1 - \mathrm{k})\ Q_{core}$.

Simulation results suggest that the AM mode feedback system developed from a biquad bandpass filter would always produce some output harmonic distortion. For any positive k, the distortion is at a negligible level; while for negative k values, the output distortion gets higher as k becomes more negative. When implementing a

feedback bandpass filter with some target Q factor, the combination of a sharper core filter and less negative k would have higher output SNR and frequency response more similar to that of the reference open loop bandpass filter. This might be due to the reconstructed $\hat{p}(t)$ contains a lot of high frequency harmonics of the down conversion sampling rate. An alternate system realization is shown in Fig. 5.7, which utilizes a biquad complex filter as the core filter. When set up with same Q_{core} and k, the feedback complex filtering system produces much less harmonic distortion and has an equivalent Q factor fits eqn. (5.1) better. Moreover, the gain spectrum of the feedback complex filter bears stronger resemblance to that of the reference open loop complex filter.

Mathematical explanation to the Q-factor tuning approach was inspired by noticing that when a first order lowpass filter cuts off at w_0 gets it output modulated by $-w_0 + \mathrm{k}\frac{\dot{y}}{y}$, where y is the modified filter's instant output, the yielded system would have a new cutoff frequency of $\frac{w_0}{1-k}$. Moreover, transformation on the state space description of the modified first order lowpass filter suggests that it could be realized by a second-order system that incorporates two terminal modulators and a biquad core filter. The state matrix specifying the biquad core filter has a formation identical to that of the state matrix in some state space representation of a biquad bandpass/complex filter. Furthermore, we proved that both the biquad bandpass filter and complex filter have the expected frequency response so as to generate a proper bandwidth control signal. Based on all the similarities, it becomes obvious that the mechanism the feedback

modulation scales the Q factor of a biquad bandpass/complex filter is exactly the same as that of the gain modulation scales the cutoff frequency of a first-order lowpass filter.

Observation made through the noise performance test is summarized as follows:

1) The feedback AM mode filtering system with a negative k is superior to its reference open loop filter in suppressing the in-filter noise. The advantage manifests itself in two aspects: First, when dealing with same amount of noise currents injecting to the filtering capacitors, the feedback filter always produces an output with lower noise floor than the open loop filter of comparable sharpness does. Second, to sharpen an open loop filter, we have to directly increase its Q factor, which amps up the input-referred noise and usually raises the output noise floor because the enhanced filtering capability could not counter balance the gain in the noise. For the feedback system, we could stick with the original core filter and simply tune the feedback scale factor k more negative. As the injected noise is not additionally amplified while the filter gets tuned sharper, the system output noise floor gets suppressed to a lower level.

2) Comparing the output spectra from feedback systems of comparable equivalent bandwidths, injected with same amount of noise, but developed with core filters of different Q factors, we discovered that the output noise level is consistently proportional to Q_{core}, so the feedback system with smaller Q_{core} always produces lower output noise floor. However, for feedback bandpass filters with very low Q_{core} and too negative scale factor k (e.g. Q_{core}=10, k=-19), large second-order harmonic distortion appears in the output (about 1.7% of the information signal size) and the recovered information signal is obviously lower than expected (about 10% lower), which greatly degrades the output SNR (Fig. 5.11(d)). So there is a tradeoff between the output noise

level, output harmonic distortion and Q_{core} value in implementing a feedback bandpass filter. Excitingly, the feedback complex filter is not subject to this issue, as shown in Fig. 5.13(c), no harmonic distortion is seen in the output from the system with Q_{core}=10 and k=-19, and the information component has larger amplitude. Therefore, the feedback complex filter demonstrates better performance than the feedback bandpass filter in dealing with in-filter noise.

3) For the feedback complex filtering system, we proposed a noisier Gm-C network model where all the transconductors are added with an input voltage noise source. The reference open loop filter models were accordingly set up noisy too. Test results in Fig. 5.17 suggest that even with noisy transconductors, the feedback complex filter and the reference open loop filter still have comparable sharpness, and the output noise floor from the feedback filter is still lower than its open loop filter counterpart. Moreover, the in-band output noise is apparently higher for the open loop filter with larger Q factor, while there is barely difference between the in-band output noise levels of the feedback filters with different sharpness, as long as they have the same Q_{core} factor. Therefore, the feedback complex filtering system provides an innovative approach to effectively sharpening a filter without raising the output noise floor in the interested frequency range.

4) Unfortunately, both the feedback bandpass filter and the feedback complex filter fail to more effectively suppress the input noise, compared to their reference open loop filters.

In the last section, a possible implementation of a biquad log-domain feedback complex filter is proposed. The schematic for the overall system is given Fig. 5.22.

Transient test, frequency response test and in-filter noise suppression test were run on the transistor-level feedback filter and its reference open loop filter. Specific test setup is given in Table 5.4, the filtering function and noise performance of the circuit is verified by simulation results in Fig. 5.23 to Fig. 5.26. Note that the proposed design has to include an assistant core filter to eliminate some undesired frequency components so as to implement the expected time-variant Q factor, which makes the circuit more power consuming and subject to more noise, further effort could be put into modifying the design and simplifying the schematic.

Chapter 6 Conclusion and Future Work

In the context of synchronous filtering, we focused on developing analog filters with improved noise performance. Specifically, a second-order bandpass filter and a second-order complex filter were implemented and modified utilizing AM mode or FM mode synchronous filtering techniques. Important discoveries and designs are summarized as follows:

1. The FM mode synchronous filtering, either static or dynamic, provides a modulator-core filter-modulator architecture that could be used to implement a high-center frequency high-Q factor complex filter with a low-center frequency low-Q filter. A dynamic synchronous complex filter, of which the core filter center frequency and both end modulating frequencies vary with time in a synchronized way, is capable of suppressing the injected in-filter single-tone noise in a certain frequency range. Consider the particular dynamic complex filter we studied that has a center frequency offset at 1MHz and a constant bandwidth of 20kHz for instance. When the center frequency varies as a square waveform at 100kHz in the range of $1\text{MHz} \pm 800\text{kHz}$, the system suppresses the single-tone noise components near 1MHz injected to the core filter to about three orders of magnitude lower than their levels in the static system output, without additionally attenuating the useful information signals.

2. We developed a few filtering systems with time-varying Q factor based on the architecture of an AM mode synchronous filter. The related block diagrams are given below. System 1 could be taken as an AM mode synchronous bandpass filter without the back end modulator, receiving input signal $u(t)$; it could also be viewed as

a filter with time-varying Q factor receiving an AM signal $u(t)p(t)$. Taking the second perspective, if System 1 has a very sharp original time-invariant core filter, then it would be able to heavily suppress the input noise while maintaining the amplitude and phase of the useful information components. Unfortunately, as it's almost impossible to generate the ideal $\frac{\dot{p}(t)}{p(t)}$ with the AM input $u(t)p(t)$, System 1 might not be implementable in practice.

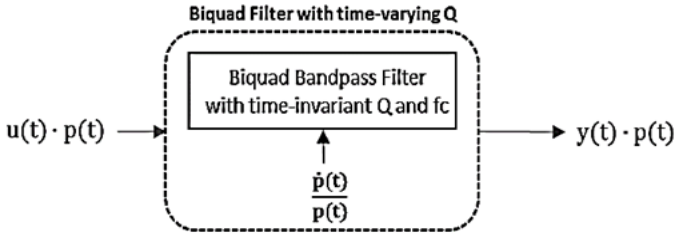

Figure 6.1 System 1: A bandpass filter with time-variant Q factor processing an AM input signal, derived by deleting the back end modulator of an AM mode synchronous bandpass filter.

Interestingly, we discovered that if we demodulate the core filter output with very little introduced phase shift to recover the information signal $\hat{p}(t)$ and generate $\frac{\dot{\hat{p}}(t)}{\hat{p}(t)}$ to time vary the core filter's Q factor, as long as the input AM signal is noiseless, the resulting system is able to produce an output very similar to what is produced by System 1. Such a feedback system is represented by System 2 with *k*=1, where the demodulator could be realized with a sample-and-hold block performing ideal sampling at the rate equal to the input carrier frequency. However, when dealing with a noisy AM signal, as the feedback Q-factor control signal becomes noisy, the system output SNR drastically drops and is even lower than that of an open loop bandpass filter with the same Q factor.

In an effort to improve the feedback system performance in processing a noisy input, we tried out several methods and came up with a system that incorporates two bandpass filters. The purpose is to generate a less noisy Q-factor control signal with the second filter. It has been shown by simulation results that for input signals with narrow bandwidths, the system is able to heavily suppress the input noise while almost maintaining the original amplitude of the useful components. The downside of this system is that the achievable highest output SNR is constrained by the bandwidth of the input signal. Namely, as the input bandwidth gets wider, the system output SNR gradually drops.

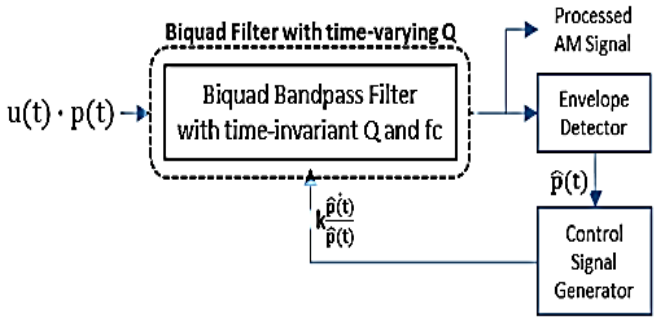

Figure 6.2 System 2: An implementable feedback system inspired by System 1. When *k*=1 and the input AM signal is noiseless, it is capable of producing an output very similar to what is produced by System 1. When *k* is negative, the equivalent Q factor of the system becomes higher than the original Q factor of the core filter.

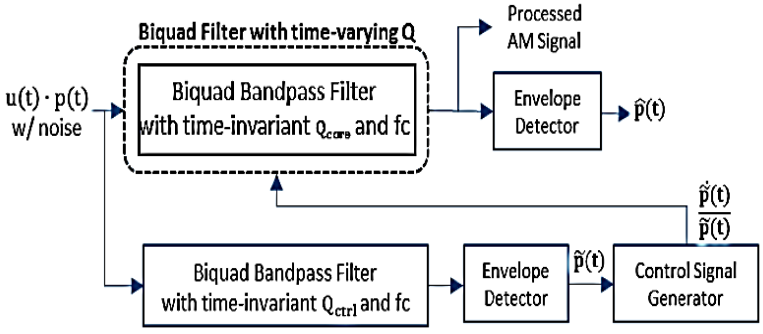

Figure 6.3 System 3: The two-filter system inspired by System 2 with k =1, for processing noisy input.

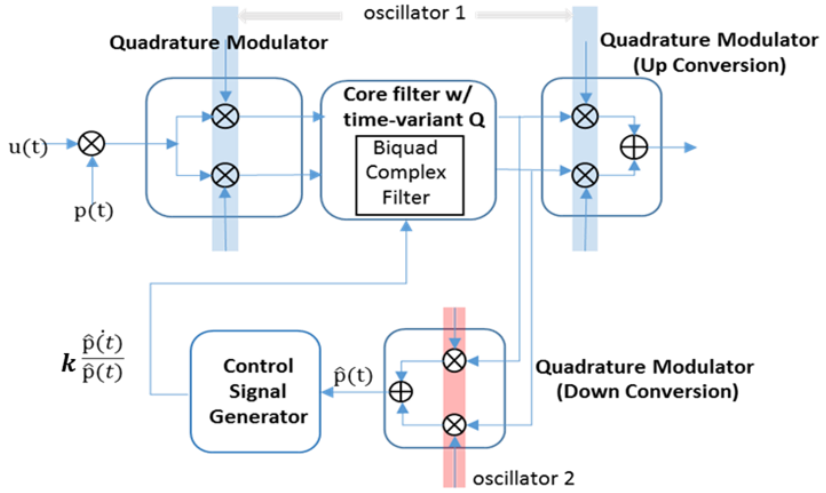

Figure 6.4 System 4: A feedback complex filtering system: an advanced version of System 2 which is easier to implement and has better noise performance.

3. It has been discovered with System 2 that the equivalent Q factor of the filtering system could be tuned by adjusting the amount of the feedback signal, denoted as $k\frac{\dot{\hat{p}}(t)}{\hat{p}(t)}$. The equivalent Q factor could roughly be evaluated with eqn. (5.1): $\mathrm{Q_{eq}} = (1-\mathrm{k})\mathrm{Q_{core}}$ for k smaller than 1. It suggests that System 2 provides an approach to the design of high-Q filters with a low-Q filter by making $\mathrm{k} < 1$. Moreover, the resulting feedback filter with time-varying Q factor is superior in suppressing the in-filter white noise to an open loop filter that has comparable bandwidth.

4. A static FM mode synchronous complex filter was modified to implement a feedback complex filter with time-varying Q factor, represented by System 4. Compared to System 2, System 4 provides a more implementable way to recover the information signal from the core filter output for generating the Q-factor control signal. Simulation on both the ideal Gm-C model and the noisier Gm-C model has verified the function and the improved noise performance of System 4. Finally, we implemented the system

as a log-domain filter and verified the frequency response and in-filter noise reduction capability of the ideal BJT-level design.

Proposals for future work include:

1. Set up a more practical Gm-C model for the feedback complex filtering system by including noise sources associated with multipliers in the demodulator and in the feedback path, checking out the performance and noise suppression capability of the model. For the transistor-level design, add noise sources in the feedback path and check out how they affect the system performance.

2. Develop a simpler transistor-level design solution to implement the feedback complex filter.

3. Derive an analytical solution for the complete response of the feedback bandpass filtering system with k=1. Determine a mathematical explanation to the emergence of the output noise peak(s) shown in Fig. 4.11, which is the result of the input white noise being processed by the feedback system.

4. Derive an analytical solution for the complete response of a dynamic FM mode synchronous complex filter. Solve it for the system where the core filter center frequency varies as a sinusoid waveform first, then as a square waveform.

5. Utilize the analytical solutions to develop new methods or architectures that lead to filtering systems with improved capability in reducing both the injected noise and the input noise.

Reference

[1] V. Gopinathan, Y. P. Tsividis, K. Tan, and R. K. Hester, "Design considerations for high-frequency continuous-time filters and implementation of an antialiasing filter for digital video," *Solid-State Circuits, IEEE Journal of,* vol. 25, no. 6, pp. 1368-1378, 1990.

[2] J. M. Khoury, "Design of a 15-MHz CMOS continuous-time filter with on-chip tuning," *Solid-State Circuits, IEEE Journal of,* vol. 26, no. 12, pp. 1988-1997, 1991.

[3] C. Chiou and R. Schaumann, "Design and performance of a fully integrated bipolar 10.7-MHz analog bandpass filter," *Solid-State Circuits, IEEE Journal of,* vol. 21, no. 1, pp. 6-14, 1986.

[4] Y. Wang and A. A. Abidi, "CMOS active filter design at very high frequencies," *Solid-State Circuits, IEEE Journal of,* vol. 25, no. 6, pp. 1562-1574, 1990.

[5] B. Wilson, "Recent developments in current conveyors and current-mode circuits," in *Circuits, Devices and Systems, IEE Proceedings G,* 1990, vol. 137, no. 2, pp. 63-77: IET.

[6] J. Dunning-Davies and F. W. Stephenson, "Sensitivity optimization of active filters containing current conveyors and controlled sources," *International Journal of Electronics Theoretical and Experimental,* vol. 48, no. 3, pp. 283-289, 1980.

[7] D. G. Haigh, J. T. Taylor, and B. Singh, "Continuous-time and switched capacitor monolithic filters based on current and charge simulation," in *Circuits, Devices and Systems, IEE Proceedings G,* 1990, vol. 137, no. 2, pp. 147-155: IET.

[8] T. S. Rathore and S. M. Dasgupta, "Current-conveyor realisation of transfer function," *Electrical Engineers, Proceedings of the Institution of,* vol. 122, no. 10, pp. 1119-1120, 1975.

[9] C. Toumazou and F. J. Ledgey, "Universal active filter using current conveyors," *Electronics Letters,* vol. 22, no. 12, pp. 662-664, 1986.

[10] G. W. Roberts and A. S. Sedra, "All current-mode frequency selective circuits," *Electronics Letters,* vol. 12, no. 25, pp. 759-761, 1989.

[11] D. R. Frey, "Synchronous Filtering," *IEEE Transactions on Circuits and Systems I-Regular Papers,* Article vol. 53, no. 8, pp. 1772-1782, Aug 2006.

[12] D. R. Frey, "Exponential state-space filters: a generic current mode-design strategy," *Circuits and Systems I: Fundamental Theory and Applications, IEEE Transactions on,* vol. 43, no. 1, pp. 34-42, 1996.

[13] D. Rowell, "State-Space Representation of LTI Systems," ed.

[14] A. A. Emira and E. Sánchez-Sinencio, "A pseudo differential complex filter for Bluetooth with frequency tuning," *Circuits and Systems II: Analog and Digital Signal Processing, IEEE Transactions on,* vol. 50, no. 10, pp. 742-754, 2003.

[15] K. W. Martin, "Approximation of complex IIR bandpass filters without arithmetic symmetry," *Circuits and Systems I: Regular Papers, IEEE Transactions on,* vol. 52, no. 4, pp. 794-803, 2005.

[16] F. Behbahani, Y. Kishigami, J. Leete, and A. A. Abidi, "CMOS mixers and polyphase filters for large image rejection," *Solid-State Circuits, IEEE Journal of*, vol. 36, no. 6, pp. 873-887, 2001.
[17] L. Der and B. Razavi, "A 2-GHz CMOS image-reject receiver with LMS calibration," *Solid-State Circuits, IEEE Journal of*, vol. 38, no. 2, pp. 167-175, 2003.
[18] K. W. Martin, "Complex signal processing is not complex," *Circuits and Systems I: Regular Papers, IEEE Transactions on*, vol. 51, no. 9, pp. 1823-1836, 2004.
[19] Y. Tsividis, "Externally linear, time-invariant systems and their application to companding signal processors," *Circuits and Systems II: Analog and Digital Signal Processing, IEEE Transactions on*, vol. 44, no. 2, pp. 65-85, 1997.
[20] R. C. Mathes and S. B. Wright, "The Compandor—An Aid Against Static in Radio Telephony*," *Bell System Technical Journal*, vol. 13, no. 3, pp. 315-332, 1934.
[21] Members *et al.*, *Transmission Systems for Communications*. Winston-Salem, NC: Western Electric Co.,, 1970.
[22] R. M. Dolby, "Signal compressors and expanders," ed. U.S. Patent 3 345416: Google Patents, 1971.
[23] D. Fisher, "Noise reduction systems," ed. Audio and Hi-Fi Handbook,(1993): Butterworth–Heinemann Ltd., Linacre House, Jordan Hill, Oxford.
[24] E. M. Blumenkrantz, "The analog floating point technique," in *Low Power Electronics, 1995., IEEE Symposium on*, 1995, pp. 72-73: IEEE.
[25] E. A. Vittoz, "Low-power low-voltage limitations and prospects in analog design," in *Analog Circuit Design*: Springer, 1995, pp. 3-15.
[26] W. A. Serdijn, A. C. v. d. Werd, J. Davidse, and A. H. M. V. Roermund, "A low-voltage low-power fully-integratable front-end for hearing instruments," *Circuits and Systems I: Fundamental Theory and Applications, IEEE Transactions on*, vol. 42, no. 11, pp. 920-932, 1995.
[27] J. O. Voorman, "Continuous-time analog integrated filters," *Integrated continuous-time filters*, pp. 27-29, 1993.
[28] G. Groenewold, B. Monna, and B. Nauta, "Micro-power analog-filter design," in *Analog Circuit Design*: Springer, 1995, pp. 73-88.
[29] L. Toth, G. Efthivoulidis, V. Gopinathan, and Y. P. Tsividis, "General results for resistive noise in active RC and MOSFET-C filters," *IEEE transactions on circuits and systems. 2, Analog and digital signal processing*, vol. 42, no. 12, pp. 785-793, 1995.
[30] Y. Tsividis, "General approach to signal processors employing companding," *Electronics Letters*, vol. 31, no. 18, pp. 1549-1550, 1995.
[31] D. R. Frey, Y. P. Tsividis, G. Efthivoulidis, and N. Krishnapura, "Syllabic-companding log domain filters," *Circuits and Systems II: Analog and Digital Signal Processing, IEEE Transactions on*, vol. 48, no. 4, pp. 329-339, 2001.
[32] R. W. Adams, "Filtering in the log domain," in *Audio Engineering Society Convention 63*, 1979: Audio Engineering Society.

[33] D. Frey, "Log-domain filtering: an approach to current-mode filtering," in *Circuits, Devices and Systems, IEE Proceedings G*, 1993, vol. 140, no. 6, pp. 406-416: IET.

[34] David Johns, Ken Martin, "*Analog integrated circuit design"*, John Wiley & Sons, Inc., 1997.

[35] Kenneth R. Laker, Willy M. C. Sansen, *"Design of analog integrated circuits and systems"*, New York: MacGraw-Hill, 1994.

[36] C. Toumazou, F.J. Lidgey, and D.G. Haigh (eds), *"Analogue IC design: The Current-Mode Approach"*. London: Peter Pereginus Ltd., 1990: Presbyterian Publishing Ltd., 1990.

[37] Jirayuth Maattanakul and Chris Toumazou, "Current-Mode Versus Voltage-mode Gm-C Biquad Filters: What the Theory Says", *IEEE Transactions on Circuits and Systems II: Analog and Digital Signal Processing*, vol. 45, no. 2, pp. 173-186, 1998.

[38] Cehan, Vlad, Radu Gabriel Bozomitu, and Daniela Ionescu. "Noise behavior of elementary transconductors stages in bipolar and CMOS technology." In *28th International Spring Seminar on Electronics Technology: Meeting the Challenges of Electronics Technology Progress, 2005.*, pp. 348-354. IEEE, 2005.

Vita

Kanlun Li was born in 1986 in Changsha, China to Mr. Jiancheng Li and Mrs. Daili Zhu. She received her B.S. degree in Electrical Engineering from Huazhong University of Science and Technology, Wuhan, China in 2008. She started studying with Professor Douglas Frey since 2010 and received her M.S. degree in Electrical Engineering from Lehigh University, Bethlehem, PA in 2011. During her graduate study at Lehigh University, she has been awarded a Sherman Fairchild Fellowship. Her research interest includes filter design and synthesis, circuits and systems, and analog/mixed-signal circuit design.